Oxygen and the ovarian follicle

A thesis presented in partial fulfilment of the requirements for the degree of

Doctor of Philosophy

in

Bioprocess Engineering

At Massey University, Palmerston North,

New Zealand

Gabe Peter Redding

2007

Abstract

The role oxygen plays in the developing ovarian follicle is of interest not only to the field of developmental biology but also to in-vitro fertilisation (IVF) technologists, as oxygenation of the oocyte is considered to be a potential determinant of oocyte competence.

Oxygen transport through the developing ovarian follicle, and practical aspects of the analysis of oxygen in human follicular fluid were investigated in this work.

Mathematical modelling of oxygen transport in the pre-antral, and antral/pre-ovulatory follicle revealed a number of interesting findings.

Contrary to previous conclusions (Gosden & Byatt-Smith, 1986), oxygen can reach the oocyte in the small pre-antral follicle. Improved estimates of diffusion coefficients through the granulosa cell layer and the inclusion of fluid voidage in this layer showed that oxygen can also reach the oocyte in large pre-antral follicles. The amount of oxygen that reaches the oocyte in the pre-antral follicle is a function of its size and degree of vascularisation. Symmetrically distributed vascularisation is superior in achieving a well oxygenated follicle.

However, the large pre-antral follicle will eventually reach a size beyond which it cannot grow without anoxic regions developing. The size at which this occurs is consistent with the size at which antrum formation is observed in human follicles.

The model predicts that the follicle can avoid an anoxic state through antrum formation, and shows that the follicle develops in a way that is consistent with overcoming mass transport limitations. The oxygen status of the follicle during the antral/pre-ovulatory phase of growth requires that the volume of granulosa cells be balanced by the volume of follicular fluid.

Further predictions suggest that oocyte respiration becomes sub-maximal at follicular fluid volumes below approximately 4ml, vascularisation levels below 38%, or fluid

dissolved oxygen levels below 5.1 vol%. These values are consistent with observations in the literature. It was also shown that the measurement of follicular fluid dissolved oxygen levels could provide a simple measure of the respiratory status of the oocyte, and this may be superior to the measurement of follicular vascularisation which requires knowledge of more parameters.

Methodology for the analysis of follicular fluid oxygen solubility and diffusivity was developed using a Clark oxygen electrode. Analysis of these parameters showed that they are similar to human plasma, and allowed the predictive uncertainty of the model to be reduced.

Experimental studies into the effects of IVF aspiration on follicular fluid were carried out. Aspiration results in significant changes in the properties of follicular fluid. Dissolved oxygen levels rose 5 ± 2 vol%, pH increased by 0.04 ± 0.01 pH units, and temperature dropped by 7.7 ± 1.3 °C. Mathematical modelling of blood contaminated follicular fluid also showed that contamination results in significant changes in the dissolved oxygen of the fluid. This suggests that if the composition of follicular fluid is to be determined (particularly dissolved oxygen), sampling and/or measurement of fluid must take place before the collection vial of the aspiration kit, and blood contamination must be eliminated.

Based on this result, the design and testing of devices capable of reliable sampling and/or measurement of oxygen levels of follicular fluid was considered. This presents a continuing challenge, including the integration of routine follicular fluid oxygen measurement into clinical practice.

Acknowledgements

I would like to thank all the staff and students at Massey University and AgResearch who have helped me during this project. Your number is too many to thank personally.

Many thanks to my supervisors, Dr. John Bronlund, and Dr. Alan Hart. John, thank you for the academic assistance, especially for focusing me on what matters. Alan, although your assistance was often academic I am particularly grateful for the day to day practical assistance and encouragement you provided me, which enabled me to get the job done. As supervisors your skills are very complimentary. To Wendy Collier thank you for all your help, and for putting up with me in general. It must surely be my turn to do the dishes now.

To all the staff at the ISIS clinic in Hamilton and in the Dairy Science building at Ruakura, thanks for having me, and making me feel welcome.

My family, Mum, Dad, Cain, Janell, and Fizz. Thank you for your support, but also for not asking too often how the thesis was going. Without you achievement is worth very little. Janell, thank you for your love and support. Without you, I simply would not have been able to finish this work.

I feel obligated by tradition to say something profound in the final paragraph of the acknowledgements section. Unfortunately I don't seem to have any runners on base in that department today. I am all spent for the next little while. So, a joke instead (somebody else's), which is best read aloud,
Why did the sperm cross the cumulus?
To get to the oocyte.

TABLE OF CONTENTS

LIST OF FIGURES

LIST OF TABLES

NOMENCLATURE

Note that some symbols which are used only once are defined in the text where they occur and are not included on this list.

A	cathode surface area	m^2
Bi	dimensionless ratio of membrane to sample layer resistance to mass transport	
c_p	heat capacity	$J.kg^{-1}.K^{-1}$
c_{pff}	heat capacity of follicular fluid	$J.kg^{-1}.K^{-1}$
C	oxygen concentration	$mol.m^{-3}$
C_o	oxygen concentration at the follicle surface	$mol.m^{-3}$
C_{crit}	Oxygen concentration of critical interest (most notably the critical oxygen concentration at which oocyte is only just respiring maximally ($R_o = 0.99R_{omax}$))	$mol.m^{-3}$
C_{0mean}	the mean surface concentration of a partially vascularised follicle	$mol.m^{-3}$
$C_{arterial}$	oxygen concentration in the plasma portion of arterial blood	$mol.m^{-3}$
C_{novasc}	oxygen concentration at a un-vascularised surface of the follicle	$mol.m^{-3}$
C_i	oxygen concentration at the granulosa/antrum interface	$mol.m^{-3}$
C_{imin}	minimum oxygen concentration required at the granulosa/antrum interface to sustain the oocyte at $R_o=0.99R_{omax}$	$mol.m^{-3}$
C_{omin}	minimum oxygen concentration required at the follicle surface to sustain the oocyte at $R_o=0.99R_{omax}$	$mol.m^{-3}$
C_{ii}	concentration of oxygen at the cumulus/antrum interface	$mol.m^{-3}$
C_a	analyte concentration	$mol.m^{-3}$
C_p	analyte concentration in plasma	$mol.m^{-3}$
C_f	analyte concentration in follicular fluid	$mol.m^{-3}$

C_H	concentration of haemoglobin in blood	$mol.m^{-3}$
d_{min}	minimum distance from oocyte centre to outer edge of either compact or expanded cumulus mass	mm
d_{max}	maximum distance from oocyte centre to outer edge of either compact or expanded cumulus mass	mm
d_f	follicle diameter	m
D_g	diffusion coefficient of oxygen in the granulosa cell layer	$m^2.s^{-1}$
D_{cell}	diffusion coefficient of oxygen through the cellular fraction of tissue	$m^2.s^{-1}$
D_p	diffusion coefficient of oxygen in plasma	$m^2.s^{-1}$
D_{eff}	effective diffusion coefficient of oxygen through tissue	$m^2.s^{-1}$
D_a	diffusion coefficient of oxygen in the antral fluid	m
D_c	diffusion coefficient of oxygen in the cumulus cell layer	$m^2.s^{-1}$
D_m	diffusivity of oxygen in the membrane of a dissolved oxygen electrode	$m^2.s^{-1}$
D_s	diffusivity of oxygen in the sample solution	$m^2.s^{-1}$
D_w	diffusivity of oxygen in water	$m^2.s^{-1}$
D_{rel}	relative diffusivity of oxygen in sample compared to water	
F	Faradays constant (number of Coulombs per mol of electrons)	$coulombs.mol^{-1}$
ΔH_{vap}	enthalpy of vaporisation of water	$J.mol^{-1}$
I	current produced by Clark oxygen electrode	A
I_g	steady-state gas phase current	A
I_s	steady-state current with sample solution layer in place	A
I_w	steady-state current with water layer in place	A
js	number of nodes in the sample solution layer	
jm	number of nodes in the membrane layer	
J	oxygen flux	$mol.s^{-1}$
K_1	first integration constant	m^{-2}
K_2	second integration constant	$mol.m^{-3}$
K_m	Michaelis-Menton constant	$mol.m^{-3}$

L_m	membrane thickness	m
L_s	sample thickness	m
L_w	water layer thickness	m
m	flow rate	$kg.s^{-1}$
n	number of electrons involved in the reduction of oxygen at the cathode	e
M_{O2}	molecular mass of oxygen	$g.mol^{-1}$
p	oxygen partial pressure	mmHg
p_o	oxygen partial pressure at follicle surface	mmHg
p_i	partial pressure of oxygen at the granulosa/antrum interface or membrane/sample interface	mmHg
p_g	partial pressure of oxygen in the gas phase	mmHg
p_m	partial pressure of oxygen in the membrane	mmHg
p_s	partial pressure of oxygen in the sample solution	mmHg
pO_2	partial pressure of oxygen	mmHg
pO_{2b}	partial pressure of oxygen in blood	mmHg
pO_{2f}	partial pressure of oxygen in follicular fluid	mmHg
pO_{2m}	partial pressure of oxygen in blood/follicular fluid mixture	mmHg
P_1	number of pixels occupied by oocyte	pixels
P_2	number of pixels occupied by oocyte and compact cumulus	pixels
P_3	number of pixels occupied by cumulus-oocyte complex (cells and fluid)	pixels
P_4	number of pixels occupied by cumulus-oocyte complex (cells only)	pixels
P_{ATM}	atmospheric pressure	atm
P_m	permeability of oxygen in the membrane of a dissolved oxygen electrode	$mol.m^{-1}.s^{-1}.mmHg^{-1}$
P_s	permeability of oxygen in the sample solution	$mol.m^{-1}.s^{-1}.mmHg^{-1}$
P_w	permeability of oxygen in water	$mol.m^{-1}.s^{-1}.mmHg^{-1}$
P_{rel}	relative permeability of oxygen in sample compared to water	

P_{50}	partial pressure of oxygen at which 50% of haemoglobin oxygen binding sites are full	mmHg
r	radial distance from follicle centre	m
r_f	follicle radius	m
r_o	oocyte radius (note this parameter expressed in mm in Chapters 7 and 8)	m
r_{anoxic}	distance from follicle centre at which follicle becomes depleted of oxygen	m
r_{fcrit}	critical follicle radius beyond which no oxygen will reach the surface of the oocyte.	m
r_a	distance from the follicle centre to the granulosa/antrum interface	m
r_c	distance from the follicle centre to the cumulus/antrum interface	m
R_{gmax}	maximal oxygen consumption rate by the granulosa cells	$mol.m^{-3}.s^{-1}$
R_g	oxygen consumption rate of the granulosa cells	$mol.m^{-3}.s^{-1}$
R_{omax}	maximal oxygen consumption rate by the oocyte	$mol.m^{-3}.s^{-1}$
R_o	oxygen consumption rate by the oocyte	$mol.m^{-3}.s^{-1}$
R	gas constant	$L.atm.mol^{-1}.K^{-1}$
R_a	oxygen consumption rate in the fluid antrum	$mol.m^{-3}.s^{-1}$
R_c	oxygen consumption rate of the cumulus cells	$mol.m^{-3}.s^{-1}$
S	solubility of oxygen in solution	$mol.m^{-3}.mmHg^{-1}$
S_a	solubility of oxygen in the antral fluid	$mol.m^{-3}.mmHg^{-1}$
S_m	solubility of oxygen in the membrane of a dissolved oxygen electrode	$mol.m^{-3}.mmHg^{-1}$
S_s	solubility of oxygen in the sample solution	$mol.m^{-3}.mmHg^{-1}$
S_w	solubility of oxygen in water	$mol.m^{-3}.mmHg^{-1}$
S_{rel}	relative solubility of oxygen in sample compared to water	
S_p	solubility of oxygen in plasma	$mol.m^{-3}.mmHg^{-1}$
t	time	s
t_f	time required for follicular fluid sample to travel through viscometer	s
t_w	time required for water to travel through viscometer	s

T	temperature	K
U_{min}	minimum gas stream velocity required to produce sustained waves on a flat liquid surface	cm.s^{-1}
$\%vasc$	mean symmetrical vascularisation	%
V_g	volume of granulosa cells in follicle	m^3
V_{cell}	volume of a single granulosa cell	m^3.cell^{-1}
V_f	total volume of follicle	m^3
V_a	volume of antral fluid	m^3
V_o	volume of the oocyte	m^3
V_b	volume of blood contamination	m^3
V_p	volume of plasma	m^3
V_{ff}	volume of follicular fluid	m^3
V_{RBC}	total volume of red blood cell sediment	m^3
x	position in membrane/sample solution system	m
x'	position in sample layer of analytical solution	m
X	weight fraction	
Y_H	fraction of haemoglobin saturated by oxygen	
y	mass of evaporated fluid	kg
Y	mass of aspirated fluid	kg
Φ	cell fraction	
Φ_L	heat flux	W
ρ_f	density of follicular fluid	kg.m^{-3}
ρ_w	density of water	kg.m^{-3}
ρ_{O2}	density of oxygen gas	g.L^{-1}
ε	fluid voidage	
τ	dimensionless time	
μ_a	kinematic viscosity of follicular fluid	mm^{2}s^{-1} (cSt)
μ_w	kinematic viscosity of water	mm^{2}s^{-1} (cSt)
θ	temperature	°C
$\Delta\theta$	temperature change	°C
$\Delta\theta_{tot}$	total temperature change over entire aspiration kit	°C
$\Delta\theta_1$	temperature drop over the collection vial when aspiration is performed normally	°C

$\Delta\theta_2$ temperature drop over the collection vial when the   °C
collection vial is heated and then insulated prior to aspiration

$\Delta\theta_3$ temperature drop over the collection vial when   °C
the collection vial is insulated only prior to aspiration

Chapter 1.   Introduction and objectives

The work presented in this thesis is part of a wider project to develop and utilise various technologies to allow improvement of the success rates of human In-Vitro Fertilisation (IVF)

Improving the success rates of IVF is desirable as the procedure currently places a significant financial burden on both individuals and taxpayers in New Zealand, as couples are eligible for funding from the government to undertake the procedure. In addition, there is also the emotional stress placed on the couple, magnified by the fact that the majority of couples need to undergo multiple treatment cycles before either success results or they discontinue treatment. It is estimated in Australia that the cost of IVF treatment per live birth is $40,000 (Wagner & St. Clair, 1989). It appears that IVF represents a significant cost to the health system without offering a substantial increase in the health of the population. Technologies with the potential to increase pregnancy rates and therefore reduce the costs of IVF, may make this process of more benefit to everyone.

This work specifically focuses on the measurement of parameters related to follicular health. This is based on the belief that follicle health can be a direct measure of the quality of the oocyte. If high quality oocytes can be selected, then higher quality embryos will probably result. In turn, high quality embryos have a greater chance of leading to a successful full term pregnancy and the birth of a healthy child. This, of course, is the ultimate goal of IVF.

The measurement of the degree of vascularisation surrounding the follicle, and the dissolved oxygen levels found in the follicular fluid are two variables which may be useful in the selection of the best oocytes. The degree of vascularisation as measured by Doppler ultrasonography has been shown to be related to the outcome of IVF (Bhal *et al.,* 1999). The dissolved oxygen content of follicular fluid has also been shown to be related to the normality (or otherwise) of the chromosomal spindle of the oocyte (Van Blerkom *et al.,* 1997).

1

In spite of the promise shown, neither of these techniques have found their way into routine clinical use as a tool for improving the success rates of IVF. In fact, other than qualitative grading of oocytes, sperm, and embryos, no tools are commonly used to assist selection (the use of pre-implantation genetic diagnosis (PGD) is increasing).

Therefore, this thesis aims to help bring the use of these technologies closer to day to day clinical practice. This work focuses on the measurement of dissolved oxygen in follicular fluid (though not exclusively because of wider contractual obligations).

Up to this point, much of the literature which seeks to relate various parameters to IVF outcome has taken on a somewhat haphazard approach. Parameters are often measured either because they are there, or based on scientific hunch. Once these parameters are measured, a correlation with IVF outcome is attempted. If no relationship is found the literature moves on to the next parameter. If a correlation is found the literature once again moves onto the next parameter. The potentially useful tools never get as far as the IVF clinic where they may be useful in improving success rates.

This work aims to take a more structured approach, which will hopefully enhance the chances of new technologies becoming a regular feature in the IVF clinic. A suggested approach is as follows,

1. Understanding what is being measured

2. Develop appropriate sampling and measurement capability

3. Integration into clinical practice

Understanding what is being measured and why, allows for better interpretation of results once measurements have been made. It also gives research the best chance of focusing on and measuring what is relevant. In this work, this was achieved through mathematical modelling of oxygen transport in the follicle. This was then used to assist in the interpretation of what the measurements of follicular vascularisation and

2

dissolved oxygen levels are actually telling us, and how the two might be related.

Sampling and measurement must be considered to eliminate and/or minimise the possibility of pre-analytical errors associated with sampling, and analytical errors associated with measurement. Too often a measurement technique is used simply because it is available, with pre-analytical and analytical errors often being overlooked. These issues as they pertain to dissolved oxygen measurement were addressed in this work.

The final hurdle for any technology in this field is integration into the clinical environment. This needs to be achieved if the full benefit of the research is to be realised. How this can be best achieved was discussed, although full treatment of this obstacle is a major project in itself.

The specific objectives of this work are,

1. To use mathematical modelling of oxygen transport and utilisation in the ovarian follicle to gain a better understanding of the role oxygen plays in the developing follicle, and to gain a greater understanding of what the measurement of follicular fluid dissolved oxygen actually means. This is achieved in Chapters 3 and 4.

2. To measure the parameters of oxygen permeability, diffusivity and solubility in human follicular fluid, so that the effect of the variability in these parameters on the conclusions drawn through the mathematical modelling of oxygen transport in the ovarian follicle can be quantified. This is achieved in Chapters 5 and 6.

3. To address the practical issues associated with the reliable measurement of dissolved oxygen levels in human follicular fluid and how this can be integrated into the clinical setting. This is achieved in Chapters 7 and 8.

Chapter 2.   Review of the literature

Before addressing the specifics of these issues, a good understanding in several key areas is required. Firstly, a basic understanding of the IVF process and the biology related to it is essential. This includes knowledge of the properties and function of the ovary, follicle, and follicular fluid. Secondly, a familiarity with the literature which relates metabolic parameters to IVF outcome is required (specifically follicular vascularisation and follicular fluid dissolved oxygen levels). Finally, a good understanding of the measurement of dissolved oxygen is required. This information is presented in this chapter in the form of a literature review.

In view of the required areas of understanding, this literature review covers a variety of topics. These are, general human reproduction (section 2.1), the IVF process (section 2.2), follicular fluid (section 2.3), the prediction of oocyte quality (section 2.4), and issues specific to the analysis of dissolved oxygen in follicular fluid (section 2.5).

2.1 Human reproduction

This section details some of the key concepts of general human reproduction common to both normal and assisted reproduction in the female.

2.1.1 The female reproductive tract

Figure 2.1 depicts the general structure of the female reproductive tract and the ovary. The ovaries are situated at one end of the fallopian tube(s) which extend down to the uterus. The ovaries lie on each side of the upper pelvic cavity against the back of the pelvic wall. Each ovary is approximately 3 cm long, 1.5 cm wide, and 1 cm thick, although size does vary (Sloane, 1985).

The ovary itself contains structures known as follicles in various stages of

development. Inside each follicle is an oocyte (egg). A mature follicle consists of granulosa cells, a fluid filled cavity, and an oocyte. Ovulation of such a follicle releases the oocyte into the fallopian tube. The remaining follicular cells form the progesterone secreting *corpus luteum*, which later recedes leaving behind scar tissue known as *corpus albicians* (Cohen, 1977). Follicles may regress and become atretic (degeneration of the follicle) at any stage of development.

2.1.2 Follicle development

Follicle development is initially controlled by hormones produced in the pituitary gland. The pituitary gland is often called the 'master gland' as it controls the function of the other glands of the body, and is itself controlled by the section of the brain just above it known as the hypothalamus. Although the pituitary gland produces many hormones, the two that are of most importance to the reproductive cycle are the follicle stimulating hormone (FSH), and the luteinising hormone (LH) (Stangel, 1979). FSH stimulates follicles to mature and grow, while LH causes mature follicles to rupture (ovulation). FSH and LH proceed to the ovary via the bloodstream, and upon arrival stimulate the ovary into the production of estrogen, which is responsible for controlling the development of the female reproductive system. The relationship between the pituitary gland and the ovaries is shown in Figure 2.2.

The process of follicle development is illustrated in Figure 2.3. Primordial germ cells become visible in the female embryo after only 3 weeks of development (Muller, 1996). Within eight to ten weeks of foetal development, the primordial germ cells undergo multiple mitotic divisions and differentiate into primordial follicles (Shostak, 1991). The primordial follicle contains a small primary oocyte that is about 30 μm in diameter. An oocyte is considered primary if it has not yet undergone the first meiotic division. The number of primordial follicles peaks at about 7 million, most of which will have perished by the 7th month of embryo development, leaving behind approximately one to two million. The primary oocyte is surrounded by a simple squamous of epithelium cells.

The Female Reproductive Tract
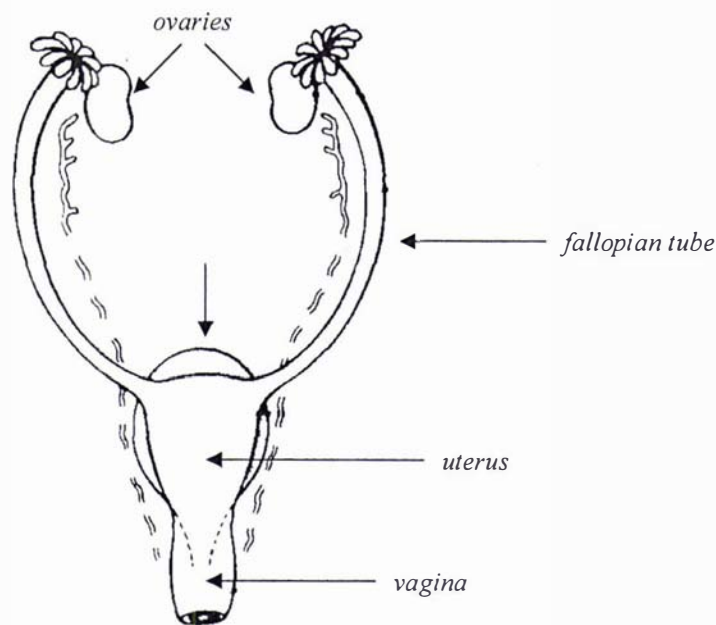
The Ovary
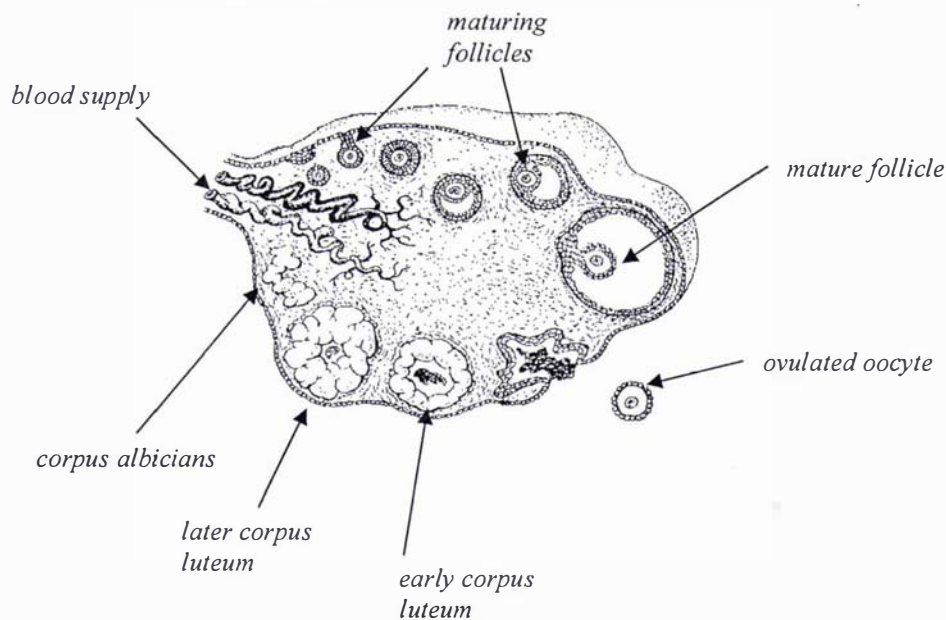
Figure 2.1   Structure of the female reproductive tract (taken from Findlay 1984) and the ovary (taken from Sloane 1985).

Even after the onset of puberty and the initiation of the ovarian cycle, 90% or more of the follicles remain primordial. These follicles serve as the source of growing follicles until the onset of menopause and the cessation of the ovarian cycle.

When puberty is reached only about 400,000 oocytes remain. At this time between 5 and 20 primordial follicles develop into primary follicles with each ovarian cycle. When the squamous cells surrounding the primordial follicle have thickened to cuboidal cells of one or more layers, the follicle is known as a pre-antral follicle (Peters & McNatty, 1980), and the squamous cells are known as granulosa cells. As still more follicular cells accumulate, and as the original simple epithelium is transformed into a multilayered cuboidal epithelium, the follicle can be considered a late pre-antral follicle. The loose connective tissue that encases the primary follicle is known as the theca. The thecal cells surrounding the follicle also differentiate into two layers: the theca interna and theca externa. As the primary follicle thickens, the zona pellucida (a layer of glycoproteins) forms between the oocyte and granulosa cells.

The pre-antral follicle enters a transition phase as small patches of fluid become evident among the granulosa cells. FSH is normally required for the formation of these cavities. During this stage intercellular contacts develop into intimate communicative connections. As the follicle grows, the fluid cavities fuse into a single antrum. The follicular fluid resembles blood serum, and is presumed to be derived from it. The follicle is now considered an antral follicle.

During a typical menstrual cycle FSH production will result in the maturation of several follicles. As the follicular cycle continues and ovulation approaches, the release of large amounts of estrogen by the leading follicle suppresses FSH and deprives smaller follicles of the stimulus for further growth. As a result this single leading follicle will generally become dominant. This follicle is characterised by an oocyte positioned eccentrically in the antrum. This follicle is known as a pre-ovulatory follicle. The oocyte and its surrounding granulosa cells now form a hillock, the cumulus oophorus, attached on one side to the follicular wall and projecting into the antrum (Mossman & Duke, 1973). The layer of cells immediately surrounding the oocyte is known as the corona radiata (Jones 1997). The oocyte has undergone the

first stage of meiosis (DNA replication) and completes the first meiotic division in response to the LH surge immediately prior to ovulation. It is during this stage of development that oocyte is aspirated for in vitro fertilisation in humans. The follicle has grown to a size of approximately 16-25 mm in diameter (McNatty, 1981).

The hypothalamus triggers the release of Gonadotrophin Releasing Hormone (GnRH), which in turn is responsible for the LH surge It is more the priming of estrogen on the cells which secrete LH that leads to the LH surge, since and LH surge can be elicited in women without hypothalamic function (i.e. no GnRH secretion) who are given regular and unvaried pulses of GnRH. The LH surge which results in the swelling and rupture of a mature pre-ovulatory follicle and the ejection of an oocyte. This is known as ovulation. Over the course of a lifetime, approximately 500 oocytes are ovulated. As a general rule, only one follicle reaches the status of a fully mature pre-ovulatory follicle per ovarian cycle (28-30 days). This status is reached after about 14 days.

Granulosa and theca cells remain in the ovary after ovulation and become the *corpus luteum* (yellow body). The *corpus luteum* gives its name to the luteinising hormone which causes its formation and sustains it (Jansen & DeCherney, 1998). The *corpus luteum* produces progesterone which upon reaching the tissue lining of the uterus causes it to change the structure of the lining such that it can provide sufficient nourishment should an egg be fertilised. The egg takes approximately five days to reach the uterus, providing it with sufficient time to develop its lining.

If fertilisation does not occur the corpus luteum has a life span of approximately 14 days for which it is sustained by LH. The *corpus luteum* then undergoes apoptosis and after several months becomes the *corpus albicans*, a white scar. Apoptosis is defined as disintegration of cells into membrane-bound particles that are then eliminated by phagocytosis or by shedding. Much of the area of an aged ovary is composed of *corpus albicans*.

If fertilisation/pregnancy does occur the corpus luteum is supported by the human chorionic gonadotropin (hCG). hCG mimics the action of LH, but has a longer duration of action. The corpus luteum continues to produce progesterone until the

placenta is formed. The *corpus luteum* also produces some estrogen.

2.2   The in-vitro fertilisation process

This section briefly details the key aspects of the in-vitro fertilisation process. The reader should refer to detailed general texts for a comprehensive review of this process (e.g. Jansen & DeCherney, 1998; Brinsden 2005).

In vitro fertilisation was the first of the assisted reproduction technologies (ART), and is still the most commonly used (McShane, 1997). The basic IVF procedure involves retrieval of oocytes from the woman, followed by insemination with prepared sperm under laboratory conditions, and the placement of the resulting embryos into the uterus.

There are currently many variations on the IVF technique available. The most commonly employed uses a precise sequence of fertility drugs, along with monitoring of ovarian response via blood estrogen levels and/or ultrasound. When oocyte readiness is confirmed, an injection of hCG is used to mimic the LH surge. hCG induces ovulation 38 hours after it is administered. Oocyte retrieval is therefore carried out approximately 36 hours after hCG dosage and before ovulation begins.

Oocyte pick-up is a relatively simple medical procedure, and is performed under anaesthetics or analgesics. The fluid in the follicle is removed via ultra-sound guided aspiration. The use of ovary stimulating fertility drugs allows an average of 10 oocytes to be obtained per procedure. Given normal semen parameters, around 70% of oocytes are expected to fertilise. The majority of fertilised oocytes will cleave (divide) forming embryos. Typically one to three embryos are transferred into the uterus. More embryos may be transferred in older women to compensate for their reduced chance of pregnancy.
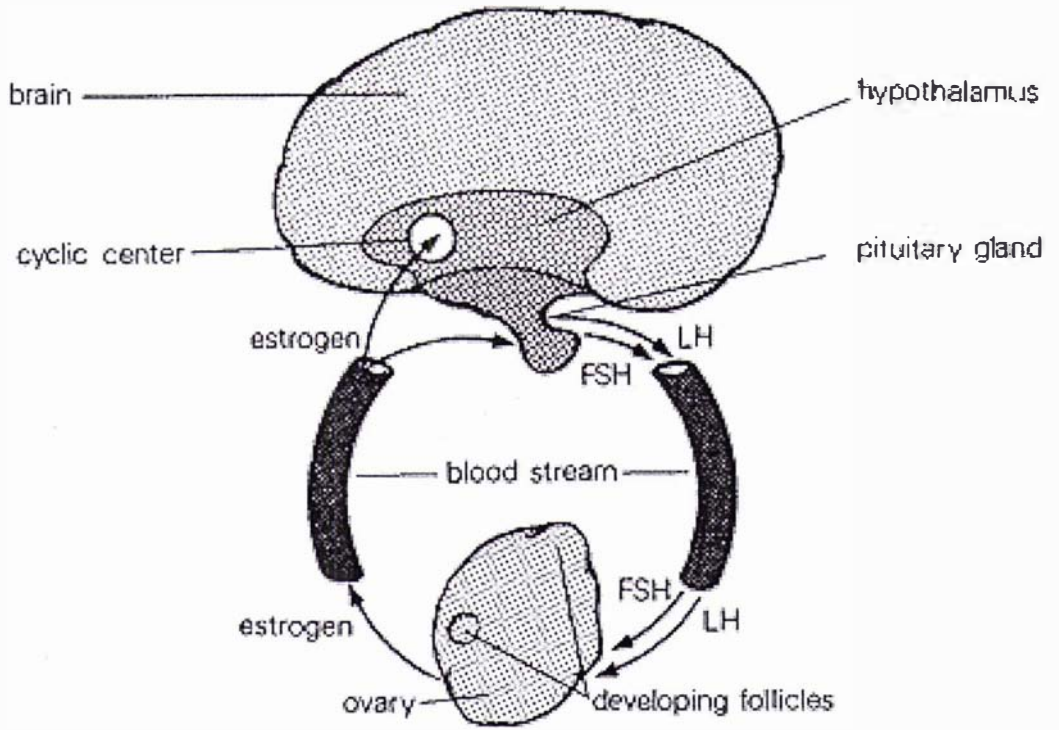
Figure 2.2   Relationship between the pituitary and the ovaries, indicating the circulation of hormones between the pituitary gland and the ovaries (taken from Stangel, 1979).
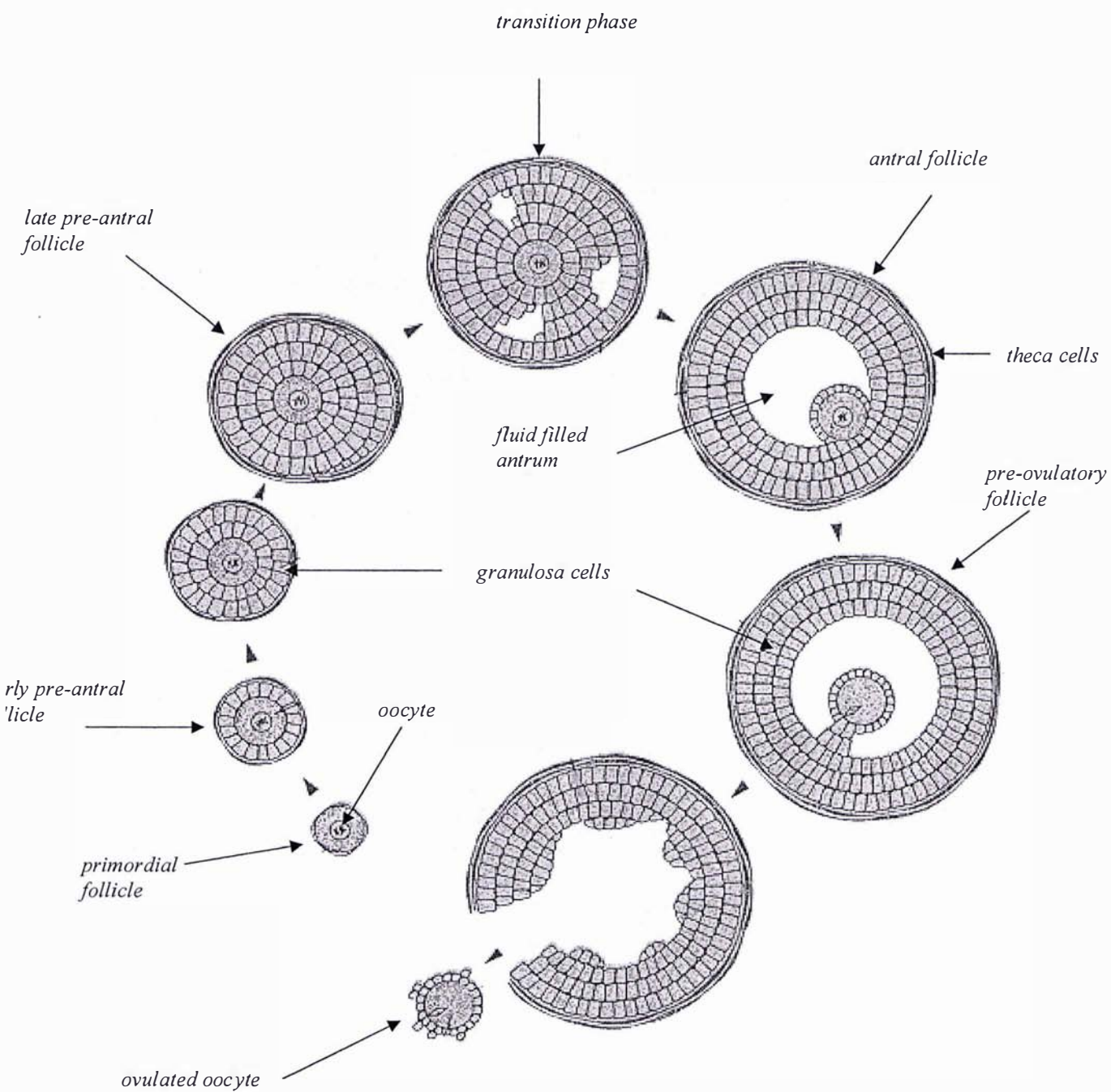
Figure 2.3   Follicle growth and development (taken from Shostak, 1991).

If more embryos are produced than are required for implantation the remainder are usually cryo-preserved and may be used if the initial procedure does not result in pregnancy.

Live birth rates after five cycles reduce with the increasing age of the women (Tan *et al.*, 1992), being 45% for ages 20-34, 29% for ages 35-39, and 14% for those 40 or older. The chance of conception after five cycles also declines with increasing age, being 54% for ages 20-34, 39% for ages 35-39, and 20% for those 40 or older. The chance of conception per cycle also decreases as more cycles of treatment are carried out.

A recent report by the Society of Assisted Reproductive Technology, has shown a continuing increase in success rates (deliveries per retrieval) for IVF (Zeitz *et al.*, 2002). The society reported on 58,937 cycles of IVF that were initiated in 1998 for which 20,241 resulted in deliveries (34%).

The fertilisation rate has also been shown to be significantly correlated with the percentage of normal semen morphology in a fresh semen sample, as well as to the motility (especially forward propulsion) of the sperm used for insemination (Duncan *et al.*, 1993). Traditionally, poor semen parameters limited the fertilisation rates for IVF, but the development of intracytoplasmic sperm injection (ICSI), has allowed normal fertilisation rates to be achieved for those with reduced semen parameters (Nagy et al., 1995). Many IVF programs use ICSI for all couples, not just those with reduced semen parameters. ICSI involves sperm microinjection, in which one or more sperm are injected through the zona pellucida, across the perivitelline space, through the vitelline membrane (the egg cell's membrane), and into the cytoplasm of the oocyte itself (Jansen & DeCherney, 1998). One disadvantage of ICSI is that the oocyte can sometimes be destroyed by this manipulation. The rate of birth defects does not seem to be affected.

Another micro-manipulation technique that has been used to successfully increase pregnancy rates is assisted hatching (Schoolcraft *et al.*, 1994). Using this technique the zona pellucida is breached chemically, mechanically, or by other means such as

12

using the energy from a laser. This allows the 'escape' of the embryo at the time of implantation. Many cultured embryos seem to have unusually thick and/or hardened zona pellucida. This seems to be a particularly valuable technique for older women or those that have been unsuccessful with multiple cycles.

IVF is a procedure described by many couples as an emotional rollercoaster ride. For this reason, as well as economic, most couples do not attempt more than three cycles of IVF.

2.2.1 The steps of the IVF procedure

The following is a description of the IVF procedure employed by Fertility Associates Inc., Hamilton, New Zealand (August 2002). The basic steps of the procedure are:

1. Use of drugs to stimulate the ovaries
2. Monitoring ovary stimulation and timing of oocyte collection
3. Aspiration of follicles for collection of oocytes
4. Fertilisation of oocytes and harvesting embryos in the laboratory
5. Transfer of embryos to the uterus
6. Use of drugs to increase receptiveness of uterus to embryos

2.2.1.1 Use of drugs to stimulate ovaries

Stimulation of the ovaries is best achieved by the 'downward regulation' or 'long course' approach. This approach seems to work best for the majority of women. Other approaches include the 'short course' and 'natural cycle'.

The 'long course' of treatment starts with the injections of a GnRH (gonadotropin stimulating hormone) agonist. GnRH agonist is administered on day 21 of the menstrual cycle. This initially stimulates the pituitary gland to produce FSH and LH, but, after a few days the pituitary gland becomes over stimulated, and stops producing FSH and LH. The pituitary gland is shut down in this manner to stop it from interfering with the artificial administration of FSH and LH. This allows the

13

suppression of the LH surge, which normally results in ovulation, which is not wanted in IVF treatment. The suppression of the production of FSH and LH is checked via a blood test around two weeks later.

Once the down regulation of the pituitary gland has been confirmed, injections of FSH begin. The purpose of FSH injections is to stimulate 6 to 12 follicles to grow to maturity. FSH is administered for 9 to 15 days, and during this time those follicles that have been appropriately stimulated will grow from 5 to 20 mm in diameter. Follicle growth is monitored by ultrasound scans, as well as by blood tests for estradiol which is the main hormone produced by the follicle cells.

When the follicles become sufficiently large an injection of hCG is administered. This triggers the final stage of oocyte development, and prepares the follicle for ovulation (aspiration will occur before ovulation can happen).

The 'short course' approach is employed for those women who do not respond well to the 'long course' approach. It basically involves larger amounts of drugs.

A 'natural cycle' may be employed by those who do not wish to use drugs, or those who have not responded well to drug treatments in the past. The major drawback of this approach is that only one follicle/oocyte develops. The chance of developing one or two oocytes is increased by the use of clomiphene citrate tablets as a mild way of stimulating the ovaries. Pregnancy rates using this method are significantly reduced as there is not the opportunity to be selective as to which embryos are replaced.

2.2.1.2 Collection of eggs from the ovaries

Following the injection of hCG the oocytes need to be aspirated from the follicles approximately 36 hours later. If aspiration is attempted earlier, recovery rates will be low as the oocytes are still attached to the wall of the follicle. If much later, ovulation may have already occurred leading to the release of the oocytes into the fallopian tube.

Initially oocyte collection was performed by laparoscopic methods which involved accessing the ovaries via a surgical incision through the abdomen. This method has a number of disadvantages, such as the requirement for general anaesthesia and a fully equipped surgical theatre. Ultrasound directed techniques can be performed in the clinical setting and do not require the patient to be unconscious. The overwhelming majority of ultrasound directed procedures are now carried out using the trans-vaginal needle approach, along with transvaginal ultrasonography.

The trans-vaginal approach using a vaginal ultrasound transducer was first described by Wikland *et al.* (1985). In this procedure the needle is introduced through the lateral fornix of the vagina and into the ovary under ultrasound guidance using a vaginal transducer and a needle guide.

The patient is placed in the lithotomy position (legs apart, secured by stirrups), in which the operator and possibly the assistant sit between her legs.

The vaginal transducer is then covered with a latex condom (spermicide free), and inserted into the vagina. The ovaries are located 2-5 cm from the top of the vagina, and as a result are reached by piercing the vaginal wall. The distance from the end of the transducer to the centre of the target follicle is estimated so that the needle can be passed down the guide an appropriate distance to penetrate through the vaginal wall into the follicle (Figure 2.4).

When the needle tip is visible and positioned appropriately, suction is applied using a syringe or vacuum pump, and the follicular fluid is aspirated. The aspirated follicular fluid is most commonly between 2-6 ml in volume. The follicular fluid often becomes contaminated with blood, and as a result varies in colour from light yellow/brown, to the deep red colour of blood. The aspirate is analysed under microscope for oocyte identification. If an oocyte is not present the follicle is often flushed in the hope that the oocyte may yet be recovered either from the dead space between the needle tip and the collection tube or in the flushing fluid itself. Flushing involves the use of a double channel needle which is more difficult to use. Although it appears that as many as 20% more oocytes can be obtained via follicular flushing, the resulting oocytes

15

have reduced fertilisation rates (Waterstone & Parsons, 1992). Another study conducted with a large sample size concluded that there was no significant difference in number of oocytes collected , number of embryos created, and pregnancy rates regardless of whether flushing was used or not (Knight *et al.*, 2001). It seems to be unclear as to what is more important, keeping the procedure short, relatively painless, safe, and uncomplicated, or attempting to maximise the chance of pregnancy.

After a follicle has been aspirated, the needle is then either advanced through the follicle wall into an adjacent follicle, or withdrawn into the ovarian stroma and redirected into another follicle. Usually the procedure will be repeated until all the follicles with diameter approximately greater than 10 mm have been aspirated (Tan *et al.*, 1990). The same process is also carried out in the opposite ovary with the vaginal wall needing to be punctured again. The procedure can normally be completed with the vaginal wall having been punctured only twice, once on each side. The most common problem associated with this procedure is vaginal bleeding.

Figures 2.5 (a) and (b) show the aspiration setup for both the single and double lumen needles (SwedMed International). Aspirating pressure is most often controlled by a foot pump at approximately -100mmHg. Needles are made from stainless steel, and tubing is constructed of Teflon. These kits are sterile and intended for single use only.

After aspiration, the test tube is passed to an embryologist who inspects the fluid under the microscope, looking for the oocyte. Oocytes are recovered from approximately 80% of the follicles aspirated.

Prior to follicle aspiration women are provided with narcotic pain relief, and during the actual procedure a short acting intravenous drug is administered. The most painful part of the procedure is usually the first time the needle pierces the vaginal wall.

2.2.1.3 Fertilisation and embryo development

After the oocytes have been collected and located they are placed in culture medium, and incubated at 37 °C.

16

Bladder in front of uterus
Bowel behind uterus
Fallopian tube
Uterus
Ovary with several follicles
Egg collection needle
Vagina
Ultrasound probe
Test tube to collect eggs
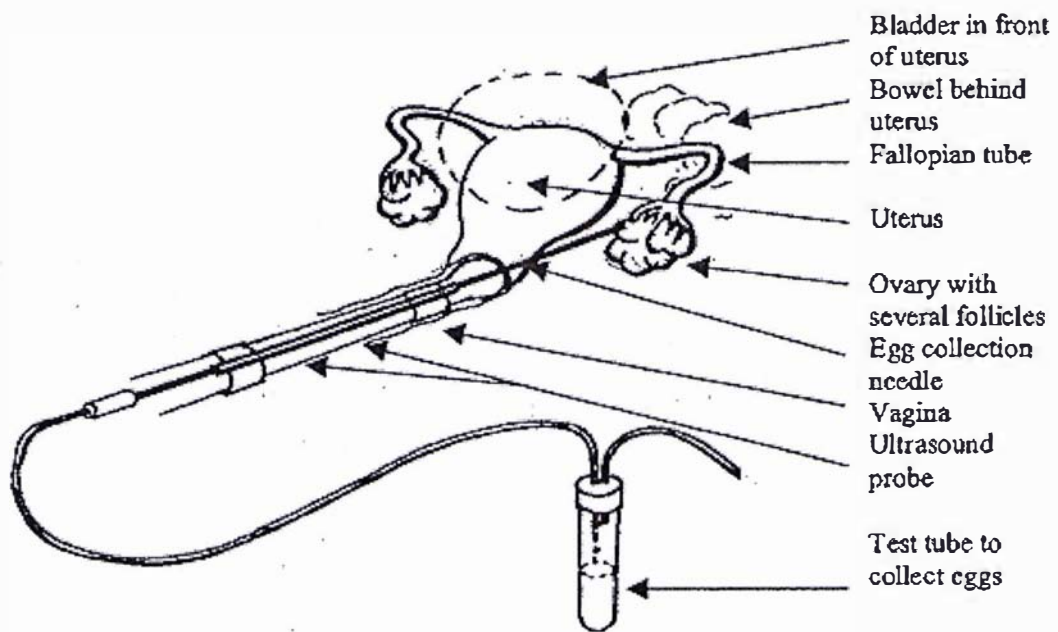
Figure 2.4   IVF aspiration for oocyte collection using ultrasound guidance (supplied by Fertility Associates Inc.).

Sperm which have been isolated from semen are added to each dish. About 50,000 sperm are added to each dish. If ICSI is used the eggs are placed in a shallow dish in micro-droplets of culture medium under oil, arranged around a central drop containing sperm. Sperm are captured one at a time using a fine glass needle. Once a sperm is captured it is injected into the egg.

Approximately 18 hours later the oocytes are examined to see if fertilisation has been successful and an embryo has developed. If the procedure has been successful the embryos will continue to divide. Around the fifth day a fluid filled cavity forms in the middle of the cells. Also visible at this stage is an outer layer of cells which will become the placenta, and an inner cell mass that will become the foetus. The embryo at this stage is called a blastocyst. During the next day or so, the shell that encases the embryo/blastocyst (the zona pellucida) thins, the embryo expands, the zona pellucida splits, and the blastocyst hatches. Such embryo development also occurs *in vivo* in a normal pregnancy.

Embryos may be transferred on day 2 or 3 after oocyte retrieval, or alternatively moved to a different culture medium for blastocyst culture. Embryos progressing to blastocysts are replaced on day 5 or 6.

2.2.1.4 Transfer of embryos to the uterus

The embryologist selects the appropriate oocytes for transfer. Except in older women , it is common practice to transfer only 1 to 2 embryos so that the chance of a multiple pregnancy is not too great.

Compared to oocyte aspiration, embryo transfer is quite a simple and painless procedure. The embryos are loaded into a thin tube along with a small amount of culture medium. A speculum is placed in the vagina and any blood or mucus present is removed. The catheter is passed through the cervix into the uterus, usually using ultrasound guidance. The procedure can become complicated depending on the size and angle of the uterus. However, having a full bladder helps to flatten the uterus and makes the transfer simpler.

2.2.1.5 Use of drugs to increase receptiveness of uterus to embryos

Progesterone is the hormone that prepares the uterus for an embryo and sustains it in the event of fertilisation. Progesterone is produced by the *corpus luteum*, which is sustained by LH, and then hCG in the event of pregnancy. As a result hCG is administered after embryo transfer to increase the receptiveness of the uterus. Alternatively progesterone can be administered directly as vaginal pessaries.

2.3   Follicular fluid

Follicular fluid is the fluid that accumulates in the extracellular spaces inside ovarian follicles (McNatty, 1978). It is first formed between granulosa cells during the early stages of follicular growth. Upon enlargement of the follicle these pockets of fluid coalesce forming a large spherical cavity of liquid known as the follicular antrum. This antrum partially surrounds the oocyte and its associated epithelial cells, which will later form cumulus oophorus cells. As more fluid accumulates, the oocyte and epithelial cells become displaced from their central position.

The majority of the volume of the antral follicle (tertiary follicle) is follicular fluid. The volume of follicular fluid in the average mature follicle of women is 4 ml (this volume varies significantly among different species, being around 65 ml in mares).

Follicular fluid contains many of the components found in blood plasma, as well as secretory products from follicle cells. The fluid filled antrum allows cells in an avascular region to be exposed to an environment that is different to that of serum. Changes in the physical properties and steroid compositions of follicular fluid facilitate steroidogenesis, oocyte maturation, ovulation, and the transport of oocytes to the uterus via the oviduct. As well as this, follicular fluid aids the subsequent development of the *corpus luteum*.

(a)
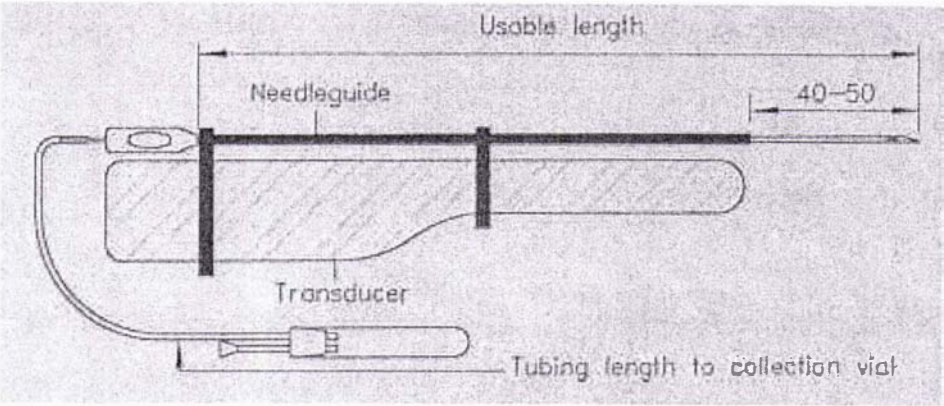
(b)
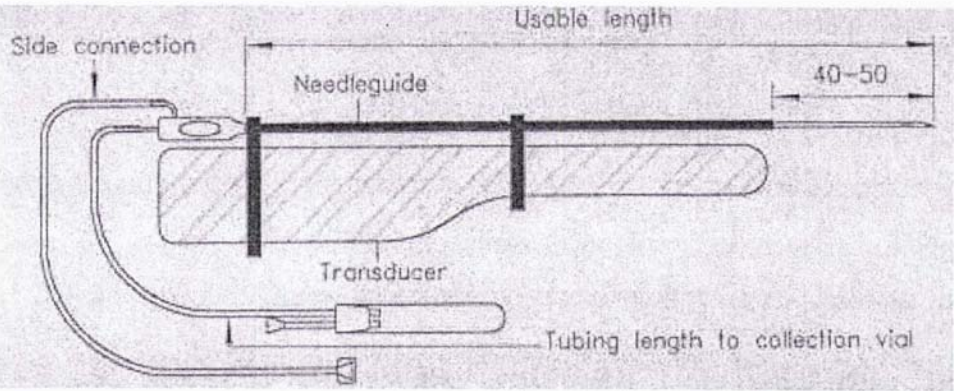
Figure 2.5   Typical IVF aspiration kits for both single(a) and double lumen needles(b) (SwedMed International).

2.3.1 Physical properties and composition

Follicular fluid is a slightly viscous solution with human follicular fluid having a viscosity of approximately 1.8 times that of water (Luck *et al.*, 2000). Its colour varies from colourless to intense yellow in ovaries that have been excised. Fluid that is aspirated directly from the follicle *in vivo* is generally straw coloured. The wider variation in the colour of excised ovaries is likely due to the effects of anoxia (McNatty, 1978).

2.3.2 pH and oxygen partial pressure (pO_2)

Changes in O_2 concentrations late in the follicular development cycle are believed to be critical to oocyte maturation. It has been suggested that the mammalian oocyte requires a relatively anaerobic environment in the follicular fluid in the later stages of development (Gull *et al.*, 1999; Gwatkin & Haidri, 1973). However it is possible that the low oxygen concentration in the follicular fluid at the later development stages could simply reflect a high level of oxygen consumption in what may be a very aerobic process. That is, if oxygen is being significantly utilised by the follicle (granulosa cells and oocyte) at a rate similar to which it is supplied, the pO_2 of the follicular fluid may be low.

Figure 2.6 compares the mean dissolved oxygen levels reported in follicular fluid by various studies. Immediately apparent from Figure 2.6 is the large variability in the reported values. Such great variability would tend to suggest that either these measurements come from different populations, or that there have been significant and variable degrees of analytical error in at least some of these studies. Taken at face value the dissolved oxygen levels shown in Figure 2.6 would not appear to support the theory that the oocyte requires a relatively anaerobic environment, with dissolved oxygen levels quite high and comparable with blood. In fact the studies of Imoedemhe *et al.* (1993) and Huey *et al.* (1999) report dissolved oxygen levels higher than that in arterial blood. Such high oxygen levels could suggest that there may be some sort of oxygen production and/or active transport in the follicle. A more likely conclusion

would be that these studies included some large analytical error, perhaps due to contamination with air (21 vol% oxygen).

The studies of Shalgi *et al.* (1972) and Fraser *et al.* (1973) obtained follicular fluid samples from patients undergoing hysterectomy. The remainder of the studies were conducted in an IVF setting, and this is one possible reason for the observed variability. Further explanation of variability may be found in the different fluid sampling methods used. The hysterectomy procedure allowed Shalgi *et al.* (1972) and Fraser *et al.* (1973) access to follicles from which fluid was directly withdrawn. The IVF aspiration process does not afford such direct access to follicles. If fluid is simply aspirated into the collection tube it may contact with air possibly causing significant changes in dissolved oxygen levels. To prevent this Imoedemhe *et al.* (1993) aspirated follicular fluid under paraffin oil. This may still result in changes in oxygen levels due to equilibration between the oxygen in the contacting follicular fluid and paraffin phases, as well as the sample tube. Arain *et al.* (2005) have shown that in liquid filled polystyrene microplates covered with paraffin oil significant oxygen transport can occur through both the polystyrene walls and the paraffin covering (the IVF collection vial is made of polystyrene). Fischer *et al.* (1992) attempted to avoid gas liquid contamination by obtaining a capillary sample from the Teflon tubing which leads to the collection tube. The remaining studies did not indicate any fluid sampling measures to prevent gas contamination. The different approaches to fluid sampling adopted by these authors may be a contributor to the observed variability.

Furthermore, the methods used to prevent/control blood contamination were also variable between studies. Shalgi *et al.* (1972) and Fraser *et al.* (1973) were able to avoid blood contamination due to the direct follicle access allowed by the hysterectomy procedure. Imoedemhe *et al.* (1993), and Fischer *et al.* (1992) did not state any method of blood contamination control, whilst Huey *et al.* (1999) accepted slightly amber samples. Blood contains large amounts of oxygen. Therefore blood contamination may lead to increased oxygen levels in follicular fluid. Once again the different measures taken to control blood contamination may be a source of the observed variability in reported dissolved oxygen levels in follicular fluid.

It seems that a fundamental understanding of oxygen transport in the human ovary/follicle is lacking. This situation may have been partly confused by the large variation in reported dissolved oxygen levels in follicular fluid.

Table 2.1 lists the values of pH reported by the same studies described above and in Figure 2.6. The pH in follicular fluid is certainly less variable than pO_2. The reported means range between 7.27 and 7.35 pH units. In human blood, pH varies from approximately 7.35 to 7.40 pH units, and from 7.30 to 7.50 pH units in human plasma (Fournier, 1998). The pH of human follicular fluid is therefore very similar to both blood and plasma. It appears to be slightly lower than blood. Dissolved carbon dioxide is probably the major determinant of follicular fluid pH. Non-volatile fatty acids also contribute.

2.3.3 Electrolytes

The concentrations of sodium and potassium in follicular fluid are important as they largely determine the osmotic pressure of the fluid (Edwards, 1974). The osmolality, sodium concentration, and potassium concentration in human follicular fluid are all comparable with human plasma (Edwards, 1974; Shalgi *et al.,* 1972). This is not surprising given that follicular fluid is presumed to be a derivative of plasma.

2.3.4 Glucose and organic acids

The concentrations of these compounds will vary according to the metabolic state of the fluid and the surrounding cells. Glucose is the primary substrate for cellular energy production, and the metabolism of glucose and its products is of considerable interest (e.g. Gregory& Leese, 1996; Hashimoto *et al.,* 2000; Sugiura *et al.,* 2005). If oxygen levels in follicular fluid are low, lactic acid can be expected to occur in follicular fluid as a result of anaerobic glycolysis by the surrounding tissues. A mean lactate concentration of 6.12 mM was observed by Leese & Lenton (1990); associated mean values of 0.26 and 3.20 mM were observed for pyruvate and glucose respectively. Typical levels of lactate in human plasma are approximately 1.2 mM

(Fournier, 1998). This level is lower than that found in follicular fluid and suggests that some anaerobic glycolysis has indeed taken place.

2.3.5 Proteins

The total protein concentration in human follicular fluid has been reported to vary between 53% to 98% that of plasma (Perloff *et al.,* 1955; Kiekhofer *et al.,* 1962; Manarang-Pangan & Menge, 1971; Shalgi *et al.,* 1972b) . Shalgi *et al.* (1973) show that the reduction in protein content is due to the cellular layers surrounding the antral fluid blocking the passage of high molecular weight proteins.

2.4   Prediction of oocyte quality

This project has been developed from the hypothesis that follicular fluid is a useful predictor of oocyte quality. Knowing the quality of an oocyte allows for use of the highest quality embryos, all other parameters being equal. If the quality of an embryo can be in some way quantified it is reasonable to expect that pregnancy rates may be increased, or at least uncompromised, while the chance of multiple gestations could be significantly reduced.

Attempting to predict oocyte and/or embryo quality is nothing new. Researchers in the field of assisted reproduction have investigated and suggested a wide variety of factors that may be useful in the prediction of oocyte/embryo quality.

Many studies into the improvement of the various success rates of IVF have focused on improving such things as culture medium. However studies have shown that many oocytes are already compromised at retrieval due to inherent biochemical, cellular or genetic defects, from which no culture medium or other system can rescue them (Van Blerkom, 1994). In light of this, prediction of oocyte quality becomes particularly important, as it may offer a way, even if indirect, of recognising such compromised oocytes at the aspiration stage.
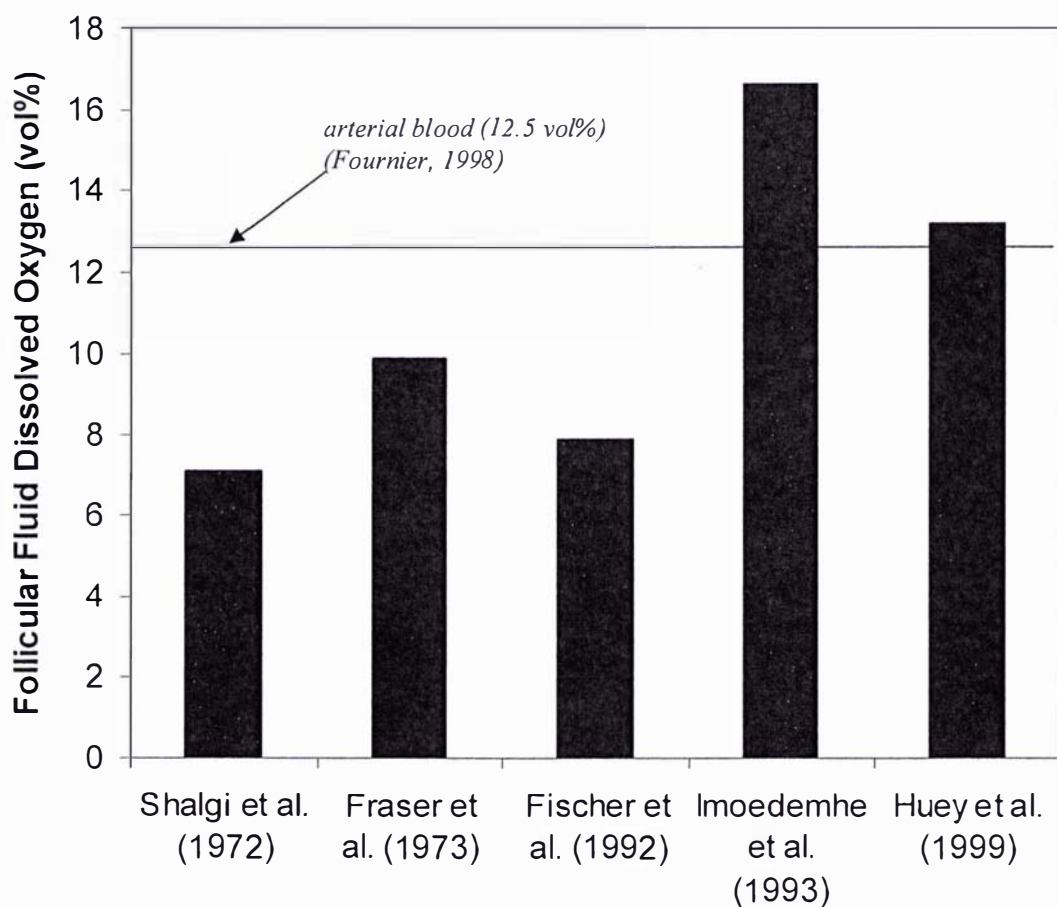
Figure 2.6   Comparison of reported values of dissolved oxygen levels in follicular fluid. Note that the study of Van Blerkom *et al.* (1997) which related oxygen levels to oocyte quality (see 2.4.1) did not report mean oxygen levels in follicular fluid and therefore was not considered in this section.

	pH	SD	n
Shalgi *et al.* (1972)	7.27	0.01	33
Fraser *et al.* (1973)	7.32	0.06	12
Fischer *et al.* (1992)	7.33	0.07	20
Imoedemhe *et al.* (1993)	7.3	0.2	107
Huey *et al.* (1999)	7.35	0.04	80

Table 2.1   Comparison of reported values of the pH of human follicular fluid.

2.4.1 Oxygen concentration in follicular fluid as a predictor of oocyte quality

The findings of Van Blerkom *et al.* (1997) from analysis of more than one thousand follicles indicate that the percentage of dissolved oxygen in follicular fluid measured at the time of ovum retrieval is associated with the developmental normality of the oocyte and with differences in follicular biochemistry. In this study follicles of similar volume and size (18-21 mm) were aspirated and the dissolved oxygen measured. The percentage of dissolved oxygen in these follicles ranged from less than 1% to approximately 5.5%. Oxygen content is seemingly unrelated to the frequency of meiotic maturation, fertilization, and cleavage. However, most oocytes with cytoplasmic defects and high frequencies of chromosomal and spindle disorders originate from severely hypoxic follicles, as do cleavage stage embryos with multinucleated blastomeres. Initial findings indicate that oocytes from follicles with dissolved oxygen contents below approximately 1.5% have low ATP contents (Van Blerkom *et al.,* 1995), and an acidic intracellular pH (Van Blerkom, 1996) that may be associated with abnormalities in spindle microtubules. Embryos derived from follicles with oxygen contents at or above 3% were more likely to implant than those derived from severely hypoxic follicles (Van Blerkom *et al.,* 1997).

2.4.2 Perifollicular blood flow and oocyte quality

Doppler ultrasonography provides an assessment of the level of vascularisation surrounding the follicle and hence the degree of perifollicular blood flow. A variety of studies have demonstrated a link between oocyte quality and/or pregnancy rates and the degree of follicular vascularisation (Kim *et al.,* 2004; Bhal *et al.,* 1999; Van Blerkom *et al.,* 1997; Huey *et al.,* 1999; Chui *et al.,* 1997).

The most comprehensive was reported by Bhal *et al.* (1999). The vascularisation surrounding the follicles was graded in 200 treatment cycles. Grading was based on the percentage of the follicular circumference that was surrounded by vascularisation, and was broken into 4 grades: <25%, $\geq$25 to <50%, $\geq$50 to <75%, and $\geq$75%. Results showed that no clinical pregnancies resulted from the embryos derived from

oocytes whose follicles had less than 25% vascularisation. Pregnancy rates were observed in all other vascularisation ranges with the rates increasing with higher vascularisation.

Using an almost identical grading system (<25%, 26 to 50%, 51 to 75%, and 76 to 100%), Chui *et al.* (1997) found that pregnancies only occurred in those patients whose embryos came from follicles graded 51% or greater. Live births resulted only from embryos derived from follicles with greater than 76% vascularisation.

Studies have also shown a correlation between follicular fluid dissolved oxygen content and the degree of vascularisation (Huey *et al.*, 1999; Van Blerkom *et al.*, 1997). Typically follicles with relatively low, moderate, and high vascularisation are associated with follicular fluids of relatively low, moderate, and high dissolved oxygen levels respectively (Van Blerkom *et al.*, 1997; Van Blerkom, 2000). Oocytes derived from follicles that exhibited perifollicular blood flow indices consistent with dissolved oxygen levels of at least 3% were associated with an increase in pregnancy rates (Van Blerkom & Henry, 1992).

Increased pregnancy rates achieved through the detection of well vascularised follicles through the use of Doppler ultrasonography have also been accompanied by an undesirable increase in the frequency of multiple gestations (Chui *et al.*, 1997; Nargund *et al.*, 1996; Van Blerkom *et al.*, 1997). Although Doppler ultrasonography appears to be a potentially useful tool its biggest disadvantage is that it is cumbersome to use (Van Blerkom, 1997).

2.4.3 Other predictive measures

Angiogenic factors are those associated with the formation of new blood vessels. In follicular fluid the relationship between vascular endothelial growth factor (VEGF) and IVF outcome has been investigated (Barroso *et al.*, 1999; Friedman *et al.*, 1998; Malamitsi-Puchner *et al.*, 2001). It has been suggested that VEGF is associated with follicles with high vascularisation and oxygenation, resulting in superior oocytes (Van Blerkom *et al.*, 1997). In contrast to this, studies have demonstrated that high levels

of VEGF in the follicular fluid can be a marker of follicular hypoxia (Barroso *et al.,* 1999; Friedman *et al.,* 1998; Malamitsi-Puchner *et al.,* 2001), suboptimal embryo development (Barroso *et al.,* 1999), and reduced oocyte fertilisation (Malamitsi-Puchner *et al.,* 2001). It is possible that high VEGF levels represent an attempt by the follicle to overcome hypoxia by increasing the formation of blood vessels. If this process is often unsuccessful this may be a potential reason for the counterintuitive finding that follicles with high levels of VEGF produce oocytes with reduced developmental potential. Although promising, it has been shown that VEGF is a poorer predictor of IVF outcome then measures of follicular blood flow.

The simple measures of follicle size and fluid volume have been related to oocyte quality. Simonetti *el al.* (1985) found that mature oocytes were associated with larger follicles with an average fluid volume of 2.7 ml. It was also suggested that these oocytes were of higher quality. Quigley *et al.* (1982) found that follicles of >20mm in diameter produced oocytes which had greater fertilisation rates. Similar results have been reported in cattle which show that oocytes originating from larger follicles had greater developmental competence than those obtained from smaller follicles (Lequarre *et al.,* 2001).

It has been reported that ATP production by human oocytes can vary greatly from patient to patient (Van Blerkom *et al.,* 1995; Magnusson, *et al.,* 1986). Very low levels of ATP do not prevent meiotic maturation or cleavage. However these oocytes appear to have a very low developmental ability (Van Blerkom *et al.,* 1995).

Oxidative stress in follicular fluid relates to the content of reactive oxygen species (ROS) and the total antioxidant capacity (TAC). Although the role of oxidative stress in reproduction is not fully understood, early results suggest that oxidative stress in the follicular environment may be a potentially useful marker for the prediction of IVF outcome (Oyawoye *et al.,* 2003; Attaran *et al.,* 2000; Weiner-Megnazi *et al.,* 2004; Pasqualotto *et al.,* 2004; Agarwal *et al.,* 2005).

2.5 Issues specific to the analysis of dissolved oxygen in follicular fluid

This section attempts to anticipate some of the possible problems that may arise in relation to measuring the dissolved oxygen levels in follicular fluid.

2.5.1 Blood contamination

It is very common, particularly in transvaginal follicular aspiration (as opposed to laparoscopic), for blood contamination to be present. Blood contamination may be present to a significant degree in approximately half of the fluid aspirated transvaginally (Huyser *et al.,* 1992). Typically blood contamination is less than 1 ml, but can be 2 ml or greater.

Blood contamination may alter the oxygen content and pH of follicular fluid, but it does not appear to have been considered by a large number of researchers investigating follicular fluid composition (Lee *et al.,* 1987). Contamination with blood also effects the concentrations of other species such as Na^+ and K^+. The impact of blood contamination on the dissolved oxygen levels of follicular fluid needs to be determined as part of this work.

2.5.2 Fouling

Fouling of pH and dissolved oxygen sensors in contact with blood occurs initially by protein adsorption and then thrombus formation (Meyerhoff, 1993). As the clotting proceeds, highly metabolic platelet cells adhere and are subsequently entrapped in the thrombus, and can coat the surface of the sensor, along with other respiring blood cells (e.g. white blood cells). These living cells consume oxygen, and liberate carbon dioxide and produce local pH and pO_2 levels that are different to that of the bulk fluid.

Generally clotting is not associated with follicular fluid. Clotting would certainly inhibit the transport of the oocyte down the fallopian tube after ovulation. As a result

thrombus formation should not be a problem except in blood contaminated samples where it may occur depending on the degree of contamination.

The degradation of sensor response in blood is quite a slow process. The responses of pH and pO_2 sensors seem to start degrading after approximately two hours of continuous contact with blood, and become severely compromised after four hours (Meyerhoff, 1993). It is anticipated that any sensor surface would only be in contact with follicular fluid for less than 10 seconds approximately 10 times per IVF pick-up. After the procedure is complete the sensors could be cleaned, sterilized, and the membrane of the oxygen sensor may be replaced. It is therefore very unlikely that fouling will represent a problem in the IVF setting. This will be true even if the sensor was to be placed in the IVF tubing line throughout the duration of the procedure (generally less than 20 min.)

2.5.3 Anaesthetic interference

The anaesthetic agents nitrous oxide (N_2O) and halothane ($CF_3CHClBr$), have been found to be electrochemically active, in aqueous electrolytes in contact with Clark dissolved oxygen sensors at polarizing voltages commonly employed for their use (Hahn, 1998). The currents generated by these agents are additive to that produced by oxygen, and result in reported readings being higher than they actually are.

No other inhalational anaesthetics have been found to be electro-active at the polarizing voltages employed for aqueous solutions. The reduction of these species is dependent both on the polarizing voltage employed and the type of material used for the cathode.

These anaesthetic agents are used by some IVF clinics. Transport of these molecules from blood to follicular fluid would need to be significant if this was to interfere in the determination of pO_2 in follicular fluid. Studies investigating the levels of oxygen in follicular fluid have used these anaesthetic agents seemingly with little effect on the magnitude of pO_2 (Fraser et al., 1973). It may be sufficient to assume at this stage that such interference is unlikely to be a factor in follicular fluid, and if it does occur it

31

will most likely be insignificant.

This issue is of course complicated by the issue of blood contamination. When this occurs, blood contamination is typically 1-2 ml of a 4 ml follicular fluid sample. As a result, interference by these anaesthetics could cause problems in this measurement system. It could have affected the findings of researchers measuring oxygen concentration in follicular fluid in the past where blood contamination was not well controlled. In fact one such study by Huey *et al.* (1999) reported oxygen concentrations significantly above those normally measured. This may be due to anaesthetic interference, although the agents used were not stated in the study. The magnitude of this problem may well depend on how commonly these anaesthetics are employed in IVF clinics.

2.5.4 Oxygen uptake post aspiration

Oxygen uptake by follicular fluid after it has been aspirated may be a source of error in the measured pO_2. Upon aspiration, the fluid travels a distance down Teflon tubing. Any oxygen present in the tubing wall may be stripped out by the fluid and result in an increase in dissolved oxygen content. Stripped oxygen may be re-supplied by diffusion from the outside atmosphere through the Teflon tubing. This, however, is likely to be a very slow process.

Oxygen may also enter the fluid through contact with the air in the collection tube. Delays in measurement may also result in the fluid oxygen levels changing through equilibration with the surrounding environment. The importance of such issues has not been discussed in the literature and needs to be determined as part of this work.

2.5.5 Oocyte shear

The sensing device must not damage or influence the oocyte being aspirated. The oocyte also needs to be a sufficient distance from the device such that it is not exposed in any way to the polarizing voltage applied to the cathode. These requirements could result in the oocyte experiencing shear damage or damage due

to exposure to an electric field, both of which may compromise its developmental capacity. These issues could be resolved by employing an oocyte filter which allows only a small portion of fluid to pass by the sensor after it has passed through a filter sufficiently large to reject the oocyte. The membrane of the cathode may also provide sufficient insulation to protect the oocyte from exposure to the electric field.

2.5.6 Sterilization

Many pH and dissolved oxygen sensors can be sterilized by way of heat, chemicals or radiation. The issue here is probably how conveniently such a regime fits in with the methods and equipment already available and in use in IVF clinics.

2.6 Conclusions and recommendations

Many couples have difficulty conceiving a child, and some are incapable of doing so for a variety of reasons. *In-vitro* fertilisation is a procedure that can allow such couples to have children.

Improvement in the success rates of assisted reproduction is desirable for a number of reasons. Most importantly such an improvement may reduce the number of cycles that need to be performed before a live birth results. This in turn reduces the resources required, and hence decreases the financial strain on both the individuals concerned and the taxpayer. Furthermore, the heavy emotional stress placed on couples undergoing the treatment would be less, due to the reduced number of treatment cycles. The number of undesirable multiple gestations could also be decreased as a result of the reduced need to implant multiple embryos.

It is hardly surprising then that a large amount of research has focused on improving the success rates of *in-vitro* fertilisation. Much of this research has focused on optimising culture conditions, and developing improved media formulations.

More recently, researchers have addressed the fact that a certain portion of oocytes

contain biological defects, and are incapable of progressing successfully through an IVF cycle and of giving rise to a successful pregnancy or birth. As a result, even under optimised conditions, the success rates of the procedure are limited.

Many investigators have now focused their resources on developing a method of predicting oocyte and/or embryo quality. If such predictions could be made, those oocytes with limited developmental capacity could be eliminated from the procedure.

Two promising predictors are the degree of follicle vascularisation and the dissolved oxygen levels in follicular fluid. A correlation between these measurements has been demonstrated, but does not appear to be fully understood. Mathematical modelling of oxygen diffusion in the follicle could assist in obtaining this understanding, and this is addressed in Chapters 3 and 4.

The reported dissolved oxygen levels in human follicular fluid are highly variable, and there seems to be no clarity in the literature as to what dissolved oxygen levels in follicular fluid might actually mean. This lack of information is also addressed in Chapters 3 and 4 through the mathematical modelling of oxygen transport in the follicle, and developed further in Chapters 5 and 6 through the experimental determination of the transport properties of follicular fluid.

Having established an understanding of oxygen transport in the follicle, the focus of this work shifts to the practical measurement of oxygen in follicular fluid (Chapters 7 and 8). It has been suggested as part of this review that oxygen levels may be effected by the IVF aspiration procedure. Chapter 7 addresses this issue.

Another potential threat is blood contamination of follicular fluid. Blood contamination is common during the *in vitro* fertilisation procedure, and in sufficient quantities may alter the readings produced by the measurement devices. Investigation into the magnitude of this problem needs to be undertaken, and if it is large enough solutions will need to be devised. These phenomena and that of oocyte shear are also addressed in Chapter 7.

Finally, Chapter 8 investigates the design and testing of devices intended for the sampling and/or analysis of dissolved oxygen levels in follicular fluid. The practical integration of any oxygen measuring system into the IVF clinical setting is also considered.

Chapter 3.   Modelling oxygen transport in the pre-antral follicle

Gosden & Byatt-Smith (1986) presented a mathematical model of oxygen transport in the pre-antral follicle. Based on this model the authors concluded that in the pre-antral follicle, no oxygen reaches the oocyte. Further, all of the oxygen entering the follicle is consumed before reaching even the outer 5% of the follicle radius. This chapter aims to revisit this model and present an improved version based on a more detailed investigation of the assumptions originally made by Gosden & Byatt-Smith (1986). This work will seek to lay a foundation which will facilitate the derivation and understanding of the more complex model of oxygen transport in the antral/pre-ovulatory follicle presented in the next chapter. The implications of the results on the metabolism of the oocyte will be considered.

3.1 The pre-antral follicle

The development of a follicle during the pre-antral stage is depicted in Figure 3.1. This phase of development is characterised by a growing oocyte surrounded by one or more layers of granulosa cells which also begin to multiply, forming multiple layers (Peters & McNatty, 1980). This development sees the oocyte increase in diameter from 25 μm to 80 μm. This rapid growth slows as the follicle approaches the antral phase. It is important to consider where and how the oocyte gets the energy which allows it to grow during this phase. The granulosa cells also multiply with the end result being the follicle has increased in size from 50 μm to 200 μm. Fluid voids become increasingly evident in the spaces between cells. This may have implications on the transport of oxygen.

3.2 The model of Gosden & Byatt-Smith (1986)

The model of oxygen transport in the pre-antral follicle proposed by Gosden & Byatt-Smith (1986) is represented pictorially in Figure 3.2.

Small pre-antral follicle

oocyte diameter ~ 25 μm

follicle diameter ~ 50 μm

oocyte

Large pre-antral follicle

granulosa
cell layer

oocyte diameter ~ 80 μm

follicle diameter ~ 400 μm
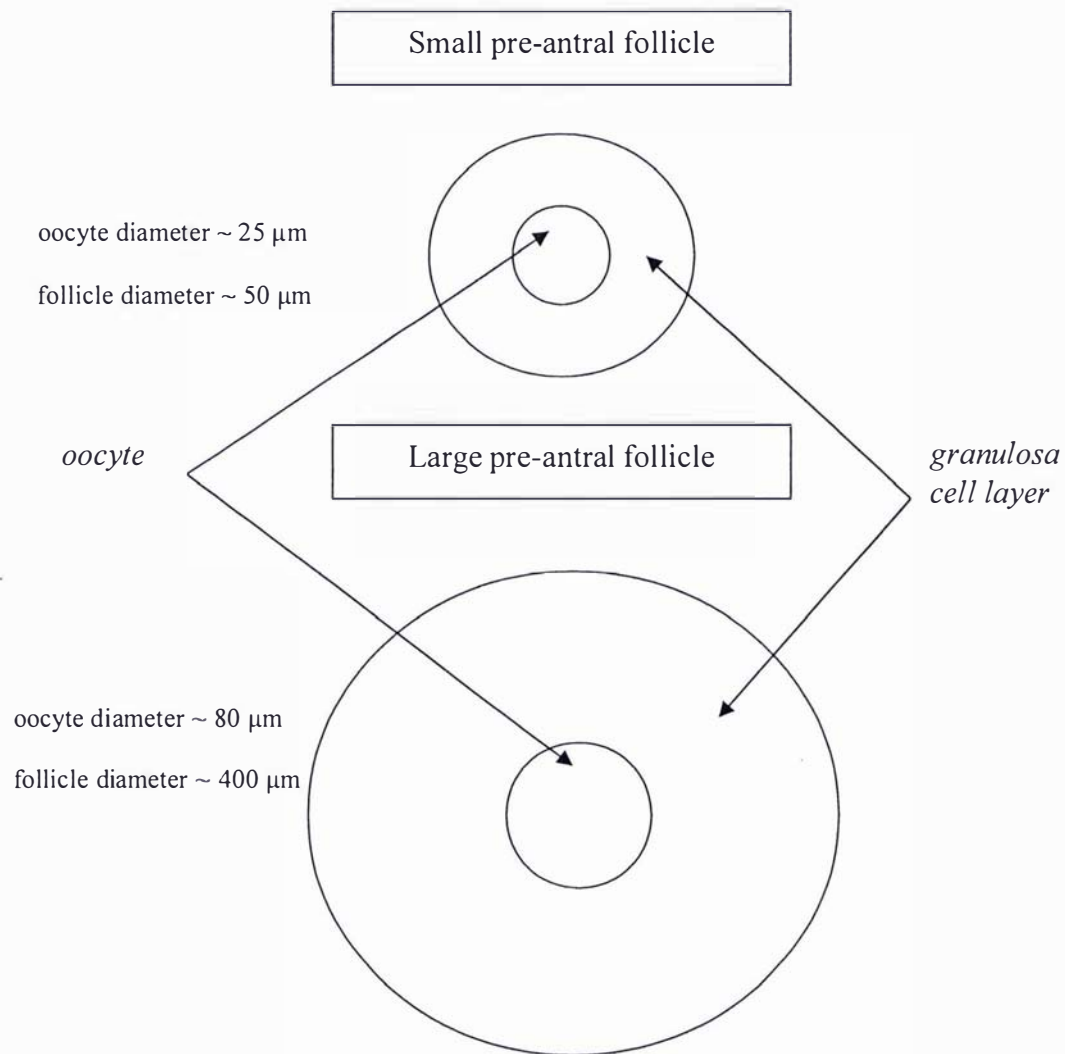
Figure 3.1   Development of the pre-antral follicle in humans.
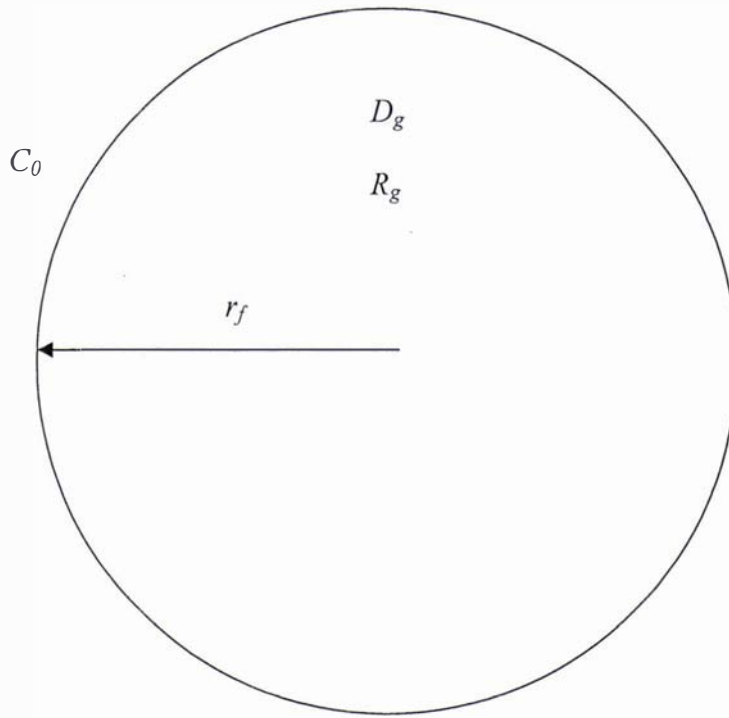
Figure 3.2   Pictorial representation of the model of oxygen transport in the pre-antral follicle proposed by Gosden & Byatt-Smith (1986). The oocyte is assumed to have the same properties as the granulosa cells and therefore its dimensions are not included. Symbols represent the concentration of oxygen at the follicle surface (C_o), the diffusion coefficient of oxygen through the granulosa layer (D_g), the oxygen consumption rate of the granulosa cells (R_g) and the follicle radius (r_f).

The model makes the following key assumptions:

1.   The follicle is spherical.

2.   The concentration of oxygen at the boundary is equal to that of arterial plasma. This concentration is uniform and hence the follicle is completely vascularised.

3.   The internal sub-domain is composed entirely of granulosa cells with no fluid voidage. Hence the model assumes that the oocyte has the same properties as the granulosa cells.

4.   Mass transport is via diffusion with consumption of oxygen. Oxygen is consumed by granulosa cells at a constant rate (i.e. independent of concentration).

The analytical solution describing this model predicts the oxygen concentration, C, at any position along the radius of the follicle. This solution is independently derived here.

Figure 3.3 provides a visual description to assist in the following derivation. The mass balance on the internal shell of a sphere is given by equation. 3.1.

| Rate of accumulation of oxygen within shell volume | = | Amount entering across inner shell surface | - | amount leaving across outer shell surface | - | rate of consumption within shell volume | (3.1) |

Units = mol.s^{-1}

The area of the inner shell is given by $4\pi\, r^2$, and that of the outer shell $4\pi(r + \Delta r)^2$. The volume of the shell is $4\pi\, r^2\, \Delta r$. Hence equation 3.2 can be written.

$$4\pi r^2 \Delta r \frac{\partial C}{\partial t} = J_r\, 4\pi r^2 - J_{r+\Delta r}\, 4\pi (r + \Delta r)^2 - R_g\, 4\pi r^2 \Delta r \qquad (3.2)$$

Dividing through by the volume of the shell ($4\,\pi\, r^2\, \Delta r$) gives equation 3.3.

$$\frac{\partial C}{\partial t} = \frac{J_r r^2 - J_{r+\Delta r}(r+\Delta r)^2}{(r+\Delta r)^2} - R_g \tag{3.3}$$

Units $= mol.m^{-3}.s^{-1}$

Taking the limit as Δr tends to zero gives equation 3.4.

$$\frac{\partial C}{\partial t} = \frac{1}{r^2}\frac{d(Jr^2)}{dr} - R_g \tag{3.4}$$

Fick's law of diffusion is given by equation 3.5.

$$J = D_g \frac{\partial C}{\partial r} \tag{3.5}$$

So, substituting equation 3.5 into equation 3.4 gives,

$$\frac{\partial C}{\partial t} = \frac{D_g}{r^2}\frac{d}{dr}\left(r^2 \frac{\partial C}{\partial r}\right) - R_g \tag{3.6}$$

Since at steady-state the rate of change of concentration with respect to time is zero, equation 3.6 becomes equation 3.7.

$$0 = \frac{D_g}{r^2}\frac{d}{dr}\left(r^2 \frac{\partial C}{\partial r}\right) - R_g \tag{3.7}$$

which can be rearranged to give equation 3.8.

$$d\left(r^2 \frac{\partial C}{\partial r}\right) = \frac{R_g r^2}{D_g} dr \tag{3.8}$$
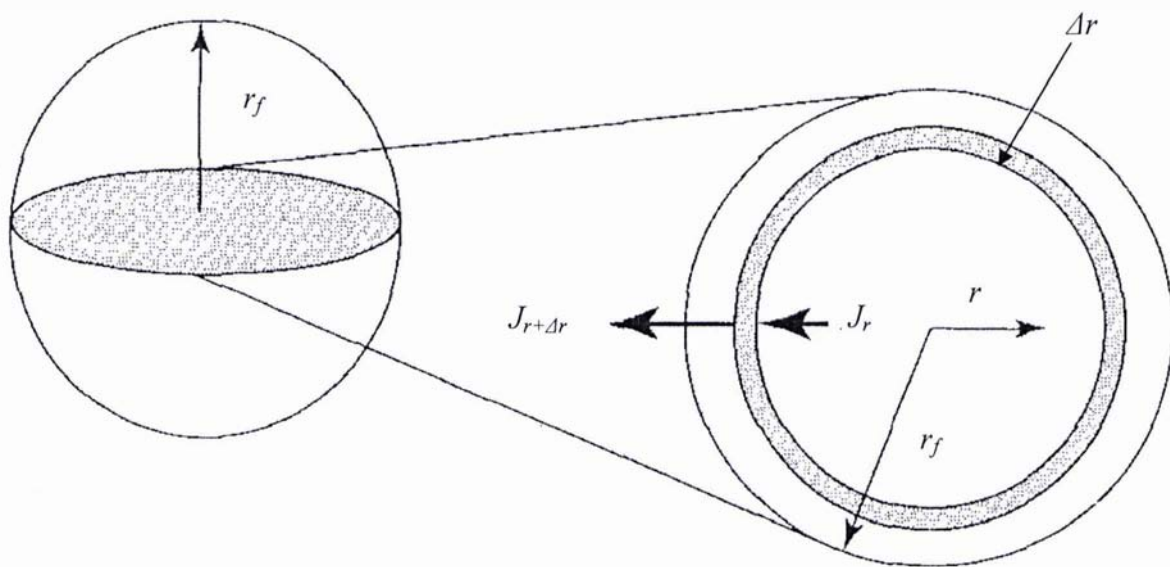
Figure 3.3.   Diffusion through an internal shell (shaded) of a spherical follicle.

Upon integration this gives equation 3.9.

$$r^2 \frac{\partial C}{\partial r} = \frac{R_g r^3}{3 D_g} + K_1$$ (3.9)

Since symmetry exists about the centre of the follicle, $\frac{\partial C}{\partial r} = 0$ at $r = 0$, and hence $K_1 = 0$. Thus, equation 3.9 can be simplified and rearranged to give equation 3.10.

$$\partial C = \frac{R_g r}{3 D_g} \partial r$$ (3.10)

which upon integration gives equation 3.11.

$$C = \frac{R_g r^2}{6 D_g} + K_2$$ (3.11)

Since at $r = r_f$, $C = C_o$

$$K_2 = C_o - \frac{R_g r_f^2}{6 D_g}$$ (3.12)

Thus, substitution of 3.12 into 3.11 gives

$$C = C_o - \frac{R_g r_f^2}{6 D_g} + \frac{R_g r^2}{6 D_g}$$ (3.13)

or

$$C = C_o - \frac{R_g}{6 D_g} \left(r_f^2 - r^2 \right)$$ (3.14)

42

Where R_g, the rate of consumption of oxygen by granulosa cells is positive. Since the concentration of oxygen at any point r cannot be zero, equation 3.14 comes with the additional requirement that if the calculated value of C is less than zero, then C is assigned the value of zero (concentration cannot be negative).

Equation 3.14 is expressed by Gosden & Byatt-Smith (1986) in terms of the relative oxygen concentration, C/C_o. Expressing equation 3.14 in this way gives

$$\frac{C}{C_o} = 1 - \frac{R_g r_f^2}{6 D_g C_o}\left(1 - \frac{r^2}{r_f^2}\right)$$

(3.15)

Converting the derivation of Gosden & Byatt-Smith (1986) to nomenclature consistent with this work gives equation 3.16.

$$\frac{C}{C_o} = 1 - \frac{R_g r_f^2}{6 D_g}\left(1 - \frac{r^2}{r_f^2}\right)$$

(3.16)

Equations 3.15 and 3.16 differ in the lack of a C_o in the denominator of the second term on the right hand side of the equation 3.16 as given by Gosden & Byatt-Smith (1986). Without this C_o included, equation 3.16 is not dimensionless, which it needs to be. For the same parameter inputs, Gosden & Byatt-Smith (1986) report the same model values as predicted here and hence this error must have been typographical only. Correcting this error the equations are identical. Equations 3.14 and 3.15 are also consistent with those derived by (Murdin *et al.,* 1988) for diffusion into a sphere.

Note that all consumption rates defined in this work, as in that of Gosden & Byatt-Smith (1986) are numerically positive.

3.3 Model improvement

This section attempts to improve the model of Gosden & Byatt-Smith (1986) and the understanding which can be obtained from it. Using the parameter values and assumptions of Gosden & Byatt-Smith (1986) as a basis of comparison, the effect of variation in these factors was investigated. Firstly the effect of the values of the basic model parameters under the assumptions presented by Gosden & Byatt-Smith (1986) was investigated. Then the effect of some of the basic assumptions was considered. Finally these two processes were combined to present a best, worst, and most likely case for oxygen transport in the pre-antral follicle.

3.3.1 Parameter estimation and variation

The parameter values used by Gosden & Byatt-Smith (1986) are presented in Table 3.1. Their values after conversion to units consistent with this investigation are also given.

The results from the model calculated using these values are shown in Figure 3.4.

Figure 3.4 shows that at these values the oxygen entering the follicle is completely consumed in the outer 1.5 μm of the follicle. Because this is a relatively large pre-antral follicle the oocyte would be expected to be approximately 70 μm in diameter (see Figure 3.1). If this is the case, and the oocyte is assumed to reside at the centre of the follicle, then the oocyte surface will be located 35 μm from the centre of the follicle. This is not even on scale in Figure 3.4, and illustrates that no oxygen is reaching the general vicinity of the oocyte.

To determine the sensitivity of the model to each of the parameters, a meaningful range over which each parameter varies needed to be estimated.

	Description	Value	Units	Value	Units	Source
C_o	oxygen concentration at the follicle surface	134	$\mu mol.L^{-1}$	0.134	$mol.m^{-3}$	As reported by Gosden & Byatt-Smith (source not stated)
D_g	diffusion coefficient of oxygen in the granulosa cell layer	7×10^{-8}	$cm^2.s^{-1}$	7×10^{-12}	$m^2.s^{-1}$	Jones & Kennedy (1982)
R_g	oxygen consumption rate of the granulosa cells	2.18 ± 0.39	$nmol.mm^{-3}.min^{-1}$	$0.0363 \pm 0.0065*$	$mol.m^{-3}.s^1$	Measurements of Gosden & Byatt-Smith (1986)
r_f	follicle radius	0.15	mm	0.00015	m	Measurements of Gosden & Byatt-Smith (1986)

Table 3.1   Parameter values used by Gosden & Byatt-Smith (1986) (* R_g is expressed ± SD). Right hand column expresses values in units appropriate to the model discussed in section 3.3.1.
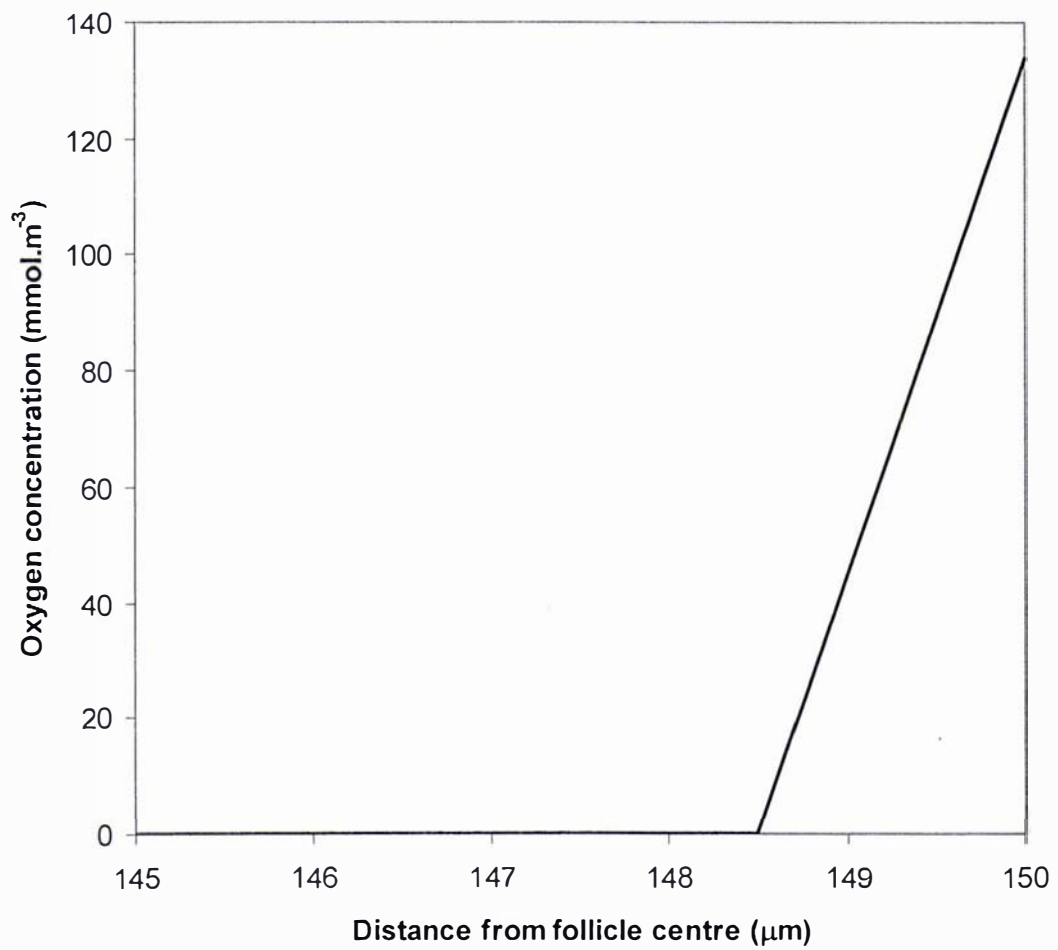
Figure 3.4   Oxygen concentration as a function of distance from the centre of a pre-antral follicle at the parameter values given by Table 3.1.

3.3.1.1 Estimation of the oxygen concentration at the follicle surface (C_o)

The value of 134 µM used by Gosden & Byatt-Smith (1986) is consistent with typical values for the plasma portion of blood which is approximately 130 µM (Fournier, 1998). More specifically, Fischer *et al.* (1992) found the partial pressure of oxygen in ovarian blood to be 102.0 ± 3.4 mmHg ($\pm$ SD).

Fournier (1998) also gives the typical partial pressure of arterial blood when the concentration is 130 µM as 95 mmHg. The partial pressure of oxygen at the follicle boundary can be related to the concentration by Henry's law

$$C_0 = p_0 S \qquad\qquad (3.17)$$

Because the solubility of oxygen in the plasma portion of arterial blood can be assumed constant the following equation can be written.

$$\frac{C_1}{C_2} = \frac{p_1 S}{p_2 S} = \frac{p_1}{p_2} \qquad\qquad (3.18)$$

Hence using equation 3.18 and the partial pressure of oxygen in ovarian arterial blood, the concentration of oxygen in ovarian arterial blood can be estimated as $C = \frac{102}{95} \times 130 = 140 \pm 5$ µM ($\pm$ SD). A range of $\pm$ 2 standard deviations of the mean was used to test the sensitivity of the model. This gives a range of 130-150 µM.

It should be noted that in this work the follicle is assumed to be at atmospheric pressure. This is in keeping with Gosden *et al.* (1988) provide evidence that intra-follicular pressure is modest (approximately 17 mmHg).

3.3.1.2 Estimation of rate of oxygen consumption by granulosa cells (R_g)

The rate of oxygen consumption by granulosa cells of sheep is reported as $0.0363 \pm$

0.0065 mol.m^{-3}.s^{-1} (Gosden & Byatt-Smith, 1986). Table 3.2 shows that this value is consistent with oxygen consumption rates reported for human tissues.

Given that the value reported by Gosden & Byatt-Smith (1986) is a direct measure of granulosa cells, and that it is in keeping with values reported for human tissue, this value ± 2 standard deviations was used to determine the range for input into the sensitivity analysis. Therefore the range is 0.0233 to 0.0493 mol.m^{-3}.s^{-1}.

3.3.1.3 Estimation of follicle radius (r_f)

For human pre-antral follicles, the range over which the follicle radius varies is 25 μm to 200 μm (Peters & McNatty, 1980, McNatty, 1978). This is the range that will be tested in the sensitivity analysis. 200 μm is the follicle radius at which the antrum first forms (McNatty, 1978).

3.3.1.4 Estimation of oxygen diffusivity in the granulosa cell layer (D_g)

The diffusion coefficient of oxygen in granulosa cells has never been explicitly measured. Granulosa cells fall into the broader category of epithelial cells which include any cells present at tissue interfaces including the stomach, intestines, lung, kidney, liver, and secretory cells. Therefore, a reasonable range over which D_g is likely to vary may be estimated from available literature. The literature available on this subject can be divided into two categories, theoretical and experimental. Careful consideration of the material in both categories will hopefully allow the estimation of a reasonable range of values for D_g.

3.3.1.4.1 Theoretical analysis

Hills (1970) presented a mathematical analysis which assumed that oxygen diffusion in tissue occurs by diffusion first through an extra-cellular fluid phase, followed by diffusion through a cellular phase composed of irregularly shaped cells. The predictions of this model suggested that the diffusion coefficient of oxygen in cellular material is $^1/_{10,000}$ that in extra-cellular fluid (plasma).

Granulosa cells	0.0363	Gosden & Byatt-Smith (1986)
Brain tissue	0.0234 – 0.0972	Truskey *et al.*, (2004)
Pancreatic tissue	0.026 – 0.046	Fournier, (1998)
Typical human tissue	0.02	Christoforides *et al.*, (1969)
Skeletal muscle	0.1	Truskey *et al.*, (2004)

Table 3.2   Oxygen consumption rates of various human tissues compared to granulosa cells. All consumption rates have units of $mol.m^{-3}.s^{-1}$.

A later mathematical analysis assumed tissue to consist of alternating layers of cells and fluid, both in series and in parallel (Tai & Chang, 1974). Tai & Chang (1974) argued that this method of analysis was more representative of real tissue, and were thus critical of the approach of Hills (1970), even pointing out errors in derivation. The results of the analysis of Tai & Chang (1974) suggested that the diffusion co-efficient in the cellular phase is far more likely to be around $^1/_{10}$ of that in plasma.

3.3.1.4.2 Experimental analysis

Experimental values for oxygen diffusion coefficients are not abundant in the literature. The data that does exist uses a wide variety of experimental set-ups and conditions. Some data are gathered at 37°C, some are not. Some data are gathered using respiring cells, some dead, whilst for others it is difficult to tell.

Further, the void volume is often not stated or considered. This makes estimation of anything other than a reasonable range impossible. Lango et $al.$ (1996) compiled the available data into a review. The eighteen reported values range from 0.1 to 1.5 x 10^{-5} cm^2.s^{-1} at 37 °C. Human plasma has a reported value of 2.2 x 10^{-5} cm^2.s^{-1} at 37°C (Goldstick et $al.$, 1976). Thus, tissue diffusion coefficients vary between 0.05 and 0.68 that of plasma. Because of the unusual assumption of Gosden & Byatt-Smith (1986) that there is no void volume in the tissue of the pre-antral follicle, it is required that the effective diffusion coefficients in the tissue be converted to cellular values. This can be achieved using Maxwell's equation which relates the effective diffusivity (D_{eff}) in a tissue composed of extra-cellular fluid and cells to the separate diffusion coefficients in the extra-cellular fluid and the cells and a(Maxwell, 1873). The diffusion coefficient of oxygen in the extra-cellular fluid can be assumed to be that of plasma (D_p) and hence Maxwell's equation can be expressed as,

$$\frac{D_{eff}}{D_p} = \frac{D_p + D_{cell} - 2\phi(D_p - D_{cell})}{D_p + D_{cell} - \phi(D_o - D_{cell})} \tag{3.19}$$

Φ is the volume fraction of cells, and is related to the fluid void volume fraction (ε) by $\Phi = 1 - \varepsilon$. For biological tissues ε can vary from 0.06 to 0.3 (Nicholson, 2001; Dutta

& Popel, 1995; Tai & Chang, 1974; Truskey *et al.*, 2004b). In theory, given Maxwell's model, the inputs of D_{eff} (such as the range obtained from Goldstick *et al.* (1976)), and the typical values of Φ, a range of D_{cell} can be solved for. Unfortunately, equation 3.19 is only accurate for void volumes of approximately $\varepsilon \leq 0.1$.

More recently empirical correlations have been developed relating D_{eff}, D_p, D_{cell} and Φ based on Monte Carlo simulations (Riley *et al.*, 1994; Riley *et al.*, 1995; Riley *et al.*, 1996). These simulations work by generating a computational structure that mimics immobilised cells. Tracer particles then undergo a 'random walk' through the structure. The empirical correlation is given by equation 3.20, and shows excellent agreement with available experimental data over a range of $0.04 < \Phi < 0.95$ (Riley *et al.*, 1994; Riley *et al.*, 1995; Riley *et al.*, 1996).

$$\frac{D_{eff}}{D_p} = 1 - \left(1 - \frac{D_{cell}}{D_p}\right)(1.727\phi - 0.8177\phi^2 + 0.09075\phi^3) \tag{3.20}$$

Solving 3.20 for D_{cell} gives equation 3.21.

$$D_{cell} = \frac{D_p\phi^3 - 9.01047D_p\phi^2 + 19.0303D_p\phi + 11.0193\left(D_{eff} - D_p\right)}{\phi^3 - 9.01047\phi^2 + 19.0303\phi} \tag{3.21}$$

From the literature, the range previously determined for D_{eff} was 0.1 to 1.5 x 10^{-5} cm^2.s^{-1}. It is fair to assume that the lower end of the range will likely relate to cells with a low void fraction ($\varepsilon = 0.06$), whilst the value at the higher end will be more relevant to a high void fraction ($\varepsilon = 0.3$). Under this assumption equation 3.21 can be used to calculate the range over which D_{cell} may vary and gives $5 \times 10^{-7} \leq D_{cell} \leq 1.4 \times 10^{-5}$ cm^2.s^{-1}. This is quite a wide range with D_{cell} varying from 0.02 to 0.67 that of the diffusion coefficient of oxygen in the plasma phase. However, this is in reasonable agreement with the value of 0.1 suggested by the theoretical analysis of Tai & Chang (1974). The value used by a standard bio-medical engineering text (without reference) was 6 x 10^{-6} cm^2.s^{-1} (Fournier, 1998), which also falls within the predicted range.

The value of D_{cell} used by Gosden & Byatt-Smith (1986) in their model of oxygen transport for the pre-antral follicle was 7×10^{-8} cm^2.s^{-1}. This falls outside the range of the D_{cell} predicted here. This value comes from the work of Jones & Kennedy (1982) who suggested that D_{cell} varied from 0.7 to 6×10^{-7} cm^2.s^{-1}. This range shows marginal overlap with the one predicted here. The range of Jones & Kennedy (1982) was calculated based on measurements of oxygen gradients across liver cells of the rat. Direct measurements of D_{cell} are obviously more desirable than the indirect calculation performed here based on D_{eff}. Unfortunately such measurements are rare. The range given by Jones & Kennedy (1982) was later disregarded in work carried out by one of the same authors (Jones, 1984). In this investigation measurements were again carried out on liver cells of the rat, and a range for D_{cell} was recalculated taking into account mitochondrial interaction. The previous work of Jones & Kennedy (1982) had assumed that regions of oxygen gradients surrounding the mitochondria do not overlap. However electron micrographs presented by Jones (1984) showed this not to be the case due to mitochondrial clustering. The improved range was reported as 1 to 5×10^{-6} cm^2.s^{-1}.

Similar studies carried out on cardiac muscle cells of the rat gave a range of D_{cell} of between 2 to 4×10^{-6} cm^2.s^{-1} (Jones & Kennedy, 1986), a range similar to that found for rat liver cells. This work was later supported by Rumsey et al. (1990) who gave a value of 3×10^{-6} cm^2.s^{-1}.also for cardiac muscle cells of the rat. The D_{cell} values given by Jones (1984), Jones & Kennedy (1986), and Rumsey et al. (1990) all fall within the range calculated here.

A summary comparing the various values of D_{cell} discussed here is presented in Figure 3.5. Figure 3.5 shows that all estimates apart from the disregarded measurements of Jones & Kennedy (1982) show an area of common overlap ranging between 1×10^{-6} to 5×10^{-6} cm^2.s^{-1}. This is perhaps the best range for D_{cell} that can be obtained from currently available literature. Dutta & Popel 1995 found that they could not reconcile the discrepancy between reported values of D_{eff} and D_{cell}. Similarly the work here suggests that trying to exactly match values of D_{eff} and D_{cell} may be impossible. Although the variability is high, the feasible ranges of D_{cell}

predicted from D_{eff}, and D_{cell} as measured experimentally, share common overlap. It is important to note that the value of D_{cell} used by Gosden & Byatt-Smith (1986) in their pre-antral follicle model is essentially the lowest value that could be reasonably derived from the literature. Further, it has since been disregarded (Jones, 1984), although Gosden & Byatt-Smith (1986) did state that values an order of magnitude above and below this value were tested.

Although future use of the model of oxygen transport in the pre-antral model may benefit from the more accurate values of D_{cell} suggested here, for the purposes of examining the models sensitivity to the input parameters it is advisable to use the full range of D_{cell} values suggested by Figure 3.5 (0.7×10^{-7} to 1.4×10^{-5} $cm^2.s^{-1}$). Doing this may allow for greater understanding of the conclusions reached by Gosden & Byatt-Smith (1986) with regard to the pre-antral follicle.

3.3.2 Sensitivity analysis

In the relationship between oxygen concentration and the distance from the follicle centre depicted in Figure 3.4, the point of most interest is that where the oxygen concentration reaches zero and the remaining tissue becomes anoxic. It is therefore sensible to investigate the sensitivity of the model to variation in parameters at this point. This can be achieved by setting equation 3.14 equal to zero and solving for r. Doing so results in equation 3.22 which gives the distance from the follicle centre at which the tissue becomes anoxic.

$$r_{anoxic} = \sqrt{r_f^2 - \frac{6 D_g C_o}{R_g}} \qquad (3.22)$$

where $D_g = D_{eff}$ as given by equation 3.20.

Using equation 3.22 the sensitivity analysis can be performed by varying each parameter over the range of interest. When a parameter was not being varied it was held at its nominal value which was either the mean or the centre of the range of

interest. For D_{cell}, the nominal value is the middle of the range of overlap described in Figure 3.5. A summary of ranges of interest and nominal values for each parameter is presented in Table 3.3.

The results of these calculations are shown in Figures 3.6 to 3.9 for variation in C_o, R_g, r_f, and D_g respectively. Also included in the figures are the results of the calculations when the parameters not being varied are held at the values used by Gosden & Byatt-Smith (1986) (see Table 3.1).

The most striking information obtained from figures 3.6 to 3.8 is that variation in C_o, R_g, and r_f causes close to no variation in the solution of equation 3.22 when the other parameter estimates of Gosden & Byatt-Smith (1986) are used.

Figure 3.9 shows that using the parameter values used by Gosden & Byatt-Smith (1986) the model is very sensitive to variations in D_g. However, this was not investigated by Gosden & Byatt-Smith (1986). The reason this sensitivity was not discovered by these authors is illustrated graphically by Figure 3.10. In Figure 3.10 D_g is varied over the range tested by Gosden & Byatt-Smith (1986) (7×10^{-9} to 7×10^{-7} $cm^2.s^{-1}$). The Figure shows that variation throughout this range results in only a 3% difference in the solution. It can be concluded that at the parameter estimates and ranges tested by Gosden & Byatt-Smith (1986) the model essentially gives the same result regardless of the values used. In light of these results it is easy to see how Gosden & Byatt-Smith (1986) arrived at the conclusion that the oxygen gradient through the follicular epithelium is very steep. This result is dictated almost solely by the low diffusion coefficient selected.

Using the improved estimates described here, Figures 3.6 to 3.9 show increased sensitivity of the solution to variation in all parameters. The solution is only moderately sensitive to variation in C_o, showing a negative linear relationship throughout the range tested. Variation of R_g over the range tested results in variation in r/r_f of ~ 0.4. If D_g is narrowed to the most likely range given in Table 3.3 then variation in this parameter causes ~ 0.61 variation in r/r_f. Hence the solution is very sensitive to variation in both R_g and D_g.

54
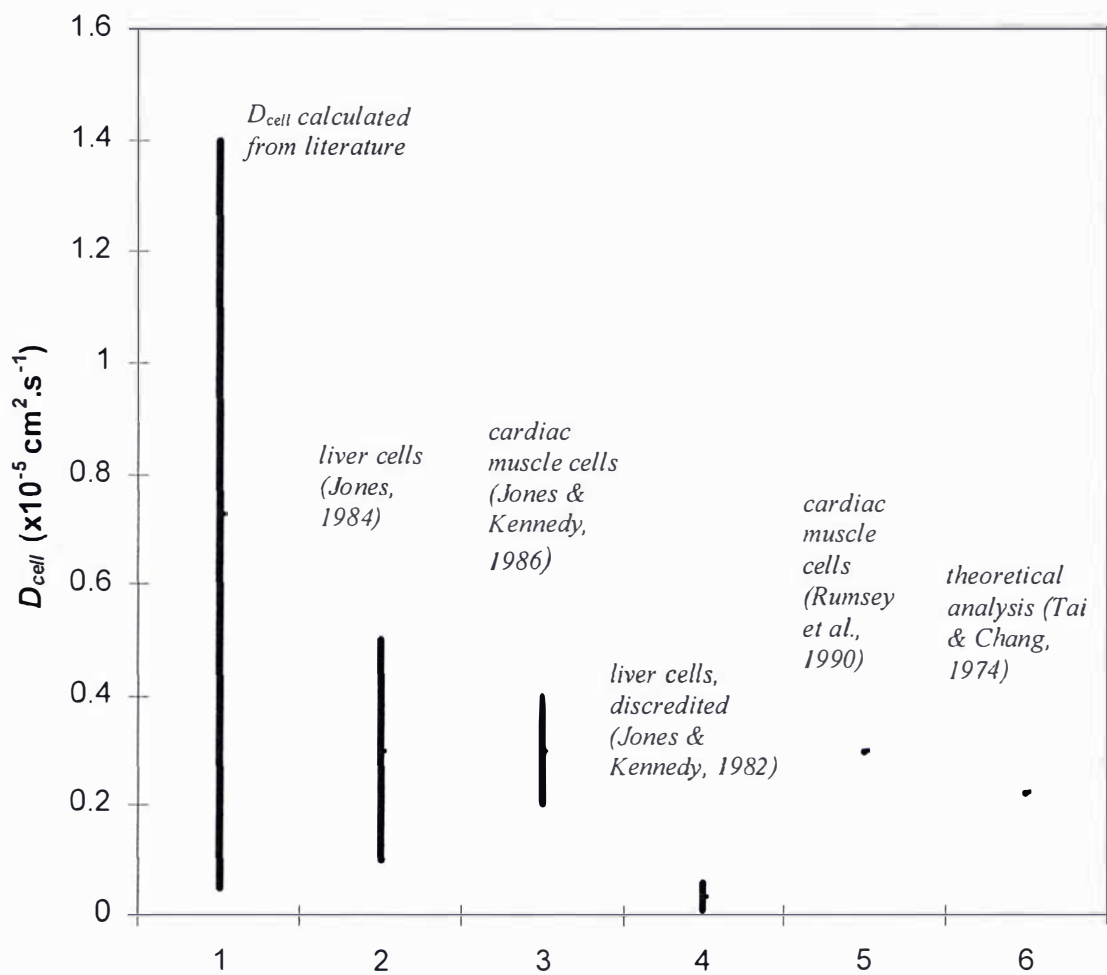
Figure 3.5   Comparison of measured values of D_{cell} from the literature with the range predicted in this work.

	Range	Units	Nominal Value
C_0	0.130 – 0.150 (μ-2SD to μ+2SD)	mol.m^{-3}	0.140 (mean from Fischer *et al.*, 1992)
D_g	7x10^{-12} to 1.4x10^{-9} likely range (1 to 5 x 10^{-10})	m^2.s^{-1}	3 x 10^{-10} (mid point of range of overlap)
R_g	0.0233 to 0.0493 (μ-2SD to μ+2SD)	mol.m^{-3}.s^{-1}	0.0363 (mean from Gosden & Byatt-Smith, 1986)
r_f	0.000025 to 0.00020	m	0.0001125 (mid point of range from Peters & McNatty, 1980 and McNatty, 1978)

Table 3.3   Ranges of interest and nominal values for the pre-antral follicle model.
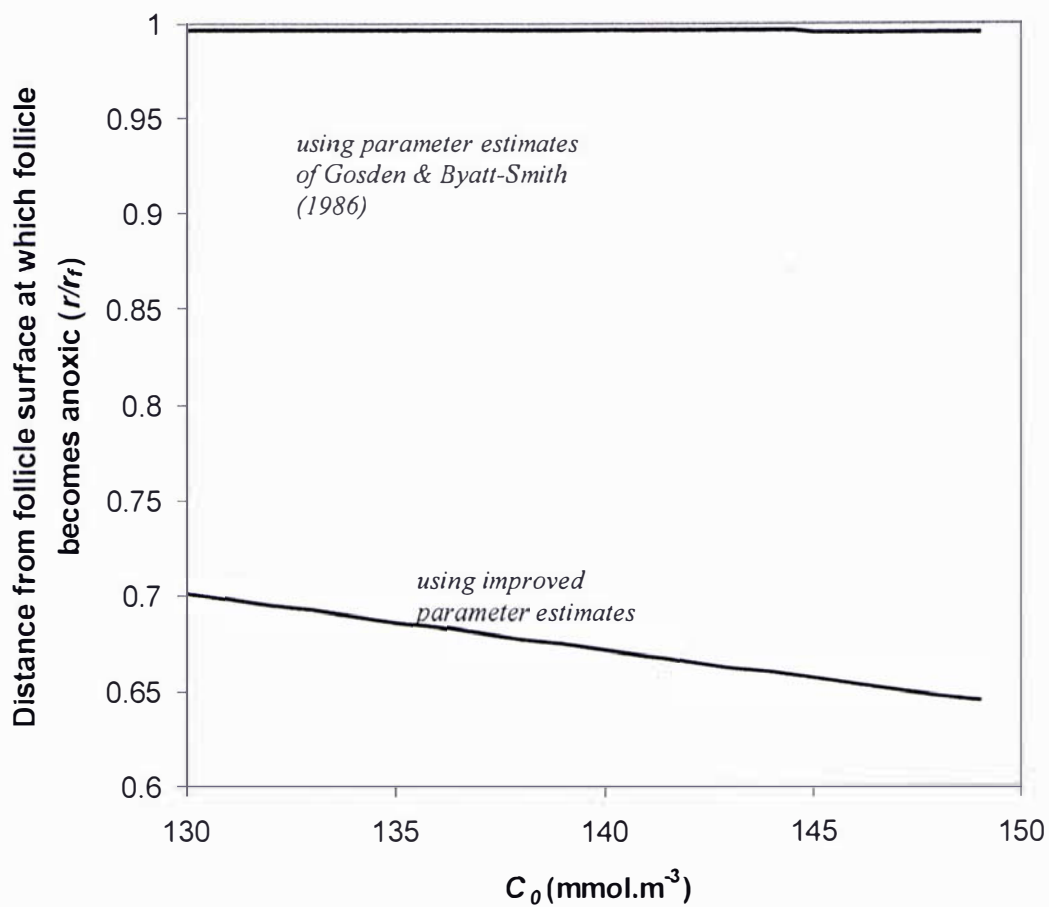
Figure 3.6   The effect of variation of C_0 on the distance from the follicle surface at which follicle becomes anoxic (note that r/r_f has a value of 1 at the follicle surface). Note that improved parameter estimate values can be found in Table 3.3 and those used by Gosden & Byatt-Smith in Table 3.1.
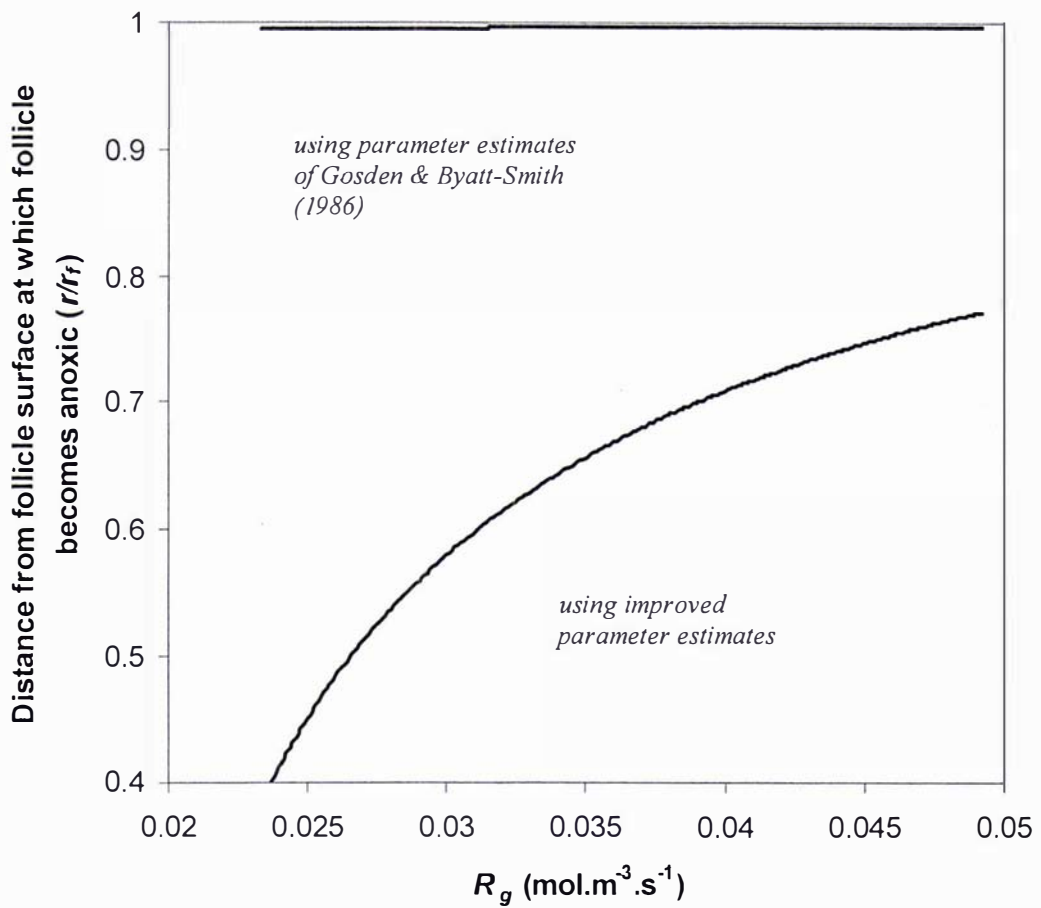
Figure 3.7   The effect of variation of R_g on the distance from the follicle surface at which follicle becomes anoxic (note that r/r_f has a value of 1 at the follicle surface). Note that improved parameter estimate values can be found in Table 3.3 and those used by Gosden & Byatt-Smith in Table 3.1.
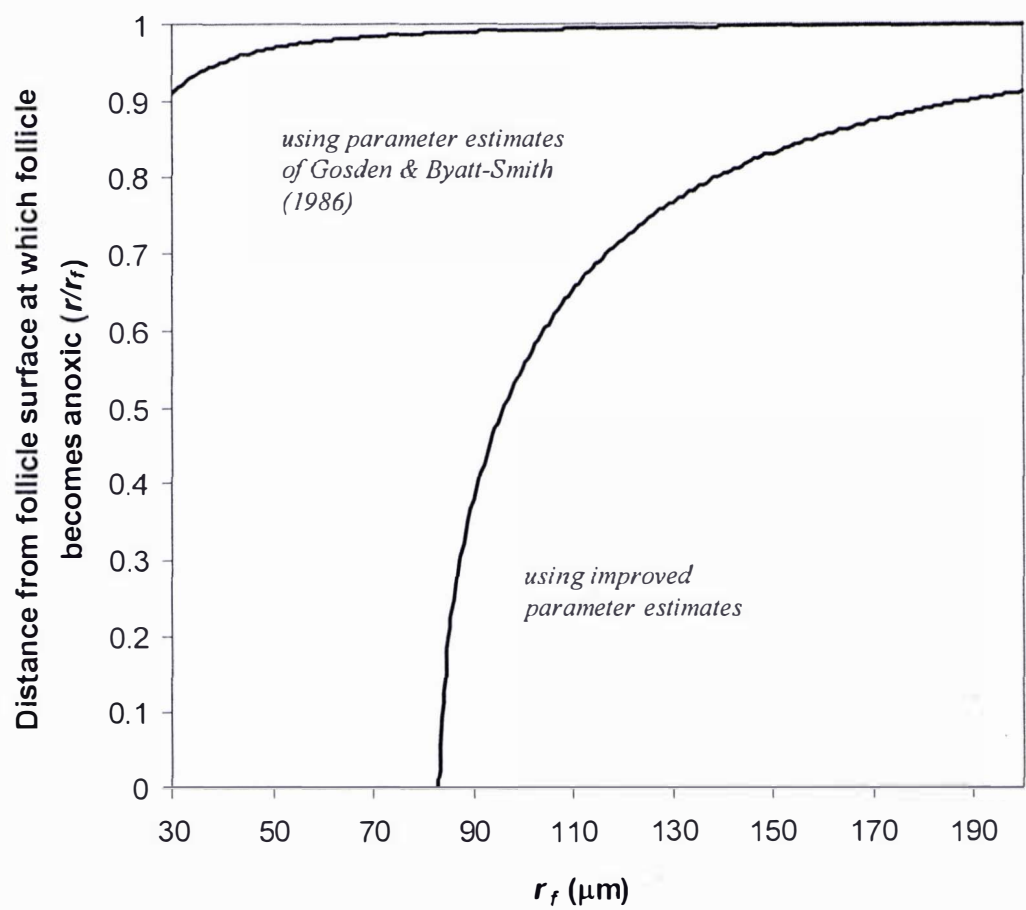
Figure 3.8   The effect of variation of r_f on the distance from the follicle surface at which follicle becomes anoxic (note that r/r_f has a value of 1 at the follicle surface). Note that improved parameter estimate values can be found in Table 3.3 and those used by Gosden & Byatt-Smith in Table 3.1.
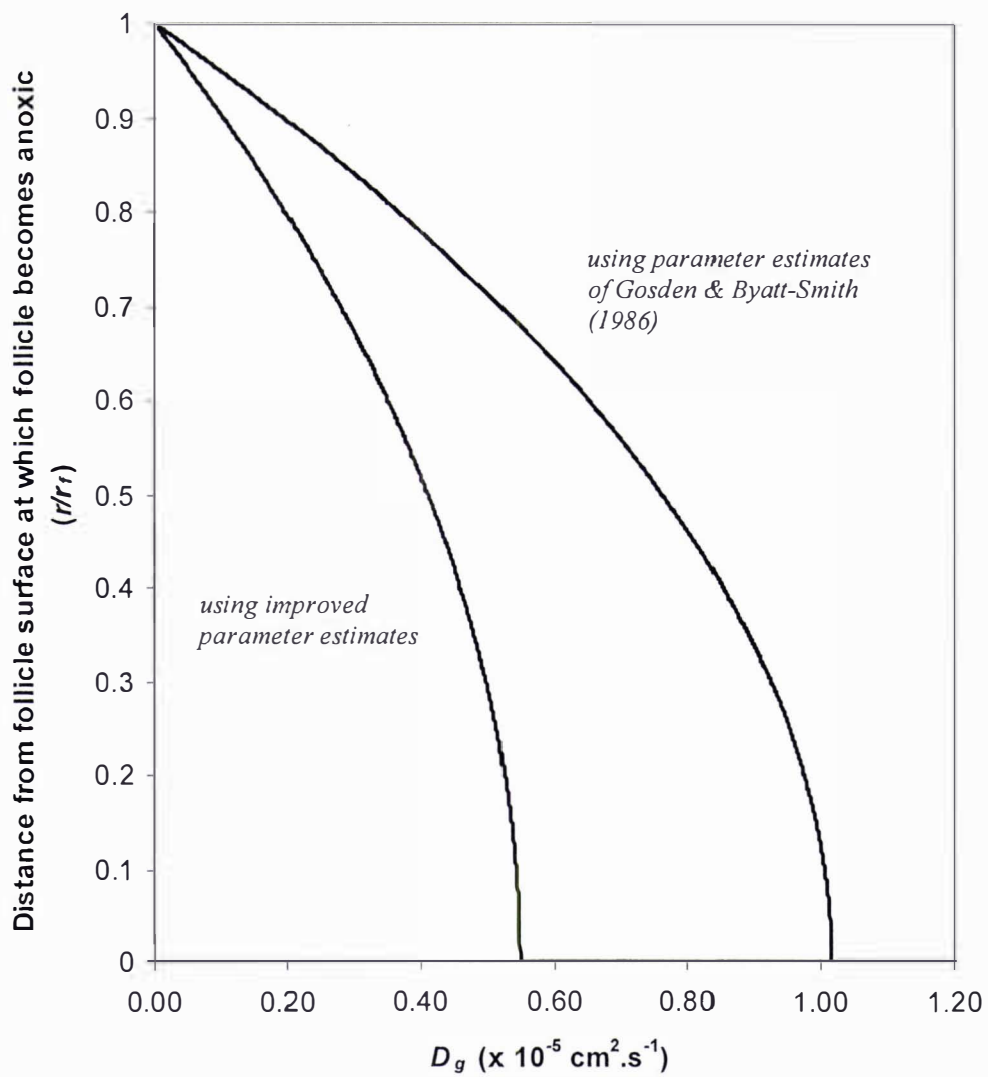
Figure 3.9   The effect of variation of D_g on the distance from the follicle surface at which follicle becomes anoxic (note that r/r_f has a value of 1 at the follicle surface). Note that improved parameter estimate values can be found in Table 3.3 and those used by Gosden & Byatt-Smith in Table 3.1.
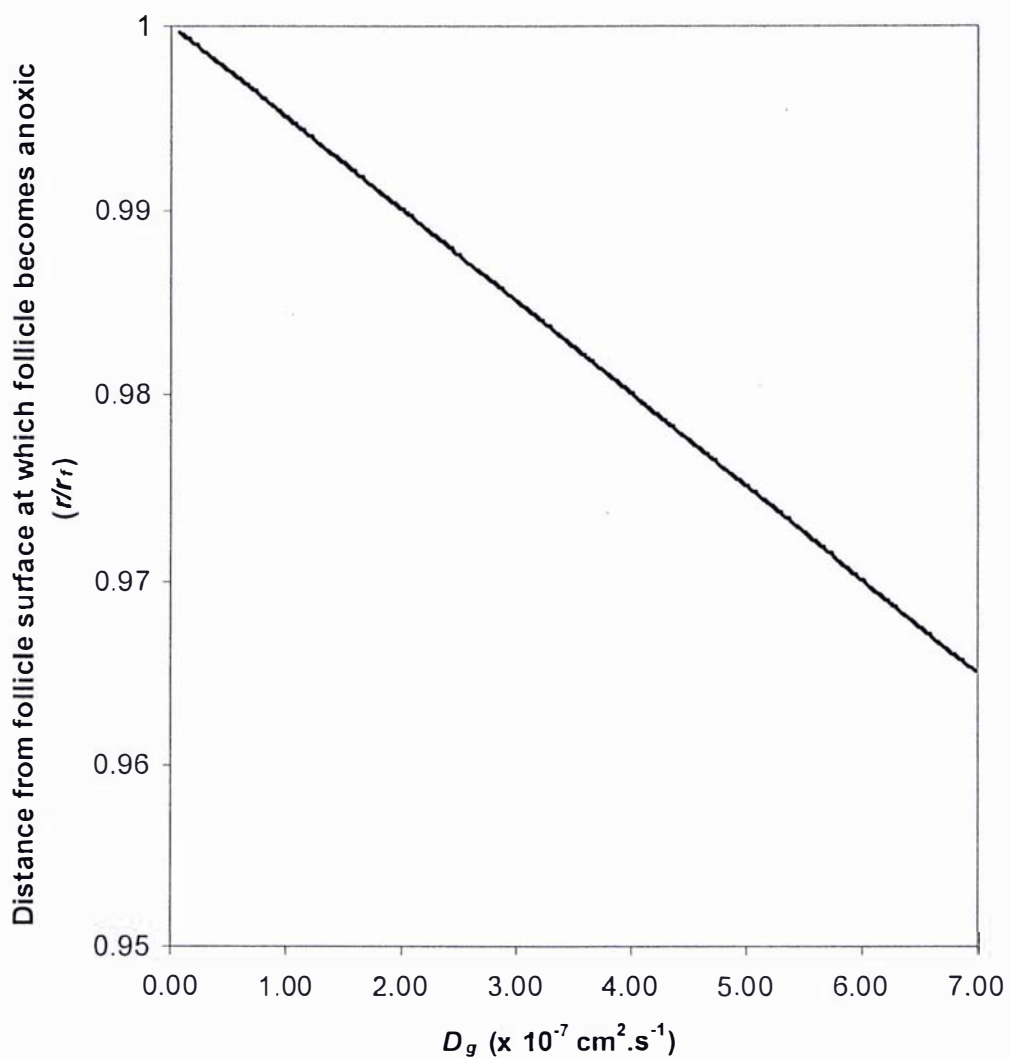
Figure 3.10   The effect of variation of D_g over the range tested by Gosden & Byatt-Smith (1986) on the distance at which the follicle becomes anoxic (note that r/r_f has a value of 1 at the follicle surface).

Variation in r_f is somewhat different as this does not represent an uncertainty range in this parameter, but rather describes the growth of the pre-antral follicle. Figure 3.8 shows that at the nominal values of each parameter the follicle has no anoxic region when it is small. As it increases in size to approximately $r_f = 83$ μm it starts to become anoxic, increasingly so as the follicle size becomes larger.

From these results it can be seen that high values of C_o, and D_g are favourable to oxygen transport, and vice versa. High consumption rates (R_g) and large follicle diameters (r_f) are unfavourable to oxygen transport, and vice versa.

Equation 3.22 shows why the solution of Gosden & Byatt-Smith (1986) was insensitive to variation in all parameters. The very small diffusion coefficient used resulted in the $6D_gC_o/R_g$ term being negligible and hence $r_{anoxic} \approx \sqrt{r_f^2} \approx r_f$. In other words the anoxic region was always in the same place, close to the follicle surface.

The use of parameter values in combinations least and most favourable to oxygen transport can now be used to view the range over which the oxygen concentration profiles will vary. The most favourable parameter combination is defined as high C_o, high D_g, and low R_g, and vice versa for the least favourable parameter combination, where high and low are the upper and lower ends respectively of the range for each parameter presented in Table 3.3. The results of such calculations are shown in Figures 3.11 and 3.12 for small and large follicles respectively.

Figure 3.11 shows that in spite of the large variation in solution for favourable and unfavourable parameter values, the conclusion remains the same. That is, oxygen is reaching the oocyte.

For large pre-antral follicles Figure 3.12 shows less variation between the curves for unfavourable and favourable parameter values for oxygen transport. The conclusion drawn from both curves is once again the same. No oxygen can reach the oocyte in a large pre-antral follicle. This model assumes no fluid voidage, no oocyte, constant consumption rate, and complete vascularisation of the follicle.
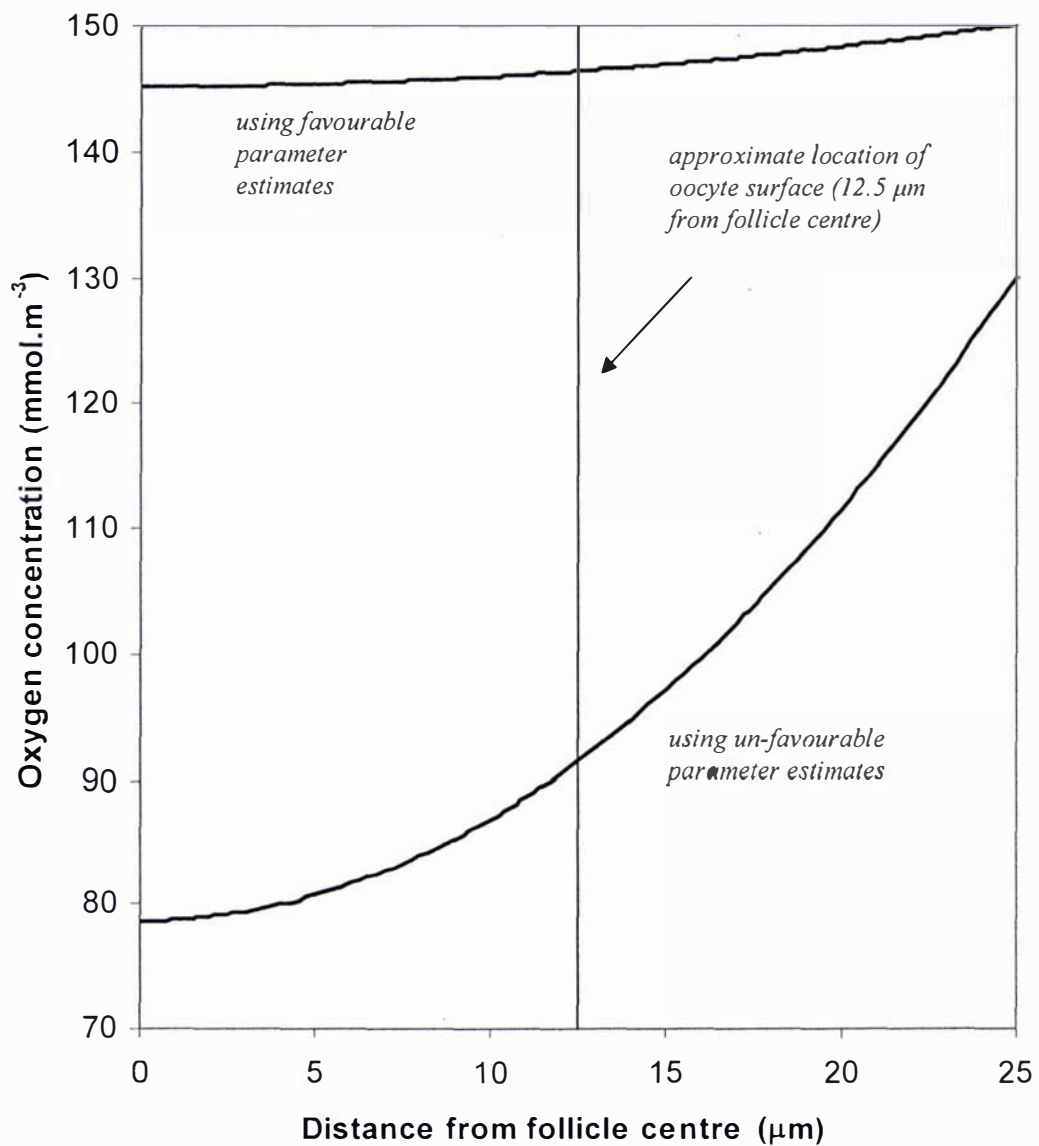
Figure 3.11   Oxygen concentration profiles across a small ($r_f = 25$ µm) pre-antral follicle using parameter values favourable and unfavourable to oxygen transport. The most favourable parameter combination is defined as high C_o, high D_g, and low R_g, and vice versa for the least favourable parameter combination, where high and low are the upper and lower ends respectively of the range for each parameter presented in Table 3.3.
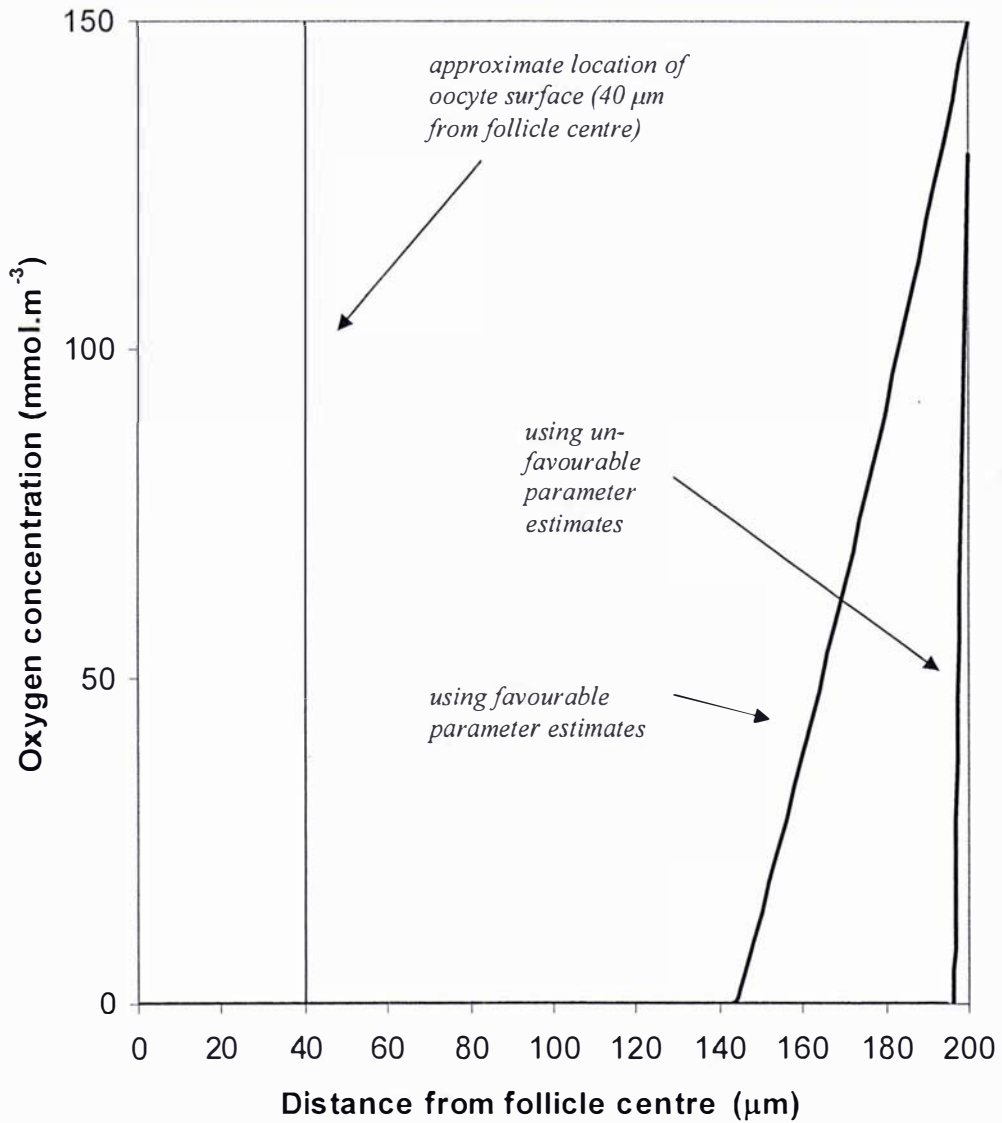
Figure 3.12   Oxygen concentration profiles across a large (r_f=200 μm) pre-antral follicle using parameter values favourable and unfavourable to oxygen transport. The most favourable parameter combination is defined as high C_o, high D_g, and low R_g, and vice versa for the least favourable parameter combination, where high and low are the upper and lower ends respectively of the range for each parameter presented in Table 3.3.

The validity of these assumptions and their impact on the model and the conclusions drawn is investigated in the next section.

3.3.3 Assumption of no fluid voidage

The fluid voidage (ε) of typical biological tissues ranges between 0.06 to 0.3 (Nicholson, 2001, Dutta & Popel, 1995, Tai & Chang, 1974, Truskey *et al.*, 2004b). It is therefore unlikely that the assumption made by Gosden & Byatt-Smith (1986) of no voidage in the pre-antral follicle is true. In the small pre-antral follicle, before sufficient fluid has been secreted, this assumption is likely to be a reasonable approximation. However as the pre-antral follicle grows and more fluid is secreted, the voidage will increase (Peters & McNatty, 1980). The increased voidage observed in the follicle tissue is somewhat unique, and it is possible that before the formation of the antrum when fluid voidage will be at its greatest, that the voidage resembles that of some tumour tissues. In tumour tissues ε can be as high as 0.6 (Truskey *et al.*, 2004b). The striking morphological, biophysical, and biochemical similarities between ovarian follicles and small tumours has been presented by Neeman *et al.* (1997). It is therefore advisable to examine the effect of voidage on the model of oxygen transport in the pre-antral follicle, particularly as it relates to large pre-antral follicles.

Fluid voidage will affect the model in two ways. Firstly the diffusion coefficient of oxygen in the granulosa cell layer, which was initially assumed to be equal to D_{cell} will now be an effective diffusion coefficient. This effective diffusion coefficient combines the diffusion coefficients of the cellular and extra-cellular components of the tissue according to equation 3.20.

The effect of increasing fluid voidage on D_{eff} is described by Figure 3.13 over the reasonable range of D_{cell} (0.1 to 0.5 x 10^{-5} cm^{2}s^{-1}, see Table 3.3). At zero fluid voidage $D_{eff} = D_{cell}$. At low fluid voidage ($\varepsilon \leq 0.1$) the effect on D_{eff} is minimal with $D_{cell} \approx D_{eff}$. Hence, the assumption that $D_{cell} = D_{eff}$ for small pre-antral follicles is fair. It is important to note that even if this assumption was not true for small pre-antral

follicles, the conclusions drawn from Figure 3.11 would not be altered. That is, oxygen would still be reaching the oocyte, indeed at increased levels.

As ε increases the effect on D_{eff} becomes more dramatic, with the difference between the low and high estimates reducing, and converging at $\varepsilon = 1.0$, at which point $D_{eff} = D_{plasma}$.

Before examining the affect of increased voidage, the model requires further modification. Fluid voidage represents space where no oxygen consumption occurs. To account for this, modification of equation 3.14 results in equation 3.23 which describes the oxygen concentration at any position, r, in the pre-antral follicle when the effect of fluid voidage is considered (assuming R_g does not already account for voidage).

$$C = C_0 - \frac{R_g (1-\varepsilon)}{6D_g}(r_f^{\,2} - r^2)$$

(3.23)

where $D_g = D_{eff}$, as calculated by equation 3.20.

Because the inclusion of voidage will not effect the conclusions drawn for the small pre-antral follicle it is sufficient to examine the effect of voidage on the distance at which a large pre-antral follicle becomes anoxic. This can be achieved by setting equation 3.23 equal to zero and solving for r_{anoxic} in the same way equation 3.22 was previously derived. Doing so results in equation 3.24 which gives the distance from the follicle centre at which the tissue becomes anoxic, for a given voidage level.

$$r_{anoxic} = \sqrt{r_f^2 - \frac{6D_g C_0}{R_g (1-\varepsilon)}}$$

(3.24)

where again $D_g = D_{eff}$.
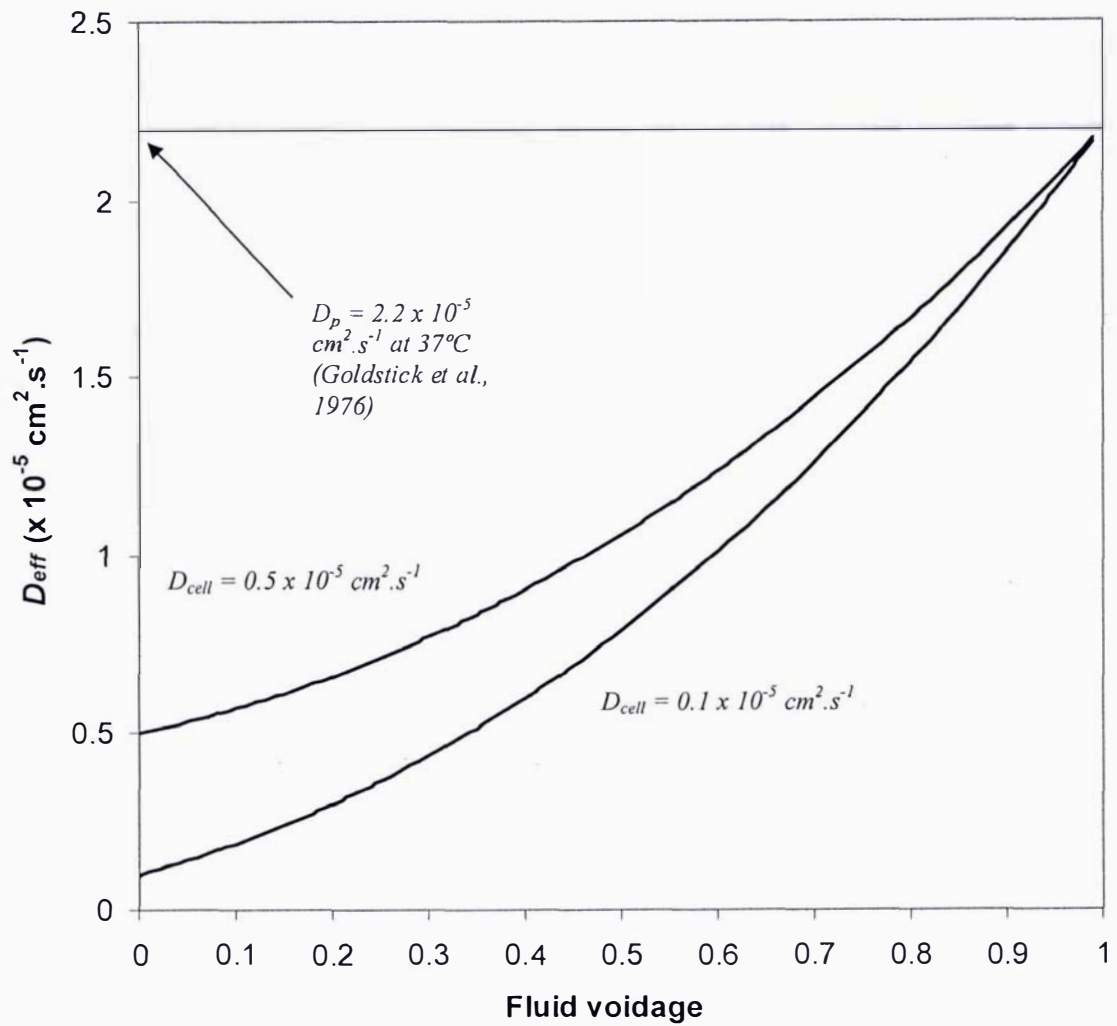
Figure 3.13   The effect of fluid voidage on the effective diffusion coefficient (D_{eff}) at low (0.1 x 10^{-5} $cm^2.s^{-1}$) and high (0.5 x 10^{-5} $cm^2.s^{-1}$) values of D_{cell} according to equation 3.20. Included is the value for the oxygen diffusion coefficient in human plasma (D_p).

Figure 3.14 shows the relationship between fluid voidage and the distance from the follicle centre at which the follicle becomes anoxic, using parameters both favourable and unfavourable to oxygen transport. As voidage increases oxygen penetrates further into the follicle. Using favourable parameters, oxygen just reaches the oocyte when $\varepsilon = 0.26$. Using unfavourable parameters, oxygen does not reach the oocyte surface until the voidage reaches approximately $\varepsilon = 0.59$.

These results suggest that oxygen can reach the oocyte in a large pre-antral follicle provided a certain level of voidage is achieved. This level of voidage may fall within a likely range of 0.26 to 0.59. The lower end of this range falls within the range of normal tissue whilst the upper end does not, and is closer to that reached by some tumour tissue. The conclusion that oxygen can reach the oocyte in large pre-antral follicles when voidage is considered is in contrast to what was shown when voidage was assumed not to exist. The idea that oxygen can reach the oocyte may help to explain the fact that the oocyte undergoes considerable growth as a pre-antral follicle progresses from small to large.

These results also imply that once the follicle has grown large enough, it will reach a critical size beyond which oxygen will never reach the oocyte for a given voidage level. The size of such a follicle can be calculated by setting equation 3.23 equal to zero, r equal to the radius of the oocyte (r_0) and solving for r_f. The result is equation 3.25.

$$r_{fcrit} = \sqrt{r_o^2 + \frac{6D_g C_0}{R_g (1 - \varepsilon)}} \tag{3.25}$$

Equation 3.25 calculates the critical follicle radius above which no oxygen will reach the oocyte surface. The relationship between r_{fcrit} and fluid voidage is shown in Figure 3.15 for parameter estimates both favourable and unfavourable for oxygen transport. The feasible region of Figure 3.15 represents the region over which voidage of a follicle could vary ($0.06 < \varepsilon < 0.6$), as previously described for normal and tumour type tissue. This being the case, the figure suggests that a follicle with low voidage ($\varepsilon = 0.06$) will not be able to grow larger than approximately $r_f = 63$ to 155

68

μm if oxygen is to be maintained at the oocyte surface. A follicle with high voidage (ε=0.6) will not be able to grow larger than approximately r_f= 205 to 350 μm if oxygen is to be maintained at the oocyte surface. So considering favourable and unfavourable parameter estimates over the range of feasible voidages, this work suggests that pre-antral follicles will be unlikely to be capable of growing larger than approximately 63 to 350 μm in radius. This concept may have important implications as to why the follicular antrum forms.

Although this range is wide it does include the value of 400 μm (r_f=200 μm) given by McNatty (1978) as the diameter of the follicle at which the antrum first forms in humans. It is possible that the formation of the antrum is a process driven by mass transport limitations encountered when the follicle reaches $r_{fcrit.}$. If this is the case, Figure 3.15 would suggest variability in the size at which the antrum forms depending on the conditions a particular follicle is presented with. No indication in the variability of the size of the follicle at antrum formation is given by McNatty (1978). The formation of the antrum and the role it might play in oxygen transport is considered in the following chapter.

3.3.4 The assumption of no oocyte

The assumption of no oocyte in the pre-antral follicle model of Gosden & Byatt-Smith (1986) (although not discussed by the authors) seems a fair one given that their results suggested that no oxygen reaches even the general vicinity of the oocyte.

This work has shown that under various conditions it is indeed possible (even likely) that oxygen will reach the oocyte. The purpose has been to lay the foundation for the modelling of the antral/pre-ovulatory follicle whilst at the same time improving the understanding of oxygen transport at this earlier stage. This improved understanding has been obtained simply by acknowledging the oocyte's position relative to the oxygen levels predicted in its absence. In this regard addition of the oocyte will further complicate the mathematical relationships but likely give little improvement in the understanding of the general phenomena described by the simpler form of the model.
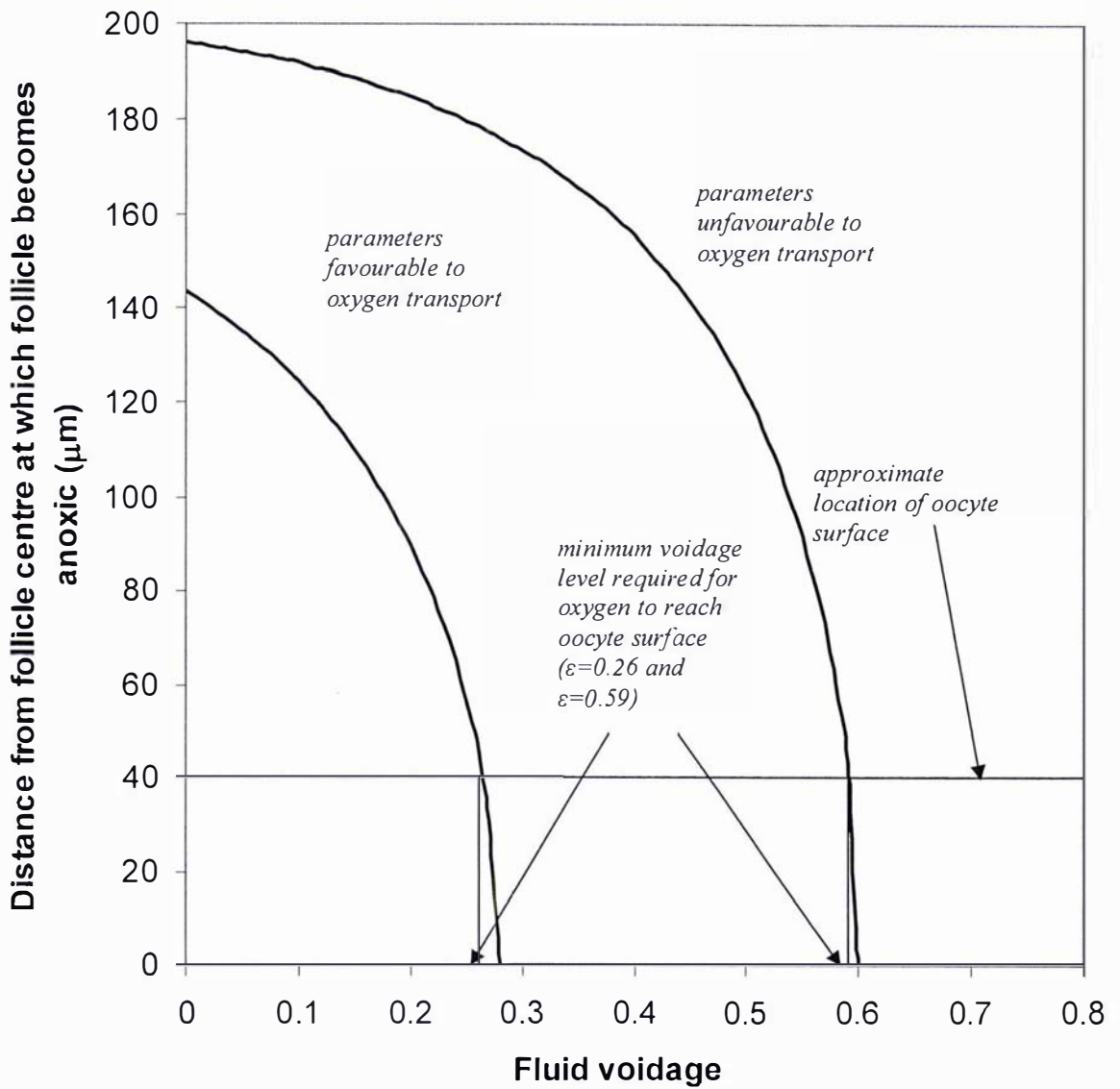
Figure 3.14   Effect of fluid voidage on the distance from the follicle centre at which a large (r_f=200 μm) pre-antral follicle becomes anoxic using parameter estimates favourable and unfavourable to oxygen transport. The most favourable parameter combination is defined as high C_o, high D_g, and low R_g, and vice versa for the least favourable parameter combination, where high and low are the upper and lower ends respectively of the range for each parameter presented in Table 3.3.
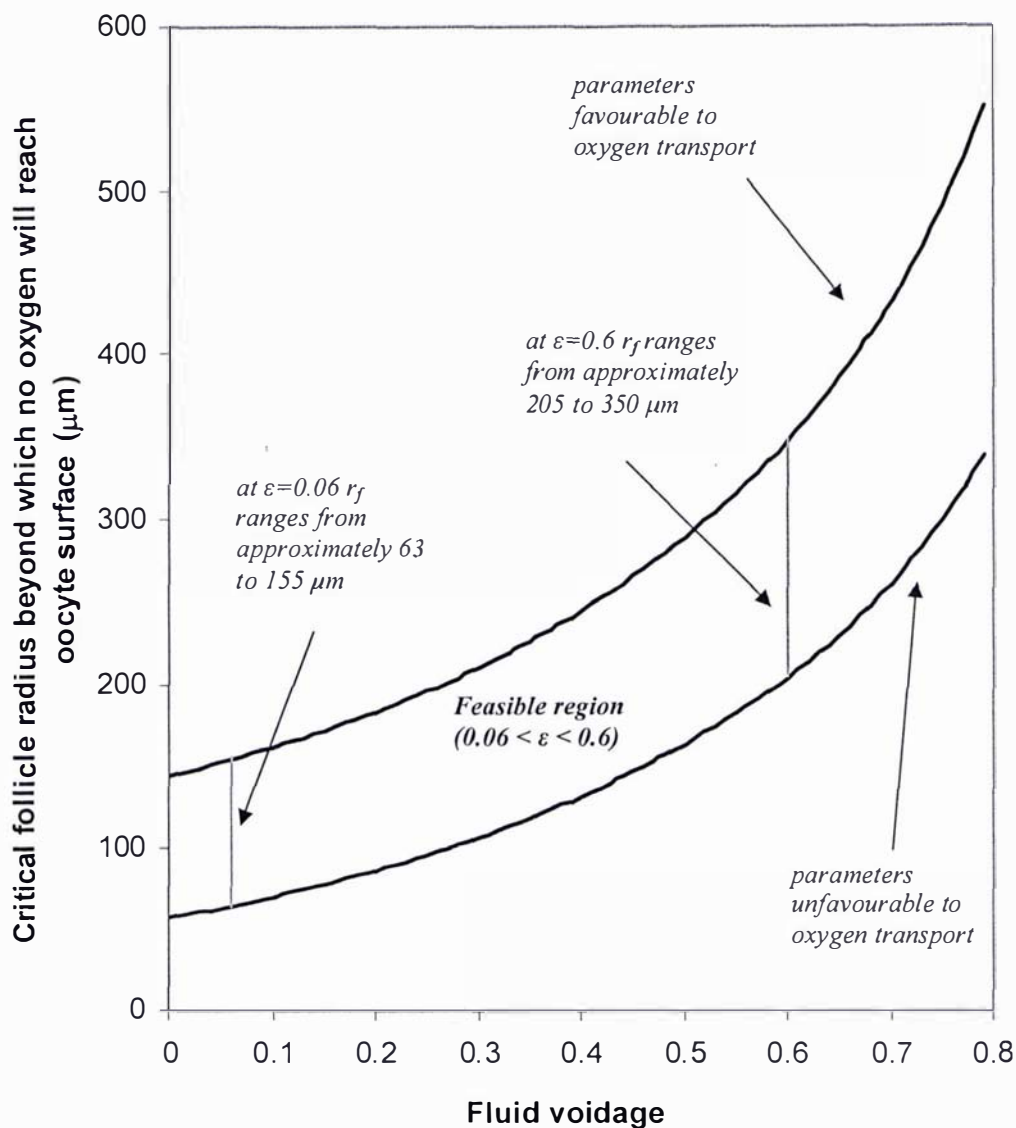
Figure 3.15   Critical follicle radius beyond which no oxygen reaches oocyte surface, as a function of fluid voidage using parameter estimates favourable and unfavourable to oxygen transport (r_o= 40 μm). The most favourable parameter combination is defined as high C_o, high D_g, and low R_g, and vice versa for the least favourable parameter combination, where high and low are the upper and lower ends respectively of the range for each parameter presented in Table 3.3.

Furthermore, parameter estimates of the oxygen consumption of the oocyte at the pre-antral stage are not available, thus making the addition of the oocyte somewhat academic. For these reasons the assumption of no oocyte was also justified here. Addition of the oocyte to the more complex antral/pre-ovulatory model is considered in the following chapter.

Figure 3.15 also suggests that at any given follicle size a certain critical level of voidage needs to be achieved if any oxygen is to reach the surface of the oocyte. At r_f = 200 µm (the radius of a large pre-antral follicle and the follicle size at which the antrum is reported to first appear) this critical level of voidage is predicted to range from $0.26 < \varepsilon < 0.59$ as predicted by Figure 3.14 (note that this same range can be obtained via Figure 3.15 from the voidage levels at which r_f=200 µm intersects with the curves for unfavourable and favourable parameter estimates). This range falls mainly outside the range reported for normal tissue ($0.06 < \varepsilon < 0.30$). In order for the oocyte to receive oxygen, the follicle would then need to increase its voidage to levels found in and above those found in tumours. It is possible that the formation of the antrum represents an alternative to high voidage.

3.3.5 The assumption of constant oxygen consumption rate of the granulosa cells (R_g)

The oxygen consumption of biological cells is not constant. Rather it varies as a function of concentration. At high oxygen concentrations oxygen consumption is constant but declines as concentration reduces. Often oxygen consumption rates are assumed constant, and when oxygen levels are close to the typical range of venous and arterial blood this assumption is indeed valid. However, this assumption breaks down as conditions approach hypoxia. Because this model is concerned with such low oxygen conditions it is worthwhile examining the oxygen consumption of the granulosa cells as a function of oxygen concentration. This can be done by describing the oxygen consumption of granulosa cells using Michaelis-Menton kinetics, which oxygen consumption is reported to follow (Truskey *et al.,* 2004). This is described by equation 3.26.

$$R_g = \frac{R_{g\,max}\,C}{K_m + C} \qquad (3.26)$$

Where K_m is the Michaelis-Menton constant, and R_{gmax} is the maximum rate of oxygen consumption by the granulosa cells (this will be the same as the previous constant rate assumed). For biological tissue K_m varies between 0.5 μM to 3.0 μM (Richmond *et al.*, 1999, Fournier, 1998, Truskey *et al.*, 2004).

Because R_g is a function of C, equation 3.26 cannot simply be substituted into any final derivation, but must be included in the integration. Substituting equation 3.26 into equation 3.8 gives,

$$d\left(r^2 \frac{dC}{dr} \right) = \left(\frac{R_{g\,max}\,C}{K_m + C} \frac{r^2}{D_g} \right) dr \qquad (3.27)$$

which upon integration gives

$$r^2 \frac{dC}{dr} = \frac{R_{g\,max}\,C}{K_m + C} \frac{r^3}{3D_g} + K_1 \qquad (3.28)$$

Since symmetry exists about the centre of the follicle ($dC/dr=0$, at $r=0$), and therefore $K_1=0$. Rearrangement of equation 3.28 gives,

$$\frac{K_m + C}{R_{g\,max}\,C} dC = \frac{r}{3D_g} dr \qquad (3.29)$$

which upon integration gives,

$$K_m \ln C + C = \frac{R_{g\,max}\,r^2}{6D_g} + K_2 \qquad (3.30)$$

Since at $r=r_f$, $C=C_0$, then

$$K_2 = K_m \ln C_0 + C_0 - \frac{R_{g\,max} r_f^2}{6 D_g} \tag{3.31}$$

Substitution of 3.31 into 3.30 and rearrangement gives,

$$K_m \ln \frac{C}{C_0} + (C - C_0) = -\frac{R_{g\,max}}{6 D_g}(r_f^2 - r^2) \tag{3.32}$$

Equation 3.32 gives the oxygen concentration at any position r in the pre-antral follicle when Michaelis-Menton oxygen consumption kinetics are considered. Equation 3.32 cannot be solved explicitly, and hence requires an iterative solution (for the purposes of comparison, equation 3.32 assumes no voidage). Setting equation 3.32 equal to zero and solving for the distance from the follicle centre at which the follicle becomes anoxic is not possible in this case. However, equation 3.32 can be used to provide a comparison with the solution of equation 3.14 for the oxygen profiles through the pre-antral follicle.

Figure 3.16 compares the solutions of equation 3.14 to that of equation 3.32 at both high and low values of K_m for a large pre-antral follicle. All parameter values other than r_f are at their nominal values (see Table 3.3).

Figure 3.16 shows that when Michaelis-Menton kinetics are considered oxygen concentration reduces more gradually at low oxygen concentrations than when the consumption rate is constant. At a high K_m value this is more dramatic.

Using Michaelis-Menton kinetics the oxygen concentration tends toward zero but does not reach a true anoxic state (although for biological purposes it is still essentially anoxic). This suggests that even under hypoxic conditions some oxygen may still be able to reach the oocyte surface. However, such small oxygen concentrations are unlikely to be of any real consequence for the oocyte. Using a high K_m value oxygen only penetrates the follicle an extra 5 μm (after which its concentration is $<1\times10^{-5}$mmol.m^{-3}, which can be considered practically zero) when

74

compared with constant respiration. Thus, even with a favourable K_m value the effect of Michaelis-Menton kinetics is small. Without any real knowledge of the oocyte's respiratory activity in a pre-antral follicle it is difficult to speculate any further than this.

Although Michaelis-Menton kinetics allow oxygen to penetrate further into the follicle, what may be of more significance is the point at which R_{gmax} can no longer be sustained. This concept is shown in Figure 3.17. Figure 3.17 illustrates that there exists a critical oxygen concentration below which R_g cannot be sustained at R_{gmax}. If C_{crit} is defined as the oxygen concentration at which $R_g = 0.99\ R_{gmax}$ then equation 3.26 can be solved (iteratively) over the feasible range of K_m (0.0005 to 0.003 mol.m^{-3}), to give a feasible range for C_{crit}. This gives a range of C_{crit} from 50 μM to 297 μM. This range is very wide, particularly when compared with the arterial blood oxygen concentrations (130 μM to 150 μM). The upper range of C_{crit} would suggest that even cells experiencing the high concentrations of arterial blood will not be able to respire maximally. With such a wide range in K_m little can be gained from pursuing a model which includes Michaelis-Menton kinetics. Still, equation 3.14 can be set equal to C_{crit} and solved for r giving equation 3.33.

$$r = \sqrt{r_f^2 + \frac{6D_g(C_{crit} - C_0)}{R_g}}$$
(3.33)

where $D_g = D_{eff}$

Or, if voidage is to be included equation 3.33 can be solved in the same way giving equation 3.34

$$r = \sqrt{r_f^2 + \frac{6D_g(C_{crit} - C_0)}{R_g(1 - \varepsilon)}}$$
(3.34)

where $D_g = D_{eff}$

75
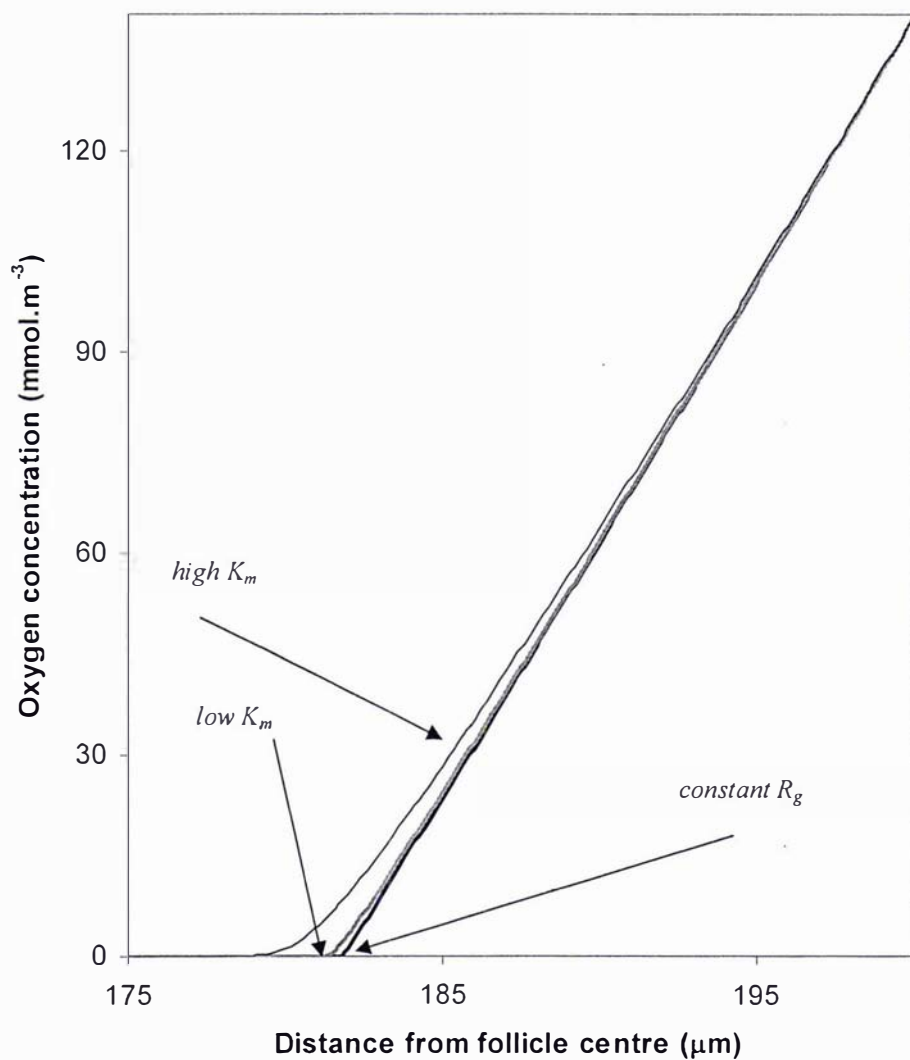
Figure 3.16   Oxygen concentration profiles in a large pre-antral follicle under the assumption of constant granulosa cell oxygen consumption (R_g) compared with Michaelis-Menton kinetics.
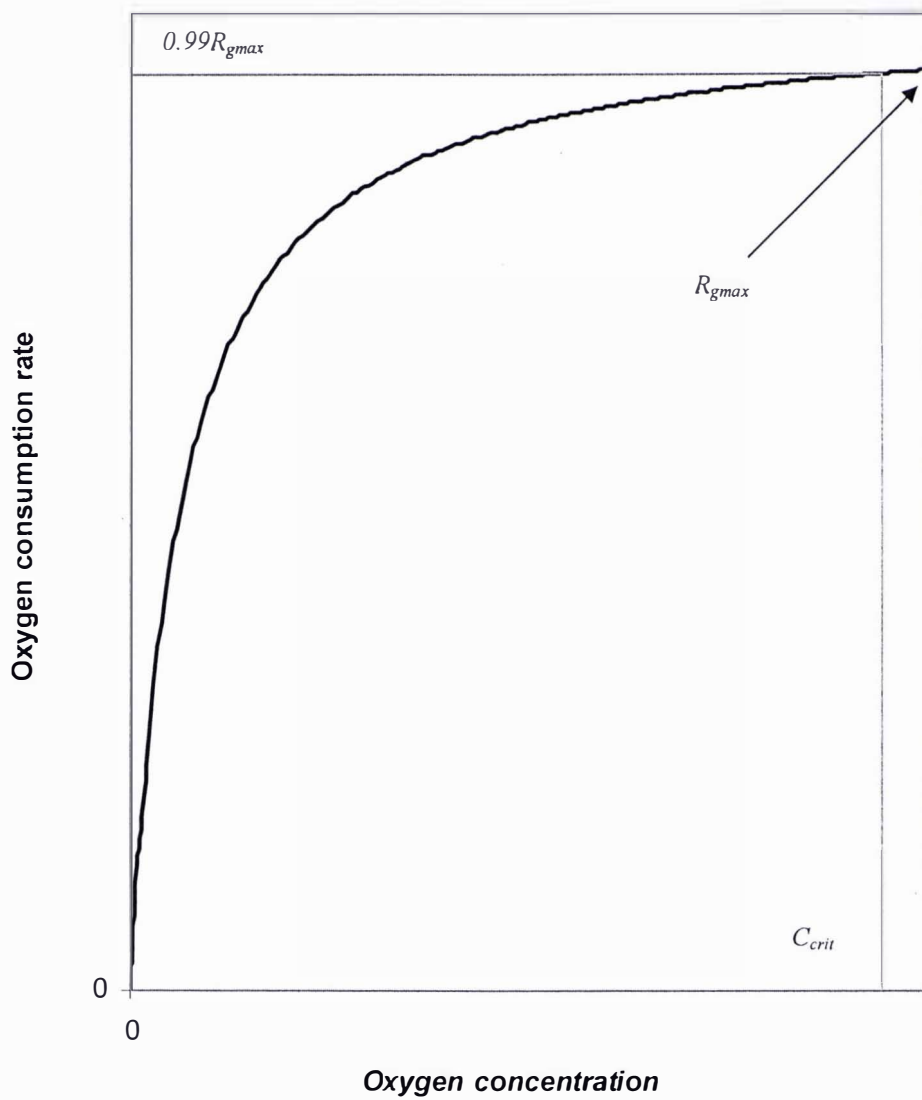
Figure 3.17   Concentration dependence of oxygen consumption described by Michaelis-Menton kinetics (not to scale).

Equations 3.33 and 3.34 can be used to calculate the distance from the centre of the follicle at which maximal respiration is no longer possible under the assumptions of no voidage and voidage respectively. Alternatively C_{crit} (and hence R_g) could just as easily be any concentration which may have some significance. For example, it may be the concentration at which cells are known to be compromised, and this could possibly be somewhat lower than C_{crit} for marginal sub-maximal respiration.

In spite of the lack of information about C_{crit} some useful general statements can still be made. If voidage is considered, there will exist a critical follicle size beyond which maximal respiration can never be achieved for any given voidage level. Similarly, at any given follicle size a certain critical voidage will be required if respiration is to be maximal.

3.3.6 The assumption of complete vascularisation

The assumption that each follicle is surrounded completely by its own vascularisation is not always true for antral follicles, and is unlikely to always be the case for pre-antral follicles. Both the amount and distribution of vascularisation around a follicle are likely to be important.

If a follicle is considered to be surrounded by areas of vascularisation and areas of no vascularisation which are distributed symmetrically, with each patch being infinitely small, then reducing the value of C_0 down from its arterial value can be used to simulate a reduced area of vascularisation.

This concept is described by equation 3.35.

$$C_{0mean} = C_{arterial} \times \frac{\%vasc}{100} + C_{novasc.} \times \frac{(100 - \%vasc)}{100} \qquad (3.35)$$

Assuming in areas of no vascularisation the oxygen concentration is zero, then $C_{novasc} = 0$. Hence, equation 3.35 can be solved to give the % vascularisation.

$$\%vasc = \frac{100C_{0mean}}{C_{arterial}} \qquad (3.36)$$

where *%vasc* is defined here as the mean symmetrical vascularisation.

Equations 3.35 and 3.36 represent a simple way of examining the effect of reduced vascularisation whilst maintaining the convenience of an analytical solution. Whilst they are useful as an illustrative tool the magnitude of the results should be treated with care. A comparison with the values calculated using this method and that of finite element modelling is detailed in the following section.

It has been demonstrated earlier (see Figure 3.11) that under parameter estimates both favourable and unfavourable to oxygen transport, the small pre-antral follicle receives oxygen at the oocyte surface. This was under the assumption of complete vascularisation. Figure 3.18 shows the effect of variation in mean symmetrical % vascularisation on the distance from the follicle centre at which a small pre-antral follicle becomes anoxic. The figure suggests that under favourable and unfavourable conditions for oxygen transport respectively, between approximately 3% and 30% vascularisation will be required for oxygen to just reach the oocyte surface. So, although under the assumption of complete vascularisation it was shown that the oocyte will always have access to oxygen, when possible limitations in blood supply are considered it can be seen that a certain critical level of vascularisation will be required to meet this same end.

Figure 3.15 demonstrated that at any given void level there will be a critical follicle radius beyond which no oxygen will reach the oocyte surface. Figures 3.19 and 3.20 show the effect of variation in vascularisation on this result at both favourable and unfavourable parameter values for oxygen transport respectively. The results show that, at a given fluid voidage, the size of the follicle at which no oxygen reaches the oocyte is reduced, at reduced vascularisation. In the same way, at any given follicle size, if the oocyte is to see any oxygen, an increased level of voidage will be required at a reduced vascularisation level.

For example, at a follicular diameter of 400 μm (size at which antrum forms, $r_f = 200$ μm), under favourable conditions for oxygen transport, Figure 3.19 shows that a follicle with a void fraction of 0.3 would require between 80 to 100% vascularisation if oxygen is to reach the oocyte surface. If this same follicle only had 20% vascularisation Figure 3.19 shows that the follicle would require a void fraction of around 0.7 to ensure that oxygen reaches the oocyte. This is unlikely to be feasible as it falls outside the range of voidage found in biological tissues. It is possible that the level of vascularisation may therefore play a role in early atresia of pre-antral follicles. Variation in vascularisation may also be linked to possible variation in the size at which the antrum forms.

Using parameter estimates unfavourable to oxygen transport, Figure 3.20 shows that at $r_f = 200$ μm, even at a high voidage level of 0.6, the follicle will require almost 100% vascularisation if the oocyte is to receive any oxygen. If the voidage is much lower than this, then even a 100% vascularised follicle will be incapable of delivering oxygen to the oocyte surface.

Again, this may suggest that poorly vascularised follicles may be destined for earlier atresia as a result of hypoxic conditions, and this could also be linked to variability in antrum formation.

For this work to gain more practical insight, observations on the voidage levels found in pre-antral follicles may be helpful. Data on the levels of follicle voidage and how this might change over time could provide useful information on the mechanisms of follicular growth and mass transport.

3.3.7 Variability in vascular distribution

Investigating the effect of variable vascular distribution requires the use of non-uniform boundary conditions. The use of such boundary conditions makes analytical solutions very difficult. For this reason the finite element method has been implemented with the aid of the multi-physics software modelling package Femlab

3.1 (Comsol, Stockholm, Sweden). In Femlab the basic approach to finite element modelling involves four sequential steps;

1.   Geometry modelling – here the geometry is defined either using the Femlab interface and drawing tools, or through equations defined in Matlab with which Femlab can interface.   The pre-antral follicle requires only a sphere.

2.   Boundary and sub-domain settings – here the boundary conditions can be described either as constants or by equations.   Sub-domain settings describe the properties of the material(s) of the geometry. The outer surface of a sphere is divided into eight equal regions by default. In the case of the pre-antral follicle each segment will be set either to $C_{arterial}$ or to no vascularisation using the insulation/symmetry boundary condition.   The sub-domain setting for diffusive mass transport with reaction in the pre-antral follicle will simply involve defining the diffusion coefficient and rate of oxygen consumption.

3.   Meshing – here Femlab generates a mesh structure within the defined geometry.   This mesh can be refined to improve the accuracy of the numerical solution at the expense of processing time.

4.   Solution and post processing – having carried out steps 1 through 3 Femlab computes the finite element solution to the problem defined. The results are available and can be viewed in a variety of graphical formats.

Femlab's division of a sphere's surface into 8 equal segments potentially allows vascularisation to be dictated from 0 to 100% at increments of 12.5%. It is sensible to investigate the effect of variation in vascular distribution for a follicle where the supply of oxygen to the oocyte is limiting (only just reaches the oocyte surface), or either side of this where the oocyte will be better supplied with oxygen as well as starved of it. This was done using the nominal values of C_o, D_g, and R_g. Figure 3.21 is equivalent to Figures 3.19 and 3.20 other than it is produced at these nominal values. Figure 3.21 can be used to select the follicle which will be in the limiting state described.
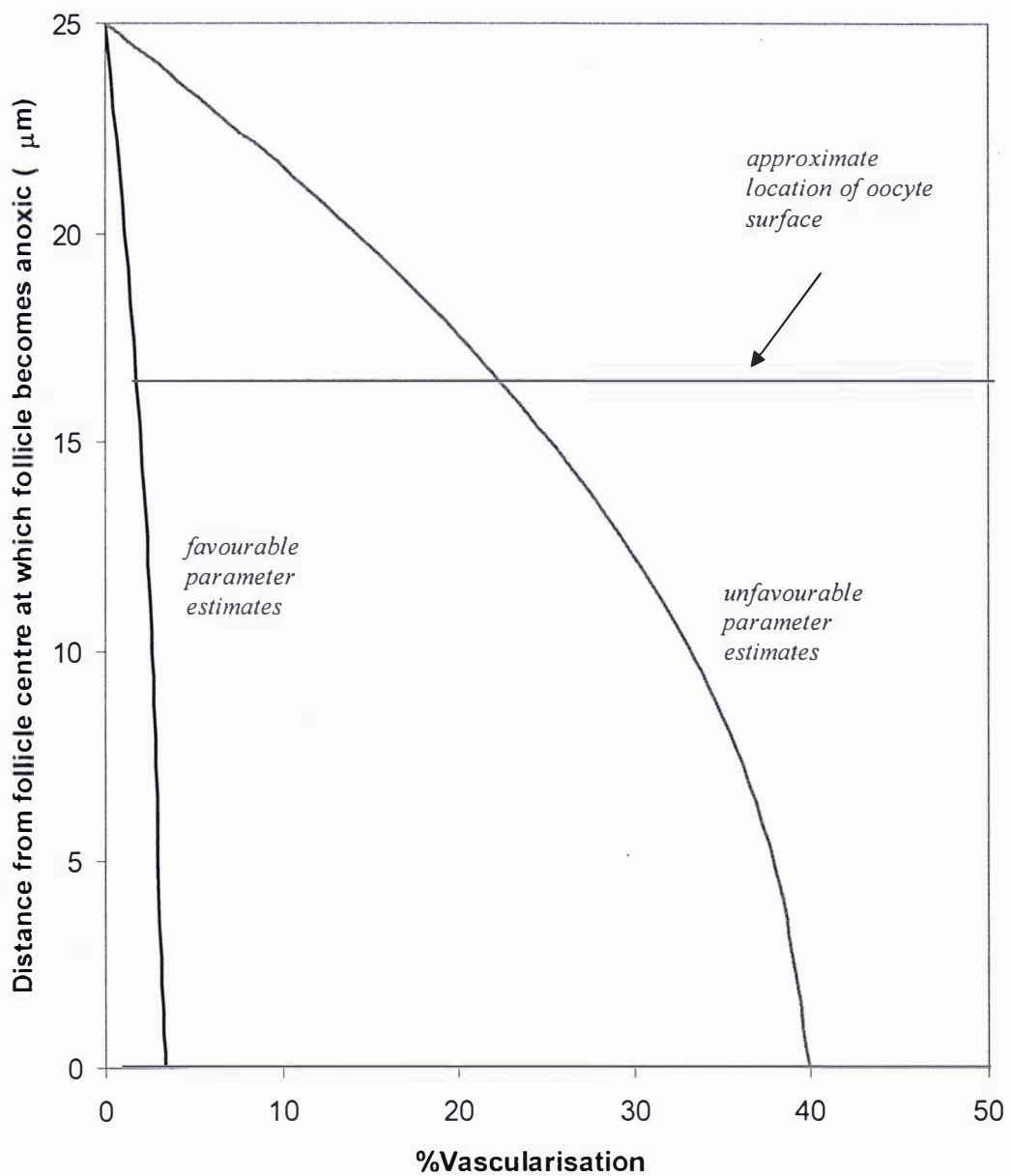
Figure 3.18 Relationship between mean symmetrical % vascularisation and the distance at which a small (r_f=25 μm) pre-antral follicle becomes anoxic for favourable and unfavourable parameter estimates. Note that using favourable estimates less vascularisation is required to maintain oxygen at the oocyte surface (~3% compared to ~30%).
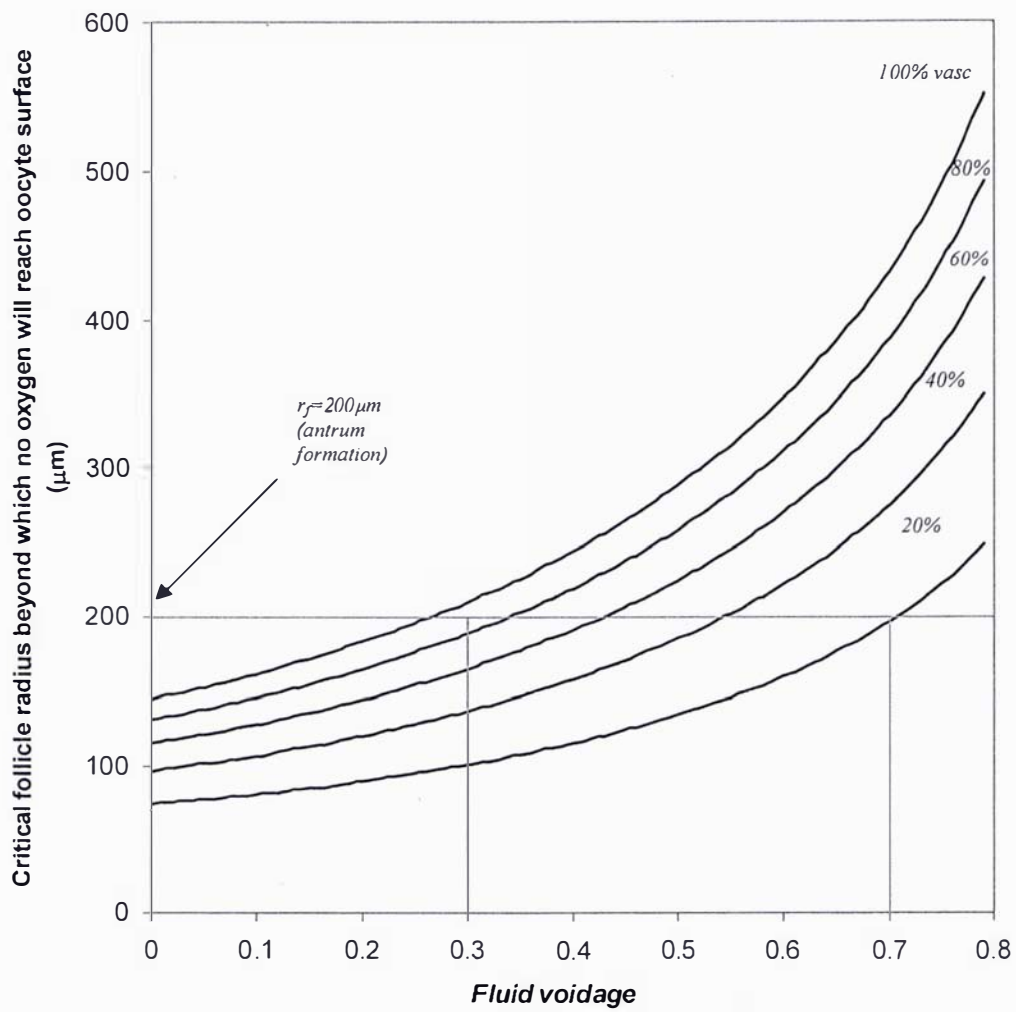
Figure 3.19 Critical follicle radius beyond which no oxygen reaches oocyte surface as a function of fluid voidage using parameter estimates favourable to oxygen transport (r_o=40 μm) at various vascularisation levels. Intersections of grey lines illustrate two example follicles each with a radius of 200 μm and with differing voidage of 0.3 and 0.7.
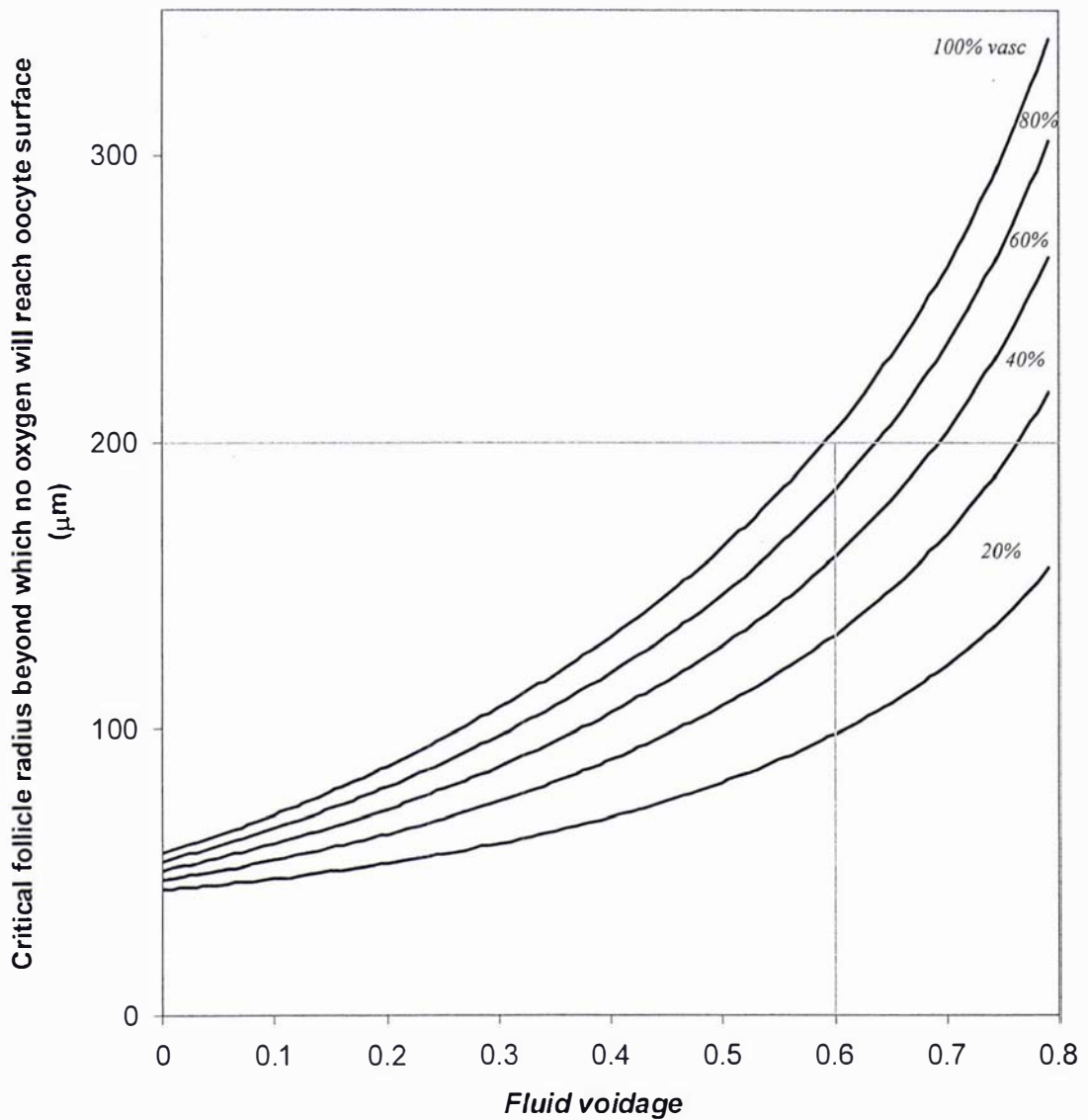
Figure 3.20 Critical follicle radius beyond which no oxygen reaches oocyte surface as a function of fluid voidage using parameter estimates unfavourable to oxygen transport (r_o=40 µm) at various vascularisation levels. Intersection of grey line illustrates an example follicle with a radius of 200 µm and a voidage of 0.6.

Somewhat arbitrarily choosing 50% vascularisation and $\varepsilon = 0.3$ (although this is intuitively interesting as it represents the voidage cut-off between normal and tumour type tissue) the size of the follicle can be read off the graph, and is 108 μm (calculated from equation 3.25 for an oocyte radius of 40 μm). Having determined that a follicle of radius 108 μm, with 50% symmetrical vascularisation, and a void fraction of 0.3 will only marginally allow oxygen to the oocyte surface, this follicle can be used in Femlab to view the results of varying vascular distribution at this marginal level, but also either side of this.

The solution for various vascular distributions at 25% vascularisation is shown in Figure 3.22.

Figure 3.22(a) shows the Femlab solution using 25% mean symmetrical vascularisation as previously defined. Note that the deep blue regions of Figure 3.22 indicate low oxygen levels, deep red indicates high oxygen levels, with other colours indicating oxygen levels in between (see scales on figure). The Femlab solution is the same in all three planes through the centre of the follicle (the x, y, and z planes), and is also identical to the analytical solution as would be expected. Figure 3.22(b) shows the solution when 25% of the follicle boundary is vascularised at the concentration of arterial blood. The two 12.5% boundaries are arranged in opposite segments so that the distribution is as even as possible. This results in profiles which are the same in each of the three planes through the centre. The solution is clearly different from the mean symmetrical case with large anoxic regions about the unvascularised boundaries. The areas that are vascularised allow oxygen to penetrate further toward the oocyte than in the mean symmetrical solution. Figures 3.22 (c and d) result from stacking the two 12.5% regions side by side so as to give the most uneven distribution possible. This results in two planes giving the same concentration profiles relative to the vascularised regions (3.22(c)) with one unique plane (3.22(d)). This results in reduced oxygen penetration in two planes with increased penetration in the other.
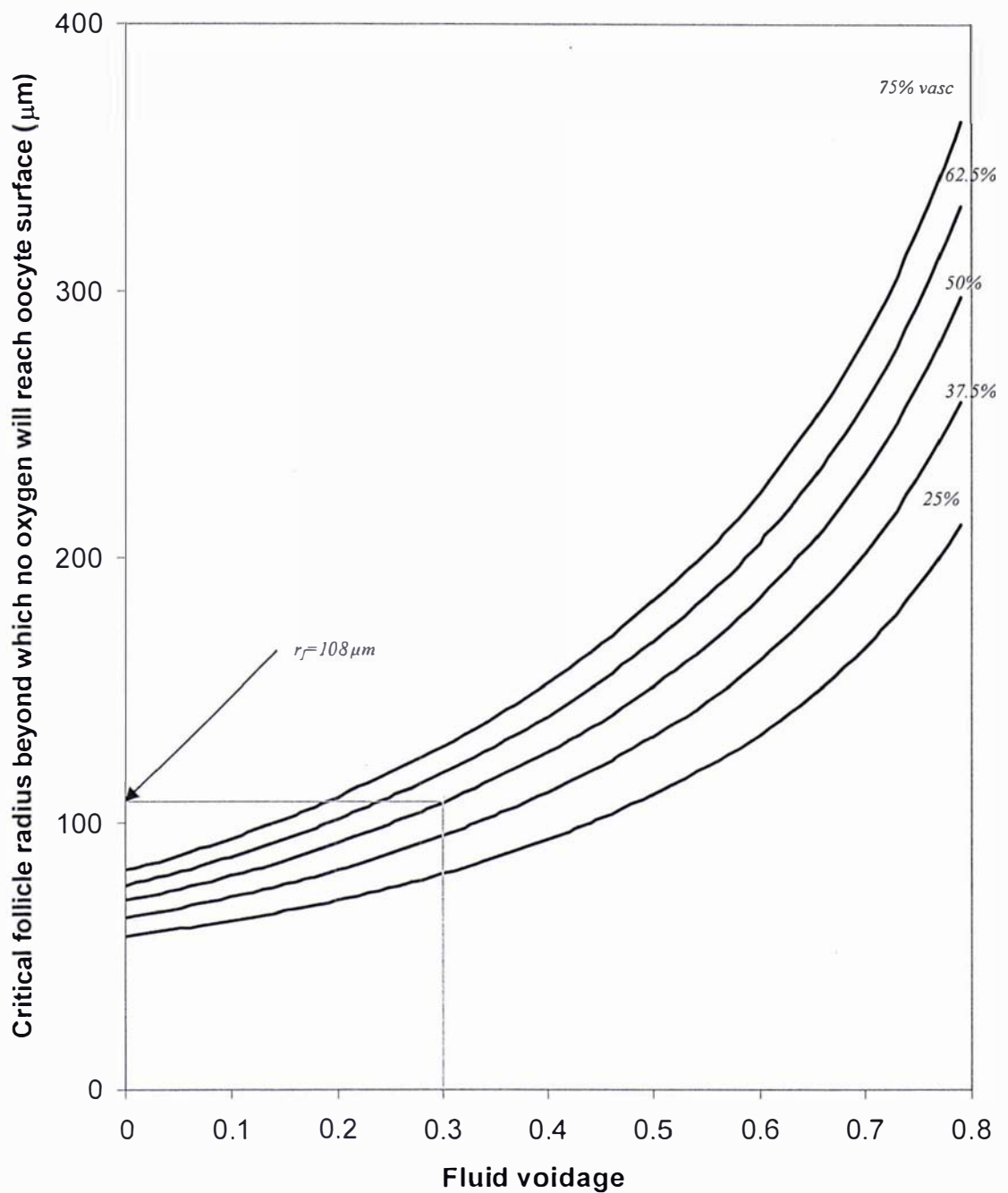
Figure 3.21   Critical follicle radius beyond which the oocyte will receive no oxygen
(r_o = 40 µm) at vascularisation increments consistent with Femlab's spherical
divisions and at nominal values for oxygen transport. Illustrated is the selection of a
follicle with 0.3 voidage and 50% vascularisation.

Figures 3.23 and 3.24 describe the same results for 50% and 75% vascularisation respectively. In both cases the most even arrangement of vascular distribution results in three identical planes through the centre relative to the areas of vascularisation, as was observed for 25% vascularisation. Once again the uneven adjacent stacking of vascularised areas results in two identical planes and one unique one relative to the areas of vascularisation.

Compared with 25% vascularisation the oxygen profiles for 50% and 75% vascularisation are much more even. At 75% vascularisation, uneven stacking of vascularised areas results in reduced variability compared with 50% vascularisation. This suggests that regardless of the vascular distribution, higher levels of vascularisation will have a reduced tendency to form anoxic regions, and hence allow oxygen to reach the oocyte. The oocyte's position at or near the centre of the follicle means that when vascular distribution is uneven it will be less likely to be found in a totally anoxic region. The key result is that distribution of vascularisation can cause large differences in oxygen profiles, particularly when vascularisation is low.

Also of importance is how the various vascular distributions impact on the total oxygen, both in the follicle, and within the area that would be occupied by the oocyte. This information can be obtained in the mean symmetrical case by integration of the analytical solution, and in the other cases integrating the subdomains numerically in Femlab.

For a follicle with voidage, the total amount of oxygen (moles) will be given by the integral of equation 3.23 between the limits of $r = r$ and $r = r_{anoxic}$ (equation 3.24) multiplied by the surface area of a spherical shell at any distance r. This is described mathematically by equation 3.37.

$$moles\ of\ oxygen = 4\pi \int_{r=r_{anoxic}}^{r} r^2 \left(C_{0mean} - \frac{R_g(1-\varepsilon)}{6D_g}(r_f^2 - r^2) \right) dr \tag{3.37}$$

Evaluation of this integral yields equation 3.38.

87

$$moles\ of\ oxygen = 4\pi\left(\frac{(r^3 - r_{anoxic}^3)}{3}\left(C_0 - \frac{R_g(1-\varepsilon)r_f^2}{6D_g}\right) + \frac{R_g(1-\varepsilon)(r^5 - r_{anoxic}^5)}{30D_g}\right) \quad (3.38)$$

where $D_g = D_{eff}$

This equation will hold true for all real values of r_{anoxic}. To calculate the amount of oxygen in the follicle, $r=r_f$ is simply substituted into equation 3.38 (solution valid provided $r_{anoxic} < r_f$). Likewise, to calculate the amount of oxygen in the area occupied by the oocyte, $r=r_o$ is simply substituted into equation 3.38 (solution valid provided $r_{anoxic} < r_o$).

Figures 3.25 and 3.26 show the result of the evaluation of this integral for follicle and oocyte respectively using both the analytical solution of equation 3.38 and the numerical value of the integrals for a variety of vascular distributions. The integrals have been divided by the total follicle volume (Figure 3.25) or by the total oocyte volume (Figure 3.26), and hence are expressed as a mean concentration.

Figure 3.25 confirms the non-equivalence of mean symmetrical vascularisation (see equation 3.36 for definition of) with the vascular distributions used in finite element modelling. However, interestingly, in all cases the mean-symmetrical vascularisation produces similar results (although slightly lower) to the finite element uneven distributions. As would be expected, the analytical and finite element solutions are the same in the mean symmetrical case. In all cases these were identical to four significant figures. At all levels of vascularisation the even distribution finite element results show greater total oxygen in the follicle. This is also true for the total oxygen in the oocyte region (Figure 3.26). Also, once again the finite element vascular distributions allow more oxygen to the oocyte region. At 50% vascularisation the mean symmetrical solutions show no oxygen in the oocyte region. At 25% vascularisation none of the vascular distributions allow any oxygen to the oocyte region. At 75% vascularisation the mean oxygen in the oocyte area is the same for both analytical and finite element solutions for the case of mean symmetrical vascularisation.

(a) Femlab mean symmetrical solution, all three planes

(b)Symmetrical distribution, all three planes

(c)Asymmetric distribution, two identical planes

(d)Asymmetric distribution, odd plane
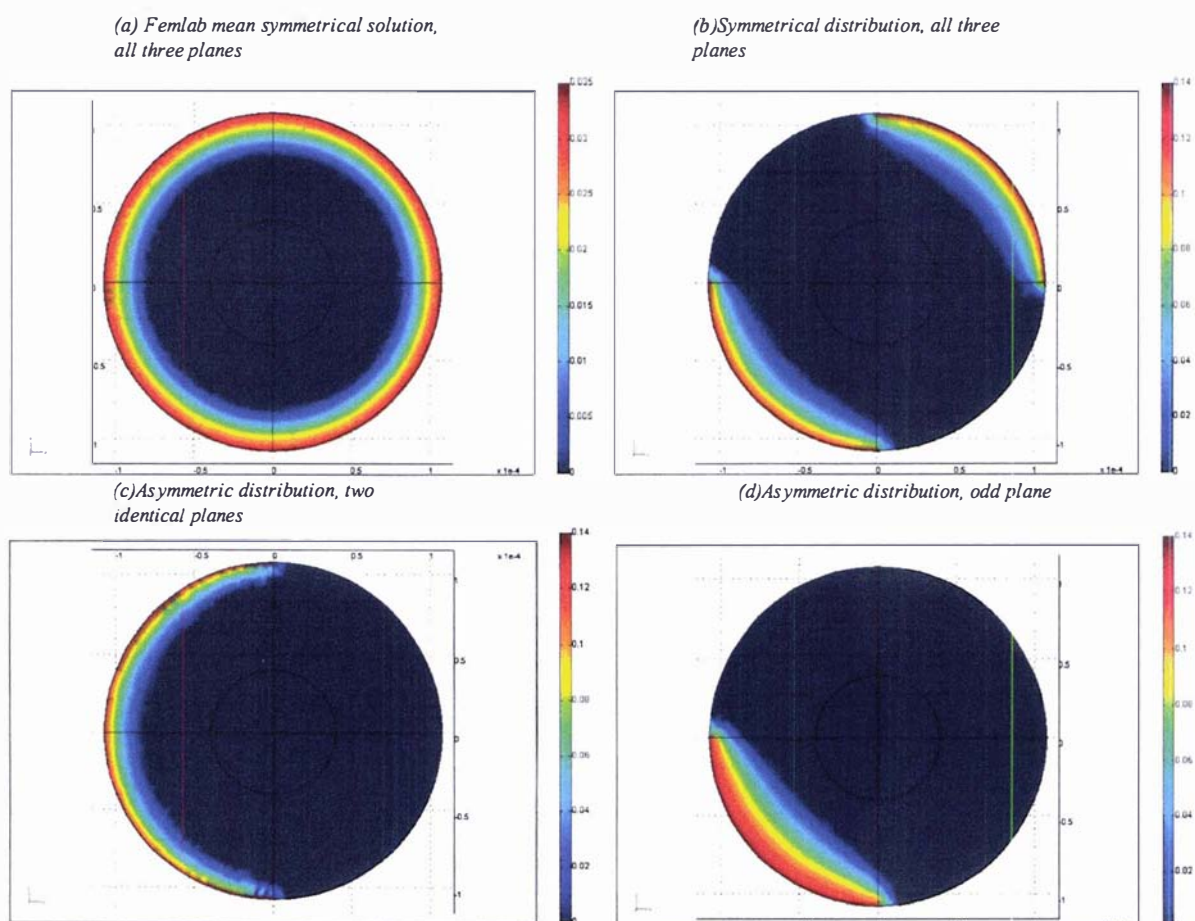
Figure 3.22   Oxygen concentration in a 108 μm radius pre-antral follicle with various vascular distributions (25% vasc, $\epsilon = 0.3$). Concentration scales have units of mol.m^{-3}.

(a) Femlab mean symmetrical solution, all three planes

(b)Symmetrical distribution, all three planes

(c)Asymmetric distribution, two identical planes

(d)Asymmetric distribution, odd plane
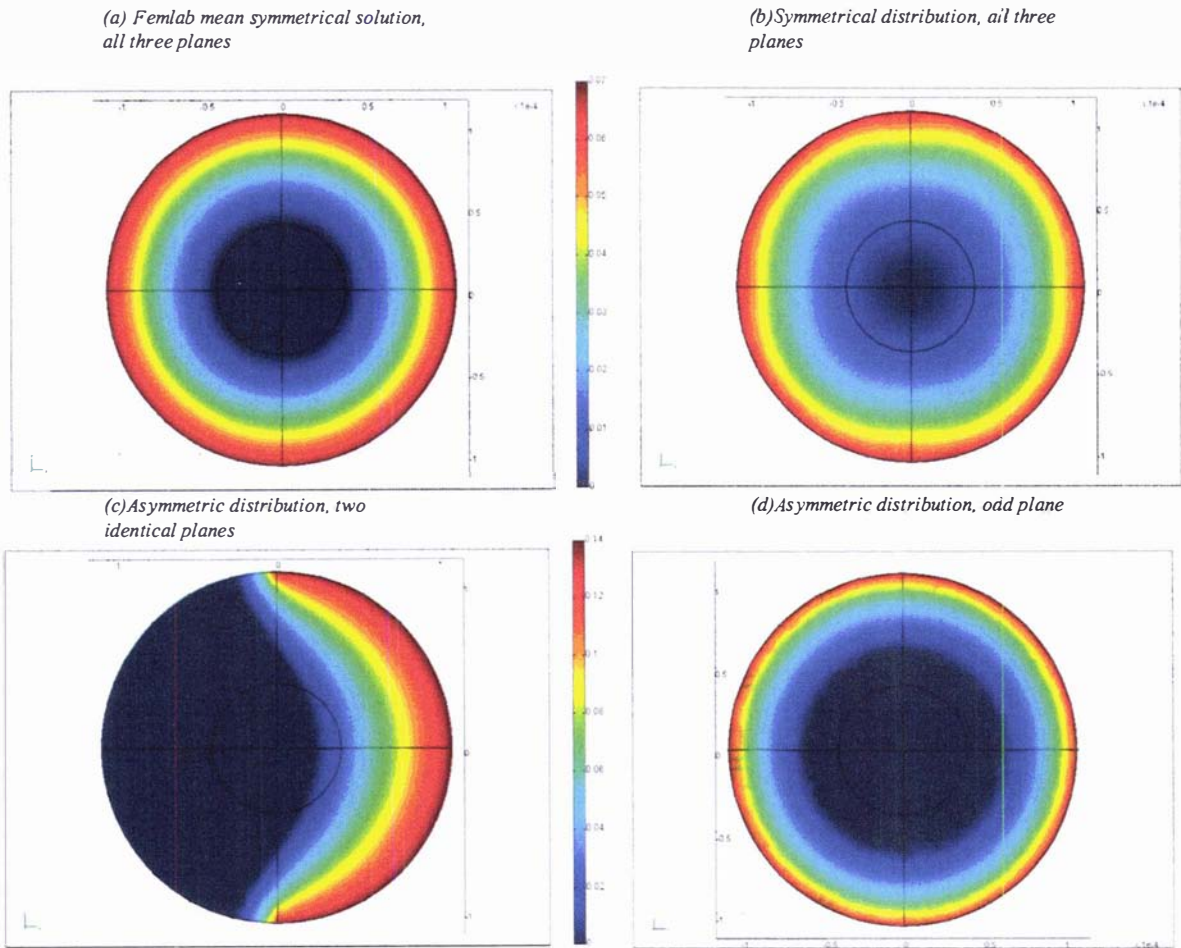
Figure 3.23   Oxygen concentration in a 108 μm radius pre-antral follicle with various vascular distributions (50% vasc, $\epsilon = 0.3$). Concentration scales have units of mol.m^{-3}.

(a) Femlab mean symmetrical solution, all three planes

(b)Symmetrical distribution, all three planes

(c)Asymmetric distribution, two identical planes

(d)Asymmetric distribution, odd plane
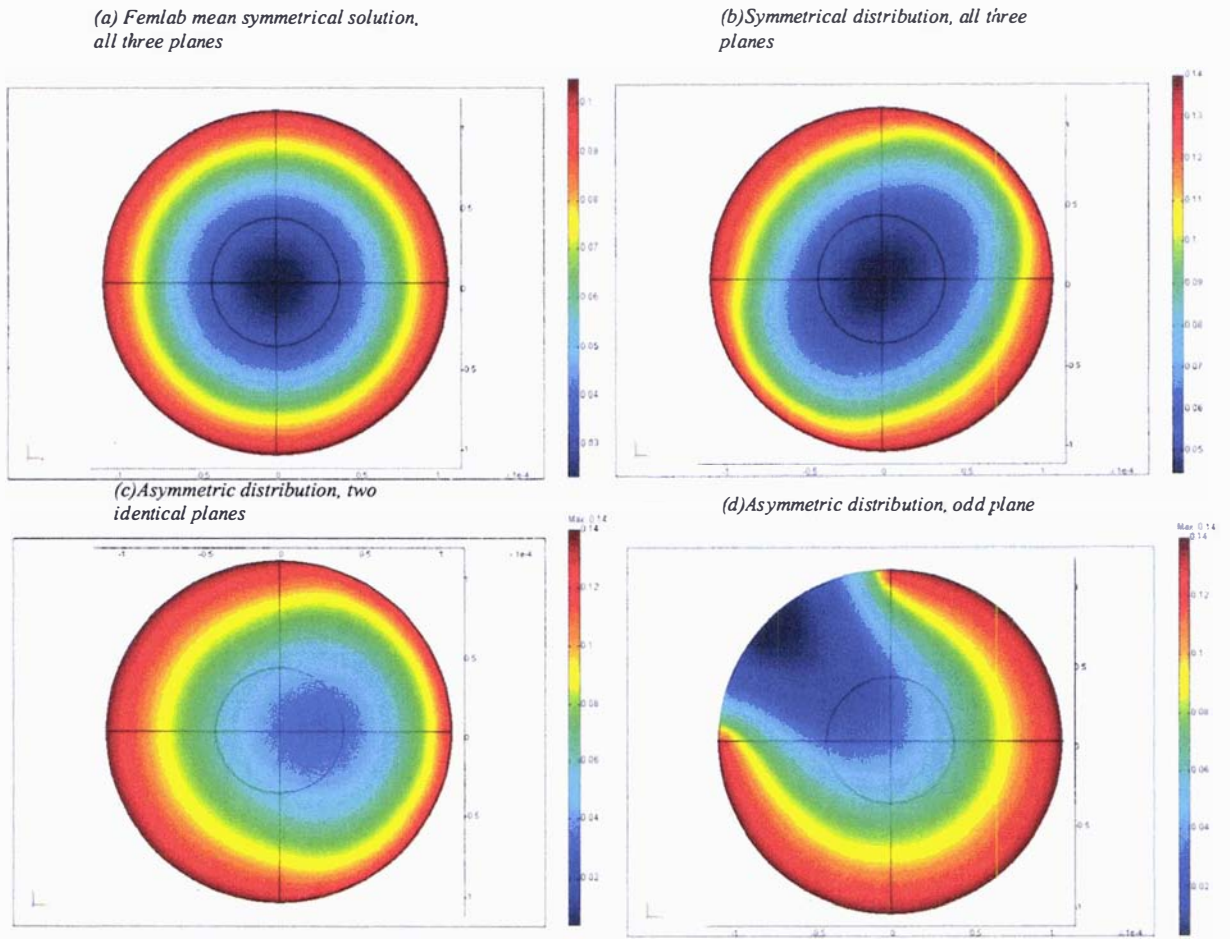
Figure 3.24   Oxygen concentration in a 108 μm radius pre-antral follicle with various vascular distributions (75% vasc, $\epsilon = 0.3$). Concentration scales have units of mol.m^{-3}.
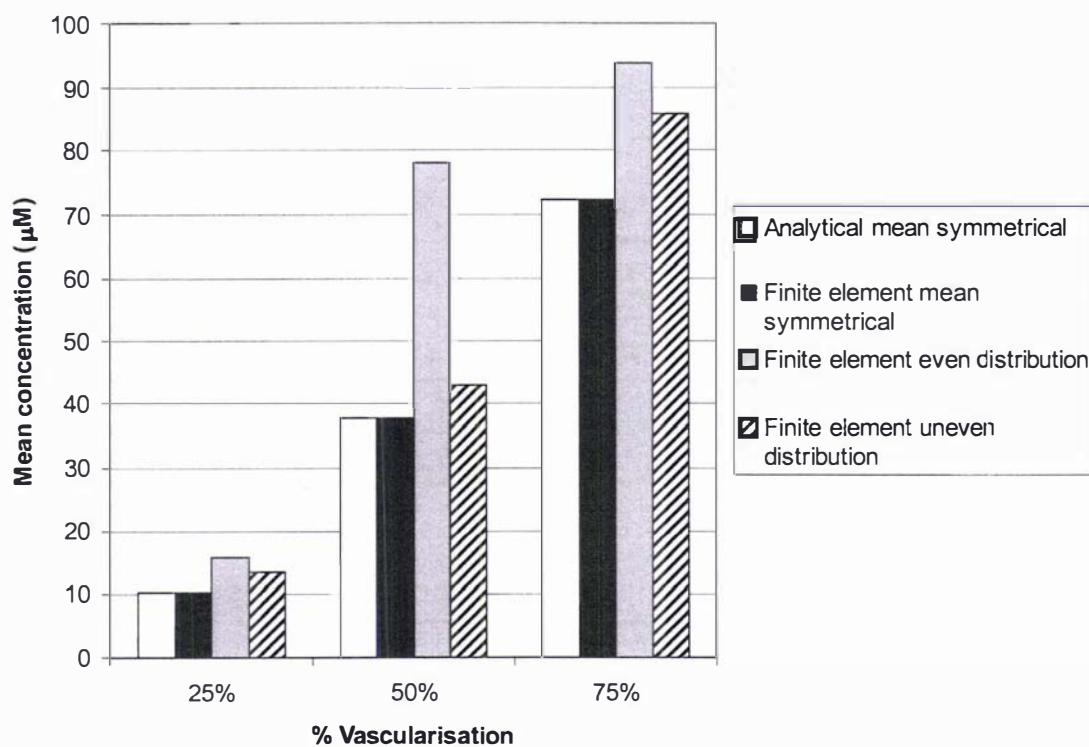
Figure 3.25   Mean total follicle oxygen concentration for various vascular distributions.
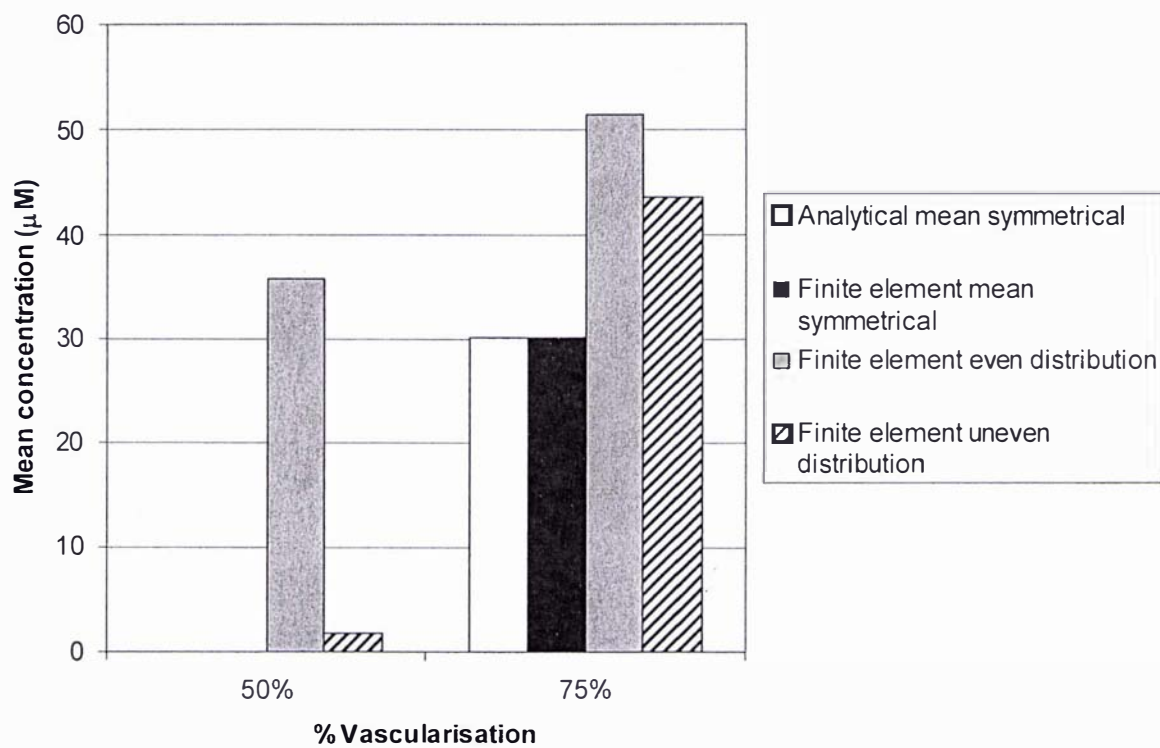
Figure 3.26   Mean oxygen concentration within the area occupied by the oocyte for various vascular distributions.

The results suggest that not only is the degree of vascularisation important to pre-antral follicle oxygenation, but the distribution of vascularisation also plays a role. Further, those follicles with evenly distributed vascularisation will have an improved oxygen status with regard to both total follicle oxygen and oxygen in the oocyte region once it gets above a certain level.

3.4 Conclusions and recommendations

This chapter revisited a model for oxygen transport in a pre-antral follicle developed by Gosden & Byatt-Smith (1986). The model was expanded upon by reconsidering the estimation of parameters, and the assumptions made.

This work has several key results,

1. Oxygen can reach the oocyte in a small pre-antral follicle.
2. Using improved parameter estimates, and on consideration of cellular voidage, it has been demonstrated that oxygen can also reach the oocyte in a large pre-antral follicle.
3. The growing pre-antral follicle will reach a limiting size beyond which it cannot grow without becoming increasingly anoxic.
4. Whether or not a pre-antral follicle is anoxic is a function of its size, voidage and degree of vascularisation.
5. Symmetrically distributed vascularisation is superior in achieving well oxygenated follicles.

In contrast to the conclusions of Gosden & Byatt-Smith (1986) it has been demonstrated that a completely vascularised small pre-antral follicle will allow oxygen to reach the oocyte positioned at the centre. This difference is largely due to the insensitivity of the model solution to all parameters at the values of cellular diffusion coefficient used by Gosden & Byatt-Smith (1986). Using improved estimates of cellular diffusion coefficients, oxygen transport in the follicle becomes less hindered and the model solution demonstrates enhanced sensitivity to all parameters.

In agreement with the conclusions reached by Gosden & Byatt-Smith (1986) a large pre-antral follicle vascularised at 100% will not allow oxygen transport through to the region occupied by the oocyte. However, if fluid voidage is considered in the model, oxygen transport becomes more easily facilitated due to the reduced mass transport resistance and zero oxygen consumption of the fluid void regions. If fluid voidage is varied over the range found in normal biological tissues, and tumours ($0.06 < \varepsilon < 0.6$) oxygen can penetrate further into the follicle, and if the voidage is high enough oxygen can reach the region occupied by the oocyte, even in large follicles. At any given voidage level there will be a critical follicle size beyond which no oxygen will reach the oocyte unless the voidage is increased.

Therefore, if the follicle reaches a limiting voidage, any increased follicle growth would result in increased anoxia moving from the core outwards. It is possible that when this scenario is encountered antrum formation may be the only way that the follicle can avoid oxygen starvation. Without any real knowledge of the degree of voidage in pre-antral follicles it is difficult to speculate any further. Studies into how the voidage of pre-antral follicles changes over time, and the voidage level at which antrum formation occurs may be very useful and provide further insight.

Considering Michaelis-Menton kinetics in the model showed that the reduced oxygen consumption of granulosa cells at low oxygen concentrations allows a small amount of oxygen to continue to penetrate regions of the follicle that were previously anoxic under the assumption of constant oxygen consumption by the granulosa cells. How useful low concentrations of oxygen are to the granulosa cells is difficult to determine without specific knowledge of the oxygen consumption kinetics of these cells. Estimates of the Michaelis-Menton constants for biological cells provided a range which is too wide to draw useful conclusions. If the oxygen consumption kinetics of granulosa cells were determined, the model could be adjusted to consider at what distance the oxygen concentration in the follicle drops below the critical level required by these cells for maximal oxygen consumption. This may provide further insight into the oxygen status of the pre-antral follicle, and hence studies investigating the oxygen consumption kinetics of granulosa cells are recommended.

It has been shown that reduced vascularisation results in reduced oxygen transport, with the follicle becoming anoxic closer to its outer boundary. In fact the oxygen status of a pre-antral follicle will be a function of its size, voidage and degree of vascularisation. The combined effect of these parameters will determine how far oxygen penetrates through the follicle and indeed if any oxygen reaches the area occupied by the oocyte. Therefore the size, voidage and degree of vascularisation may control whether or not the follicle prospers or becomes atresic. If the follicle size and voidage have physical limitations imposed on them, then the amount of vascularisation may be key in determining the fate of the follicle. It is possible that at the pre-antral stage oxygen limitations may play a role in not only atresia but also antrum formation. The effect of antrum formation on oxygen transport will be considered in the next chapter. Studies which look at the degree of vascularisation of pre-antral follicles, and whether this is related to the ultimate fate of the follicle, would provide further insight.

Although the amount of vascularisation appears to be critically important, how this vascularisation is distributed also has an impact on the oxygen status of the follicle. Perhaps not surprisingly, symmetrical distribution of vascularisation about the follicular boundary results in more even distribution of oxygen throughout the follicle. More interesting is the fact that even distribution of the same level of vascularisation allows greater oxygen into the follicle as well as into the region occupied by the oocyte.

In summary, modelling oxygen transport in the pre-antral follicle has shown that oxygen can penetrate this structure, and indeed reach the oocyte. Whether or not it does will depend most heavily on the follicular volume, voidage, and degree of vascularisation. Studies investigating these variables, their possible interaction, and role in determining follicular fate through either atresia or antrum formation, would be valuable in providing further insight. Knowledge of the oxygen requirements of the pre-antral oocyte may also be useful. Perhaps the key result here is that if a follicle is receiving oxygen and continues to grow, it will eventually reach a state where no combination of variables will be able to prevent it from becoming hypoxic. Unless, of

course, something different happens.

This chapter has laid the foundation to investigate and understand what does happen next in the antral and pre-ovulatory follicles, which is critical to this work, and to a better understanding of oxygen's role in IVF follicles.

Chapter 4.   Modelling oxygen transport in the antral / pre-ovulatory follicle

There are no mathematical models in the literature which describe mass transport of any substance in the antral/pre-ovulatory follicle. This is somewhat surprising given the importance of the pre-ovulatory follicle to human reproduction generally, as well as to IVF. This chapter describes the development of a mathematical model concerned with oxygen transport in the antral/pre-ovulatory follicle. The purpose of the model is to gain an insight into the effect of antrum formation on oxygen transport, but most importantly to use the model to gain an understanding of what real world measurements of follicle vascularisation and dissolved oxygen levels in the follicular fluid can actually tell us about the oxygen status of the follicle.

The vascularisation surrounding the follicle (perifollicular blood flow) has been shown to be related to oocyte competence and IVF outcome (Bhal *et al.*, 1999, Huey *et al.*, 1999), as has the dissolved oxygen content of the follicular fluid (Van Blerkom *et al.*, 1997). Hence these measurements may provide a useful tool for IVF clinics when selecting oocytes. This modelling work also seeks to compare these two methods to see if one appears to have any advantage over the other with regard to determining the oxygen status of the follicle. Although every effort was made to ensure the best possible parameter estimates are obtained, and that the model assumptions are fair, it must be stressed that the purpose of this work was not to establish absolute predictions of follicle oxygen concentrations. Rather, general relationships which provide useful information about follicle oxygenation are sought.

4.1 The antral and pre-ovulatory follicle

The antral and pre-ovulatory follicles are shown in Figure 4.1. As the granulosa cells continue to produce fluid, this fluid accumulates, resulting in the formation of a fluid cavity known as the antrum (Peters & McNatty, 1980). The oocyte is pushed to one

98

side. The surrounding granulosa cells now form a hillock, the *cumulus oophorus*, attached on one side to the follicular wall and projecting into the antrum.

The follicle enlarges from approximately 0.4 to 16 mm in diameter at which point it is considered a pre-ovulatory follicle (McNatty, 1978, McNatty, 1981). During this expansion, the fluid voidage increases (Peters & McNatty, 1980).

The pre-ovulatory follicle continues to expand to approximately 25 mm in diameter (Peters & McNatty, 1980), although it can become much larger than this. The cumulus cells may detach from the granulosa cells releasing the cumulus/oocyte complex into the antrum. Both the granulosa and cumulus cells show continued expansion in size (Peters & McNatty, 1980).

From its pre-antral size of approximately 80 μm in diameter the oocyte increases moderately in size during the antral/pre-ovulatory phase to around 116 μm (Tsuji, *et al.,* 1985).

4.2 Antral follicle model – description and assumptions

The proposed model of oxygen transport in the antral follicle is represented pictorially in Figure 4.2. The model makes the following assumptions:

1. The follicle is spherical.

2. The concentration of oxygen at the boundary is equal to that of arterial plasma. This concentration is uniform and hence follicle is completely vascularised. The effect of reduced vascularisation is considered later.

3. The granulosa cell layer is composed of both cells and fluid voidage.

4. The granulosa cell layer is a uniform spherical shell. This assumption allows symmetry to be maintained, and hence an analytical solution to be achieved. Useful inferences can be made by considering the oocyte to occupy a volume

99

within the granulosa cell layer, and just touching the cell/antrum interface.

5. Mass transport is via diffusion in both the granulosa layer and fluid antrum. The granulosa cells consume oxygen at a constant rate. There is no oxygen consumption in the antrum.

6. The solubility of oxygen is equal in the granulosa layer and fluid antrum. The assumption of equal solubility of oxygen in the granulosa and fluid layer simplifies the model by eliminating oxygen partitioning between the phases.

It should be noted that in the antral follicle the influx of fluid as the antrum expands may lead to convective transport within the follicle. This is most likely to occur during and leading up to the pre-ovulatory phase of follicle growth when fluid accumulation is most rapid. It is also possible that temperature gradients observed between the follicle and surrounding tissue (Hunter *et al.*, 2006) may result in convection in the follicle. Furthermore, any significant convection is most likely to occur in the fluid antrum and not the granulosa layer. Therefore the effect of convection will be reduced for an oocyte attached to the granulosa layer. Furthermore because there is no oxygen consumption in the fluid antrum the steady-state solution will be unaffected. Thus, although such phenomena are worthy of further investigation, they do not affect any of the limiting scenarios considered in this work and should be given due consideration in any simulation of dynamic mass transport in the follicle.

4.3 Antral follicle model derivation

Because it has been assumed that the fluid space is symmetrically surrounded by granulosa cells and that there is no oxygen consumption within the fluid space, at steady-state the oxygen concentration in the fluid will be uniform throughout and equal to the oxygen concentration at the cell/antrum interface.

$$C = C_i \qquad\qquad (4.1)$$

For the granulosa cell layer the equation for the steady-state oxygen balance is the same as that given by equation 3.8, which upon inclusion of fluid voidage and integration yields equation 4.2.

$$r^2 \frac{dC}{dr} = \frac{R_g (1-\varepsilon) r^3}{3D_g} + K_1 \qquad (4.2)$$

At steady-state the rate of change of concentration with respect to radius at the spherical shell interface where $r = r_a$ is zero, since there is no consumption of oxygen in the antrum. Mathematically stated,

$$D_g \left(\frac{dC}{dr} \right)_g = D_a \left(\frac{dC}{dr} \right)_a = 0 \qquad (4.3)$$

Where the subscripts g and a refer to the granulosa and antrum sides of the interface at $r = r_a$.

Hence substitution of $\frac{dC}{dr} = 0$. at $r = r_a$ into Equation 4.2 and rearrangement yields.

$$K_1 = -\frac{R_g(1-\varepsilon)}{3D_g} r_a^3 \qquad (4.4)$$

Hence substitution of K_1, into equation 4.2 and rearrangement gives,

$$\frac{dC}{dr} = \frac{R_g (1-\varepsilon)r}{3D_g} - \frac{R_g (1-\varepsilon)r_a^3}{3D_g\, r^2} \qquad (4.5)$$

Which upon integration with respect to r results in,

$$C = \frac{R_g (1-\varepsilon)r^2}{6D_g} + \frac{R_g (1-\varepsilon)r_a^3}{3D_g\, r} + K_2 \qquad (4.6)$$

Antral follicle

1. Granulosa cell layer

2. Fluid filled antrum

3. Oocyte, $r_o=58\pm10\mu m$ (Tsuji et al., 1985)

4. Cumulus cells

Follicle diameter (d_f) 0.4 to 16 mm (McNatty, 1981)

Pre-ovulatory follicle

Follicle diameter (d_f) > 16 mm (McNatty, 1981)
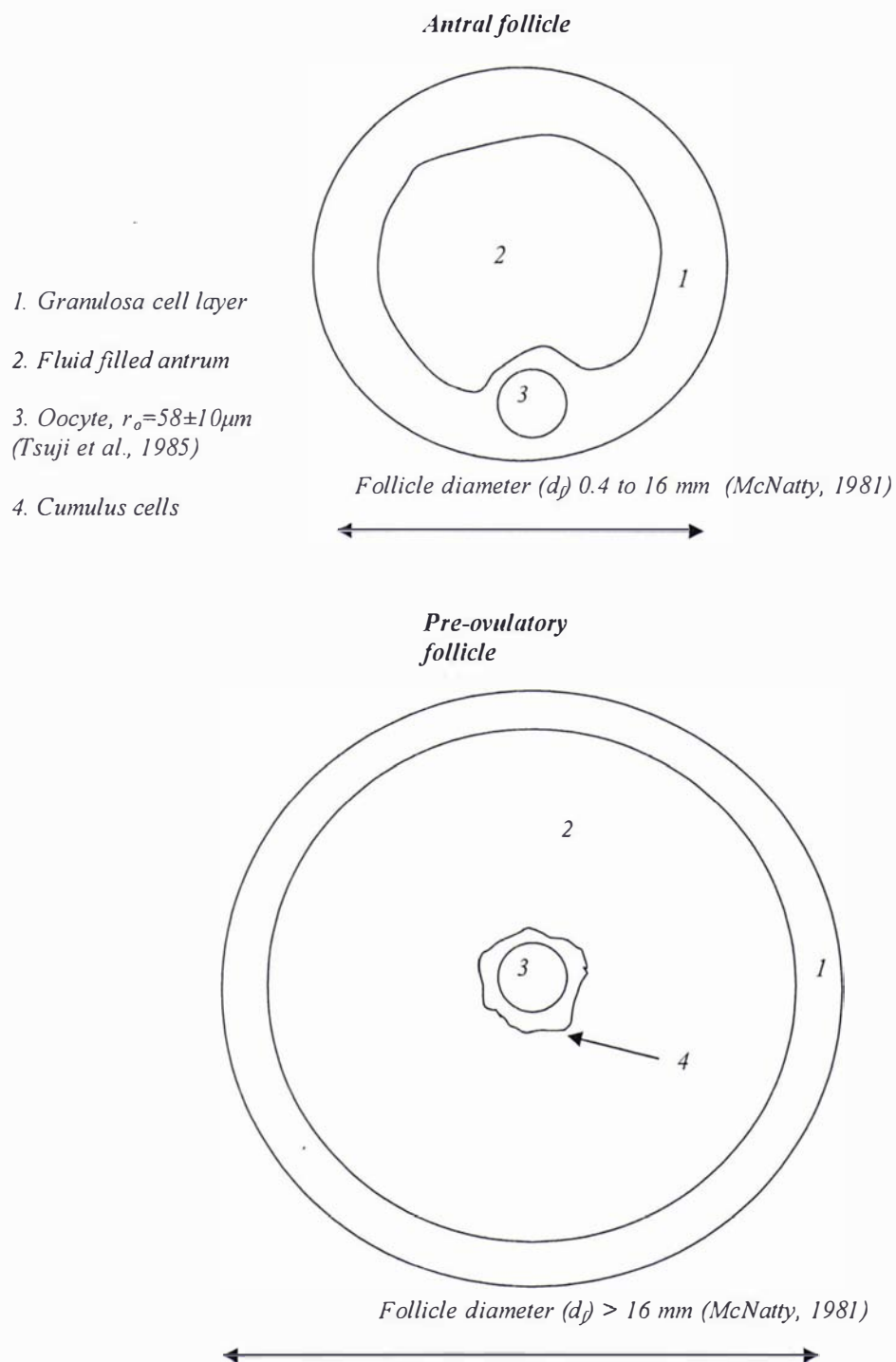
Figure 4.1.   The antral and pre-ovulatory follicles.
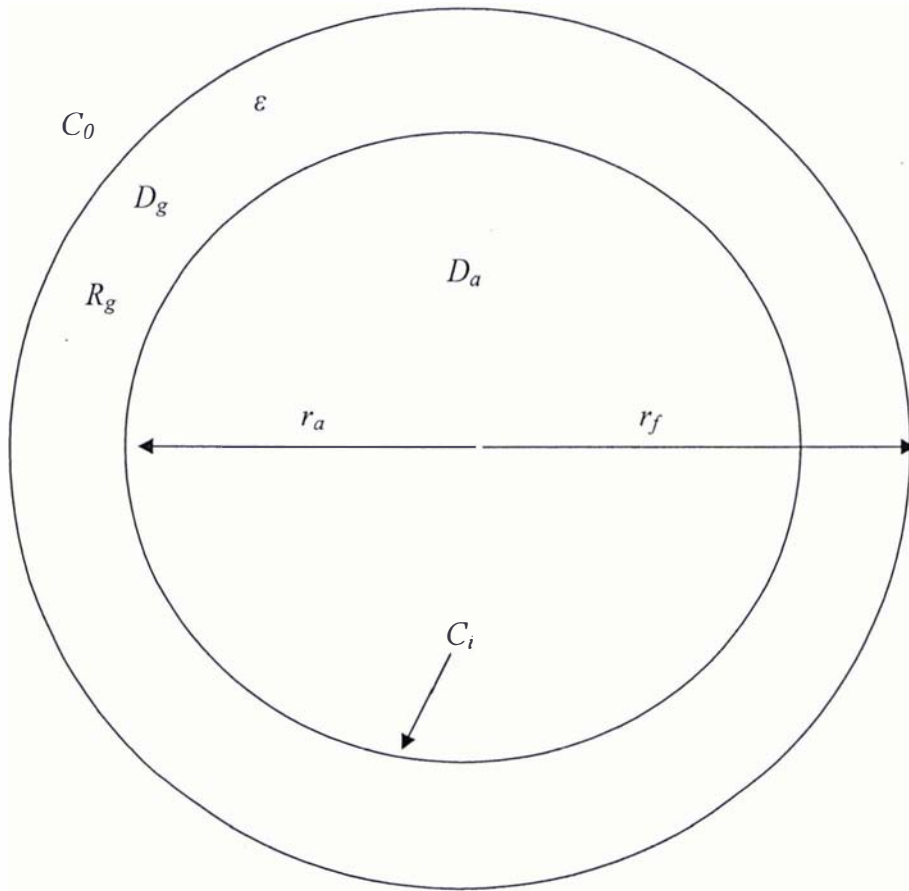
Figure 4.2   Pictorial representation of the model of oxygen transport in the antral follicle. See nomenclature for symbols.

Substitution of the second boundary condition $C = C_0$ at $r = r_f$ into equation 4.6 and solving for K_2 gives,

$$K_2 = C_0 - \frac{R_g (1-\varepsilon) r_f^2}{6D_g} - \frac{R_g (1-\varepsilon) r_a^3}{3D_g \, r_f} \qquad (4.7)$$

Substitution of K_2 back into equation 4.6 gives,

$$C = C_0 - \frac{R_g (1-\varepsilon)}{6D_g}(r_f^2 - r^2) - \frac{R_g (1-\varepsilon) r_a^3}{3D_g}\left(\frac{1}{r_f} - \frac{1}{r}\right) \qquad (4.8)$$

Equation 4.8 describes the oxygen concentration at any position r in the granulosa cell layer of an antral follicle. It should be noted that, if no fluid antrum exists $r_a = 0$, equation 4.8 reduces back to equation 3.23 which describes oxygen transport in a pre-antral follicle composed solely of cellular matter and fluid voidage.

Using the nominal parameter estimates presented in Chapter 3, Figure 4.3 uses equation 4.8 to describe the oxygen transport in a follicle of radius $r_f = 200$ μm. The figure shows that when the antrum does not exist and when it is small, the oxygen concentration profiles are similar. As the radius of the antrum increases, oxygen levels drop less dramatically, particularly as the fluid/cell interface is approached. After the antrum has reached a certain size, oxygen can penetrate the entire cell layer and enter the fluid where concentration remains constant.

Here oxygen transport is facilitated by the antrum, as at constant follicle size its inclusion represents a reduction in the total resistance to mass transport because the diffusion coefficient is greater than in the granulosa layer.

It is important to realise that viewed in isolation, the fluid simply represents another resistance to mass transport. In Figure 4.3, the increasing antrum volume reduces the volume of the granulosa cell layer and hence mass transport becomes less hindered. In reality the volume of granulosa cells increases rapidly throughout the antral phase. As

does the volume of the fluid antrum (McNatty, 1981). The increase in the volume of the granulosa cells, the fluid volume, and the total volume of the follicle will have several implications for oxygen transport.

Consider the situation, described in the previous chapter, of a pre-antral follicle which has reached a critical size, which only just allows oxygen to reach the oocyte. If the follicle becomes larger through increasing granulosa cell volume alone then the oocyte will become oxygen starved. If the volume of the follicle increases by the addition of antral fluid only, then the constant volume of granulosa cells will become dispersed around the outer layer of the follicle and their thickness $(r_f - r_a)$ will be reduced. Mass transport through this layer will be more easily achieved and the oocyte will still see some level of oxygen.

Therefore because both granulosa cell volume and follicular fluid volume are increasing, then at any give total follicle volume the relationship between the increase in each parameter will have to be such that it maintains or improves the oxygen transport status, otherwise the follicle will become increasingly anoxic.

If we consider the situation of critical interest for the antral follicle to be when the concentration of oxygen only just falls to zero at the cell/fluid interface, then setting equation 4.8 equal to zero at $r = r_a$ gives,

$$0 = C_0 - \frac{R_g(1\text{-}\varepsilon)}{6 D_g}(r_f^2 - r_a^2) - \frac{R_g(1\text{-}\varepsilon) r_a^3}{3 D_g}\left(\frac{1}{r_f} - \frac{1}{r_a}\right) \tag{4.9}$$

where $D_g = D_{eff}$.

For any given follicle volume (known r_f) equation 4.9 can be used to solve for the radius, r_a, of the antrum at which oxygen will only just make it through the layer of granulosa cells. From the granulosa cell layer thickness ($r_g = r_f - r_a$), the volume of granulosa cells can also be obtained.
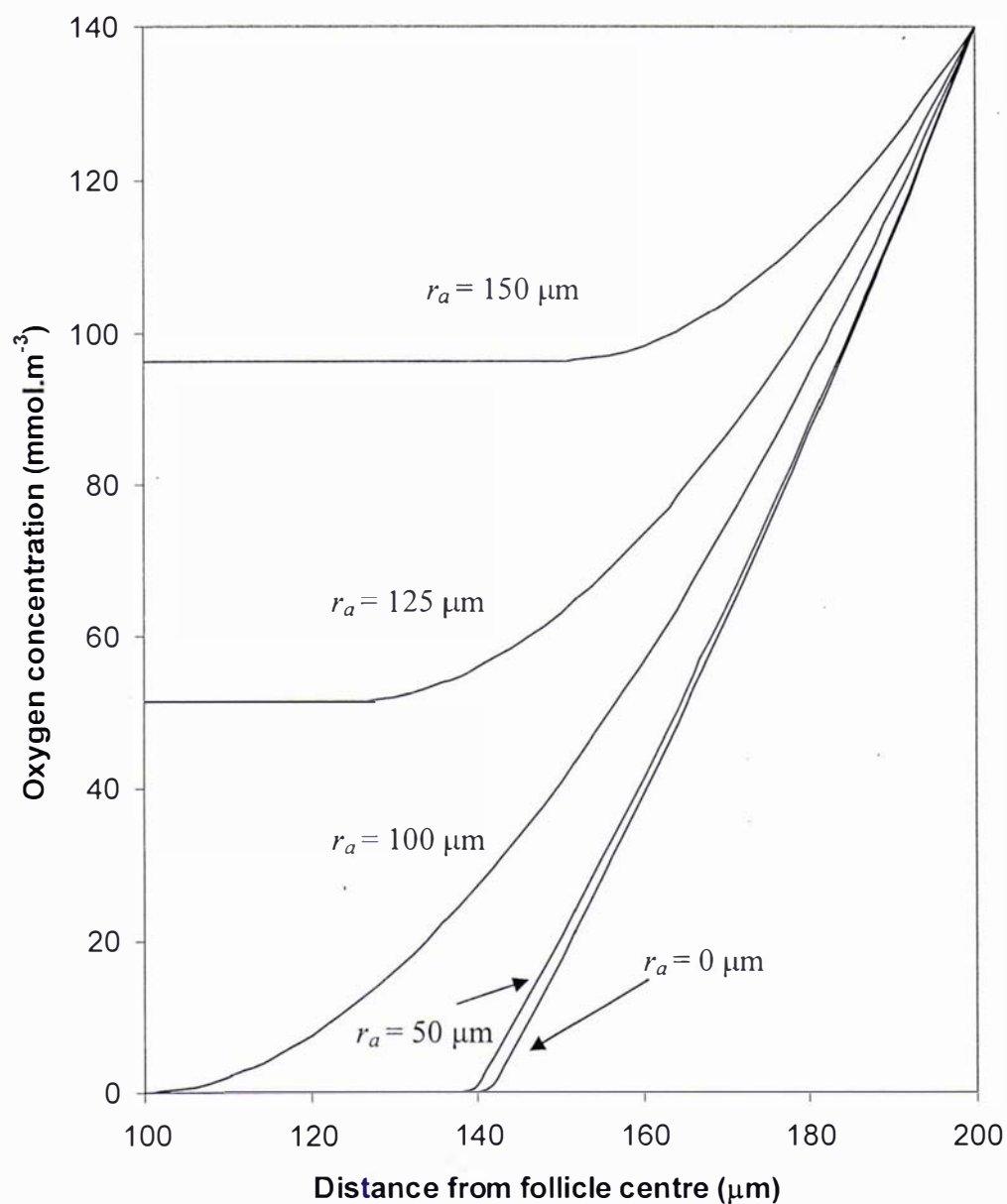
Figure 4.3   Oxygen concentration profiles across a follicle (r_f=200 μm) with various antrum sizes (parameters at nominal values).

Equation 4.9 cannot be solved explicitly for r_a, rather an iterative solution must be obtained. The cubic term r_a^3 in equation 4.9 dictates that only real solutions for which $r_a < r_f$ are of interest.

Figure 4.4 shows the relationship between the granulosa cell volume, antral fluid volume, and total follicle volume. The calculations were carried out at the nominal values of the parameters in equation 4.9 with a void fraction of 0.3. The starting point of the figure is where there is no antrum at all. The starting follicle radius is 147 μm which is the critical radius, determined from equation 3.25, at which the oocyte of the pre-antral follicle would only just be receiving oxygen. The figure spans the total follicle volumes associated with antral follicles ($r_f \leq 8000$ μm). Initially only a small volume of antral fluid is required to maintain oxygenation of the granulosa cell layer. However, as the follicle becomes a large antral follicle, a comparatively large antral fluid volume is required to sustain oxygenation of the granulosa cell layer.

Of key interest is the ratio of antral fluid volume to total follicle volume that needs to be achieved to keep the granulosa cell layer oxygenated as the total follicle volume increases. This relationship is shown in Figure 4.5. Figure 4.5 shows that at small total follicle volumes, only a small fluid volume is required relative to granulosa cell volume to ensure full oxygenation of the granulosa cell layer. As the follicle increases in volume the required ratio rises steeply before becoming relatively constant. At the nominal parameter estimate values used and a voidage of $\varepsilon = 0.3$ this constant value of the ratio V_a/V_f is approximately 0.97. If V_a/V_f rises above 0.97 even more oxygen will penetrate the granulosa cell layer and will reach the fluid space, but if $V_a/V_f < 0.97$ at least some granulosa cells will be anoxic.

The key result here is that if the granulosa cell number/volume keeps on growing then antrum formation represents the only possible way that the follicle can avoid becoming anoxic. It is therefore possible that the formation of the follicular antrum may be a mechanism to overcome mass transport limitations.
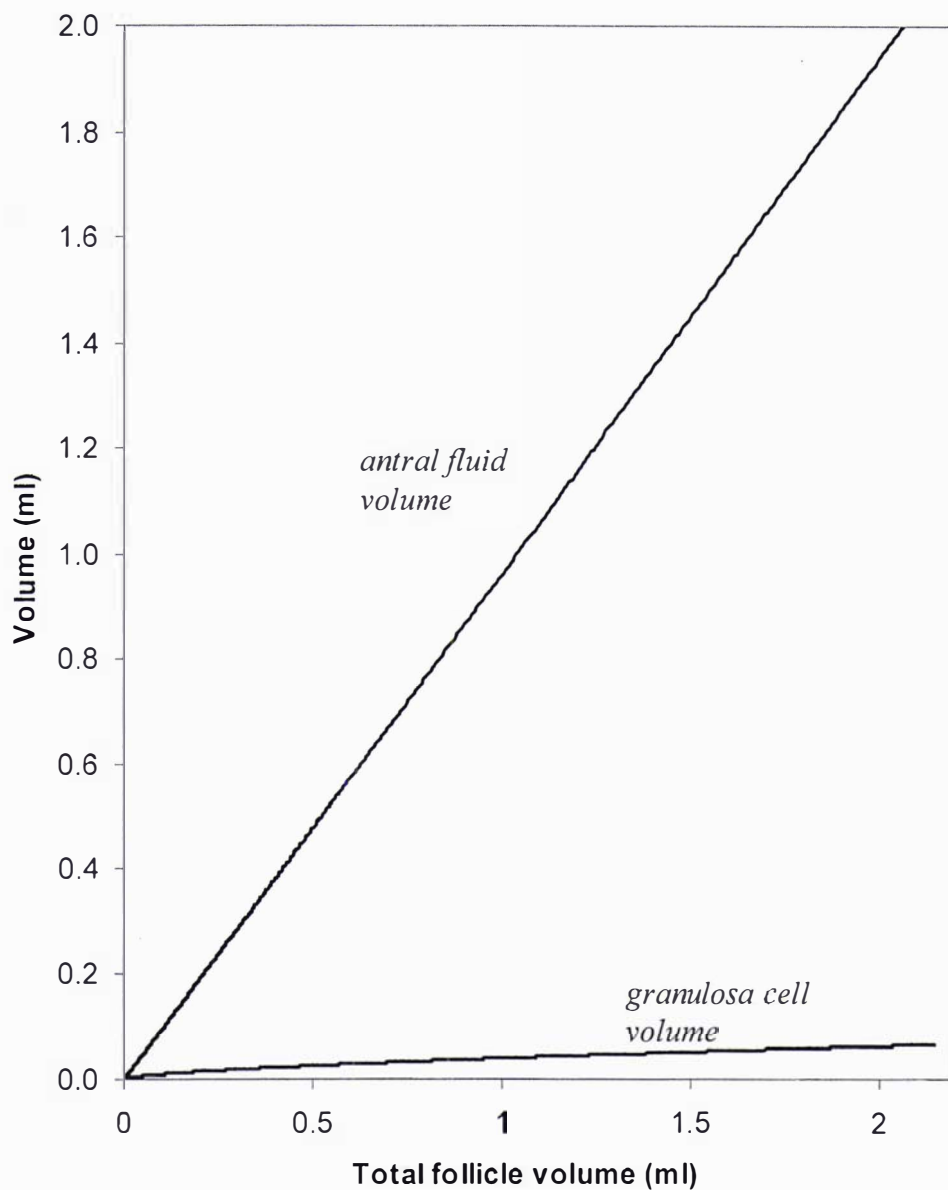
Figure 4.4   Volume of antral fluid and granulosa cells required to maintain oxygenation of the granulosa cell layer as a function of total follicle volume (solution obtained for the case when oxygen concentration only just drops to zero at the granulosa/antrum interface).

Although the mathematical model of Gosden & Byatt-Smith (1986) did not extend to include antrum formation, the authors did speculate that the formation of the antrum in which there is negligible oxygen consumption and greater oxygen diffusivity may be a mechanism for coping with the problem of oxygenating a vascular structure. The results presented here appear to lend support to this hypothesis.

Based on the model of Gosden & Byatt-Smith (1986), Van Blerkom (1998) speculated that intrafollicular oxygen should rise with antrum formation. This work suggests that this will be the case only if antrum formation is taken in isolation, and occurs without accompanying granulosa cell growth. However, if antrum formation occurs in conjunction with an increase in granulosa cell numbers the oxygen status of the follicle will be determined by the balance between V_a/V_f. Depending on this ratio antrum formation and enlargement may or may not give rise to an oxygenated follicle.

McNatty (1981) reports the granulosa cell numbers and antral fluid volume in developing human follicles. This data is reproduced in Figure 4.6(a) and (b) and shows that both the granulosa cell number and antral fluid volume increase as the follicle diameter progresses through the early and late antral phases of follicular development. As the pre-ovulatory phase is entered both granulosa cell numbers and antral fluid volume increase, plateau and become fairly constant. To allow comparison of this data with the concepts illustrated in Figures 4.4 and 4.5, requires estimation of the volume of granulosa cells.

4.3.1 Estimation of the volume of granulosa cells

Two studies have estimated the cellular volume of human granulosa cells using electron microscopy (Delforge *et al.*, 1972; Dhar *et al.*, 1996). Delforge *et al.* (1972) gives a range of 942 to 2207 μm^3/granulosa cell. Dhar *et al.* (1996) gives a mean value of 1140 ± 200 μm^3/granulosa cell ($\pm$SD). Because the mean of Dhar *et al.* (1996) falls within the range given by Delforge *et al.* (1972), it is sensible to use the upper and lower range of Delforge *et al.* (1972) to convert granulosa cell number to granulosa cell volume. The calculations in Figures 4.4 and 4.5 are based on a void

fraction of $\varepsilon = 0.3$. So for a fair comparison the granulosa cell numbers from McNatty (1981) can be converted to granulosa layer volume by equation 4.10.

$$V_g = \frac{n V_{cell}}{(1-\varepsilon)} \qquad (4.10)$$

Where n is the number of granulosa cells, V_{cell} is the volume of a single granulosa cell and ε is the void fraction of the granulosa cell layer ($\varepsilon = 0.3$ used here). The result of these calculations is compared in Figures 4.7 and 4.8 to the calculations of the model previously described in Figures 4.4 and 4.5.

Figure 4.7 shows the increase in both antral fluid volume and granulosa cell volume in human follicles. Included also are the model calculations of Figure 4.4. Comparison of the two shows that real human antral volume increase, and granulosa cell volume increase, follow a similar pattern to that predicted by the model, suggesting these volumes increase in such a way as to avoid oxygen mass transport limitations.

Of course, cause and effect should not be deduced from this model. Rather it is possible to make the general statement that real human granulosa and antral fluid volumes increase in such a way that is consistent with what would be expected if follicle growth is mass transport limited. Hence follicle growth occurs in such a way that the chances of sufficient oxygen supply to both oocyte and granulosa cells is improved.

Figure 4.7 is not an attempt to match the real world data to that of the model predictions. Given the range over which many of the parameter estimates vary, attempting this would not reveal any additional information to the general trend shown here. Yet the closeness of the real world observations to the model calculations lends some support to the nominal, best estimate values used in this work.
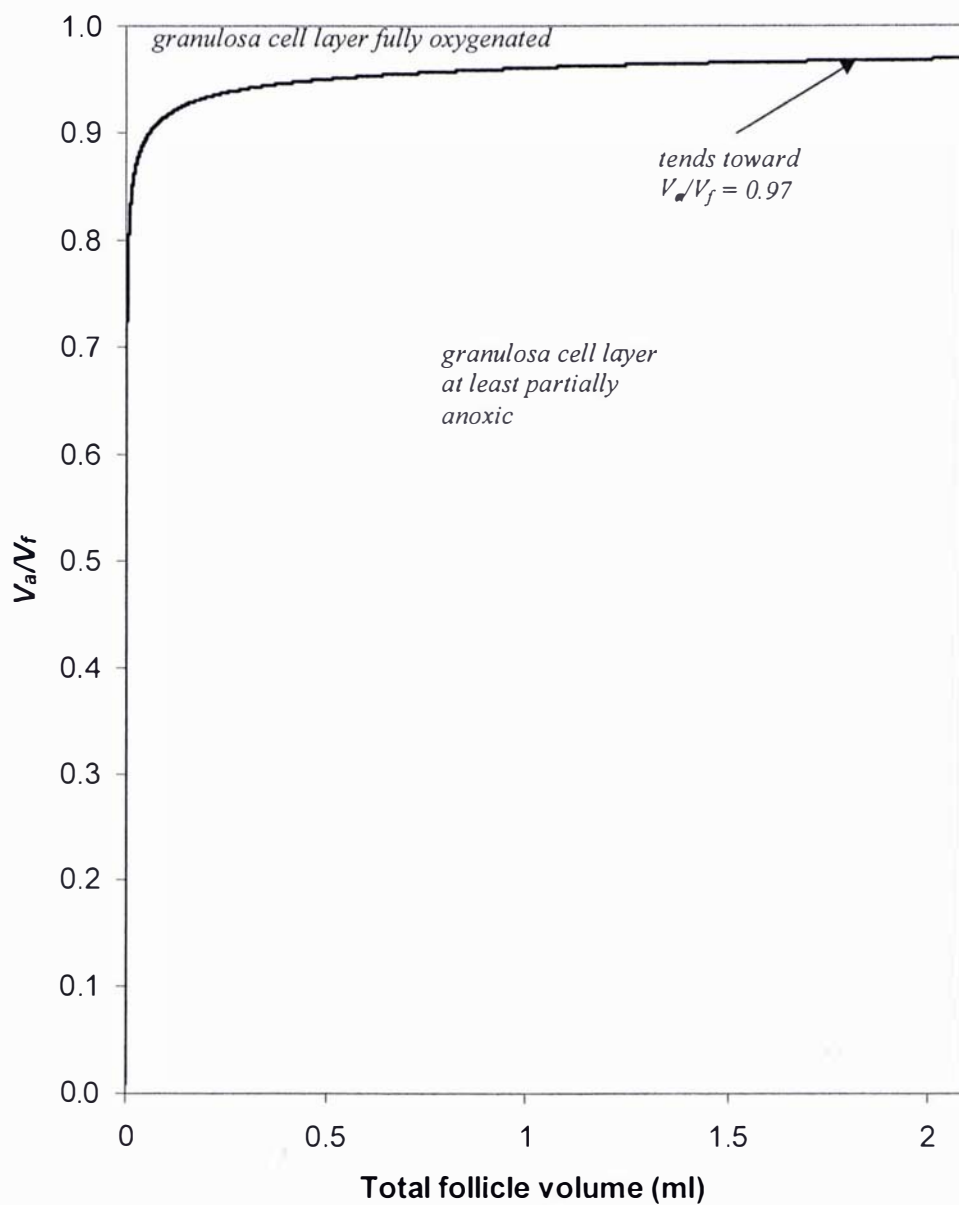
Figure 4.5   The ratio of antral fluid volume to total follicle volume required to maintain oxygenation of the granulosa cell layer as a function of total follicle volume.

(a)

Early   Late   Preovulatory
antral   antral   25mm

No. of granulosa cells $\times 10^{-6}$

Follicle diameter (mm)

(b)

Early   Late   Preovulatory
antral antral   25mm

Antral fluid volume (ml)

Follicle diameter (mm)
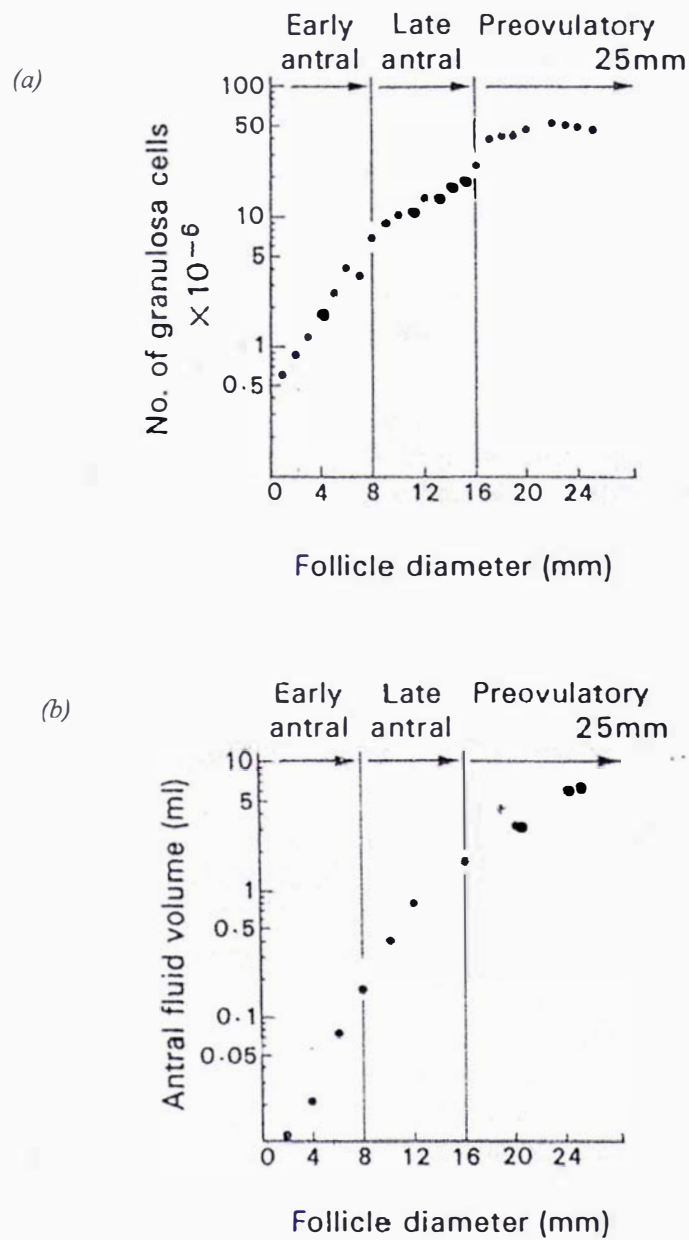
Figure 4.6   Changes in human granulosa cell number (a) and antral fluid volume
(b) as a function of follicle diameter throughout the early antral, late antral, and pre-
ovulatory stages of follicle development (taken from McNatty, 1981).
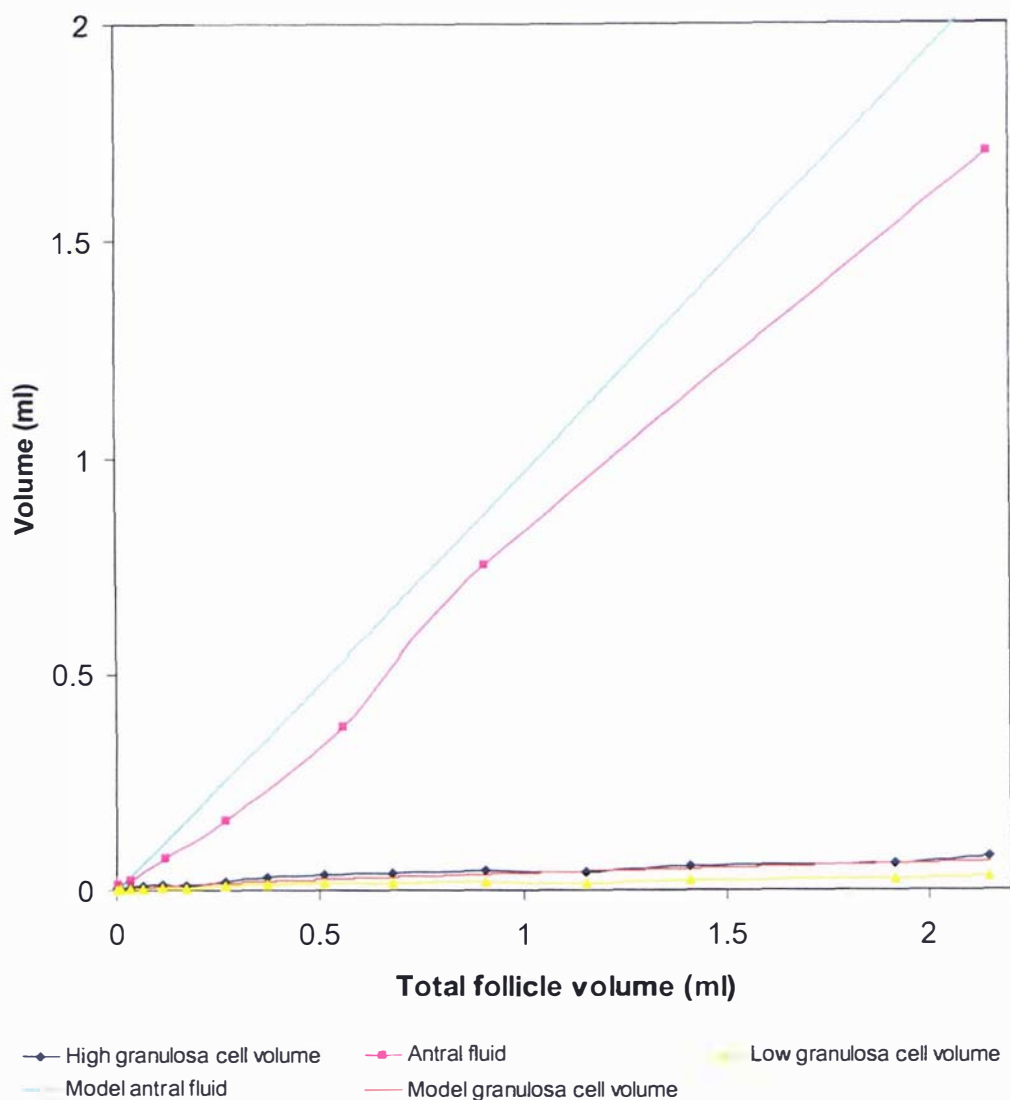
Figure 4.7   Antral and granulosa cell volume increase in the human follicle (data adapted from McNatty, 1981) compared to model calculations for mass transport limited follicle growth (solution obtained for the case when oxygen concentration only just drops to zero at the granulosa/antrum interface). Low and high single granulosa cell volumes used in converting human follicle data from McNatty (1981) are 942 and 2207 μm^3/cell respectively.

113
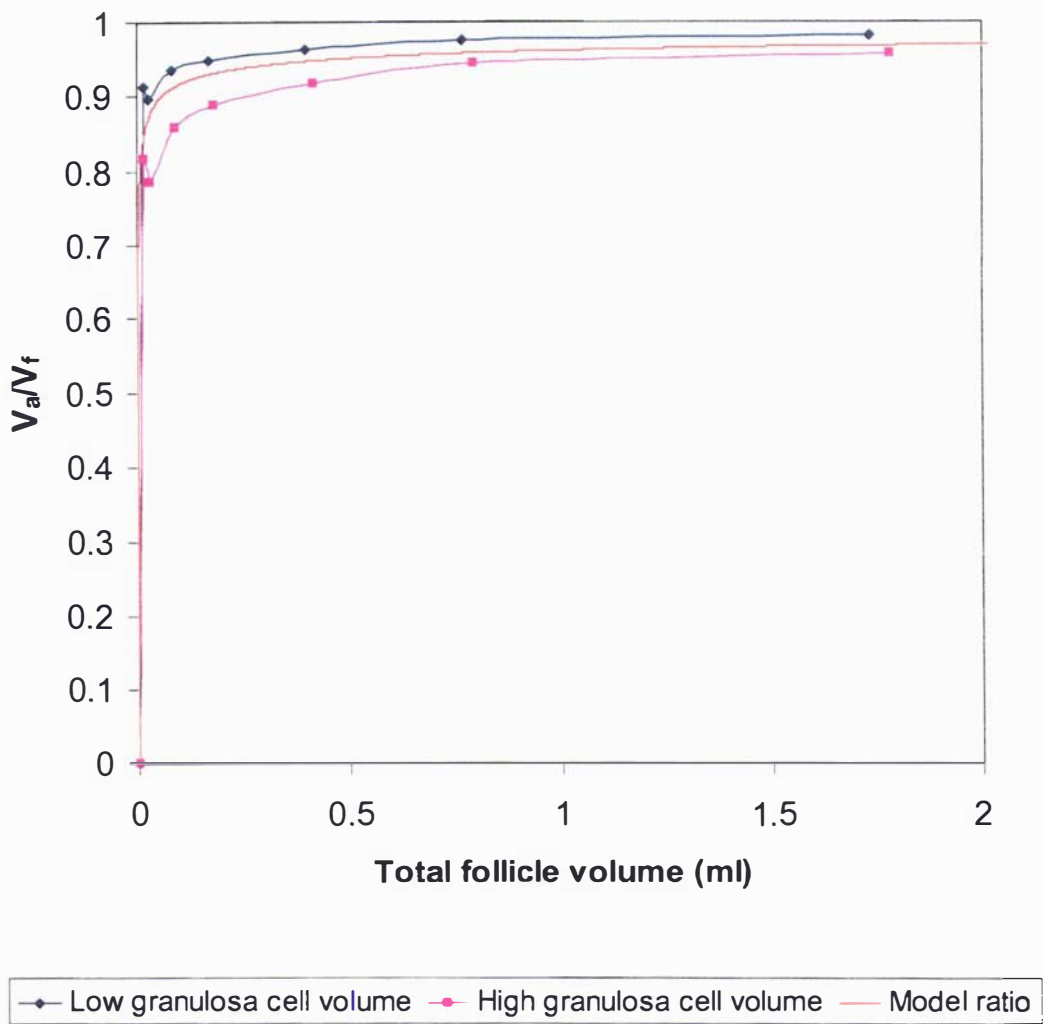
Figure 4.8 V_a/V_f in the human follicle (data adapted from McNatty, 1981) using both high and low granulosa cell volume estimates compared to model calculations for mass transport limited follicle growth.

With this in mind perhaps a more valid comparison is that shown in Figure 4.8 which compares how the dimensionless quantity V_a/V_f changes as a function of total follicle volume for both real human data and the model predictions of Figure 4.5. The human data has been compiled from the McNatty (1981) data shown in Figure 4.6 (a) and (b) at those follicle diameters that have data points for both granulosa cell number, and antral fluid. Because of the common follicle diameters, total follicle volume has been calculated using $V_f = V_a + V_g$ as opposed to Figure 4.7 where $V_f = \frac{4}{3}\pi\left(\frac{d_f}{2}\right)^3$.

$V_f = V_a + V_g$ is considered a better estimate as it is based on two measured values, where as $V_f = \frac{4}{3}\pi\left(\frac{d_f}{2}\right)^3$ is prone to small errors in follicle diameter measurement. Since $V_f = V_a + V_g$, the calculations once again include upper and lower estimates as dictated by the upper and lower estimates of single V_{cell} given by Delforge *et al.* (1972).

From Figure 4.8 it can be seen that both model and human data show a similar trend whereby the ratio of antral fluid volume to total follicle volume increases as follicle volume increases. The point at which $\frac{V_a}{V_f} = 0$ is not from the same data set, but has been taken from the same author and is the point at which antrum formation occurs, that is $V_a = 0$ (McNatty, 1978).

Figure 4.8 essentially offers the same information as Figure 4.7, that the observed increase in antral and granulosa volume ($V_f = V_a + V_g$) observed in humans is consistent with what would be expected if the increase in follicle volume was related to oxygen transport limitations. Because of the dimensionless nature of Figure 4.8 it can also be stated that not just the general trend, but the absolute value of the ratio in which granulosa cell volume and fluid volume increase, is consistent between both model and human data, and that the predicted ratio seems to fall within the range calculated from the data. Once again, this does not demonstrate cause and effect, but adds further support to the fact that observed characteristics of follicle growth enhance the ability of the follicle to be oxygenated.

115

4.3.2 Oxygen supply to the oocyte and Michaelis-Menton kinetics

The previous calculations relate to the formation of anoxic regions. What may be of greater importance to the oocyte is whether or not it receives enough oxygen to meet its respiratory demands? As discussed in Chapter 3 oxygen consumption by biological cells can be described by Michaelis-Menton kinetics. The effect of including such kinetics is that at low oxygen concentrations oxygen consumption is reduced and hence the oxygen concentration profile declines less rapidly. A small amount of oxygen penetrates into areas of the follicle which would previously have been predicted as being anoxic, but the usefulness of such low levels of oxygen is unclear. What is more likely to be important is whether or not a cell receives enough oxygen to sustain maximal respiration. If the oocyte is within the granulosa cell layer of the antral follicle and is assumed to require a certain critical level of oxygen C_{crit} then equation 4.9 can be set equal to C_{crit} instead of zero giving equation 4.11.

$$C_{crit} = C_0 + -\frac{R_g(1-\varepsilon)}{6D_g}\left(r_f^2 - r_a^2\right) - \frac{R_g(1-\varepsilon)\,r_a^3}{3D_g}\left(\frac{1}{r_f} - \frac{1}{r_a}\right) \tag{4.11}$$

where $D_g = D_{eff}$.

Equation 4.11 still assumes constant oxygen consumption rate of the granulosa cells and that the overall oxygen consumption of the follicle is not affected by the presence of the oocyte. That is, the volume of the granulosa cells sufficiently dominates the total cellular volume rendering the oocyte volume negligible. This is more likely to be true for larger follicles which contain a greater volume of granulosa cells. Given that this work is largely concerned with the implications of oxygen transport in the IVF clinic, and hence IVF sized follicles, the validity of this assumption can be inferred from the size of IVF follicles and the relative importance of antral type follicles in human IVF.

This information was obtained by collecting follicular fluid samples from patients undergoing IVF treatment at the ISIS clinic in Hamilton, New Zealand. Appropriate ethical approval and patient consent were obtained prior to collecting samples.

116

Samples were collected from 12 patients and the volume of fluid was measured in the graduated tubes in which the fluid was collected to the nearest 0.5 ml (14 ml Falcon round bottom polystyrene tube, product no. 352057, Becton Dickinson Labware, NJ, USA).

Where possible samples were collected from individual follicles, where this was not the case the number of follicles from which the total sample was composed was recorded, so that an average follicle volume could be obtained. Samples which contained follicular flushing fluid were not considered.

Figure 4.9 shows the distribution of antral fluid volumes in samples taken from 12 women undergoing IVF treatment. The data of Figure 4.9 includes volumes measured when only one follicle was sampled per collection vial. The follicle volumes ranged between 1 and 26 ml with a mean of 5±4 (±SD). Most of the volumes are clustered between 1.5 to 7.5 ml with a drop in frequency between 4.5 and 5.5 ml where the mean lies. Of the 54 follicles measured, two were particularly large, with volumes of 16 and 26 ml respectively.

From Figure 4.6 it can be seen that an antral follicle can be considered any follicle whose fluid volume is lower than approximately 1.5 ml. Thus, from Figure 4.9, the relative frequency of antral follicles can be calculated as 4/54 = 0.07. The volumes of these antral follicles ranged from 1.2 to 1.4 ml, and hence can be considered large antral follicles.

However, it is important to realise that in IVF clinics, small follicles will often be aspirated into a collection tube with other follicles. This saves both inconvenient changeover of collection tubes and also reduces the total cost of collection tubes. Therefore, considering only the data from single follicles is likely to cause overestimation of the mean follicle volume, and underestimation of the frequency of small follicle volumes. For this reason, Figure 4.10 shows that distribution of antral volumes when tubes containing fluid from multiple follicles are also considered.
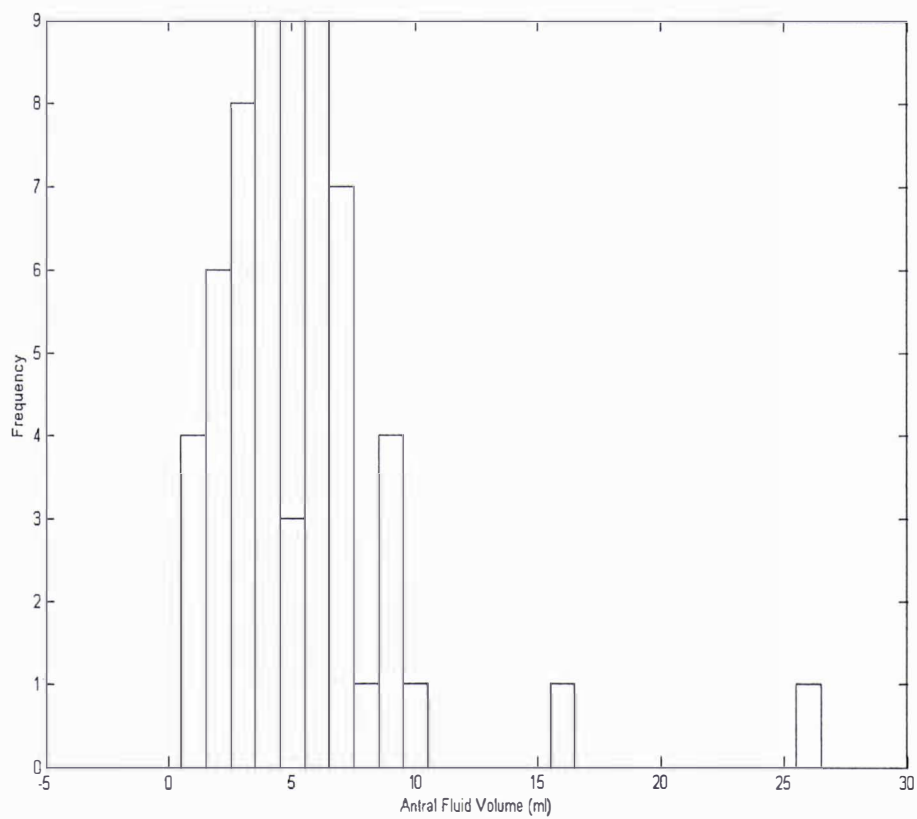
Figure 4.9   Distribution of human IVF antral fluid volumes for samples taken from single follicles.
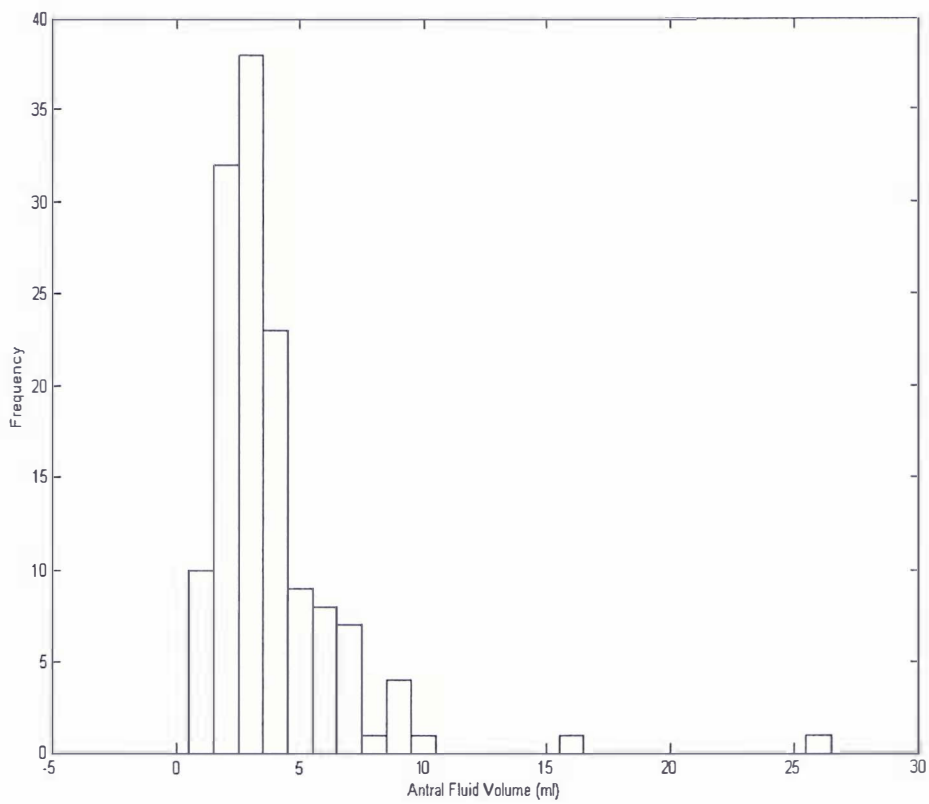
Figure 4.10 Distribution of human IVF antral fluid volumes including samples from multiple follicles.

Where a tube contains the fluid from multiple follicles the total volume of the tube has been averaged over the follicle number, with the frequency being recorded as the follicle number. For example, a collection tube containing 9 ml of antral fluid from three follicles is recorded as three, 3ml follicles. Although this situation is not ideal it does not affect the mean fluid volume that would be obtained via measurement of single follicles only. It also allows for an improved estimate of follicular volume through the elimination of bias bought about through measuring only single follicles, and through a greater sample size.

When this is done for the same 12 women, 135 follicles are included, and the mean fluid volume is 4±3 ml. Although this mean is not significantly different from that of the smaller sample size, the likelihood of the bias discussed above is indicated by the drop in the mean antral fluid volume from 5 to 4 ml. The antral volumes appear to be more uniformly distributed with the bulk of measurements ranging between 1.5 to 4.5 ml. The relative frequency of antral sized follicles is now $10/135 = 0.07$ and is hence unchanged from its previous estimate. The range of these antral fluid volumes for antral follicles is now between 1 and 1.4 ml. Hence it can be concluded that the majority of IVF follicles can be considered pre-ovulatory follicles. Antral follicles are only of minor importance, and their occurrence is restricted to large antral follicles. For this reason, the implications of equation 4.11 will be restricted to large antral follicles or follicles with a volume of at least 1.5 ml.

For large antral follicles (V_a=1.5 ml), using the granulosa cell numbers given by McNatty (1981) and the upper and lower estimates of total granulosa cell volume previously determined, the total granulosa cell layer volume can be calculated, and ranges from approximately 2×10^{10} to 6×10^{10} μm^3. The diameter of the oocyte is approximately 116 μm. Hence the volume of the oocyte can be estimated, by assuming it is spherical, as approximately 8×10^5 μm^3. Thus, even at a low granulosa cell volumes, the fraction of cellular volume occupied by the oocyte will be less than 0.0001, which will be even further reduced when voidage is considered. Hence the assumption that the projected area (which is an important variable for two dimensional mass transport through the granulosa layer) occupied by the oocyte can be neglected in the antral model is certainly reasonable for the large antral follicles

120

found in IVF clinics.

Although the oocyte can be excluded from the calculation it will still be effected by whether or not it receives oxygen sufficient for it to respire maximally. If the oocyte resides in the granulosa cell layer, then the point of critical interest will be when the granulosa cell layer oxygen concentration is $\geq C_{crit}$. If $C \geq C_{crit}$ at the granulosa cell/fluid interface $(r=r_a)$, then regardless of the position of the oocyte within the granulosa cell layer it will receive sufficient oxygen to allow it to respire maximally. In the previous chapter it was discussed that obtaining an estimate of C_{crit} for the pre-antral follicle was somewhat fruitless due to the scarcity of knowledge of oocyte respiration in the early pre-antral follicle. This situation was further complicated by the wide ranging Michaelis-Menton constant values reported for oxygen consumption by animal cells. For the purposes of making some at least illustrative calculations, a reasonable estimate of C_{crit} for the antral and pre-ovulatory follicle is required.

4.3.2.1 Michaelis-Menton kinetics and the antral/pre-ovulatory follicle

More information is available about the oxygen consumption of the antral/pre-ovulatory oocyte. The oxygen consumption of human oocytes has been reported as 530 ± 80 pL.hr^{-1}.oocyte^{-1} (Magnusson *et al.*, 1986). Table 4.1 compares this value with the oocyte oxygen consumption reported for other species. The oxygen consumption is highest in the human, but the human has the largest oocyte. When the results are expressed on a per volume basis, they all become more similar. The value for oxygen consumption of the human oocyte given by Magnusson *et al.* (1986), although only from a single study, seems to be a good estimate to use for model calculations, and is in keeping with values reported for other species.

The value of oxygen consumption for humans in pL.hr^{-1}.oocyte^{-1} needs to be converted to units consistent with the model (mol.m^{-3}.s^{-1}) The density of oxygen at 37°C can be calculated from the ideal gas law using equation 4.12.

$$\rho_{0_2}\left(\frac{g}{L}\right) = \frac{P_{ATM}\, M_{O_2}}{RT} \tag{4.12}$$

where, P_{ATM} = 1 atm., M_{O2} = 32 g.mol^{-1}, R = 0.082 L.atm.mol^{-1}.K^{-1} (the gas constant), and T = 310.15 K (37 °C).

Evaluating equation 4.12 gives the density of oxygen at 37°C as 1.26 g.L^{-1}. Finally the oxygen consumption rate of an oocyte per unit volume can be calculated using equation 4.13.

$$R_o\left(\frac{mol}{m^3 s}\right) = R_o\left(\frac{pL}{hr.oocyte}\right) \times \frac{\rho_{O_2}}{3600 \; M_{O_2} V_o} \times 10^{-12} \tag{4.13}$$

where 3600 is the number of seconds per hour, and V_o is the volume of a single oocyte calculated by assuming it is spherical and of diameter 116 µm . Evaluating equation 4.13 gives the volumetric oxygen consumption rate of a human oocyte as 0.00709 mol.m^{-3}.s^{-1}.

No data on the Michaelis-Menton constant for oocytes are available. It was shown in the previous chapter that the range over which reported values for other cells vary is too large to perform any meaningful calculations. For the purpose of investigating the implications on the antral follicle here, it is then necessary to select a best estimate from the literature.

Of the cells for which K_m values have been reported, pancreatic islets of the rat seem to be the most similar to oocytes (Fournier, 1998, Dionne *et al.,* 1991). These islets have a diameter of 150 µm which is similar to that of 116 µm for the oocyte. The oxygen consumption rate of these islets varies between 26 µM.s^{-1} to 46 µM.s^{-1}, which is similar to the oocyte oxygen consumption rate of 7 µM.s^{-1}. The value of K_m reported for these islets is 0.44 mm Hg, and this value will be used here as a best estimate to facilitate some illustrative calculations.

	R_o (pL.hr^{-1}.oocyte^{-1})	Reference	r_o (µm)	Reference	R_o (pL.hr^{-1}.µm^{-3})
Human	530	Magnusson et al., 1986	58	Tsuji et al., 1985	6.48×10^{-4}
Bovine	240	Thompson et al., 1996	55	Clark et al., 2006	3.44×10^{-4}
Mouse	141	Houghton et al., 1996	40	Clark et al., 2006	5.26×10^{-4}
Rat	135-173	Magnusson et al., 1977	31	Daniel et al., 1989	$10.8\text{-}13.9 \times 10^{-4}$

Table 4.1   A comparison of human oocyte oxygen consumption to that of other species. Note that R_o is reported both on a per oocyte basis and after normalisation for oocyte volume of a given species.

To be consistent with the units of the model, this value of K_m needs to be converted to a concentration in $mol.m^{-3}$. This can be achieved using Henry's Law ($C = pS$), provided the solubility of oxygen in the follicle is known or can be estimated. As already stated, the solubility of oxygen in the granulosa layer and fluid layers is assumed to be the same, and equal to that of human plasma. The solubility of oxygen in water is well defined over a large temperature range. Battino *et al.* (1983) has taken data from 15 studies which meet their inclusion criteria, to give an excellent resource for obtaining a reliable value for oxygen solubility in water. Taking data from this review, a value of 0.00137 $mol.m^{-3}.mmHg^{-1}$ was used for the solubility of oxygen in water at 37°C. The relative solubility of oxygen in human plasma to water is also well defined and is given as 0.895 (Christoforides *et al.*, 1969, Dittmer & Grebe, 1958). This ratio remains constant with temperature (Christoforides *et al.*, 1969). Hence, the solubility of oxygen in human plasma can be calculated as $0.00137 \times 0.895 = 0.00123$ $mol.m^{-3}.mmHg^{-1}$. Thus, the Michaelis-Menton constant of $K_m = 0.044$ mmHg can be expressed as a concentration of $0.44 \times 0.00123 = 0.000541$ $mol.m^{-3}$ via Henry's Law.

If R_o is defined as R_{omax}, and C_{crit} defined as the oxygen concentration at which R_{omax} just drops below its maximal level to be 0.99 R_{omax}, then according to Michaelis-Menton kinetics, equation 4.14 can be written.

$$0.99\,R_{o\,max} = \frac{R_{o\,max}\,C_{crit}}{K_m + C_{crit}} \qquad (4.14)$$

Iterative solution of equation 4.14 yields C_{crit}, the oxygen concentration at which respiration rate has dropped from R_{omax} to 0.99 R_{omax}. This value is 0.0536 $mol.m^{-3}$. Expressed as a partial pressure this is 42.5 mmHg, or as a volume percentage, 5.7 vol %. It should be noted that the selection 99% of maximal respiration is used in this work only for illustrative purposes. It could easily be replaced by any respiration rate (or critical oxygen concentration) of interest. Perhaps most interesting would be experimentally determined values of R_o and C_{crit} at which the oocyte becomes compromised. Unfortunately no such values have been directly measured.

124

Equation 4.11 can now be solved. The result of this solution is shown in Figure 4.11 for the same input parameters used to solve equation 4.9. Figure 4.11 shows that to maintain the granulosa cell layer oxygen concentration $\geq C_{crit}$ a greater ratio of V_a/V_f is required at any given follicle volume when compared with maintenance of the granulosa cell layer at $C \geq 0$. As the follicle volume increases, the curve for $C \geq 0$ tends towards 0.97 as previously calculated. For $C \geq C_{crit}$ the curve tends towards 0.98. So although a greater ratio of V_a/V_f is required for maintenance of $C \geq C_{crit}$ the difference is small, particularly at the larger follicle volumes encountered in IVF. These results suggest that the ratio V_a/V_f may be useful as a measure of follicle oxygenation, and hence of oocyte competence. It is important to realise that the results this far have assumed complete vascularisation of the follicle, and hence it is important to investigate the implications of reduced vascularisation on the results and conclusions to this point.

4.3.3 Effect of reduced vascularisation

Using the previously defined mean symmetrical vascularisation to simulate the effect of reduction in vascularisation, equation 4.9 can be solved at various vascularisation levels. Figure 4.12 shows the effect of reduced vascularisation on the ratio V_a/V_f required at any given follicle volume to sustain the granulosa cell layer at $C \geq 0$. The results show that if a follicle's oxygen status is to be determined, the ratio V_a/V_f, must be known along with the total follicle volume and the degree of vascularisation. In reality, this requires knowledge of three parameters. Any two of V_a, V_g or V_f (since $V_f = V_a + V_g$), as well as the level of vascularisation. This has important implications in terms of the measurement of follicle oxygen status using Doppler ultrasonography. These results suggest that for the oxygen status of one follicle to be compared with another not only the vascularisation needs to be known, but also any two of V_a, V_g, and V_f. Although Figure 4.12 shows results for the granulosa cell layer at $C \geq 0$, the same will be true if the granulosa cell layer is oxygenated at $C \geq C_{crit}$, except the curves will be shifted accordingly to accommodate the fact that $C_{crit} > 0$ as shown by Figure 4.11.

Figure 4.12 also shows that the ratio V_a/V_f is quite insensitive to changes in the level

of vascularisation even over the large range of 25 to 100%. This is particularly the case for large antral follicles such as those encountered in IVF ($V_f > 1$ ml). For a follicle vascularised at 100%, V_a/V_f required to maintain $C \geq 0$ in the granulosa cell layer tends toward 0.969. For a follicle vascularised at 25%, the required V_a/V_f tends towards 0.985.

The relative insensitivity of V_a/V_f to the required concentration (Figure 4.11) and level of vascularisation (Figure 4.12) means that this ratio would really only be useful as a selection tool if V_a/V_f is well below the required level. For example if V_a/V_f was measured as 0.2 for a given follicle it would be unlikely that this follicle would be well oxygenated and in this way measurement of V_a/V_f may be useful. If, however, a follicle's ratio of V_a/V_f was measured at 0.96, it would be difficult to determine what level of C the follicle concentration was greater than or equal to. Similarly, just how well vascularised it was would also be difficult to determine.

The reason this would be so difficult is due to the experimental uncertainty that would be associated with the measurement of V_a/V_f. As Figures 4.11 and 4.12 show, to discriminate accurately among follicles, V_a/V_f would have to be able to be measured with an uncertainty of <1% to be of any real value. Consideration of how V_a/V_f might be measured experimentally provides some insight into how feasible an uncertainty of <1% really is. As already stated measurement of V_a/V_f requires knowledge of any two of V_a, V_g and V_f. V_f could be measured by measuring the volume of the aspirate during or after the IVF procedure, as this aspirate in theory is made up of both V_a and V_g. Accurate measurement of this volume would be complicated by any residual volume that remains in the system after aspiration and as a result does not reach the collection tube.

Subsequent measurement of V_a or V_g would require separation of the cellular and fluid phases of the aspirate (not to mention knowledge of the void fraction). The accuracy of this procedure would be compromised by the fact that it is unlikely all the granulosa cells would be extracted by aspiration, with some remaining in the evacuated follicle.
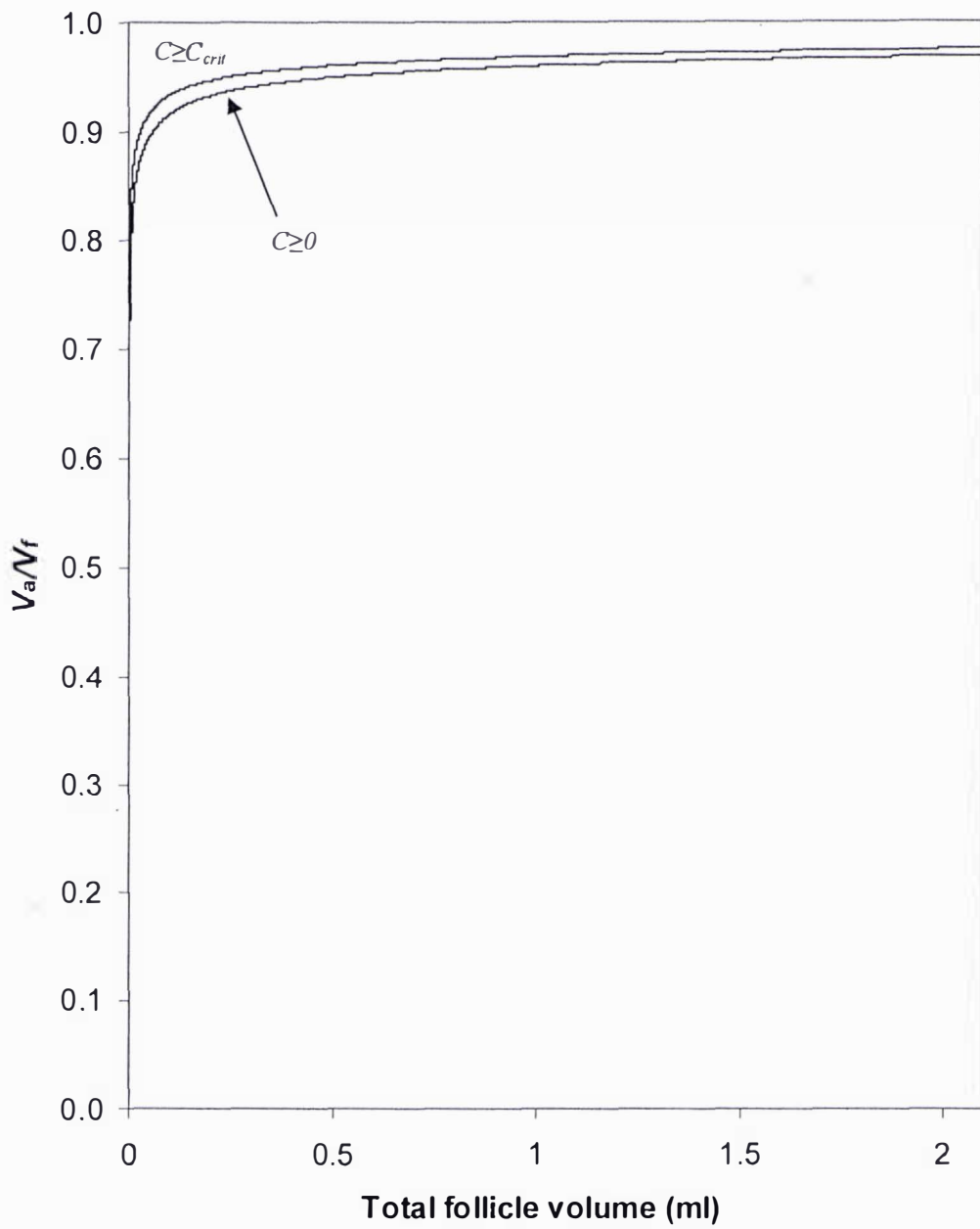
Figure 4.11 V_a/V_f as a function of total follicle volume when the granulosa cell layer is oxygenated at $C{\geq}0$ and $C{\geq}C_{crit}$.
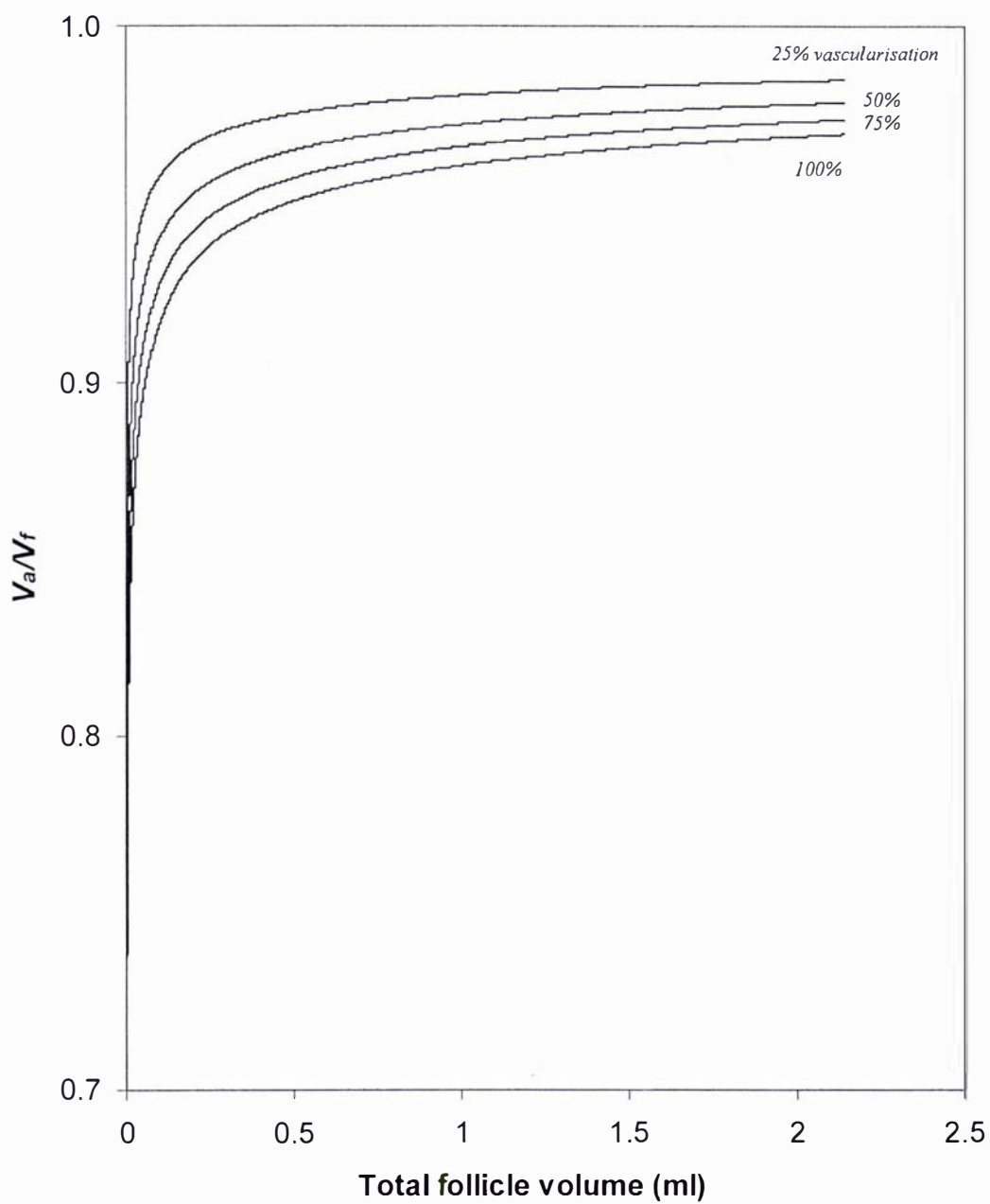
Figure 4.12   The effect of reducing mean symmetrical vascularisation on V_a/V_f and its relation to total follicle volume (granulosa cell layer oxygenated at $C \geq 0$).

Another way of determining V_f would be from ultra-sound measurements of follicle diameter at the time of aspiration. However, this would rely on the follicle being perfectly spherical if accurate determinations of V_f are to be achieved. Although assuming a follicle to be spherical is a reasonable approximation, it is unlikely to produce uncertainties of <1%. However, if sonography could be used it would allow for coupling with the measurement of V_a after removal of cells from the aspirate. This would eliminate the requirement of measurement of V_g, and the problems associated with failure to extract all of the granulosa cells.

The measurement of V_a/V_f may be useful in determining if a follicle lies far away from being well oxygenated, or in other words if it has a very low value of V_a/V_f. How useful such a measure would be will depend on how common such low values are. If V_a/V_f values are all high relative to one another and have minimal variability then V_a/V_f will not be useful in itself, due to its likely inability to differentiate between small differences among follicles. To be more useful in this regard it will need to be coupled with the measurement of follicle vascularisation.

Returning to the measurement of vascularisation for IVF sized follicles, Figure 4.12 shows that for follicles greater than approximately 1 ml in total volume, the relationship between V_a/V_f and vascularisation becomes essentially constant. Hence follicle oxygenation no longer depends on follicle volume but only on V_a/V_f and % vascularisation. Keeping nominal parameter values the same as previously described, Figure 4.13 shows the relationship between V_a/V_f and follicle vascularisation for a large antral follicle ($V_a = 1.5$ ml), with the granulosa cell layer oxygenated at $C \geq 0$ throughout. This is achieved through the solution of equation 4.9 at various vascularisation levels.

Figure 4.13 reinforces again that if follicle vascularisation is to provide a useful measure of follicle oxygen status, it needs to be coupled with knowledge of V_a/V_f for large antral follicles. Furthermore, this relationship is very sensitive to small variations in V_a/V_f. Because of this sensitivity and the difficulties already discussed in measuring small variations in V_a/V_f, the coupling of vascularisation and measurement of V_a/V_f to produce meaningful results may be difficult to achieve in practice. For

129

example, a follicle vascularised at 70% with a V_a/V_f ratio of 0.97 will not be oxygenated at $C \geq 0$ whereas the same follicle with a V_a/V_f ratio of 0.99 will be (see Figure 4.13).

It is important to realize that these predictions are based on best estimates of model parameters, and it is possible that in reality the sensitivity of the predictions to changes in V_a/V_f may be reduced making the task of measuring follicle oxygenation easier (alternatively it may get worse!).

The information provided here suggests that just using follicle vascularisation as a measure of oxygen status could be misleading. For example a follicle vascularised at 100% but with a V_a/V_f ratio less than 0.96 will have a worse oxygen status than a follicle vascularised at 70% with a V_a/V_f ratio of 0.99. In fact, the asymptotic nature of Figure 4.13 can provide some additional information. Because vascularisation greater than 100% is not possible, Figure 4.13 suggests that there exists a critical level of V_a/V_f slightly greater than 0.965. If the follicle does not achieve this, it will not be oxygenated at $C \geq 0$, regardless of how well it is vascularised.

The right-hand asymptote tends to a V_a/V_f ratio of 1. As long as there are granulosa cells, such a ratio cannot be achieved. Because the curve rapidly approaches 1 at approximately 20% vascularisation this suggests that any follicle below 20% vascularisation will be unlikely to be able to achieve oxygenation at $C \geq 0$ regardless of its V_a/V_f ratio. This information is potentially very useful as it provides a way in which conclusions can be drawn from vascularisation data independent of V_a/V_f.

Although the absolute values of Figure 4.13 and its asymptotes are only estimates, they provide useful information from which some general statements can be made. These are, for large antral follicles, determining oxygen status from vascularisation data will also require knowledge of V_a/V_f. However, if V_a/V_f is below a certain critical level, vascularisation level becomes irrelevant and the follicle will not be fully oxygenated. In a similar way, below a certain critical level of vascularisation, the ratio of V_a/V_f becomes irrelevant, and the follicle will not be well oxygenated. Experimental determination of these critical levels of V_a/V_f and vascularisation is a

topic worthy of further investigation, as is verification of the relationship between vascularisation and V_a/V_f. Both fall outside the expertise and scope of this thesis. More knowledge is certainly required about the variability of the ratio V_a/V_f. If this ratio is not highly variable in IVF sized follicles, then follicle vascularisation as measured by Doppler ultrasonagraphy would essentially become a good independent measure of follicle oxygenation. This is because, all other things being equal, higher vascularisation will mean more oxygen in the follicle.

With regard to Doppler ultrasonagraphy it is interesting to consider the study of Bhal *et al.* (1999) which measured follicle oxygenation in four ranges, <25%, ≥25% to <50%, ≥50% to <75%, and ≥75%. Interestingly, pregnancies were recorded in all ranges ≥25%. None were recorded for follicles with vascularisation of <25%. This data seems supportive of the cut-off predicted by the asymptotic nature of Figure 4.13. The value of <25% is also consistent with the predictions made in the figure.

In contrast to the measurement of vascularisation, this work suggests that the measurement of dissolved oxygen in antral fluid may provide a simpler method of obtaining the same information. To determine if the follicle contains greater than or equal to a certain oxygen concentration, knowledge of both vascularisation and V_a/V_f would be required. However, measurement of the oxygen concentration in the antral fluid provides this information directly with a single measurement. Just how the measurement of oxygen concentration is interpreted may depend on whether or not any gradients exist within the fluid. The work this far has assumed uniform vascular distribution, and under this assumption no oxygen gradients exist within the fluid since $C_a = C_i$, for all values of r_a. This means that a sample of antral fluid will be representative of the entire fluid space.

The figure shows a graph with:
- Y-axis labeled "% Vascularisation" ranging from 0.0 to 100.0
- X-axis labeled "V_a/V_f" ranging from 0.96 to 1

Text labels on the figure:
- critical level of V_d/V_f as follicle vascularisation greater than 100% is not possible
- fully oxygenated granulosa cell layer
- right asymptote
- partially oxygenated granulosa cell layer
- granulosa cell layer partially oxygenated at 70% vasc, and $V_d/V_f = 0.97$
- granulosa cell layer fully oxygenated at 70% vasc, and $V_d/V_f = 0.99$

Figure 4.13   Relationship between follicle vascularisation and V_d/V_f for a large antral follicle ($V_f = 1.5$ ml, granulosa cell layer oxygenated at $C \geq 0$). The effect of an increase in V_d/V_f, for a follicle with 70% vascularisation, on oxygen status is highlighted.

132

4.3.3.1 Effect of variable vascular distribution on oxygen concentration profiles in the antral fluid

The effect of variable vascular distribution can in theory be examined in the same way it was for the pre-antral follicle in Chapter 3, by using finite element modelling. However the growth of the antrum in the antral/pre-ovulatory follicle results in a very thin layer of granulosa cells. It is difficult in the finite element modelling software Femlab 3.1 to mesh such a thin layer. Therefore it has not been possible to investigate the effect of variable vascular distribution. Although not covered here, this is certainly worthy of further investigation, and will likely require some special modelling techniques, and considerable expertise in using a finite element modelling software package such as Femlab.

4.4 Pre-ovulatory follicle model – description and assumptions

It is important to realise that the results of the previous section for the antral follicle will also be relevant to any pre-ovulatory follicle where the oocyte has not broken away to reside in the antrum.

In the pre-ovulatory follicle, if the oocyte has broken away from the granulosa cells and resides in the antrum, then it might be expected to reside on average, at the centre of the follicle. Hence, the proposed model of oxygen transport in the pre-ovulatory follicle is represented pictorially by Figure 4.14. The assumptions on which this model is based are the same as those made in the antral follicle for the granulosa and fluid layers. Additional assumptions due to the presence of the oocyte are:

1.   The oocyte resides in the fluid antrum at the centre of the follicle. This assumption seems reasonable as a free floating oocyte would be expected to reside at the centre on average. This assumption also allows analytical solution of the problem, and represents the worst case position for the oocyte in terms of oxygen supply.

2. The oocyte respires according to Michaelis-Menton kinetics.

3. Oxygen diffusion through the oocyte is ignored, with consumption assumed to take place at the oocyte surface.

4. The oocyte is not surrounded by cumulus cell mass. The impact of cumulus cells will be investigated later.

4.5 Pre-Ovulatory follicle model derivation

4.5.1 Antral fluid

In the antral fluid layer, the equation for the steady-state oxygen balance is similar to that given by equation 3.7 and is expressed here by equation 4.15.

$$0 = \frac{D_a}{r^2} \frac{d}{dr}\left(r^2 \frac{dC}{dr}\right) - R_a \qquad (4.15)$$

Since there is no oxygen consumption in the antral fluid, substituting $R_a = 0$ and multiplying through by r^2/D_a gives equation 4.16.

$$0 = \frac{d}{dr}\left(r^2 \frac{dC}{dr}\right) \qquad (4.16)$$

which upon integration yields equation 4.17.

$$K_1 = r^2 \frac{dC}{dr} \qquad (4.17)$$
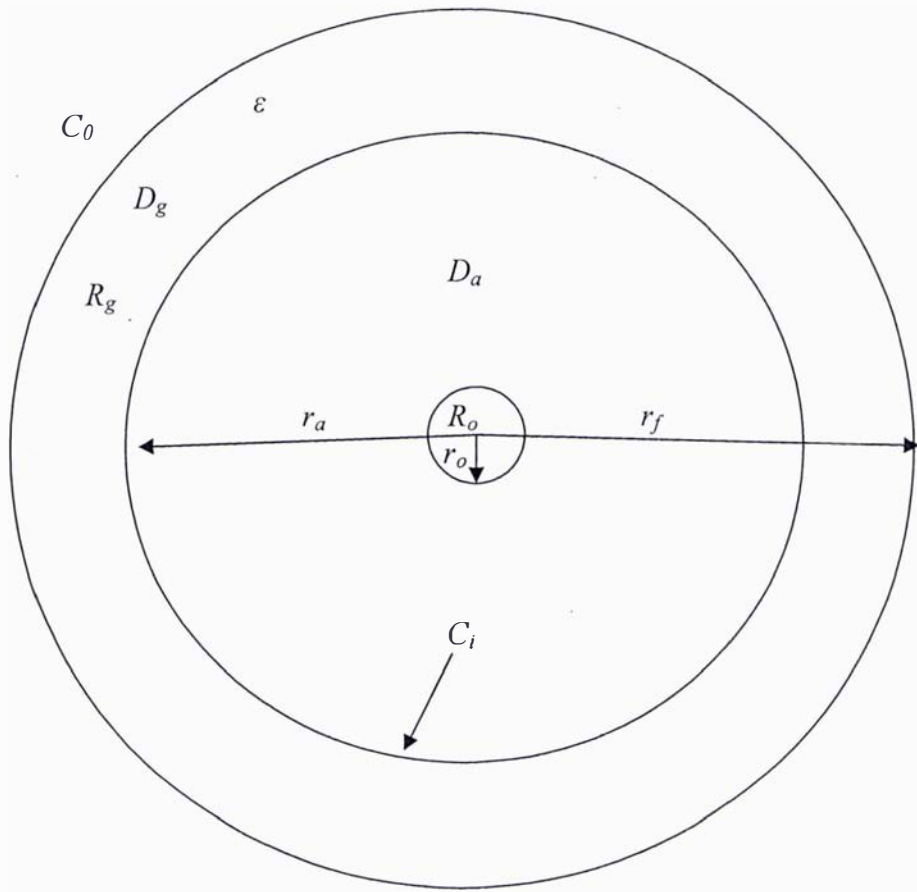
Figure 4.14   Pictorial representation of the model of oxygen transport in the pre-ovulatory follicle (refer to nomenclature section for symbol meanings).

At the oocyte surface, $r=r_o$, and the rate of diffusion of oxygen through the antral fluid to the surface of the oocyte is equal to the rate of oxygen utilisation by the oocyte. Expressed mathematically,

$$4\pi r_o^{\,2} D_a \left(\frac{dC}{dr}\right)_{r_o} = R_o \frac{4}{3}\pi r_o^{\,3} \tag{4.18}$$

Rearrangement of equation 4.18 results in the first boundary condition.

$$\left(\frac{dC}{dr}\right)_{r_o} = \frac{R_o\, r_o}{3D_a} \tag{4.19}$$

Substitution of equation 4.19 into equation 4.17 at $r = r_o$ reveals,

$$K_1 = \frac{R_o\, r_o^{\,3}}{3D_a} \tag{4.20}$$

Substitution of K_1, into equation 4.17 and subsequent rearrangement gives equation 4.21.

$$dC = \frac{R_o\, r_o^{\,3}}{3D_a r^2}\, dr \tag{4.21}$$

which upon integration results in,

$$C = K_2 - \frac{R_o\, r_o^{\,3}}{3D_a r} \tag{4.22}$$

Since $C=C_i$ at $r=r_a$, substitution of this boundary condition and subsequent rearrangement gives,

$$K_2 = C_i + \frac{R_o\, r_o^{\,3}}{3D_a\, r_a} \tag{4.23}$$

Finally substitution of K_2 back into equation 4.22 gives equation 4.24.

$$C = C_i + \frac{R_o r_o^{\,3}}{3D_a}\left(\frac{1}{r_a} - \frac{1}{r}\right) \tag{4.24}$$

Equation 4.24 describes the oxygen concentration at any position r in the fluid space of a pre-ovulatory follicle containing an oocyte at the centre. Equation 4.24 assumes a constant oxygen consumption rate of the oocyte. Considering Michaelis-Menton kinetics, the Michaelis-Menton equation can be substituted into equation 4.18 for R_o giving,

$$4\,\pi\, r_o^{\;2} D_a \frac{dC}{dr} = \frac{R_{o\,max}\, C}{K_m + C} \frac{4}{3}\,\pi\, r_o^{\,3} \tag{4.25}$$

Because R_o is a function of C, the Michaelis-Menton equation must be included in all integration. Thus, rearrangement of equation 4.25 for dC/dr and substitution of dC/dr into equation 4.17 at $r = r_o$ gives,

$$K_1 = \frac{R_{o\,max}\, C}{K_m + C} \frac{r_o^{\,3}}{3D_a} \tag{4.26}$$

Substitution of K_1, back into equation 4.17 and rearrangement gives,

$$\frac{K_m + C}{R_{o\,max}\, C}\, dC = \frac{r_o^{\,3}}{3D_a r^2}\, dr \tag{4.27}$$

Which upon integration and subsequent rearrangement gives,

$$K_2 = \frac{K_m \ln C + C}{R_{o\,max}} + \frac{r_o^3}{3 D_a r} \tag{4.28}$$

Substituting the boundary condition $C = C_i$ at $r = r_a$ into equation 4.28 gives,

$$K_2 = \frac{K_m \ln C_i + C_i}{R_{o\,max}} + \frac{r_o^3}{3 D_a r_a} \tag{4.29}$$

Which upon substitution into equation 4.28 and rearrangement gives equation 4.30.

$$K_m \ln \left(\frac{C}{C_i} \right) + (C - C_i) = \frac{R_{o\,max}\, r_o^3}{3 D_a} \left(\frac{1}{r_a} - \frac{1}{r} \right) \tag{4.30}$$

Equation 4.30 describes the oxygen concentration at any position r in the fluid antrum under the assumption of Michaelis-Menton kinetics. Equation 4.30 cannot be solved explicitly, and requires an iterative solution. Given that in this work the interest was in what was happening in the pre-ovulatory follicle at a critical oxygen level $C = C_{crit}$ when $R_o = 0.99\, R_{omax}$, the consumption rate of oxygen by the oocyte can essentially be assumed to be constant, i.e. not a function of concentration. In this case rather than using the more complex iterative procedure required to solve equation 4.30, $C = C_{crit}$ and $R_o = 0.99 R_{omax}$ can simply be substituted into equation 4.24 directly.

Since for the oocyte to be only just respiring maximally $C = C_{crit}$ at $r = r_o$ then substitution of this into equation 4.24 and rearrangement gives equation 4.31.

$$C_i = C_{crit} - \frac{R_o r_o^3}{3 D_a} \left(\frac{1}{r_a} - \frac{1}{r_o} \right) \tag{4.31}$$

Equation 4.31 describes the minimum oxygen concentration required at the granulosa/antrum interface to sustain the oocyte at $C \geq C_{crit}$ where $C_{crit} = C$ at $R_o = 0.99\, R_{omax}$.

4.5.2 In the granulosa cell layer

For the granulosa cell layer the steady-state oxygen balance is once again similar to equation 3.7, and is expressed here, including fluid voidage by equation 4.32.

$$0 = \frac{D_g}{r^2} \frac{d}{dr}\left(r^2 \frac{dC}{dr}\right) - R_g(1-\varepsilon)$$

(4.32)

where $D_g = D_{eff}$.

Which upon rearrangement and integration gives,

$$r^2 \frac{dC}{dr} = \frac{R_g (1-\varepsilon) r^3}{3D_g} + K_1$$

(4.33)

At the interface between the granulosa cell layer and the antral fluid the rate of oxygen diffusion to the interface through the granulosa cell layer equals the rate of oxygen diffusion away from the interface through the antral fluid layer. This is described mathematically by equation 4.34.

$$D_g \left(\frac{dC}{dr}\right)_{granulosa} = D_a \left(\frac{dC}{dr}\right)_{fluid}$$

(4.34)

From differentiation of equation 4.24 for the oxygen concentration at any position r in the antral fluid, equation 4.35 can be written.

$$\left(\frac{dC}{dr}\right)_{fluid} = \frac{R_o r_o^3}{3D_a r^2}$$

(4.35)

Setting $r = r_a$ in equation 4.35, substituting into equation 4.34 for $(dC/dr)_{fluid}$ and rearrangement gives,

$$\left(\frac{dC}{dr}\right)_{r_a} = \frac{R_o \, r_o^{\,3}}{3D_g \, r_a^{\,2}}$$

(4.36)

Substitution of equation 4.36 into equation 4.33, and rearrangement for K_1 at $r = r_a$ gives,

$$K_1 = \frac{R_o \, r_o^{\,3}}{3D_g} - \frac{R_g \, (1-\varepsilon) \, r_a^{\,3}}{3D_g}$$

(4.37)

Then substitution of K_1 back into equation 4.33 and subsequent rearrangement gives,

$$dC = \left(\frac{R_g \, (1-\varepsilon) \, r}{3D_g} - \frac{R_g \, (1-\varepsilon) \, r_a^{\,3}}{3D_g \, r^2} + \frac{R_o \, r_o^{\,3}}{3D_g \, r^2}\right) dr$$

(4.38)

which upon integration gives,

$$C = \frac{R_g \, (1-\varepsilon) \, r^2}{6D_g} + \frac{R_g \, (1-\varepsilon) \, r_a^{\,3}}{3D_g \, r} - \frac{R_o \, r_o^{\,3}}{3D_g \, r} + K_2$$

(4.39)

Since at $r = r_f$, $C = C_o$

$$K_2 = C_0 - \frac{R_g \, (1-\varepsilon) \, r_f^{\,2}}{6D_g} - \frac{R_g \, (1-\varepsilon) \, r_a^{\,3}}{3D_g \, r_f} + \frac{R_o \, r_o^{\,3}}{3D_g \, r_f}$$

(4.40)

Hence substitution of K_2 back into equation 4.39 gives,

$$C = C_o - \frac{R_g \, (1-\varepsilon)}{6D_g}(r_f^{\,2} - r^2) - \frac{R_g \, (1-\varepsilon) \, r_a^{\,3}}{3D_g}\left(\frac{1}{r_f} - \frac{1}{r}\right) + \frac{R_o \, r_o^{\,3}}{3D_g}\left(\frac{1}{r_f} - \frac{1}{r}\right)$$

(4.41)

Equation 4.41 describes the oxygen concentration at any position r within the granulosa cell layer. At $r = r_a$ evaluation of equation 4.41 yields C_i for input into

equations describing oxygen transport in the antral fluid space. Coupling of such equations allows for comparison of the oxygen concentration profiles in the antral and pre-ovulatory follicles.

To do this the nominal values of each parameter previously described can be used, and it is assumed that R_o is at R_{omax}. A nominal value of V_g as calculated by equation 4.10 needs to be selected. The data of McNatty (1981) suggests that for pre-ovulatory follicles the number of granulosa cells becomes fairly constant ranging between 40 and 54 x 10^6 cells. Choosing a follicle with antral fluid volume of 4 ml (the mean value for IVF sized follicles measured in this work) the number of granulosa cells is approximately 50 x 10^6. Given that the reported granulosa cell volumes range from 942 to 2207 μm^3 a sensible nominal value for V_{cell} is in the middle of this range, a value of 1576 μm^3. Evaluation of equations 4.41 and 4.24 (concentration profiles in pre-ovulatory granulosa and fluid layers respectively) as well as equations 4.8 and 4.1 (concentration profiles in antral granulosa and fluid layers respectively) requires knowledge of both r_a and r_f. Assuming the volume of the oocyte to be negligible allows direct comparison of the pre-ovulatory and antral models by allowing the granulosa cell layers to be the same distance from the follicle centre. Assuming this to be the case, and since V_a and V_g are known, r_a can be calculated.

$$r_a = \left(V_a \frac{3}{4\pi} \right)^{\frac{1}{3}} \qquad (4.42)$$

And since $V_f = V_a + V_g$, r_f will be given by,

$$r_f = \left(\frac{3}{4\pi} (V_a + V_g) \right)^{\frac{1}{3}} \qquad (4.43)$$

Subsequent evaluation of equations 4.41 and 4.8 reveals that at these parameter values all oxygen is consumed in the granulosa cell layer before it gets to the fluid space. If the nominal value of V_{cell} is changed to the lower limit of 942 μm^3 this is no longer the case and the follicle is oxygenated throughout. This reinforces what was already

known, that the model solution is very sensitive to small variations in V_a/V_f. To allow comparison of complete oxygen profiles in antral and pre-ovulatory follicles, a value of 942 μm^3 was used as a nominal value. The results of the evaluation of the complete antral and pre-ovulatory models are shown in Figure 4.15.

Figure 4.15 shows that the antral and pre-ovulatory models show the same rapid drop off in oxygen concentration through the granulosa cell layer, as predicted for an IVF sized follicle with 4 ml of antral fluid. The reason the profiles are the same here is due to the fact that the term involving the oocyte in equation 4.41 is negligible. If this term is omitted equations 4.41 and 4.8 become identical.

In the fluid space the solutions are also the same except when in the vicinity of the oocyte, where the pre-ovulatory model shows a rapid non-linear decline in oxygen concentration as the surface of the oocyte is approached. This pattern is observed because at the granulosa/fluid interface, $C=C_i$. As the oocyte is approached the consumption term starts to have an effect and hence the decline in oxygen concentration is observed as r approaches r_o.

The drop of in oxygen concentration near the oocyte surface appears to result in only a very localised oxygen gradient. This is important to the clinical analysis of dissolved oxygen as it suggests that the fluid can essentially be assumed to be at an overall bulk concentration. The important question now is what oxygen concentration, C_i, the granulosa/fluid interface must be at to maintain oocyte respiration at C_{crit}, and how is this effected by the volume of the fluid antrum. This can be determined through solution of equation 4.31. Evaluation of equation 4.31 is shown in Figure 4.16 at $R_o = 0.99\ R_{omax}$. Figure 4.16 shows that the minimum required interfacial oxygen concentration starts at $C = C_i$ and rapidly increases with increasing fluid volume as the total resistance to mass transport increases. As the size of the antral fluid space increases the required interfacial oxygen concentration becomes constant. This happens because as r_a becomes large $^1/r_a \rightarrow 0$, and hence the required interfacial oxygen concentration becomes independent of fluid volume and equation 4.31 reduces to,

$$C_i = C_{crit} + \frac{R_o \, r_o^{\,2}}{3D_a}$$

(4.44)

Figure 4.16 shows that the interfacial oxygen concentration (C_i) required becomes constant well before typical IVF fluid volumes are encountered. This suggests that for IVF follicles equation 4.44 will apply. If the follicle is antral (not pre-ovulatory), equation 4.44 simply reduces to $C_i = C_{crit}$. Figure 4.17 shows the relationship between fluid volume and required interfacial oxygen concentration for IVF sized follicles. For easier interpretation the oxygen concentrations are expressed as vol%. Figure 4.17 shows that the required interfacial oxygen level is independent of fluid volume for IVF size follicles. An antral follicle with antral fluid dissolved oxygen above 5.7 vol% will be able to support maximal oocyte respiration, and below this level it will not. For a pre-ovulatory follicle this oxygen level is elevated to 6.1 vol% (using best parameter estimates). If whether or not the follicle is antral or pre-ovulatory is unknown, or if the location of the oocyte is not known, then these concentrations can be used to form a zone of uncertainty (Figure 4.17). This zone exists between the oxygen levels of 5.7 to 6.1 vol%, between which the respiratory status will be undetermined. It should be noted that the 0.4 vol% width of the zone of uncertainty would be only marginally detectable within the limits of many oxygen analysis techniques, including the commonly used Clark-style dissolved oxygen electrode. Hence, at least at the nominal values used here, it is suggested that comparison of dissolved oxygen values from follicle to follicle is relatively independent of oocyte position, if attempting to infer respiratory status. Not requiring information about oocyte position is clearly an advantage and greatly simplifies any potential analysis.

Figure 4.17 suggests the existence of a cut-off level, or band of dissolved oxygen level, above which the oocyte can respire maximally and below which it cannot. This is an important concept and suggests that the measurement of follicular fluid dissolved oxygen may represent a very simple method of assessing oocyte respiratory status, or perhaps more correctly whether or not the oocyte is in an environment that facilitates maximal respiration.

143
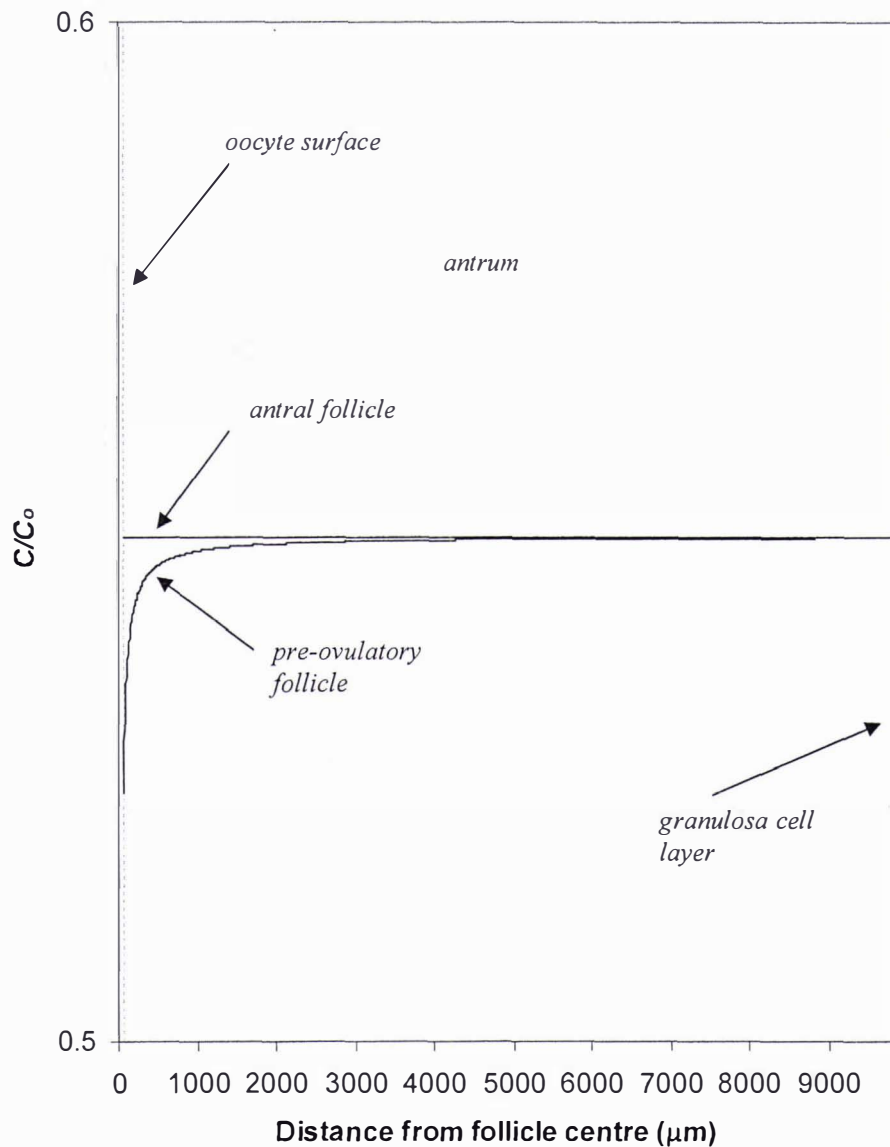
Figure 4.15   Comparison of oxygen concentration profiles across antral and pre-ovulatory follicles for IVF sized follicles (4 ml antral fluid volume (V_a)). Calculations performed by evaluating of equations 4.41 and 4.24 (concentration profiles in pre-ovulatory granulosa and fluid layers respectively) as well as equations 4.8 and 4.1 (concentration profiles in antral granulosa and fluid layers respectively) and using the nominal values of each parameter (Tables 3.3 and 4.1 and including a constant granulosa cell volume calculated at V_{cell} = 942 μm^3).
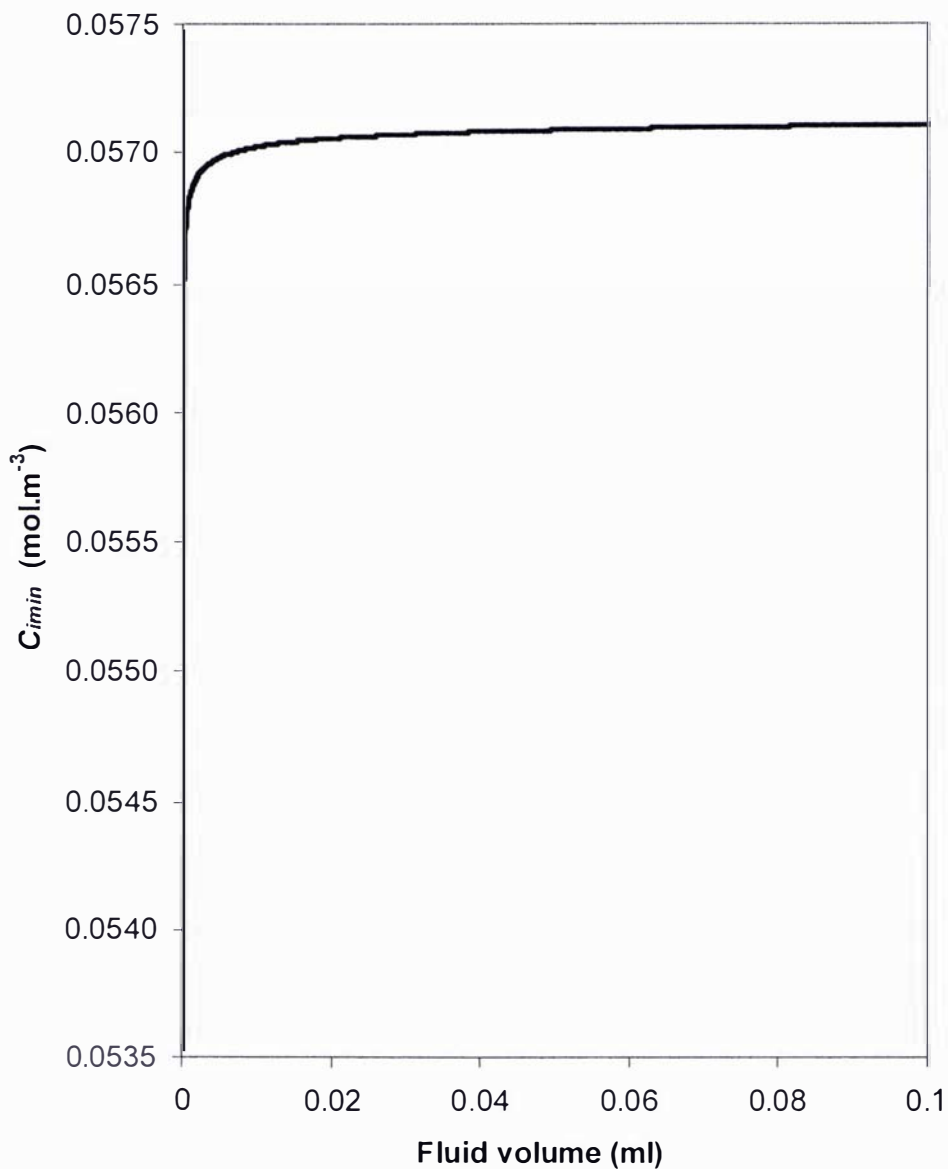
Figure 4.16   Minimum interfacial oxygen concentration (C_{imin}) required to sustain the oocyte at 99% maximal respiration as a function of follicular fluid volume (V_a). Note that oxygen concentration becomes constant before typical IVF volumes attained. Calculations performed by evaluating equation 4.31 at $R_o = 0.99R_{omax}$ and using the nominal values of each parameter.

The concept of a cut-off level in dissolved oxygen is supported in the literature by Van Blerkom *et al.* (1997) who found that oocytes originating from follicles with ≤ 3 vol% dissolved oxygen in the antral fluid are much more likely to be abnormal and have reduced development frequency. The value of 3% is somewhat similar to that calculated here (approximately 5.7% as shown by lower band of Figure 4.17). It should be noted that this work assumes a cut-off to occur when the oocyte can no longer respire maximally. It is possible that the oxygen level at which the oocyte actually becomes compromised may be below this. Of course, care should be taken comparing the absolute values calculated here with experimental values due to the unknown accuracy of some of the parameter estimates. In any case, this work is seen as being very useful in illustrating the concept of an oxygen cut-off level.

For this concept to be used effectively, analysis would benefit from a zone of uncertainty that is as narrow as possible, and ideally lack any great variability from follicle to follicle. For IVF sized follicles, equation 4.44 suggests that four parameters will impact on the width of the zone of uncertainty, namely C_{crit}, R_o, r_o, and D_a.

The first two parameters C_{crit}, and R_o relate to the oxygen consumption kinetics of the oocyte. Studies investigating the oxygen consumption kinetics of human oocytes would be very useful in assisting with the interpretation of dissolved oxygen data. Studies involving oocytes (particularly human) are complicated by the difficulty in obtaining oocytes due to ethical and clinical issues, and considered beyond the resources available for this work. If C_{crit} and/or R_o are significantly variable they will need to be known as a function of dissolved oxygen to be meaningfully interpreted, thus greatly complicating any analysis.
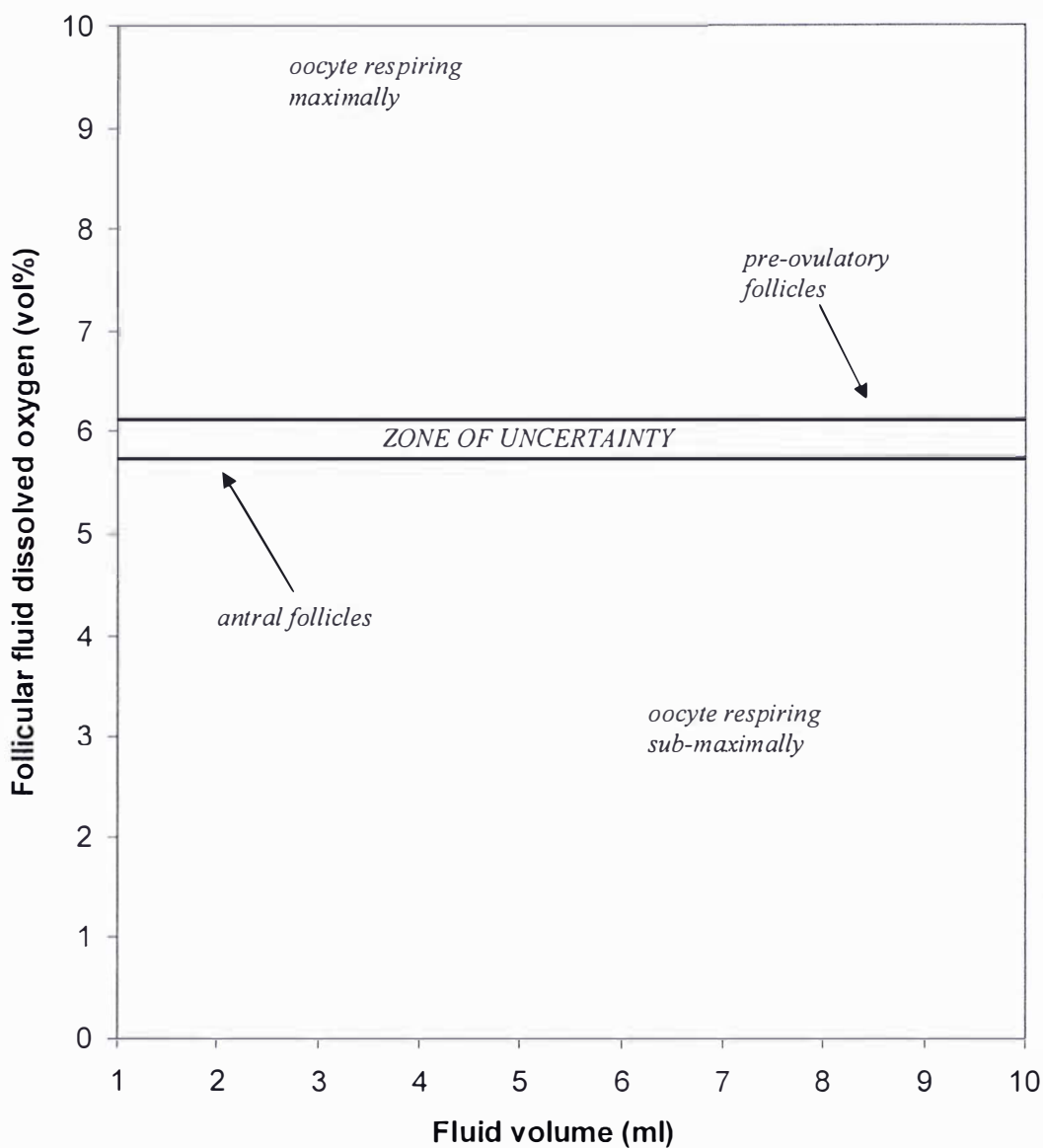
Figure 4.17   Minimum interfacial oxygen concentration required to sustain oocyte at 99% maximal respiration for antral and pre-ovulatory across a range of follicular fluid volumes typical of IVF. The zone of uncertainty represents the dissolved oxygen range within which the respiratory status of the oocyte will be uncertain. Here this is due to the uncertainty in the position of the oocyte.

147
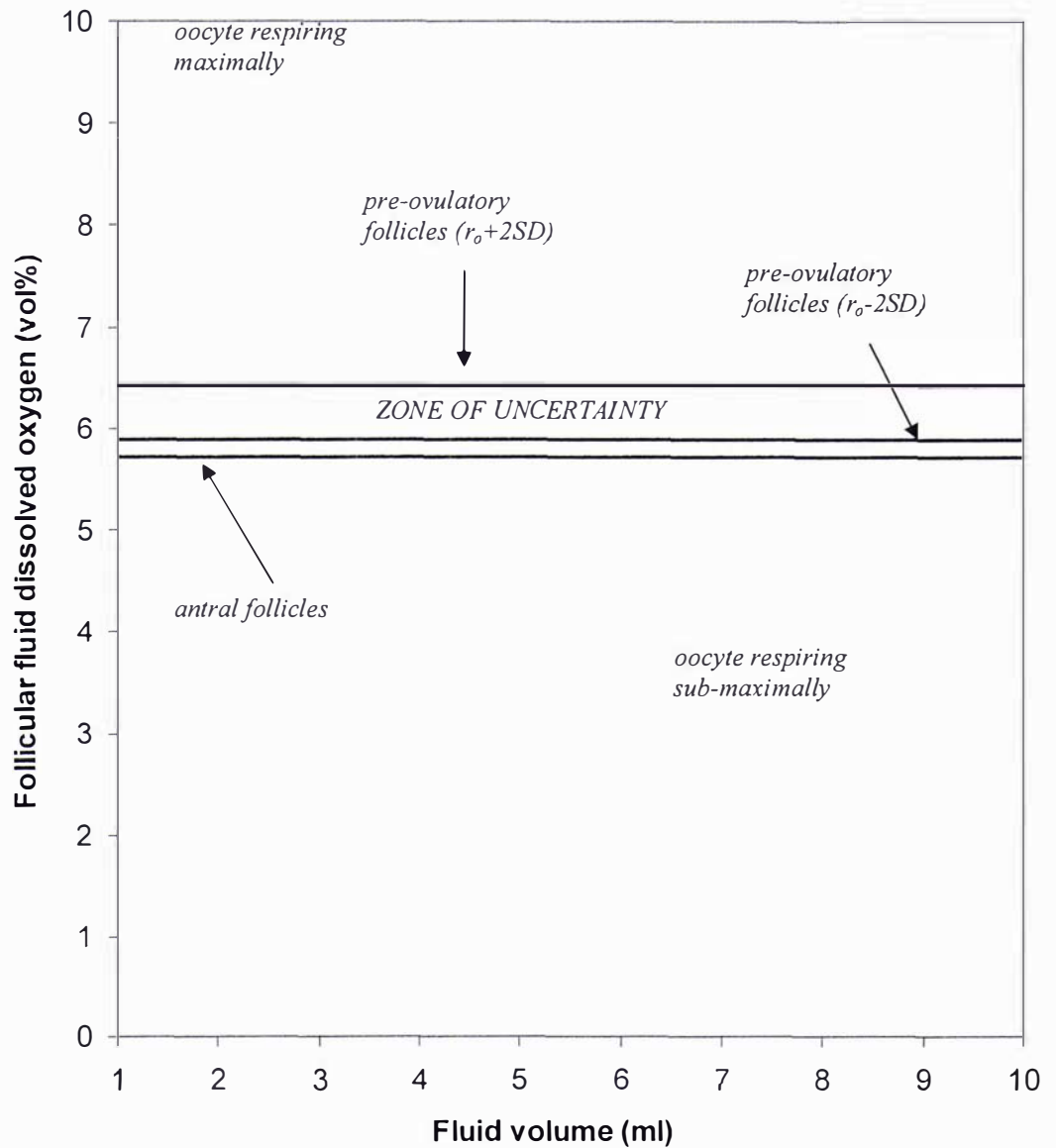
Figure 4.18   Effect of variability in oocyte radius (r_o) through mean ± 2SD on minimum interfacial oxygen concentration required to sustain oocyte at 99% maximal respiration (IVF size follicle range). The width of the zone of uncertainty is now determined by positional uncertainty of the oocyte (antral or pre-ovulatory) and variability in parameter estimates (in this case r_o).

Information on the variability of r_o is available with Tsuji *et al.* (1985) giving the radius of the human oocyte as 58 ± 10 µm ($\pm$ SD). Figure 4.18 shows the impact of variation in r_o through a feasible range of the mean $\pm$ 2SD, on the width of the zone of uncertainty. The zone of uncertainty then spans from 5.9 to 6.4 vol % if the oocyte is centred in the antrum (pre-ovulatory follicle). Again this difference is only marginally detectable. If the position of the oocyte is unknown, then the zone of uncertainty ranges from 5.7 to 6.4 vol %. Whilst this is starting to become a detectable difference, it is still small enough to allow reasonable inference about the respiratory status of the oocyte if the radius of the oocyte is unknown. That said, given that the oocyte is viewed under the microscope during the IVF procedure, it may be a simple matter to measure its radius if this is seen to be worthwhile. This may provide additional useful information. For example Figure 4.18 suggests, if two oocytes were derived from fluids of the same oxygen concentration but one was significantly larger, this oocyte may be less likely to have an oxygen supply that meets its demands (all other things being equal).

Diffusion coefficients of oxygen in follicular fluid have not been reported. In a review of diffusion coefficients Lango *et al.* (1996) give a preferred value of the diffusivity of oxygen in water as 3.0×10^{-5} cm^2.s^{-1} at 37°C. This value would likely be the maximum that follicular fluid could be expected to have. Goldstick *et al.* (1976) give the value of the diffusion coefficient of oxygen in normal human plasma as 2.2×10^{-5} cm^2.s^{-1} at 37°C. Given that follicular fluid is a derivative of plasma it would be fair to expect the diffusion coefficient of oxygen in follicular fluid to be similar to this value. To give a reasonably conservative estimate of the range over which D_a might vary, 50% of the plasma value has been selected as the lower limit. Hence the range for input into the model is 1.1 to 3.0×10^{-5} cm^2.s^{-1}.

Figure 4.19 shows the impact of variation of D_a throughout this range on the size of the zone of uncertainty. The effect on the size of the zone is similar to that caused by variation in oocyte radius, with the range being 6.0 to 6.5 vol% for variation of D_a from 3.0 to 1.1×10^{-5} cm^2.s^{-1}. If the position of the oocyte is unknown then variation is from 5.7 to 6.5 vol%. Although this is once again only marginally detectable, this range is based on estimated values, with variability in D_a not as well quantified as it is

for R_o. Therefore investigation into variability in the diffusion coefficients of oxygen in follicular fluid is considered worthwhile.

Reinforcing this is Figure 4.20 which shows the variability in the zone of uncertainty between the extreme limits of a small oocyte ($r_o - 2SD$) in a highly diffusive fluid (3.0×10^{-5} cm^2.s^{-1}) and a large oocyte ($r_o + 2SD$) in a less diffusive fluid (1.1×10^{-5} cm^2.s^{-1}). As would be expected, the required interfacial concentration tends toward the antral situation of $C_i = C_{crit}$ for the small oocyte in the highly diffusive fluid. The total range is now quite large. If the diffusivity of oxygen in follicular fluid was measured and was found not to vary greatly then this range would narrow considerably. If diffusion coefficients of oxygen in follicular fluid are found to be highly variable, then measurement of oocyte radius may help in reducing the zone of uncertainty. This may be more convenient than measuring diffusion coefficients in individual fluids which would be a very time consuming exercise, unless an efficient technique could be developed. Measurement of diffusion coefficients could of course be coupled with measurements of oocyte radius to further reduce the zone of uncertainty. In any case, it is considered an important exercise to determine the variability of diffusion coefficients of oxygen in follicular fluid, and this is one of the focal points of the following chapters.

4.5.3 Vascularisation and required interfacial oxygen concentration

It has been shown that in the pre-ovulatory follicle the oxygen concentration at the cell/fluid interface needs to be at a certain level if the oocyte is to receive sufficient oxygen to respire maximally. Perhaps the key question now becomes, what level of vascularisation is required to achieve this concentration at the interface, and how does this depend on follicle size? Since it is known that if the interfacial oxygen concentration drops below a certain minimum level the oocyte can no longer respire maximally, this question can be answered through the solution of simultaneous equations. The oocyte will just sustain maximal respiration when $C_i = C_{i\,min}$ at $r = r_a$. So setting $C = C_{i\,min}$ in equation 4.41 and $r = r_a$ gives (C_{imin} is the minimum oxygen concentration required at the granulosa/antrum interface to sustain the oocyte at $R_o = 0.99 R_{omax}$),

$$C_{i\,min} = C_o - \frac{R_g(1-\varepsilon)}{6\,D_g}(r_f^2 - r_a^2) - \frac{R_g(1-\varepsilon)r_a^3}{3\,D_g}\left(\frac{1}{r_f} - \frac{1}{r_a}\right) + \frac{R_o\,r_o^3}{3\,D_g}\left(\frac{1}{r_f} - \frac{1}{r_a}\right)$$

(4.45)

Also from equation 4.44 for IVF follicles,

$$\dot{C}_{i\,min} = C_{crit} + \frac{R_o\,r_o^2}{3\,D_a}$$

(4.46)

So setting equation 4.45 equal to equation 4.46 and $C_o{=}C_{omin}$ allows the following expression for C_{omin} (minimum oxygen concentration required at the follicle surface to sustain the oocyte at $R_o{=}0.99R_{omax}$) to be solved for,

$$C_{o\,min} = C_{crit} + \frac{R_g(1-\varepsilon)}{6\,D_g}(r_f^2 - r_a^2) + \frac{R_g(1-\varepsilon)r_a^3}{3\,D_g}\left(\frac{1}{r_f} - \frac{1}{r_a}\right) - \frac{R_o\,r_o^3}{3\,D_g}\left(\frac{1}{r_f} - \frac{1}{r_a}\right) + \frac{R_o\,r_o^2}{3\,D_a}$$

(4.47)

where C_{crit} is as previously defined at $R_o = 0.99\,R_{o\,max}$

This equation can be evaluated at any given values of follicle and antral radius to give the minimum follicle surface vascularisation level to sustain the oocyte at $0.99\,R_{o\,max}$. This concentration can then be easily converted to a mean symmetrical vascularisation percentage as previously described (see 3.3.6). For the pre-ovulatory follicle, making the assumption that the volume of granulosa cells is constant as previously described, then for a given fluid volume V_a the radius of the antrum will be given by,

$$r_a = \left(\frac{3}{4\pi}V_a + r_o^3\right)^{\frac{1}{3}}$$

(4.48)

And hence the total radius of the follicle with constant granulosa cell layer volume (V_g) will be given by,

$$r_f = \left(\frac{3}{4\pi}V_g + r_a^3\right)^{\frac{1}{3}}$$

(4.49)

151

10

oocyte respiring
maximally

9

8

pre-ovulatory follicles
$(D_a=1.1x10^{-9}\ m^2.s^{-1})$

pre-ovulatory follicles
$(D_a=3.0x10^{-9}\ m^2.s^{-1})$

Follicular fluid dissolved oxygen (vol%)

7

ZONE OF UNCERTAINTY

6

5

antral follicles

4

oocyte respiring
sub-maximally

3

2

1

0

1   2   3   4   5   6   7   8   9   10

Fluid volume (ml)
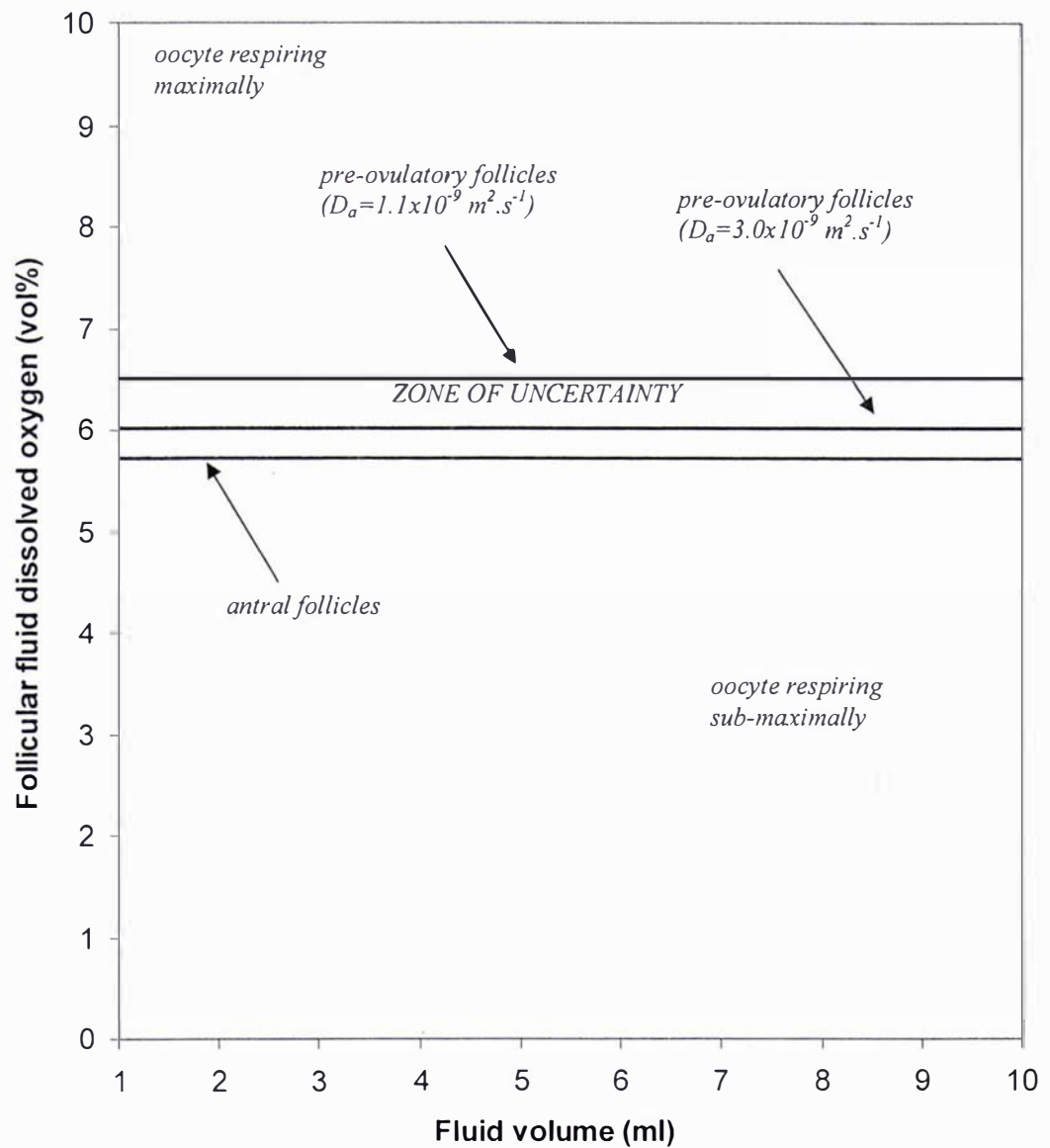
Figure 4.19   Effect of variability in follicular fluid oxygen diffusion coefficient (D_a) on the minimum interfacial oxygen concentration required to sustain the oocyte at 99% maximal respiration (IVF size follicle range).
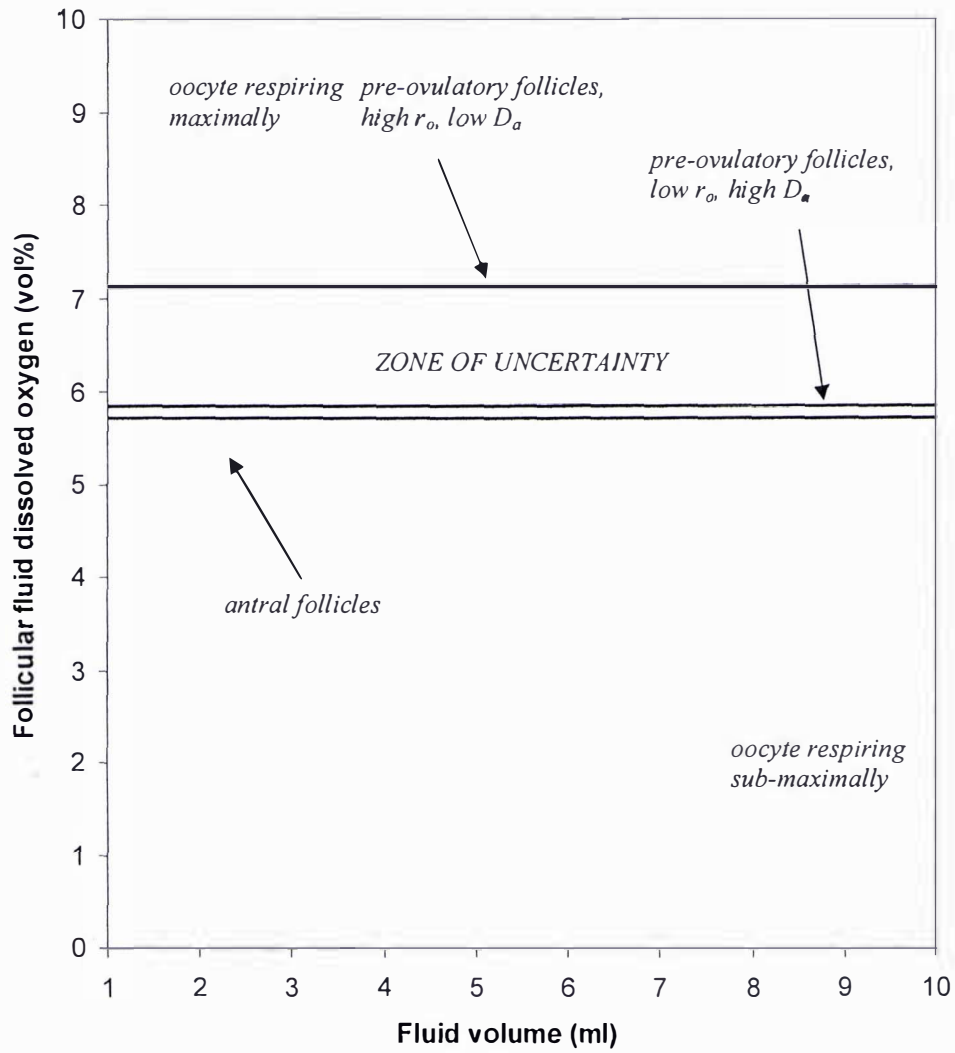
Figure 4.20   Effect of variability in both r_o and D_a on the minimum interfacial oxygen concentration required to sustain the oocyte at 99% maximal respiration (IVF size follicle range).

Using the nominal values of each parameter (Tables 3.3 and 4.1 and including a constant granulosa cell volume calculated at $V_{cell} = 942$ μm^3), Figure 4.21 shows the relationships between antral fluid volume and required vascularisation to sustain the oocyte at $R_o = 0.99\ R_{o\ max}$ as calculated using equation 4.47.

Figure 4.21 shows that if the ability of the oocyte to respire maximally is to be determined from follicle vascularisation, then the volume of the antral fluid must also be known. This figure and those for the measurement of dissolved oxygen level (Figures 4.17 to 4.20), give the same information, but measurement of vascularisation requires knowledge of additional parameters. Putting aside any issues associated with measurement technique, this once again suggests that Doppler ultrasonography, as a measure of oxygen status, is a more complicated procedure. It should be stressed that Figure 4.21 assumes constant granulosa cell volume. If this is not the case the situation becomes even more complex, requiring knowledge not only of vascularisation and fluid volume, but also either total follicle volume or granulosa cell volume. Further, equation 4.44 showed that the reliability of the use of dissolved oxygen concentration will depend on the variability in the oxygen consumption kinetics of oocytes, as well as oocyte size and fluid diffusivity. Because these parameters also feature in equation 4.47, the measurement of follicle vascularisation will also be subject to variability in these parameters. Additionally, follicle vascularisation as a measure of oxygen status will be subject to variability in the other parameters of equation 4.47, namely granulosa cell oxygen consumption rate, fluid voidage, and cellular diffusion coefficient. The direct measurement of dissolved oxygen is independent of these parameters, making it potentially a far simpler and more attractive procedure overall.

In spite of all this, some very useful information can still be derived from Figure 4.21. The figure shows that, as the volume of the follicle increases, the level of required vascularisation reduces. As the total volume of the spherical follicle increases, the constant volume of granulosa cells is spread across a greater surface and hence becomes thinner, offering less resistance to mass transport, and hence results in a reduction in the required vascularisation level. This reduced level of vascularisation tends toward the horizontal asymptote of Figure 4.21 as fluid volume increases and r_a

$\approx r_f$. As $r_a \to r_f$ equation 4.47 reduces to,

$$C_{o\,min} = C_{crit} + \frac{R_\sigma \, r_o^{\,2}}{3 \, D_a} \qquad\qquad (4.50)$$

This equation is identical to equation 4.44 for the fluid filled antrum. This is because, as the follicle becomes very large and $V_a >> V_g$, the follicle is essentially just a fluid filled sphere with the cellular layer becoming negligible. Evaluation of equation 4.47 yields a vascularisation level of approximately 38%. This is an important piece of information, as it suggests there is a critical level of vascularisation below which the oocyte will not be capable of maximal respiration, irrespective of fluid volume. So Doppler ultrasonography could potentially provide some very useful information without knowledge of fluid volume. That is, above a certain critical vascularisation the respiratory status of the oocyte may be uncertain but below this level the oocyte can be considered as incapable of maximal respiration. This suggests that Doppler ultrasonagraphy may be able to be used to select oocytes using cut-off values.

The concept of a cut-off level of vascularisation below which the oocyte may be compromised appears to be supported by data in the literature. It was found by Bhal *et al.* (1999) through the use of Doppler ultrasonography, that below 50% vascularisation only 7.3% of IVF cycles resulted in pregnancy with a 100% loss rate. Greater than or equal to 50% vascularisation resulted in 28% pregnancy with only a 48% loss rate. Furthermore less than 25% vascularisation resulted in no pregnancies. This suggests that somewhere between 25 and 50% there exists a cut-off level of vascularisation below which the oocyte becomes extremely compromised. The 38% calculated here for the horizontal asymptote lies within this range, and although the value calculated here should not be considered absolute (as it is based on best parameter estimates), the ability of the oocyte to respire maximally may explain the observations of Bhal *et al.* (1999).
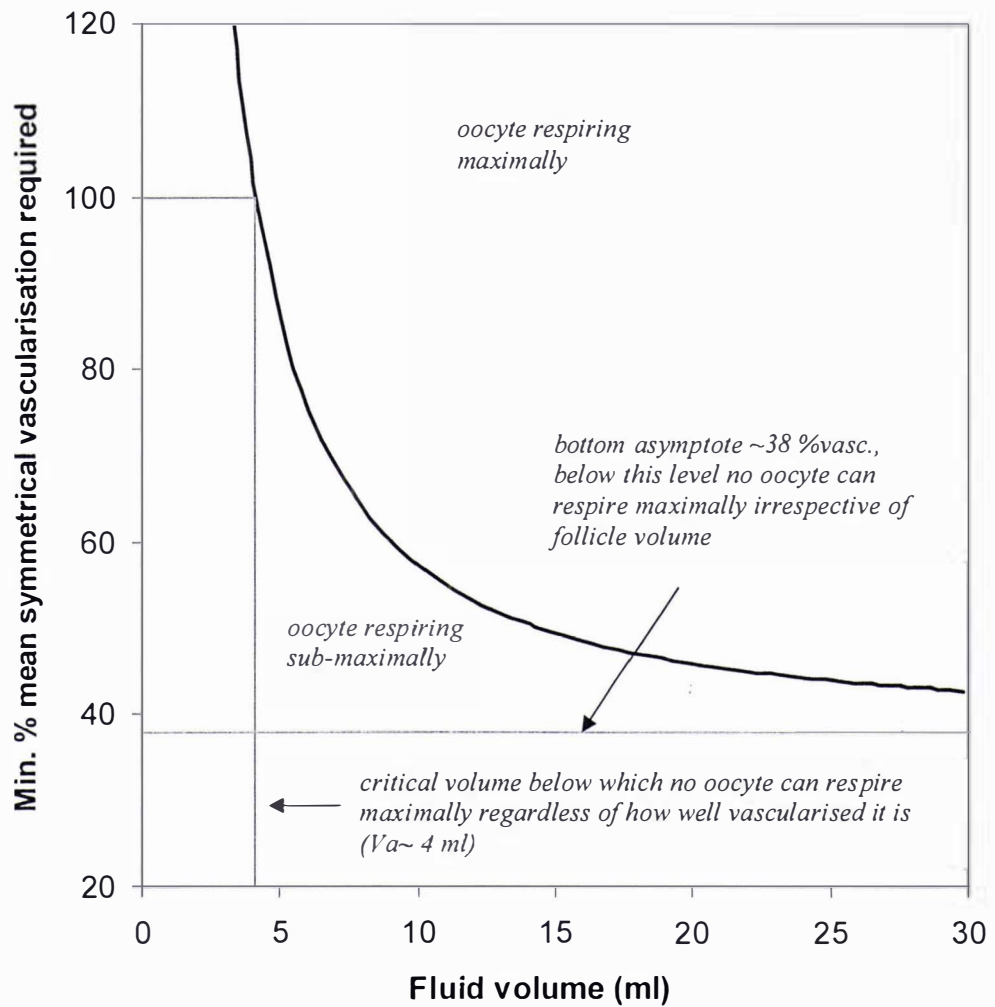
Figure 4.21   Minimum % vascularisation required to sustain oocyte at 99% maximal respiration as a function of follicular fluid volume (V_a) using the nominal values of each parameter (Tables 3.3 and 4.1 and including a constant granulosa cell volume calculated at $V_{cell} = 942 \; \mu m^3$)

It can also be suggested from Figure 4.21, that below a certain critical volume the oocyte will not be able to respire maximally regardless of how well vascularised it is. By reading off fluid volume at 100% vascularisation from Figure 4.21, this critical volume is approximately 4 ml.

The concept of a cut-off fluid volume also seems to be supported in the literature. In a brief review, Fisch *et al.,* (1990) claim that a relationship between fluid volume and IVF outcome is well established. Perhaps more specifically Quigley *et al.* (1982) found that follicles with a diameter of greater than 20 mm showed higher oocyte recovery rates, higher fertilisation rates, and higher cleavage rates. By considering granulosa cell volume to be negligible, a 20 mm follicle represents approximately 4.2 ml of antral fluid, similar to the 4 ml value in Figure 4.21. It is suggested here that the observation of a cut-off volume level may be related to mass transport limitations of oxygen and the subsequent ability of the oocyte to respire maximally.

Interestingly, Scott *et al.* (1989) found that follicles with antral fluid volume greater than approximately 1.5 ml are more likely to contain mature oocytes. Simonetti *et al.* (1985) found a similar association between mature oocytes and follicles with fluid volume greater than 2.8 ml. Although speculative, it is possible that oxygen limitations may play a role in oocyte maturation. Perhaps further insight on this result could be developed if data for oocyte respiration as a function of maturity could be measured.

4.5.4 Effect of addition of cumulus cells

The previous pre-ovulatory model assumed the oocyte to be naked. In reality the oocyte will likely be surrounded by a mass of granulosa cells known as the *cumulus oophorus*. This section looks at the impact of such cells on oxygen transport in the follicle, and the implications on the conclusions drawn thus far. A mathematical model for oxygen transport in the isolated cumulus-oocyte complex has been described by Clark *et al.* (2006). In the work presented here, this structure is modelled as part of a complete follicle. The proposed model of oxygen transport in the pre-ovulatory follicle with cumulus cells is represented pictorially in Figure 4.22.

The assumptions made by this up-dated model are the same as those made for the pre-ovulatory follicle with no cumulus (section 4.5) except for the following,

1.   The oocyte is surrounded by a mass of cumulus cells.

2.   The cumulus cells consume oxygen at a constant rate.

3.   The cumulus-oocyte complex is spherical.

4.5.4.1 Model derivation

4.5.4.1.1 Cumulus Layer

For the cumulus cell layer the steady-state oxygen balance is given by,

$$0 = \frac{D_c}{r^2} \frac{d}{dr}\left(r^2 \frac{dC}{dr}\right) + R_c \tag{4.51}$$

which upon integration gives,

$$r^2 \frac{dC}{dr} = \frac{R_c \, r^3}{3D_c} + K_1 \tag{4.52}$$

At the interface between the cumulus cell layer and the oocyte ($r=r_o$) the rate of oxygen diffusion through the cumulus cell layer to the oocyte surface is equal to the rate of oxygen consumption by the oocyte.

$$4\pi r_o{}^2 D_c \frac{dC}{dr} = R_o \frac{4}{3}\pi r_o{}^3 \tag{4.53}$$

Rearrangement of equation 4.53 gives the first boundary condition,

$$\frac{dC}{dr} = \frac{R_o \, r_o}{3D_c} \tag{4.54}$$
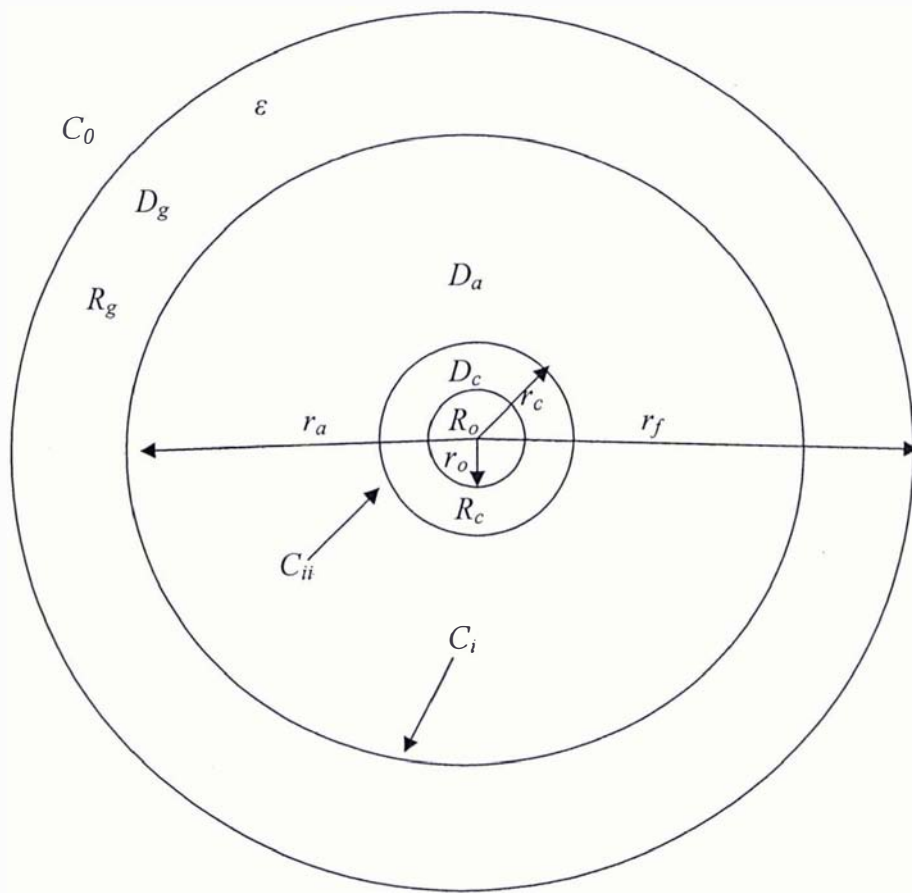
Figure 4.22   Pictorial representation of the model of oxygen transport in the pre-ovulatory follicle with cumulus (see nomenclature section for description of symbols).

At $r=r_o$ substitution of equation 4.54 into equation 4.52 and subsequent rearrangement reveals,

$$K_1 = -\frac{R_c r_o^3}{3D_c} + \frac{R_o r_o^3}{3D_c} \tag{4.55}$$

Substitution of equation 4.55 back into equation 4.52 and subsequent rearrangement gives,

$$dC = \left(\frac{R_c r}{3D_c} - \frac{R_c r_o^3}{3D_c r^2} + \frac{R_o r_o^3}{3D_c r^2} \right) dr \tag{4.56}$$

Which upon integration gives,

$$C = K_2 + \frac{R_c r^2}{6D_c} + \frac{R_c r_o^3}{3D_c r} - \frac{R_o r_o^3}{3D_c r} \tag{4.57}$$

Since at $C=C_{ii}$ at $r=r_c$, substitution of this boundary condition into equation 4.57 and subsequent rearrangement gives,

$$K_2 = C_{ii} - \frac{R_c r_c^2}{6D_c} - \frac{R_c r_o^3}{3D_c r_c} + \frac{R_o r_o^3}{3D_c r_c} \tag{4.58}$$

Finally substitution of K_2 back into equation 4.57 gives equation 4.59.

$$C = C_{ii} - \frac{R_c}{6D_c}(r_c^2 - r^2) - \frac{R_c r_o^3}{3D_c}\left(\frac{1}{r_c} - \frac{1}{r} \right) + \frac{R_o r_o^3}{3D_c}\left(\frac{1}{r_c} - \frac{1}{r} \right) \tag{4.59}$$

Equation 4.59 describes the oxygen concentration at any position r in the cumulus cell layer.

4.5.4.1.2 Antral Fluid

Since there is no oxygen consumption in the antral fluid the steady-state oxygen balance is given by,

$$0 = \frac{d}{dr}\left(r^2 \frac{dC}{dr}\right) \tag{4.60}$$

which upon integration yields equation 4.61.

$$K_1 = r^2 \frac{dC}{dr} \tag{4.61}$$

At the interface between the antral fluid and the cumulus cells the rate of oxygen diffusion to the interface through the antral fluid equals the rate of oxygen diffusion away from the interface through the cumulus cell layer. This is described mathematically by equation 4.62.

$$D_a \left(\frac{dC}{dr}\right)_{fluid(rc)} = D_c \left(\frac{dC}{dr}\right)_{cumulus(rc)} \tag{4.62}$$

From differentiation of equation 4.59 for the oxygen concentration at any position r in the cumulus cell layer, equation 4.63 can be written,

$$\frac{dC}{dr} = \frac{R_c r}{3D_c} - \frac{R_c r_o^3}{3D_c r^2} + \frac{R_o r_o^3}{3D_c r^2} \tag{4.63}$$

Setting $r = r_c$ in equation 4.63, defines $(dC/dr)_{cumulus}$ which when substituted into equation 4.62 and rearranged, gives the antral side concentration gradient at the antrum/cumulus interface,

$$\left(\frac{dC}{dr}\right)_{fluid(rc)} = \frac{R_c r_c}{3D_a} - \frac{R_c r_o^3}{3D_a r_c^2} + \frac{R_o r_o^3}{3D_a r_c^2} \tag{4.64}$$

161

Substitution of equation 4.63 into equation 4.61 at $r = r_c$ gives,

$$K_1 = \frac{R_c r_c^3}{3D_a} - \frac{R_c r_o^3}{3D_a} + \frac{R_o r_o^3}{3D_a}$$

(4.65)

Then substitution of K_1 back into equation 4.61 and subsequent rearrangement gives equation 4.66.

$$dC = \left(\frac{R_c r_c^3}{3D_a r^2} - \frac{R_c r_o^3}{3D_a r^2} + \frac{R_o r_o^3}{3D_a r^2} \right) dr$$

(4.66)

which upon integration gives,

$$C = -\frac{R_c r_c^3}{3D_a r} + \frac{R_c r_o^3}{3D_a r} - \frac{R_o r_o^3}{3D_a r} + K_2$$

(4.67)

Since at $r = r_a$, $C = C_i$

$$K_2 = C_i + \frac{R_c r_c^3}{3D_a r_a} - \frac{R_c r_o^3}{3D_a r_a} + \frac{R_o r_o^3}{3D_a r_a}$$

(4.68)

Finally substitution of K_2 back into equation 4.67 gives,

$$C = C_i + \frac{R_c r_c^3}{3D_a} \left(\frac{1}{r_a} - \frac{1}{r} \right) - \frac{R_c r_o^3}{3D_a} \left(\frac{1}{r_a} - \frac{1}{r} \right) + \frac{R_o r_o^3}{3D_a} \left(\frac{1}{r_a} - \frac{1}{r} \right)$$

(4.69)

Equation 4.69 describes the oxygen concentration at any position r in the antral fluid layer. Note that if $r_c = 0$, and hence $R_c = 0$, equation 4.69 reduces to the same equation derived for the pre-ovulatory follicle without a cumulus layer (equation 4.24).

4.5.4.1.3 Granulosa cell layer

In the granulosa cell layer the steady-state oxygen balance is given by,

$$0 = \frac{D_g}{r^2} \frac{d}{dr}\left(r^2 \frac{dC}{dr}\right) - R_g (1-\varepsilon) \qquad (4.70)$$

which upon integration gives,

$$r^2 \frac{dC}{dr} = \frac{R_g(1-\varepsilon)\,r^3}{3D_g} + K_1 \qquad (4.71)$$

At the interface between the granulosa cell layer and the antral fluid, the rate of oxygen diffusion to the interface through the granulosa cell layer equals the rate of oxygen diffusion away from the interface through the antral fluid. This is described by equation 4.72.

$$D_g \left(\frac{dC}{dr}\right)_{granulosa(ra)} = D_a \left(\frac{dC}{dr}\right)_{fluid\,(ra)} \qquad (4.72)$$

From differentiation of equation 4.69 for the oxygen concentration at any position r in the cumulus cell layer equation 4.73 can be written,

$$\frac{dC}{dr} = \frac{R_c r_c^3}{3D_a r^2} - \frac{R_c r_o^3}{3D_a r^2} + \frac{R_o r_o^3}{3D_a r^2} \qquad (4.73)$$

Setting $r = r_a$ in equation 4.73, defines $(dC/dr)_{fluid}$ which when substituted into equation 4.72 and rearranged, gives the granulosa side concentration gradient at the granulosa/antrum interface,

$$\left(\frac{dC}{dr}\right)_{granulosa(ra)} = \frac{R_c r_c^3}{3D_g r_a^2} - \frac{R_c r_o^3}{3D_g r_a^2} + \frac{R_o r_o^3}{3D_g r_a^2} \qquad (4.74)$$

163

Substitution of equation 4.74 into equation 4.71, and rearrangement for K_1 at $r = r_a$ gives,

$$K_1 = -\frac{R_g(1-\varepsilon)r_a^3}{3D_g} + \frac{R_c r_c^3}{3D_g} - \frac{R_c r_o^3}{3D_g} + \frac{R_o r_o^3}{3D_g}$$

(4.75)

Then substitution of K_1 back into equation 4.71 and subsequent rearrangement gives equation 4.76,

$$dC = \left(\frac{R_g(1-\varepsilon)r}{3D_g} - \frac{R_g(1-\varepsilon)r_a^3}{3D_g r^2} + \frac{R_c r_c^3}{3D_g r^2} - \frac{R_c r_o^3}{3D_g r^2} + \frac{R_o r_o^3}{3D_g r^2} \right) dr$$

(4.76)

which upon integration gives,

$$C = \frac{R_g(1-\varepsilon)r^2}{6D_g} + \frac{R_g(1-\varepsilon)r_a^3}{3D_g r} - \frac{R_c r_c^3}{3D_g r} + \frac{R_c r_o^3}{3D_g r} - \frac{R_o r_o^3}{3D_g r} + K_2$$

(4.77)

Since at $r=r_f$, $C=C_o$

$$K_2 = C_o - \frac{R_g(1-\varepsilon)r_f^2}{6D_g} - \frac{R_g(1-\varepsilon)r_a^3}{3D_g r_f} + \frac{R_c r_c^3}{3D_g r_f} - \frac{R_c r_o^3}{3D_g r_f} + \frac{R_o r_o^3}{3D_g r_f}$$

(4.78)

Finally substitution of K_2 back into equation 4.77 gives,

$$C = C_o - \frac{R_g(1-\varepsilon)}{6D_g}(r_f^2 - r^2) - \frac{R_g(1-\varepsilon)r_a^3}{3D_g}\left(\frac{1}{r_f} - \frac{1}{r}\right) + \frac{R_c r_c^3}{3D_g}\left(\frac{1}{r_f} - \frac{1}{r}\right) - \frac{R_c r_o^3}{3D_g}\left(\frac{1}{r_f} - \frac{1}{r}\right) + \frac{R_o r_o^3}{3D_g}\left(\frac{1}{r_f} - \frac{1}{r}\right)$$

(4.79)

where $D_g = D_{eff}$

Equation 4.79 describes the oxygen concentration at any position r in the granulosa cell layer. Note that if $r_c=0$, and hence $R_c=0$, equation 4.79 reduces to the same

equation derived for the pre-ovulatory follicle without a cumulus layer (equation 4.41).

4.5.4.2 Estimation of r_c, R_c, and D_c

To use the equations derived for the pre-ovulatory follicle with cumulus requires that the parameters r_c, R_c, and D_c be estimated. Using images of mature human cumulus-oocyte complexes (the type found in pre-ovulatory follicles) from Ng *et al.* (1999), and Veeck *et al.* (1983), the relative thickness of the cumulus cell layer (r_c/r_o) can be estimated to range from approximately 2 to 4. This is consistent with the mean value of 2.9 (r_c/r_o) given for bovine cumulus-oocyte complexes by Clark *et al.* (2006). Because this work seeks to determine the effect of increased resistance to oxygen transport provided by the cumulus cell layer, the higher value of 4 for r_c/r_o will be used in this work as a conservative estimate. The disperse nature of a mature cumulus-oocyte complex means that it has a very high proportion of fluid voidage. Although this voidage has not been quantified, it is a fair assumption that the diffusion coefficient of oxygen in this layer will be similar to that in pure follicular fluid (refer to equation 3.21 which shows that at high fluid voidage the effective diffusion coefficient of oxygen in tissue will approach that of the fluid phase). Therefore, once again using the diffusion coefficient of oxygen in plasma (D_p) as the best available estimate of the diffusion coefficient in follicular fluid, this work makes the assumption that $D_c \approx D_p$. This is consistent with Clark *et al.* (2006) who approximated D_c as being equal to the diffusion coefficient of oxygen in water. Although the difference between the diffusion coefficients of oxygen in water and plasma are small, $D_c \approx D_p$ is assumed to be more accurate than the assumption of $D_c \approx D_w$ made by Clark *et al.* (2006), because follicular fluid is a derivative of plasma. Due to the lack of data on oxygen consumption rates of human cumulus cells, the value of R_c/R_o of 0.29 for bovine cumulus cells will be used to calculate R_c for human cumulus cells. Therefore using the nominal values of r_o and R_o previously described, r_c and R_c can be estimated according to the above discussion. Using these parameter estimates, the equations for cumulus, antral, and granulosa oxygen concentration can be evaluated (equations 4.59, 4.69, and 4.79 respectively). Figure 4.23 compares the oxygen concentration

profiles in the pre-ovulatory follicle with no cumulus, to the pre-ovulatory follicle with cumulus. This comparison is analogous to that of Figure 4.15 which compared the oxygen concentration profiles in the antral follicle with the pre-ovulatory follicle.

Figure 4.23 shows that the increased oxygen demand of the cumulus cells surrounding the oocyte causes a more pronounced nonlinear decrease in oxygen in the follicle compared with the pre-ovulatory follicle with no cumulus. It has been assumed to this point that any oxygen gradients which occur in the vicinity of the oocyte will not have a significant effect on the bulk oxygen concentration of the follicular fluid. Whether or not this is the case can be determined by calculating if the mean concentration of follicular fluid in the antrum is significantly different from that at the granulosa/fluid interface. The mean concentration of oxygen in the antral fluid can be determined for the pre-ovulatory follicle with cumulus, by multiplying equation 4.69 by the surface area of a sphere, integrating between the limits of $r=r_c$ and $r=r_a$, and dividing the result by the volume of antral fluid,

$$\text{moles of oxygen} = 4\pi \int_{r=r_c}^{r=r_a} r^2 \left(C_i + \frac{R_c r_c^3}{3D_a}\left(\frac{1}{r_a}-\frac{1}{r}\right) - \frac{R_c r_o^3}{3D_a}\left(\frac{1}{r_a}-\frac{1}{r}\right) + \frac{R_o r_o^3}{3D_a}\left(\frac{1}{r_a}-\frac{1}{r}\right) \right) dr$$

(4.80)

where C_i is calculated from equation 4.79 at $r=r_a$.

Integrating equation 4.80 and dividing the result by the volume of antral fluid gives the mean concentration of oxygen in follicular fluid,

$$\text{mean oxygen conc.} = \frac{2\pi(6C_i D_a r_a(r_a^3 - r_c^3) - (r_a^3 - 3r_a r_c^2 + 2r_c^3)(R_c(r_c^3 - r_o^3) + R_o r_o^3)}{9D_a r_a V_a}$$

(4.81)
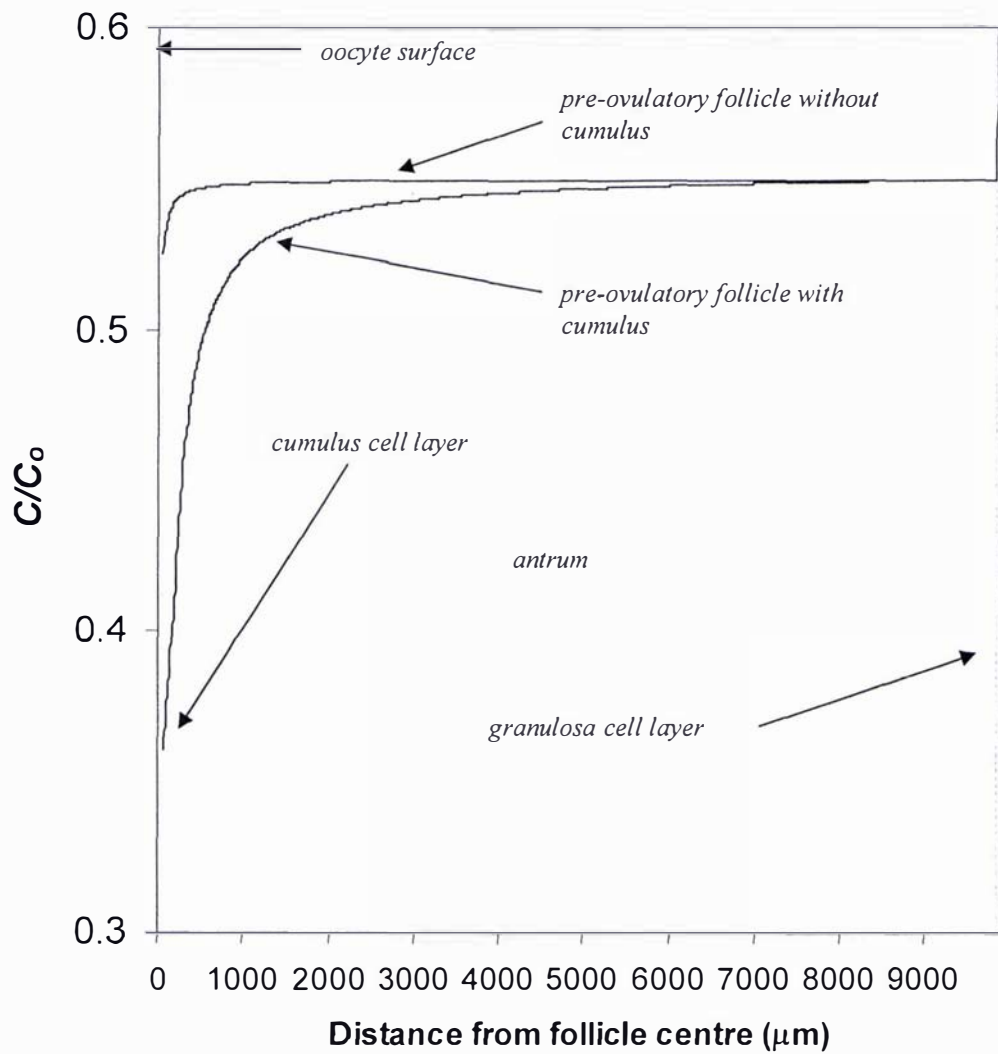
Figure 4.23   Comparison of oxygen concentration profiles across a pre-ovulatory follicle with no cumulus and a pre-ovulatory follicle with cumulus (4 ml antral fluid volume (V_a)).

Evaluation of equation 4.81 for the same 4 ml IVF sized follicle of Figure 4.23 reveals that the mean oxygen concentration in the follicle is 98% of the oxygen concentration at the granulosa fluid interface. Hence, the addition of cumulus cells does not greatly effect the assumption that the fluid can be considered to be at a bulk concentration. This assumption would only break down if a fluid sample was taken from the region of the follicle where oxygen declines rapidly. This rapid decline is most apparent when $r<3000$ μm. The fluid volume associated with this part of the follicle is only approximately 0.1 ml of the 4 ml of antral fluid. Therefore, provided that the volume of fluid sampled for dissolved oxygen is much larger than this, the fluid can be assumed to be at a bulk concentration which is slightly less than the concentration of oxygen at the granulosa/fluid interface. A sample volume of approximately 1 ml or greater is recommended.

Given that the bulk oxygen concentration of the follicular fluid is essentially the same as the concentration at the granulosa/fluid interface, the critical question is once again at what level does C_i need to be to sustain the oocyte at C_{crit} at the oocyte surface. Rearrangement of equation 4.59 at $C=C_{crit}$ and $r=r_o$ gives,

$$C_{ii} = C_{crit} + \frac{R_c}{6D_c}(r_c^2 - r_o^2) + \frac{R_c r_o^3}{3D_c}\left(\frac{1}{r_c} - \frac{1}{r_o}\right) - \frac{R_o r_o^3}{3D_c}\left(\frac{1}{r_c} - \frac{1}{r_o}\right) \tag{4.82}$$

where once again $R_o=0.99R_{omax}$

Since C_{ii} is the oxygen concentration at $r=r_c$, equation 4.69 can be rearranged at $r=r_c$ and $C=C_{ii}$ to give the minimum required interfacial oxygen concentration to sustain the oocyte at $C=C_{crit}$,

$$C_{i\,min} = C_{ii} - \frac{R_c r_c^3}{3D_a}\left(\frac{1}{r_a} - \frac{1}{r_c}\right) + \frac{R_c r_o^3}{3D_a}\left(\frac{1}{r_a} - \frac{1}{r_c}\right) - \frac{R_o r_o^3}{3D_a}\left(\frac{1}{r_a} - \frac{1}{r_c}\right) \tag{4.83}$$

where C_{ii} is given by equation 4.82 and $R_o=0.99R_{omax}$.

substitution of equation 4.82 into equation 4.83 gives,

168

$$C_{i\,min} = C_{crit} - \frac{R_c r_c^3}{3D_a}\left(\frac{1}{r_a} - \frac{1}{r_c}\right) + \frac{R_c r_o^3}{3D_a}\left(\frac{1}{r_a} - \frac{1}{r_c}\right) - \frac{R_o r_o^3}{3D_a}\left(\frac{1}{r_a} - \frac{1}{r_c}\right) + \frac{R_c}{6D_c}(r_c^2 - r_o^2) + \frac{R_c r_o^3}{3D_c}\left(\frac{1}{r_c} - \frac{1}{r_o}\right)$$
$$- \frac{R_o r_o^3}{3D_c}\left(\frac{1}{r_c} - \frac{1}{r_o}\right)$$

<div align="right">(4.84)</div>

Figure 4.24 plots the minimum required granulosa/fluid interfacial oxygen concentration to sustain the oocyte at $C=C_{crit}$ as a function of total antral fluid volume according to equation 4.83. The result is compared to the previous result of Figure 4.16 for the pre-ovulatory follicle with no cumulus.

Figure 4.24 shows that the minimum required interfacial oxygen concentration for the pre-ovulatory follicle with cumulus, increases rapidly from C_{crit} with increasing follicle volume. Like the pre-ovulatory follicle with no cumulus, the required interfacial oxygen level becomes essentially constant, albeit at a higher oxygen concentration, owing to the increased oxygen demand of the cumulus cells. Once again the oxygen level becomes constant well before fluid volumes of typical IVF follicles are encountered. This happens because as r_a becomes large $1/r_a$ tends towards zero, and hence the required interfacial oxygen concentration becomes independent of fluid volume, and equation 4.84 reduces to,

$$C_{i\,min} = C_{crit} + \frac{R_c r_c^2}{3D_a} + \frac{r_o^3}{3D_a r_c}(R_o - R_c) + \frac{R_c}{6D_c}(r_c^2 - r_o^2) + \frac{R_c r_o^3}{3D_c}\left(\frac{1}{r_c} - \frac{1}{r_o}\right) - \frac{R_o r_o^3}{3D_c}\left(\frac{1}{r_c} - \frac{1}{r_o}\right)$$

<div align="right">(4.85)</div>

Equation 4.85 will apply to IVF sized follicles. Evaluation of equation 4.85 at the nominal parameter values gives a required interfacial oxygen level of 6.6 vol%. Figure 4.25 compares this value with those previously calculated for IVF sized antral, and pre-ovulatory follicles with no cumulus, and demonstrates the impact of the addition of cumulus cells on the zone of uncertainty.

Figure 4.25 shows that the zone of uncertainty now extends from 5.1 to 6.6 vol%. Such a difference would be detectable by a standard Clark electrode. What this zone of uncertainty reflects is the variability resulting from the uncertainty in the location of the oocyte, or cumulus-oocyte complex, within the follicle. The central position essentially represents a worst case scenario in terms of oxygen mass transport. If the oocyte or cumulus-oocyte complex resides here, oxygen must diffuse through additional resistance to mass transport, and hence the required interfacial oxygen level is elevated.

In many small mammals the oocyte remains in a relatively central position in the antral fluid space. However, in man the cumulus-oocyte complex is most often located in a more eccentric position (Mossman & Duke, 1973). Therefore it is likely that in reality the upper limit of the zone of uncertainty will, in most cases, lie below the so called worst case scenario calculated here. Variability in this upper limit will not be solely due to positional uncertainty, but also to variability in cumulus thickness and oxygen consumption. However, the upper range of r_c/r_o, used here to calculate the cumulus thickness, suggests that the upper limit of Figure of 4.25 is still a conservative estimate.

4.5.5 Effect of variability in follicular fluid solubility

Up to this point it has been assumed that oxygen solubility in follicular fluid is not variable among follicles. If solubility is variable this will not affect the oxygen concentration required by the oocyte (C_{crit}) or the minimum required interfacial oxygen concentration. However, since $C=pS$, follicular fluid with low oxygen solubility will require a higher partial pressure of oxygen at the granulosa/fluid interface to sustain the oocyte. Conversely, a follicular fluid with greater oxygen solubility will require a lower oxygen partial pressure at the granulosa/fluid interface to sustain the oocyte. This can be represented by expressing the equations for minimum required interfacial oxygen concentration in terms of partial pressure. For the antral follicle,
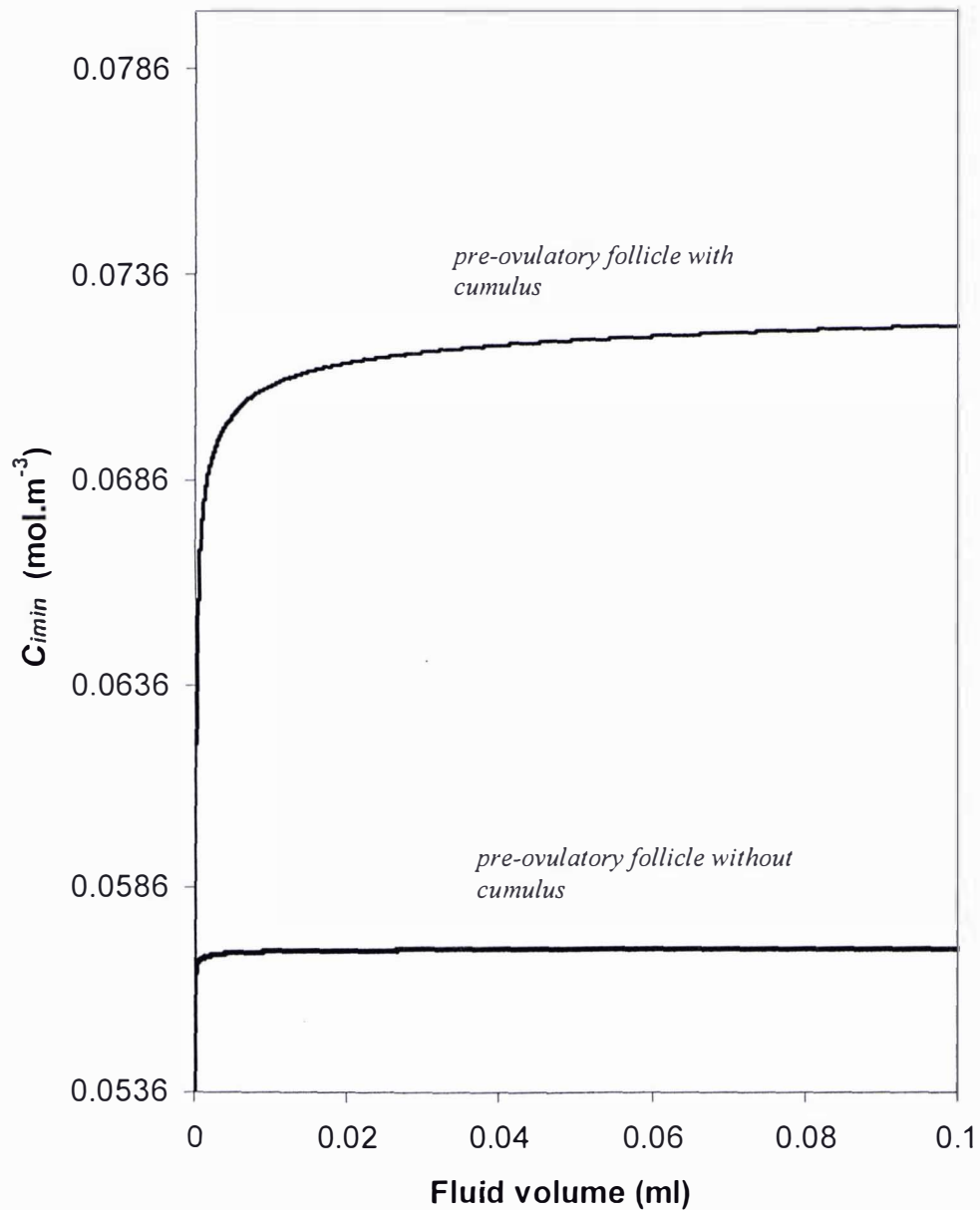
Figure 4.24   Comparison of the minimum interfacial oxygen concentration required to sustain the oocyte at 99% of maximal respiration as a function of follicular fluid volume for the pre-ovulatory follicle with and without cumulus. Note that oxygen concentration becomes constant well before typical IVF volumes are reached. Using nominal parameter estimates (Tables 3.3 and 4.1 and including those given for the cumulus in section 4.5.4.2)
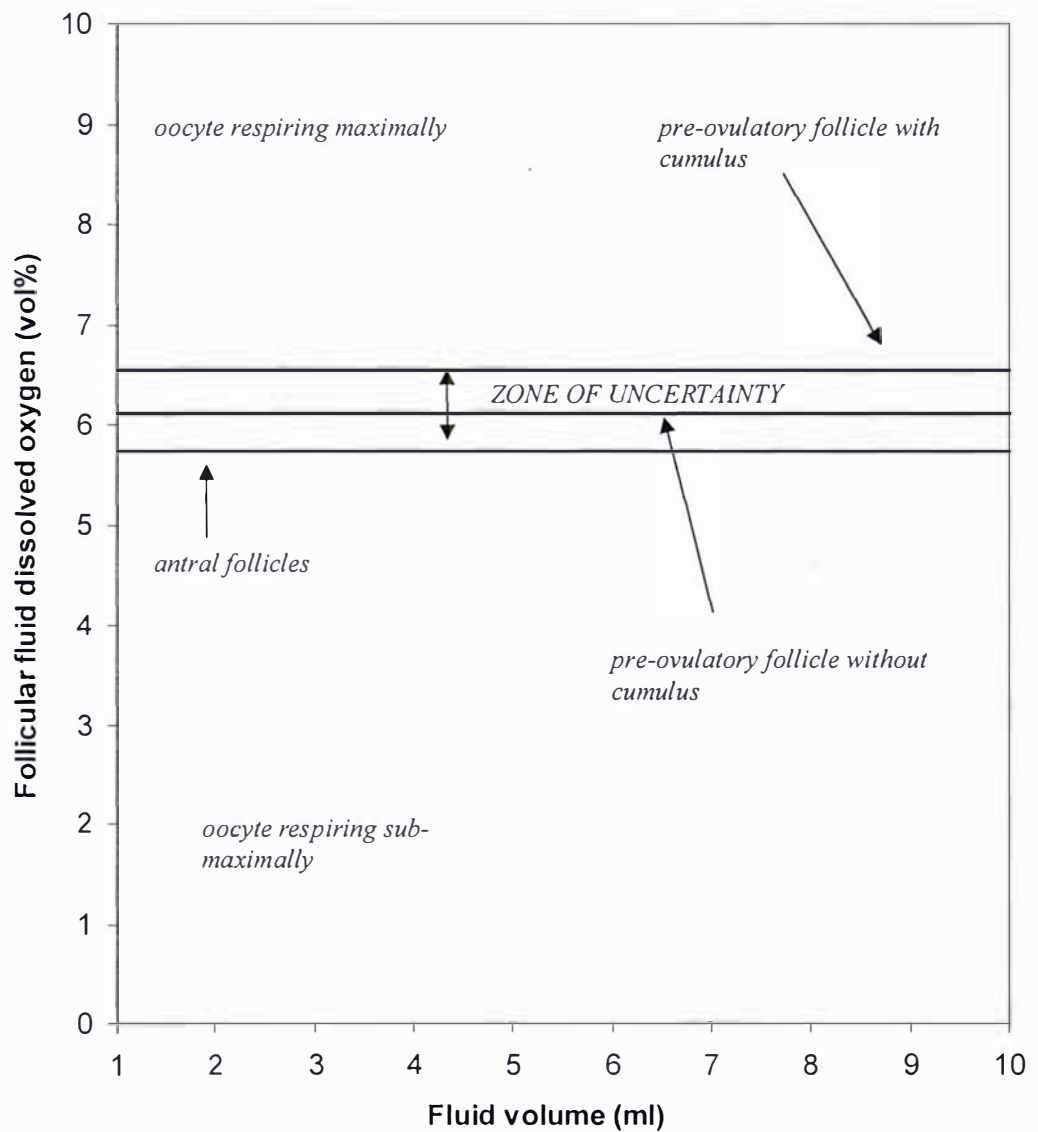
Figure 4.25   Minimum interfacial oxygen concentration required to sustain oocyte at 99% maximal respiration for antral, pre-ovulatory with no cumulus, and pre-ovulatory follicles with cumulus (IVF sized follicle range). These concentrations can once again be used to form a zone of uncertainty.

$$p_i = \frac{C_{crit}}{S_a} \tag{4.86}$$

For the pre-ovulatory follicle with no cumulus, equation 4.44 becomes

$$p_i = \frac{1}{S_a}\left(C_{crit} + \frac{R_o r_o^2}{3D_a}\right) \tag{4.87}$$

For the pre-ovulatory follicle with cumulus, equation 4.85 becomes

$$p_i = \frac{1}{S_a}\left(C_{crit} + \frac{R_c r_c^2}{3D_a} + \frac{r_o^3}{3D_a r_c}(R_o - R_c) + \frac{R_c}{6D_c}(r_c^2 - r_o^2) + \frac{R_c r_o^3}{3D_c}\left(\frac{1}{r_c} - \frac{1}{r_o}\right) - \frac{R_o r_o^3}{3D_c}\left(\frac{1}{r_c} - \frac{1}{r_o}\right)\right)$$

$$(4.88)$$

The solubility of oxygen in follicular fluid has never been determined. To this point it has been assumed to be equal to that of plasma and invariable. Figure 4.26 shows the effect on the lower (equation 4.86) and upper (equation 4.88) limits of the zone of uncertainty, of assuming that follicular fluid solubility varies between 50% greater and 50% lower than that of plasma.

Figure 4.26 shows that the zone of uncertainty now extends from 3.8 to 13.1 vol%. The width of this zone is so great that drawing useful conclusions from the measurement of follicular fluid dissolved oxygen would be very difficult. Of course, it is unlikely that follicular fluid oxygen solubility is this variable. However Figure 4.26 highlights the need to quantify this variability, and this is addressed in Chapters 5 and 6.
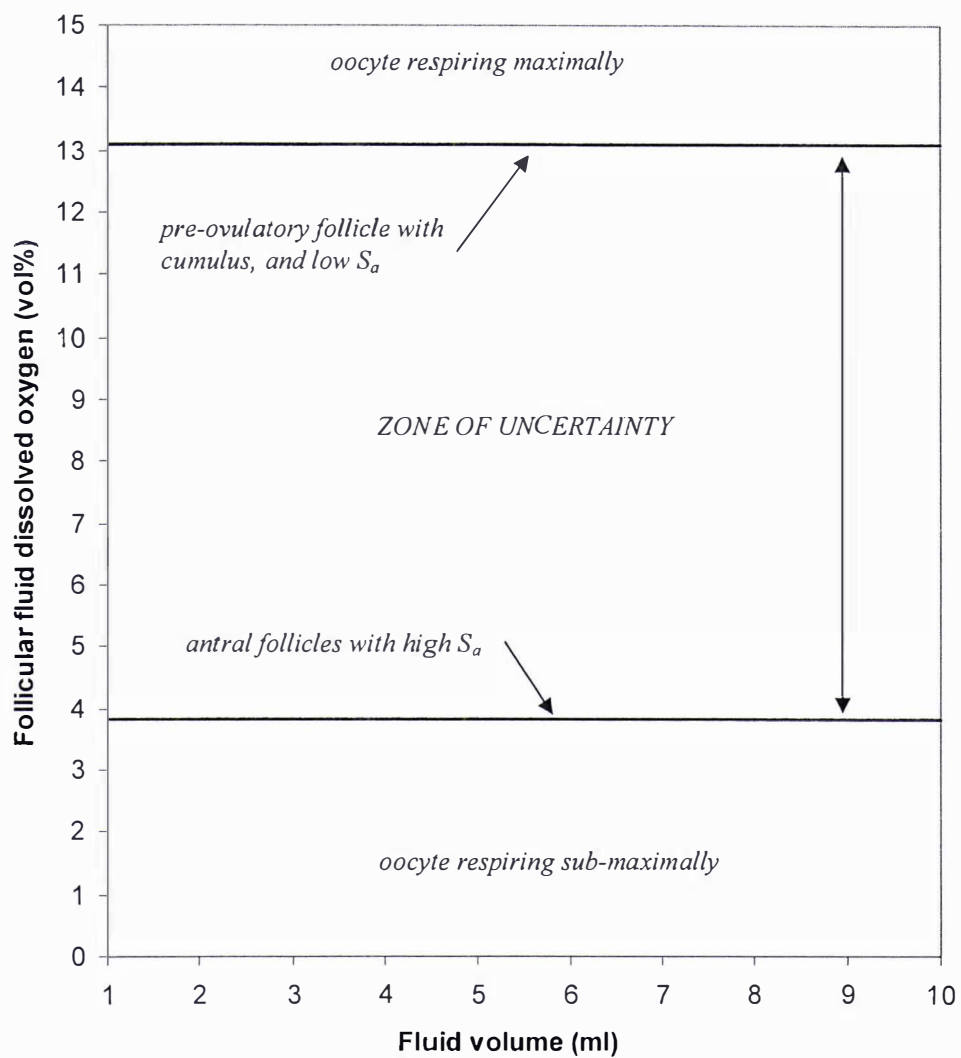
Figure 4.26   Effect of variability in follicular fluid solubility between 50% below and 50% above that of plasma on the zone of uncertainty.

4.6 Conclusions and recommendations

Chapter 3 demonstrated that pre-antral follicles will reach a certain size beyond which they cannot grow any further without becoming anoxic. The work presented here suggests that the formation of the follicular antrum represents one way in which the follicle can continue to grow yet still meet its oxygen requirements.

This work has several key results,

1. The ratio of granulosa cell volume to total follicle volume is critical to the oxygen status of the follicle.
2. The measurement of dissolved oxygen in follicular fluid may be a simple indicator of the oxygen status of the follicle.
3. The measurement of follicular vascularisation also provides information about the oxygen status of the follicle. However, this information is more complex than the measurement of dissolved oxygen in follicular fluid, and ideally needs to be coupled with knowledge of follicle volume.

If the ratio of granulosa cell volume to total follicle volume is too high at any given follicle volume, the follicle will become anoxic. Comparison of model predictions with human data reveals that observed follicle growth is consistent with maintaining a balance between granulosa cell volume and total follicle volume.

Assuming that the oocyte requires a certain critical level of oxygen, this work has demonstrated that the measurement of dissolved oxygen in the follicular fluid may provide a simple indication of whether or not the oocyte from a given follicle would have had sufficient oxygen to sustain it at this critical level. For IVF sized follicles a cut-off level of oxygen in the fluid may exist. Below this level the oocyte will not be able to respire maximally. Above this level it will be able to respire maximally. This cut-off level carries with it some uncertainty as a result of variability in oocyte position, size, level of oxygen consumption, size of the cumulus mass, and level of oxygen consumption by the cumulus mass. Variability in the properties of oxygen diffusivity and solubility in the follicular fluid also impact on this uncertainty.

In contrast to the measurement of dissolved oxygen, the relationship between follicle oxygen status and the degree of follicle vascularisation is more complex. The degree of vascularisation needs to be coupled with knowledge of the volume of the antral fluid as well as the total volume of the follicle, if the oxygen status of the follicle is to be determined. Follicular vascularisation as a measure of oxygen status will also be subject to uncertainty due to variability in the same parameters discussed above for the measurement of dissolved oxygen. However vascularisation level will also be subject to uncertainty resulting from variability in granulosa cell oxygen consumption, granulosa cell layer voidage and the diffusion coefficient of oxygen in the granulosa cell layer. The measurement of dissolved oxygen is independent of these parameters.

In summary, the modelling work presented in this chapter suggests that the measurement of dissolved oxygen in follicular fluid may be able to provide a measure of the oxygen status of the follicle and oocyte. The measurement of dissolved oxygen is considered to be simpler than the measurement of follicle vascularisation, as it requires less knowledge to provide the same amount of information. To get the most information out of the measurement of dissolved oxygen requires that the uncertainty associated with the measurements be as low as possible. Knowledge of the variability of oxygen diffusivity in follicular fluid, and oxygen solubility in follicular fluid may allow for reduction in this uncertainty. Determination of the variability of these parameters is the subject of the following two chapters.

Knowledge of the variability in oocyte position, size, level of oxygen consumption, size of the cumulus mass, and level of oxygen consumption by the cumulus mass would also reduce the uncertainty associated with drawing conclusions from the measurement of dissolved oxygen in follicular fluid.

It is also recommended that the type of modelling approach applied here to the transport of oxygen in the follicle may also be applied to other substances in the follicle. This will further improve understanding of follicle development. This modelling approach may identify other potential predictive measures of oocyte health as well as improve the understanding of those parameters which have already been identified as having predictive potential (see for examples section 2.1.3).

Chapter 5. Methodology for the analysis of the permeability, diffusivity and solubility of oxygen in aqueous fluids

The work of previous chapters demonstrated that drawing reliable conclusions from measurements of dissolved oxygen in follicular fluid depends on knowledge of the diffusivity and solubility of oxygen in the fluid. In particular, knowledge of the variability of these parameters in follicular fluid will reduce the uncertainty associated with the measurement of follicular fluid dissolved oxygen.

The objective of this chapter was to develop the methodology for determining the diffusivity and solubility of oxygen in standard aqueous solutions. This methodology would then allow the latter quantification of the variability of these parameters in human follicular fluid.

5.1 Methods for the measurement of gas diffusivity in liquids

A variety of methods for the measurement of gas diffusion coefficients in liquids have been described in the literature. Those most commonly applied to the measurement of oxygen diffusivity in aqueous solutions are:

1. Diaphragm cell
2. Bubble dissolution
3. Laminar flow
4. Electrochemical methods

The basic diaphragm cell consists of two well stirred fluid volumes separated by a permeable diaphragm. Variation in the concentration gradient across the diaphragm is related to the flux, and used to calculate the diffusivity. Vivian & King (1964) describe the use of this method to measure the diffusion coefficient of oxygen in

water. Oxygen concentrations were monitored by Winkler titration. Diaphragm cells are cheap to build and simple to operate. The main disadvantage of the diaphragm cell method is that individual runs take between a few hours to several days (Cussler, 1976; Ferrell & Himmeblau, 1967). For this reason this method is not seen to be suitable for the analysis of biological material such as follicular fluid which may change composition over such long time periods. Diaphragm cells also require initial calibration with a fluid of known diffusivity.

The rate at which a gas bubble dissolves in solution is related to the solubility and diffusion coefficient of the gas in the liquid. If the solubility of the gas in the liquid is known, then the radius of the bubble as a function of time can be used to determine the diffusion coefficient. This approach has been described by Krieger *et al*. (1967) for the determination of oxygen diffusivity in water. The radius of the bubble was monitored by taking a series of photographs at known time intervals. Values reported using this method are often greater than those reported by other methods (Lango *et al.,* 1996), and this may be due to vibration and other movement leading to convective dissolution (Krieger *et al*. 1967). The use of this method for determination of diffusion coefficients in follicular fluid would require independent determination of the solubility of oxygen in the fluid.

Laminar flow methods involve the measurement of the rate of gas absorption into a liquid stream in laminar flow. The absorption rate can then be related to the diffusion coefficient. This basic approach has been employed in a variety of configurations to measure the diffusion coefficient of oxygen in water (Chiang & Toor, 1959; Duda & Vrentas, 1968; Ferrell & Himmeblau, 1967). This method is capable of very rapid measurements, however the experimental set-up is somewhat elaborate compared to other methods.

Electrochemical methods (as they relate to oxygen) generally refer to those which employ a Clark-style oxygen electrode. A layer of the solution is placed over the electrode and exposed to gases of various oxygen levels. The steady-state response of the electrode can be used to determine the permeability of a fluid to oxygen. Since permeability is the product of diffusivity and solubility, then if the solubility of

oxygen in the fluid is known, the diffusivity can be calculated (Tham *et al.,* 1970, Akita, 1981). Alternatively, the transient response of the oxygen electrode can be coupled with the steady-state response to determine both the permeability and the diffusivity with the solubility being subsequently calculated (Ju *et al.,* 1988, Ho *et al.,* 1988).

This method has been selected for use in the remainder of this chapter for a variety of reasons. Firstly, the required equipment is readily available, and expertise in the use of Clark-style oxygen electrodes already existed at the laboratory where the work was carried out. This method allows for the simultaneous determination of solubility and diffusivity, both of which were required in this work. This is a distinct advantage over other methods which would require independent measurement of oxygen solubility.

The basic procedure employed was similar to that described by Ho *et al.* (1988), and is described in detail throughout the remainder of this chapter. Some novel extensions of this method are described.

5.2 Materials and methods

A schematic diagram of the diffusion cell setup is presented in Figure 5.1. The diffusion cell consisted of an oxygen electrode (Yellow Springs Instruments, product no. 5739, Ohio, USA), housed in a water-tight Perspex container. The Perspex container accommodated outlets which allowed the oxygen electrode to be connected to a potentiostat and data logging software (CH Instruments, Model 1030, Texas, USA). The outlets also accommodated the gas flow tubing which was equipped with valves allowing the flow to be switched between different gases as well as providing flow-rate control. The oxygen electrode was also fitted with a stainless steel cap which allowed a layer of sample solution to be added on top of the electrode without run-off. The oxygen electrode was set-up according to the manufacturer's instructions, using KCl electrolyte solution and fluorinated ethylene-propylene (FEP) Teflon membranes (Yellow Springs Instruments, YSI standard membrane, Ohio, USA). The device was submerged in a water bath and the temperature controlled at 25 ±0.5 °C. Measurements were made at 25 °C rather than 37 °C, as the probe was

observed to behave erratically at 37 °C. Furthermore it is more difficult to control the temperature at 37 °C, which may result in undesirable convection. This was not seen to pose a problem for the analysis of follicular fluid (as carried out in the following chapter), as relative diffusivity remains constant in such dilute aqueous solutions over this temperature range (e.g. human plasma, Christoforides et al., 1969). Hence the relative diffusivity at 25 °C will be essentially the same as that at 37 °C and can be used to estimate the absolute diffusivity simply by multiplying by the known diffusivity of oxygen in water at 37 °C.

The two gases used in these experiments were instrument grade air and nitrogen (BOC Ltd., Auckland, New Zealand). Before entering the diffusion cell, gases were sparged through a beaker containing the sample solution. This was done to try to ensure that the vapour pressure above the sample solution layer, and that of the gas, were the same, and hence prevent any evaporation or condensation. For the same reasons a sponge wetted with the sample solution was also placed over the top of the stainless steel cap. As described by Ho *et al.* (1988), the minimum gas stream velocity that can produce sustained waves on a flat liquid surface is given by,

$$U_{min} = 3\left(\frac{4\sigma g}{\rho}\right)^{\frac{1}{4}}$$
(5.1)

where σ is the surface tension of the fluid (dyn.cm^{-1}), ρ is its density (g.cm^{-3}), and g is the acceleration due to gravity (cm.s^{-2}). Using equation 5.1 the minimum gas stream velocity was estimated for each of the solutions used. The flow-rate was adjusted to be at least 20% below this value. This precaution helped to prevent undesirable convective mass transport which would result from significant surface disturbances.

The aqueous sample solutions used in this study were made from analytical grade NaCl, and sucrose (Mallinckrodt Baker Inc., New Jersey, USA). All sample solutions that were not used within a 24 hour period were discarded. Before a sample solution was added to the diffusion cell, the oxygen electrode was calibrated using air and nitrogen. 0.5 ml of sample was added over the top of the electrode/membrane surface. 0.5 ml was found to be the minimum volume of solution required to ensure a

complete and even covering of the membrane. The addition of the sample solution involved removal of the chamber lid, expelling the 0.5 ml sample from a glass syringe (product no. MD-0100, Bioanalytical Systems Inc., Indiana, USA) over the membrane surface, before replacing the lid. This process was done as rapidly as possible, with an even membrane covering being visually assessed. The electrode current was then allowed to reach steady-state with the gas of interest, which took approximately an hour. Upon reaching steady-state, the gas flow was either step-changed or the sample removed, depending on the type of experiment being performed.

After application of the step-change, data was gathered for an additional period (usually 10 to 15 minutes) after which time the sample was removed. After sample removal the membrane surface was cleaned by performing multiple rinses with distilled water. A calibration run was then performed in the same way except that distilled water was used as the fluid layer.

Figure 5.2 shows an example data trace of electrode current vs. time. The current was normalised by dividing all current values by the current measured in air. Therefore the electrode which is exposed to air with no sample layer in place shows a constant initial period. A layer of sample solution equilibrated with air was then added to cover the membrane surface, with air continuously flowing over the sample. The response then undergoes a long transient period as oxygen in the sample is consumed at the cathode surface, thus creating a concentration gradient in the sample layer. Eventually a new steady-state is reached. This occurs when the concentration gradient in the sample becomes linear. After this the gas phase was step changed to nitrogen, and the response entered another transient period. Theoretically, if data collection continued, the response would once again reach steady-state, this time at a normalised response of zero. The following sections detail the analysis of data obtained from traces such as that shown in Figure 5.2, so that the oxygen solubility and diffusivity in liquid samples can be determined.

The assumptions made by this work require that the thickness of the sample solution layer and the calibration fluid (water) be the same. The thickness of these layers was not measured during an experimental run, but 225 measurements of sample thickness were made using a stand mounted vernier caliper. The mean sample thickness was

found to be 2900 ± 110 μm ($\pm$SD). No significant differences between the thickness of sample solutions and water were found. The thickness of the YSI standard membrane was also measured and found to be 25.3 ± 0.3 μm ($\pm$SD, n = 15).

5.3 Steady-state analysis

Figure 5.3(a) represents an oxygen electrode running at steady-state in contact with a gas of partial pressure, p_g. The electrolyte layer was assumed to offer negligible resistance to mass transport. It was also assumed that all oxygen is instantaneously consumed at the cathode surface, and therefore the partial pressure of oxygen at this surface is zero. Under these conditions the steady-state flux of oxygen to the cathode surface will be given by equation 5.2.

$$J = \frac{D_m S_m}{L_m} (p_g - 0) = \frac{P_m}{L_m} p_g \tag{5.2}$$

And hence the steady-state current will be given by,

$$I_g = nAF \frac{P_m}{L_m} p_g \tag{5.3}$$

where n is the number of electrons involved in the reduction of oxygen at the cathode, and F is Faraday's constant (96485 coulombs.mol^{-1} of electrons).

Figure 5.3(b) describes the situation where the oxygen electrode is running at steady-state with a gas of partial pressure p_g after a layer of aqueous sample solution has been placed on top of the membrane. Making the same assumptions as above, the steady-state flux of oxygen to the cathode surface will be given by equation 5.4.

$$J = \frac{D_s S_s}{L_s} (p_g - p_i) = \frac{P_m}{L_m} p_i \tag{5.4}$$
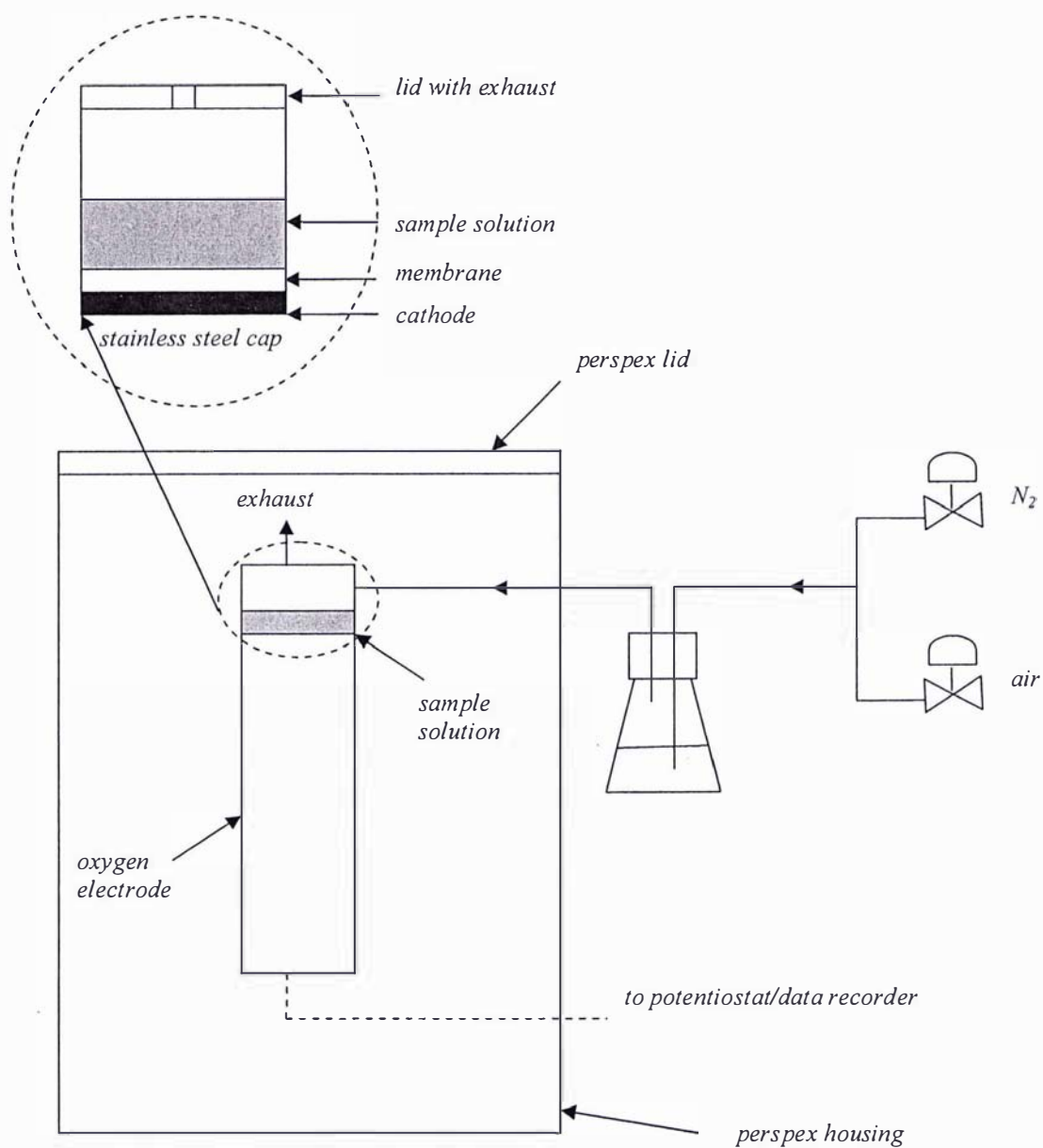
Figure 5.1   Schematic of the experimental set-up. Inset shows details of the stainless steel cap which houses the cathode, membrane, sample, and lid with exhaust.
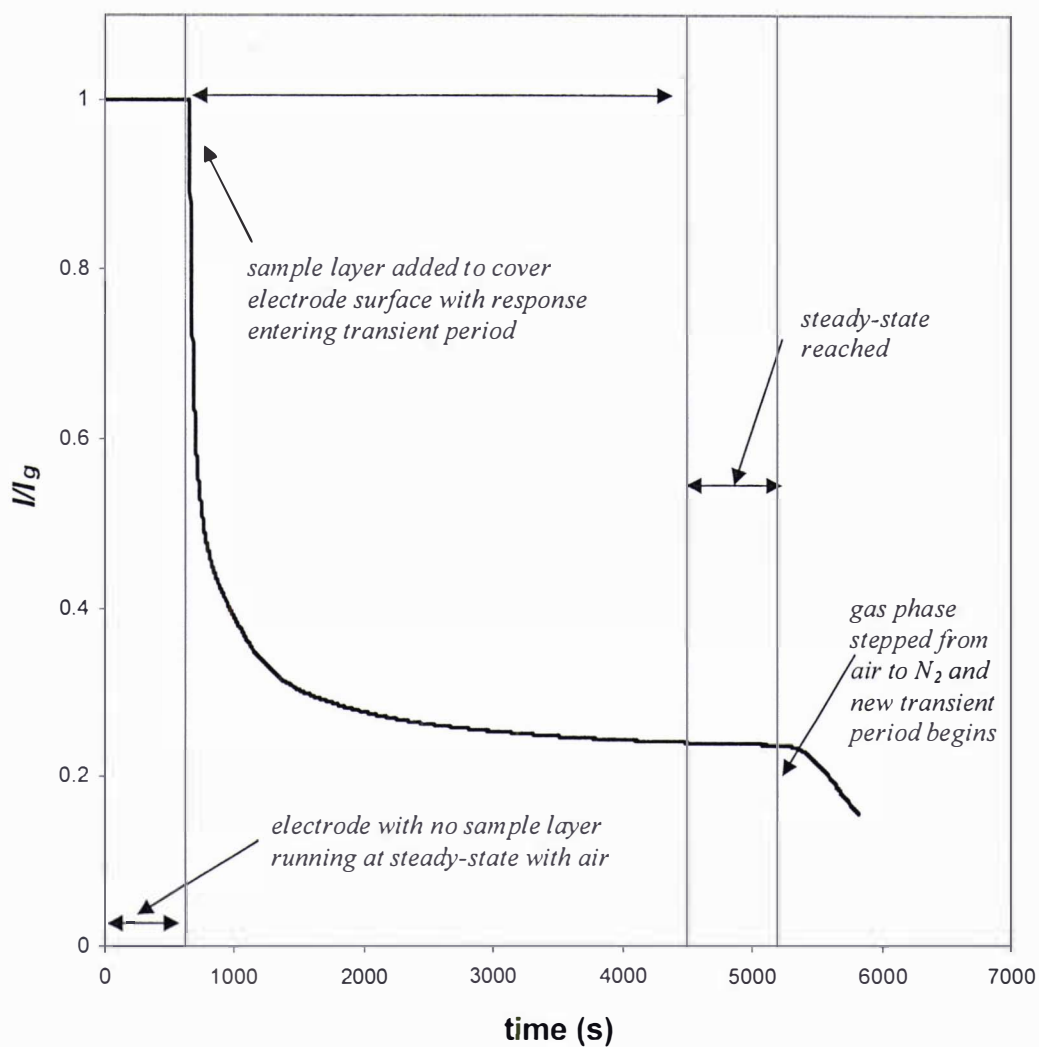
Figure 5.2.   An example data trace of normalised current vs. time showing progression through various steady-state and transient periods.

Since from equation 5.4 $p_i = \dfrac{L_m}{P_m} J$, solution of simultaneous equations allows the steady-state flux of oxygen to the cathode surface to be simplified to,

$$J = \frac{D_s S_s P_m}{L_s P_m + D_s S_s L_m} p_g \tag{5.5}$$

And hence the steady-state current for the electrode, membrane and sample layer system will be,

$$I_s = nAF \frac{D_s S_s P_m}{L_s P_m + D_s S_s L_m} p_g \tag{5.6}$$

The response of the electrode in air (I_g) and the steady-state response while in contact with a sample layer (I_s) can be compared by combining equations 5.3 and 5.6.

$$\frac{I_g}{I_s} = \frac{P_s L_m + P_m L_s}{P_s L_m} \tag{5.7}$$

where P_s is the permeability of the sample layer ($D_s S_s$).

Furthermore,

$$\frac{I_g}{I_s} - 1 = \frac{P_m L_s}{P_s L_m} \tag{5.8}$$

Therefore, if the steady-state response of the probe is measured in the gas-phase (I_g), in the presence of a water layer (I_w), and in the presence of an unknown sample solution layer (I_s), the following relationship exists which is independent of the electrode and membrane properties.

$$\frac{\left(\dfrac{I_g}{I_w}-1\right)}{\left(\dfrac{I_g}{I_s}-1\right)} = \frac{P_s L_w}{P_w L_s} \qquad (5.9)$$

Hence (according to equation 5.9), if the thickness of the water and sample layers are either known, or equal, then the relative permeability of the sample to water can be calculated.

Table 5.1 shows relative oxygen permeability results for sucrose and NaCI solutions of various concentrations. Relative permeabilities have been calculated according to equation 5.9. As expected, for both sucrose and NaCI, Table 5.1 shows oxygen permeability reduces with increasing solute concentration. This is consistent with what is expected because the solubility of oxygen in aqueous solutions is known to reduce with increasing solute concentration (the diffusivity often reduces, though not always).The results in Table 5.1 are not compared to any values in the literature because measurements of oxygen permeability and diffusivity in standard solutions are scarce, and most often not at comparable concentrations. In fact, even for water, the quantification of oxygen diffusivity has produced highly variable results in the literature. However, reliable values for oxygen solubility for the standards used here are available. These can only be compared to the data obtained here once permeability has been separated into diffusivity and solubility. This was done in a later section (see Table 5.3). It should also be noted that the variability in permeabilities reported in Table 5.1 increase with increasing solute concentration.

The objective of this work was to measure the diffusivity and solubility of these solutions, and this permeability data is the basis from which this can be achieved. If the permeability is known, then if either the diffusivity or solubility of the sample is also known, P_s can separated into D_s and S_s (since $P=DS$). Typically S_s will be known (after measurement by an independent method) and hence used to calculate D_s. This approach was employed by Tham *et al.* (1970) and Akita (1981), but carries with it the disadvantage of having to independently measure the solubility of oxygen in the sample.

186

(a) Electrode without sample layer

Gas, $p=p_g$

$p = p_g$

$p = 0$

Membrane, $P_m=D_mS_m$

Cathode surface

$x = L_m$

L_m

$x = 0$
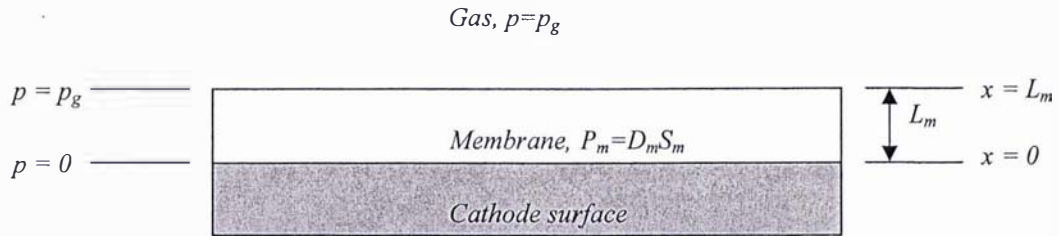
(b) Electrode with sample layer

Gas, $p=p_g$

$p = p_g$

$p = p_i$

$p = 0$

Samples solution, $P_s=D_sS_s$

Membrane, $P_m=D_mS_m$

Cathode surface

$x = L_m+L_s$

L_s

$x = L_m$

L_m

$x = 0$
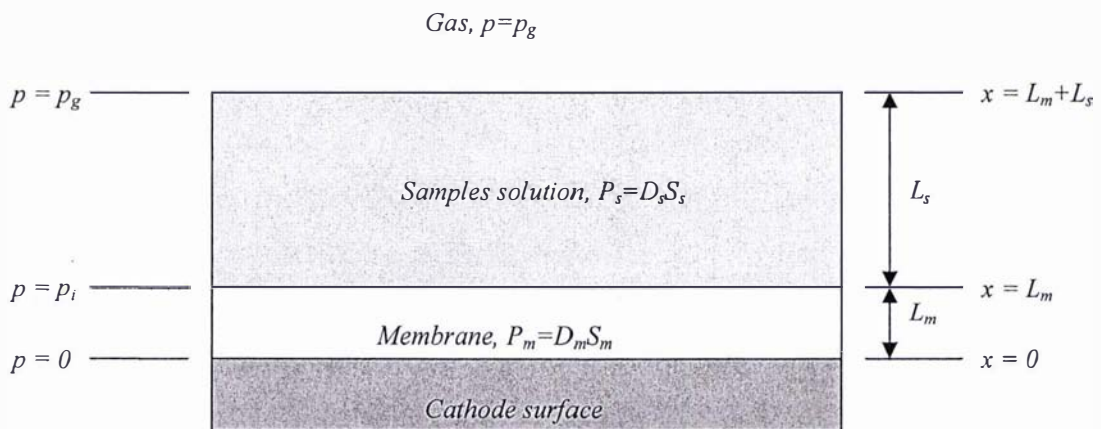
Figure 5.3   The dissolved oxygen electrode, without (a), and with (b) a sample solution layer.

Alternatively the permeability can be separated into diffusivity and solubility through the analysis of the transient electrode response. This method has been previously employed by Ho *et al.* (1988). This method is detailed and expanded on in the next section.

5.4 Transient analysis

The step change from one steady-state to another is dependent on the specific values of diffusivity and solubility of the sample solution. The transient portion of the step change can therefore be used to determine the values of these properties.

Previous investigators have used the transient response of an oxygen electrode with a sample solution layer initially at steady-state with a gas of partial pressure p_g, to a sudden down-step $(p_g=0)$ (Ju *et al.*, 1988; Ho *et al.*, 1988). However, this is only one possible combination of boundary and initial conditions. This combination, along with several others suggested in this investigation, are described and presented in mathematical form below. Figure 5.4 offers a visual representation of the expected transients for the different boundary and initial condition combinations possible to apply experimentally. The different combinations are referred to here as 'switch on', 'sample steady-state addition', 'up-step', and 'down-step'. How these conditions are achieved experimentally and mathematically are described in sections 5.4.2 to 5.4.5 respectively.

5.4.1 Transient model development

For each of the scenarios of Figure 5.4, the system, and therefore the model, is the same. Each case differs only in the initial and boundary conditions used.

In all cases the bi-layer system consists of a sample solution layer and membrane layer, described by the following diffusion equations (refer to nomenclature section and Figure 5.2 for symbols),

$$\frac{\partial p_m}{\partial t} = D_m \frac{\partial^2 p_m}{\partial x^2} \qquad 0 < x < L_m, \ t > 0 \qquad\qquad (5.10)$$

$$\frac{\partial p_s}{\partial t} = D_s \frac{\partial^2 p_s}{\partial x^2} \qquad L_m < x < L_m + L_s, \ t > 0 \qquad (5.11)$$

All cases have common boundary conditions at the membrane/sample layer interface

$$p_m = p_s \text{ at } x = L_m, \ t > 0 \qquad\qquad\qquad (5.12)$$

and $\qquad P_m \dfrac{\partial p_m}{\partial x} = P_s \dfrac{\partial p_s}{\partial x} \qquad$ at $x = L_m, \ t > 0 \qquad\qquad (5.13)$

Also common to all cases is the boundary condition at the cathode surface where oxygen is assumed to be consumed instantaneously.

$$p_m = 0 \text{ at } x = 0, \ t > 0 \qquad\qquad\qquad (5.14)$$

To complete the model for each case shown in Figure 5.4 the upper boundary condition (gas/sample interface), and initial conditions must be defined. These are different for each case. Once specified the model can be solved for each case.

5.4.2 Switch on

In this case the electrode is not running and has no potential applied. Both the sample and membrane are in equilibrium with the ambient environment, and hence have a uniform initial partial pressure profile equal to p_g. In this work p_g represents the partial pressure of oxygen in air (however in theory any gas environment could be used). The electrode is suddenly switched on (potential applied). Curve (a) of Figure 5.4 provides an example transient for this approach. The current is initially high as excess oxygen in the highly permeable membrane is consumed. The decline in current then becomes less rapid as steady-state is approached. During this period excess oxygen in the less permeable sample is being consumed. Steady-state is achieved when the partial pressure profile through the sample layer becomes linear.

	1/8M Sucrose	1/4M Sucrose	1/2M Sucrose	1M Sucrose
	0.874	0.753	0.579	0.334
	0.901	0.794	0.600	0.353
	0.897	0.765	0.584	0.351
	0.887	0.786	0.615	0.320
	0.858	0.774	0.581	0.345
	0.877	0.790	0.621	0.322
	0.920	0.751	0.576	0.327
	0.899	0.786	0.591	0.347
Mean	0.889	0.775	0.593	0.337
SE (%)	2.2	2.2	2.9	3.9

	1/4M NaCl	1M NaCl	2M NaCl	3M NaCl
	0.911	0.676	0.465	0.339
	0.962	0.661	0.471	0.317
	0.934	0.650	0.452	0.324
	0.908	0.699	0.448	0.300
	0.935	0.645	0.443	0.320
	0.901	0.708	0.447	0.296
	0.903	0.684	0.466	0.331
	0.954	0.670	0.468	0.326
Mean	0.926	0.674	0.458	0.319
SE (%)	2.6	3.3	2.4	4.6

Table 5.1.   Relative permeability (sample to water) of sucrose and NaCl standards of various concentrations.

190
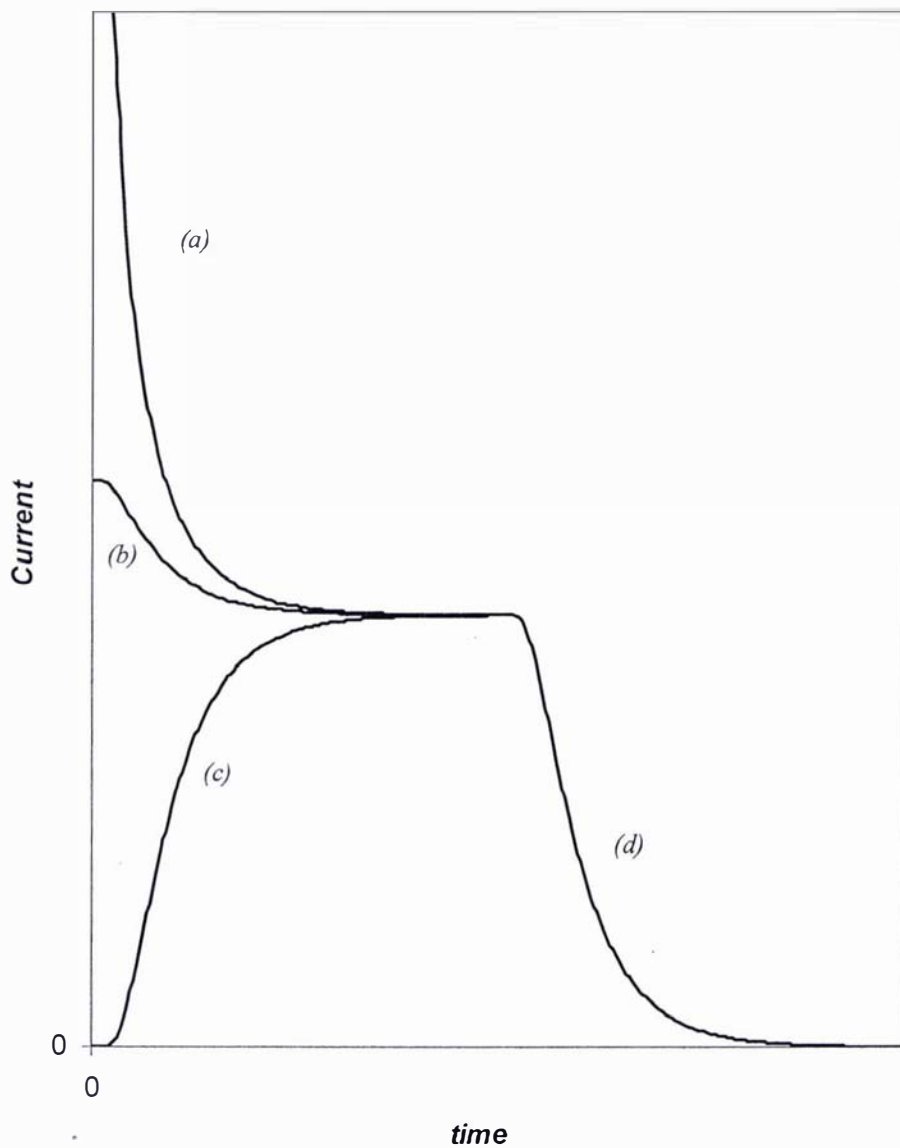
Figure 5.4   Expected schematic transients for different combinations of boundary and initial conditions: (a) switch on, (b) steady-state sample addition, (c) up-step from p_g=0, (d) down-step to p_g=0.

Initial condition

Initially the oxygen partial pressure is uniform throughout the system at $p=p_g$.

$$p_s = p_m = p_g \qquad \text{for} \quad 0 \leq x \leq L_m + L_s, \qquad t=0 \qquad (5.15)$$

Sample surface boundary condition

The sample surface is maintained at p_g for the duration of the experiment.

$$p_s = p_g \qquad \text{at} \quad x = L_m + L_s, \qquad t>0 \qquad (5.16)$$

5.4.3 Steady-state sample addition

In the 'steady-state sample addition' method, the electrode is initially at steady-state with gas of partial pressure p_g, without a sample solution layer. A sample layer at equilibrium with a gas of partial pressure p_g is rapidly added to cover the surface of the membrane. Curve (b) of Figure 5.4 provides an example transient for this approach. The initial current is lower than that of the 'switch on' current (curve (a)). This is because, in this case, excess oxygen in the highly permeable membrane has already been consumed and the electrode is running at steady state. After the addition of the sample layer, steady-state is approached with the excess oxygen in the sample being consumed. Steady-state is again achieved when the partial pressure profile in the sample is linear. Hence steady-state current is the same as for the 'switch on' method.

Initial conditions

In this approach there is a linear gradient initially through the membrane layer.

$$p_m = \frac{p_g}{L_m} x \qquad 0 \leq x \leq L_m, \qquad t = 0 \qquad (5.17)$$

The sample layer once applied to the system, has uniform partial pressure.

$$p_s = p_g \qquad L_m \leq x \leq L_m + L_s, \qquad t = 0 \tag{5.18}$$

Sample surface boundary condition

The sample surface is maintained at p_g for the duration of the experiment.

$$p_s = p_g \qquad x = L_m + L_s, \quad t > 0 \tag{5.19}$$

5.4.4 Up-step

In this experiment the probe with sample layer in place runs initially at steady-state with a gas of known partial pressure which is suddenly stepped to a gas of higher partial pressure. The special case considered here is when the probe is initially running at steady-state at $p=0$ and the up-step is to p_g, but in theory any gas environment could be used. Curve (c) of Figure 5.4 provides an example transient for this approach. The partial pressure is initially zero throughout the entire membrane and sample system. Once stepped to a higher partial pressure, oxygen diffuses through the system to the cathode surface. Once again, steady-state is reached when the partial pressure profile through the solution becomes linear. Therefore, the steady-state current is the same as both the 'switch on' and 'sample steady-state addition methods' (given the same sample solution layer).

Initial conditions

Initially there is no oxygen present throughout the system.

$$p_s = p_m = 0 \quad for\ 0 \leq x \leq L_m + L_s,\ t = 0 \tag{5.20}$$

Sample surface boundary condition

The sample surface is maintained at p_g for the duration of the experiment.

$$p_s = p_g \ at \ \ x = L_m + L_s, \ t > 0 \qquad\qquad (5.21)$$

5.4.5 Down-step

In the 'down-step' experiment the electrode runs with a sample solution layer on top of the membrane, at steady-state with a gas of partial pressure p_g, and is exposed to a sudden down-step, by switching the gas flow to a lower oxygen partial pressure. The particular case considered here, and by Ju *et al.* (1988) and Ho *et al.* (1988), is when the down-step is to a gas containing no oxygen (p_g=0). The down-step could, in practice, employ any gas partial pressure which is lower than p_g. Curve (c) of Figure 5.4 provides an example transient for this approach. In this case the system is already running at the steady-state described for the previous three methods. Upon stepping to a gas flow of zero oxygen, the response declines as excess oxygen in the system is consumed. A new steady-state is eventually reached where the current is zero. The unique initial and boundary conditions for this case are;

Initial conditions

As the system is initially at steady-state, the initial conditions are given by a linear gradient through each of the membrane and solution layers. For the membrane this gradient is given by,

$$p_m = \frac{p_i}{L_m} x \qquad 0 \le x \le L_m, t = 0 \qquad\qquad (5.22)$$

For the sample solution this gradient is given by,

$$p_s = \frac{p_g - p_i}{L_s} x - \frac{L_m(p_g - p_i) - L_s p_i}{L_s} \qquad L_m \le x < L_m + L_s, t = 0 \qquad\qquad (5.23)$$

where p_i is the partial pressure at the interface between sample solution and membrane, and can be derived from equation 5.4 as,

$$p_i = \frac{L_m P_s}{L_m P_s + L_s P_m} \, p_g \tag{5.24}$$

Sample surface boundary condition

At the surface the boundary is exposed to a gas with zero oxygen partial pressure for the duration of the experiment.

$$p_s = 0 \ \ at \ x = L_m + L_s, \ t > 0 \tag{5.25}$$

5.4.6 Model solution

The complex derivation of the analytical solution to the down-step scenario has been described in full by Ho *et al.* (1988). Obtaining analytical solutions for such bi-layer systems is very difficult, providing a solution exists. For these reasons the mathematical problems described above were initially solved here by the much more generically applicable method of finite differences. Figure 5.5 provides a schematic representation of the finite difference solution, to assist with the following derivation.

The sample solution layer can be divided into equally spaced intervals such that the first node $j=1$, falls on the boundary at the gas/sample interface, and the node js falls on the interface between the sample solution and the membrane. If this is done the node spacing of $j=js$ equally spaced nodes will be $\Delta x_1 = \dfrac{L_s}{js-1}$. In a similar way the membrane can be divided into $j=jm$ equally spaced nodes with the final node falling at the membrane/cathode interface ($js + jm$) and the node spacing given by $\Delta x_2 = \dfrac{L_m}{jm}$.

The finite difference equations follow.

For the node at the boundary between the sample/gas interface ($j = 1$)

$$\frac{\partial p_1}{\partial t} = 0 \tag{5.26}$$

For all nodes internal to the sample solution ($j = 2$ to $j = js\text{-}1$).

$$AS_s \, \Delta x_1 \frac{\partial p_j}{\partial t} = \frac{AD_s S_s (p_{j-1} - p_j)}{\Delta x_1} - \frac{AD_s S_s (p_j - p_{j+1})}{\Delta x_1} \tag{5.27}$$

giving,

$$\frac{\partial p_j}{\partial t} = D_s \frac{(p_{j-1} - 2p_j + p_{j+1})}{\Delta x_1^2} \tag{5.28}$$

For the node at the boundary between the sample solution and the membrane ($j=js$).

$$\frac{AS_s \Delta x_1, + S_m \Delta x_2}{2} \frac{\partial p_{js}}{\partial t} = \frac{AP_s (p_{js-1} - p_{js})}{\Delta x_1} - \frac{AP_m (p_{js} - p_{js+1})}{\Delta x_2} \tag{5.29}$$

giving,

$$\frac{\partial p_{js}}{\partial t} = \frac{2P_s \Delta x_2 (p_{js-1} - p_{js}) - 2p_m \Delta x_1 (p_{js} - p_{js+1})}{\Delta x_1 \Delta x_2 (S_s \Delta x_1 + S_m \Delta x_2)} \tag{5.30}$$

For all nodes internal to the membrane ($j = j_s + 1$ to $j = j_s + j_m - 1$)

$$AS_m \Delta x_2 \frac{\partial p_j}{\partial t} = \frac{AP_m (p_{j-1} - p_j)}{\Delta x_2} - \frac{AP_m (p_j - p_{j+1})}{\Delta x_2} \tag{5.31}$$

giving,

$$\frac{\partial p_j}{\partial t} = \frac{D_m(P_{j-1} - 2P_j + P_{j+1})}{\Delta x_2^2} \tag{5.32}$$

For the node at the boundary between the membrane and cathode surface $(j=j_s+j_m)$

$$\frac{\partial p_{js+jm}}{\partial t} = 0 \tag{5.33}$$

The above equations show that in order for a solution to be obtained, explicit knowledge of two of the three membrane properties P_m, D_m or S_m is required (with the remaining property being deduced from $P_m=D_mS_m$). In a practical sense this complicates experimental analysis, as these parameters must be measured. Further, the nature of the oxygen probe requires these parameters to be measured on a regular basis, as membrane characteristics are known to change with time.

Explicit knowledge of the membrane properties can be avoided if linear partial pressure profiles are assumed in the membrane, both in transient and steady-state periods (the reason for this will be explained shortly). This assumption requires that the resistance to mass transport offered by the membrane is small enough (high P_m, and small L_m) that equilibrium with the partial pressure at the membrane/sample interface p_i, is essentially achieved instantaneously. Hence the partial pressure profile across the membrane will always be linear.

In order to identify whether this assumption is sensible, an alternative solution where the membrane layer is assumed to be at steady-state was developed. If this is the case, the finite difference equations in the membrane layer are no longer required (equations 5.31/5.32), nor is the equation at the cathode surface (equation 5.33). The equation at the gas/sample interface (equation 5.22), and the equations internal to the sample layer (equations 5.23/5.24) remain the same. The equations at the sample/membrane interface (equations 5.29/5.30) are altered to become,

gas, $p=p_g$

$j=1$

$p = p_g$ $x = L_m + L_s$

sample solution,
$P_s = D_s S_s$

Δx_1

L_s

internal node
($j=2$ to $j=js-1$)

$j=js$

$p = p_i$ $x = L_m$

membrane,
$P_m = D_m S_m$

Δx_2

internal node
($j=js+1$ to
$j=js+jm-1$)

L_m

$j=js+jm-1$

$p = 0$ $x = 0$

cathode surface
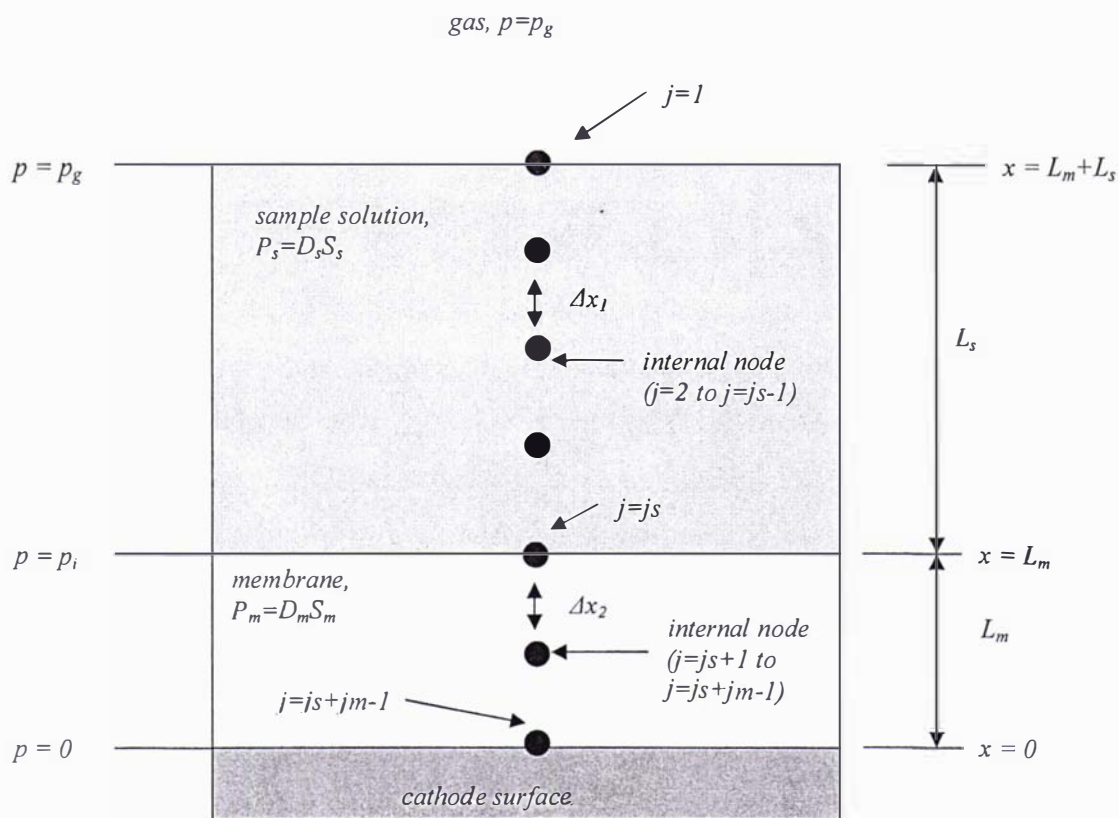
Figure 5.5.   Schematic representation of the finite difference solution to the model.

$$\frac{A\Delta x_1 S_s}{2} \frac{\partial p_{js}}{\partial t} = \frac{AP_s(p_{js-1} - p_{js})}{\Delta x_1} - \frac{AP_m(p_{ys} - 0)}{L_m} \tag{5.34}$$

giving,

$$\frac{\partial p_{js}}{\partial t} = \frac{2D_s S_s \Delta x1 L_m (p_{js-1} - p_{js}) - 2\Delta x_1^2 P_m p_{js}}{S_s \Delta x_1^3 L_m} \tag{5.35}$$

The finite difference equations, under the assumption of non-linear and linear partial pressure profiles in the membrane, could then be solved and compared to see if the simplified model is applicable to the experimental set-up.

Before this could be done, some feasible parameter estimates need to be obtained. For the case of a water sample layer and an FEP Teflon membrane (as used in this investigation), Table 5.2 provides a list of parameter estimates at 25°C. The sample solution thickness of 2.9 mm given in Table 5.2 resulted from the addition of 0.5 ml of sample solution to the diffusion cell. It was the minimum practical thickness achievable with this experimental set-up. If <0.5 ml was added, incomplete and uneven coverage of the membrane resulted. The listed membrane thicknesses are those of the standard YSI, and high-sensitivity YSI FEP Teflon membranes. A variety of membranes could be used, but these were selected as they are readily available.

The series of finite difference equations for each model were solved using Matlab's ordinary differential equation solver (ode45). Upon solution, the transient current response is described under the assumption of non-linear partial pressure profiles as,

$$I(t) = nAF \frac{P_m}{\Delta x_2} p_{js+jm-1} \tag{5.36}$$

and under the assumption of linear partial pressure profiles by,

$$I(t) = nAF \frac{P_m}{L_m} p_{js} \qquad\qquad (5.37)$$

The transient current can be made dimensionless by dividing by the initial current, by the steady-state current, the current in the pure gas phase, or some other appropriate combination. Further comparison of transients is also more readily accomplished through the use of dimensionless time (τ).

$$\tau = \frac{D_s t}{L_s^2} \qquad\qquad (5.38)$$

Figures 5.6 to 5.9 show the simulated dimensionless transients, under the assumption of both non-linear and linear partial pressure profiles in the membrane, at various ratios in the L_s/L_m for the 'down-step', 'up-step', 'switch-on', and 'steady-state sample addition' scenarios respectively.

5.4.7 Comparison of techniques

Figures 5.6 to 5.9 all reveal the same general trend in that as the ratio L_s/L_m becomes larger, the assumption of linear partial pressure profiles in the membrane becomes more valid. This is evidenced by the fact that the non-linear and linear assumption curves become closer together as L_s/L_m becomes larger. As would be expected, the assumption is most valid for the YSI high-sensitivity membrane. Unfortunately, experimental work performed with this membrane was very cumbersome, with the fragile membrane being very prone to breakage and subsequently giving variable results. For the purposes of practicality, the YSI standard membrane was employed in this work, as it is much easier to work with, producing reliable, reproducible results. For the 'down-step' experimental method, the assumption of linear partial pressure profiles in the membrane gave results that were accurate for $L_s/L_m > 115$ (see Figure 5.6), which is the value measured in the experimental set-up ($Ls/L_m = 115$)

Parameter	Value	Reference
P_m $(mol.m.m^{-2}.s^{-1}.mmHg^{-1})$	2.03×10^{-13}	Pauly (1999)
S_m $(mol.m^{-3}.mmHg^{-1})$	0.011	Pauly (1999)
L_m Standard (μm)	25.3 ± 0.3 ($\pm SD$, n = 15)	Own measurements
L_m High sensitivity (μm)	13.3 ± 0.9 ($\pm SD$, n = 15)	Own measurements
D_s $(m^2.s^{-1})$	2.2×10^{-9}	Lango *et al.* (1996)
S_s $(mol.m^{-3}.mmHg^{-1})$	0.00162	Battino *et al.* (1983)
L_s (μm)	2900 ± 110 ($\pm SD$, n=225)	Own measurements
A (m^2)	$2.9 \times 10^{-5} \pm 0.3 \times 10^{-5}$	Own measurements

Table 5.2   Parameter estimates for input into finite difference solutions at 25°C.

Figure 5.7 shows that the assumption of linear membrane partial pressure profiles may also be fair for the YSI standard membrane for the 'up-step' experimental method. However, great practical experimental difficulty was experienced trying to get a zero reading before the system was exposed to an up-step. The probe simply failed to reach a steady-state with the zero oxygen partial pressure environment. This could potentially be resolved by equilibrating the system with a higher partial pressure before up-step. However this makes the analysis more difficult. Therefore, the 'up-step' experimental method was not considered any further.

Figure 5.8 shows that for the 'switch-on' boundary and initial conditions, the assumption of linear membrane partial pressure profiles in the membrane is particularly flawed in the initial stages. This is to be expected, as before the probe is switched on, the membrane is equilibrated with gas at ambient p_g. This excess oxygen must be initially consumed before the partial pressure profiles of oxygen in the membrane can ever be considered linear. This is evident in Figure 5.8, by the non-linear and linear membrane simulation predictions being closer to one another when the membrane is thin. The thin membrane holds less excess oxygen, and hence less needs to be consumed before the partial pressure profiles can be linear. In fact, when the membrane is very thin, holding little oxygen, the 'switch-on' experiment transients tend toward the 'steady-state sample addition' transients.

In reality when the probe is switched on significant and unpredictable charging currents are observed. These could possibly be avoided by applying a zero potential before 'switch-on'. However, for these reasons as well as the theoretical reasons stated above, the 'switch-on' method was not investigated any further.

Figure 5.9 shows that the large initial differences in non-linear and linear membrane model predictions observed in the switch-on method are significantly reduced for the 'steady-state sample addition' method. This is particularly true when L_s/L_m is large (thin membrane). The reason for this is that because the probe is already running, the excess oxygen which was previously problematic, has already been consumed. Still, the assumption of linear membrane partial pressure profiles does not seem to be

particularly valid initially for the YSI standard membrane. However, this situation is greatly improved at larger values of time. The 'steady-state sample addition' method may be a useful method for measuring P, D, and S, particularly if transient data at greater elapsed time intervals is used. Furthermore, because the probe is already running, charging currents are not problematic.

This mathematical and practical analysis has revealed that it may be feasible to measure P, D, and S of sample solutions using both the 'down-step', and 'steady-state sample addition' methods. For these methods the assumption of linear partial pressure profiles seems reasonable, at least under certain conditions, using appropriate YSI standard membranes and minimum sample layer thicknesses. These methods were therefore investigated further by way of experiment. Note that the ratio of L_s/L_m could be further increased by increasing L_s. However, at the current value of L_s (2.9 mm), samples already took approximately one hour to reach steady-state. Increasing L_s would further increase this time. Given that the long term objective was to analyse and compare biological samples, analysis time must be kept to a practical minimum.

5.5 Analytical solution development

It was stated earlier that if the assumption of linear partial pressure profiles in the membrane is valid, then the parameters P, D and S can be determined without explicit knowledge of the membrane properties. This can be more easily realised through the use of analytical solutions for the 'down-step' and 'steady-state sample addition' transients. The use of the numerical solutions described above to do this would require multiple simulations and be prone to error. For the 'down-step' and 'steady-state sample addition' methods under the assumption of linear partial pressure profiles in the membrane, the system can now be considered a single slab (as opposed to a bi-layer) consisting of a sample solution layer only, and described by the diffusion equation,

$$\frac{\partial p_s}{\partial t} = D_s \frac{\partial^2 p_s}{\partial x'^2}$$
(5.39)
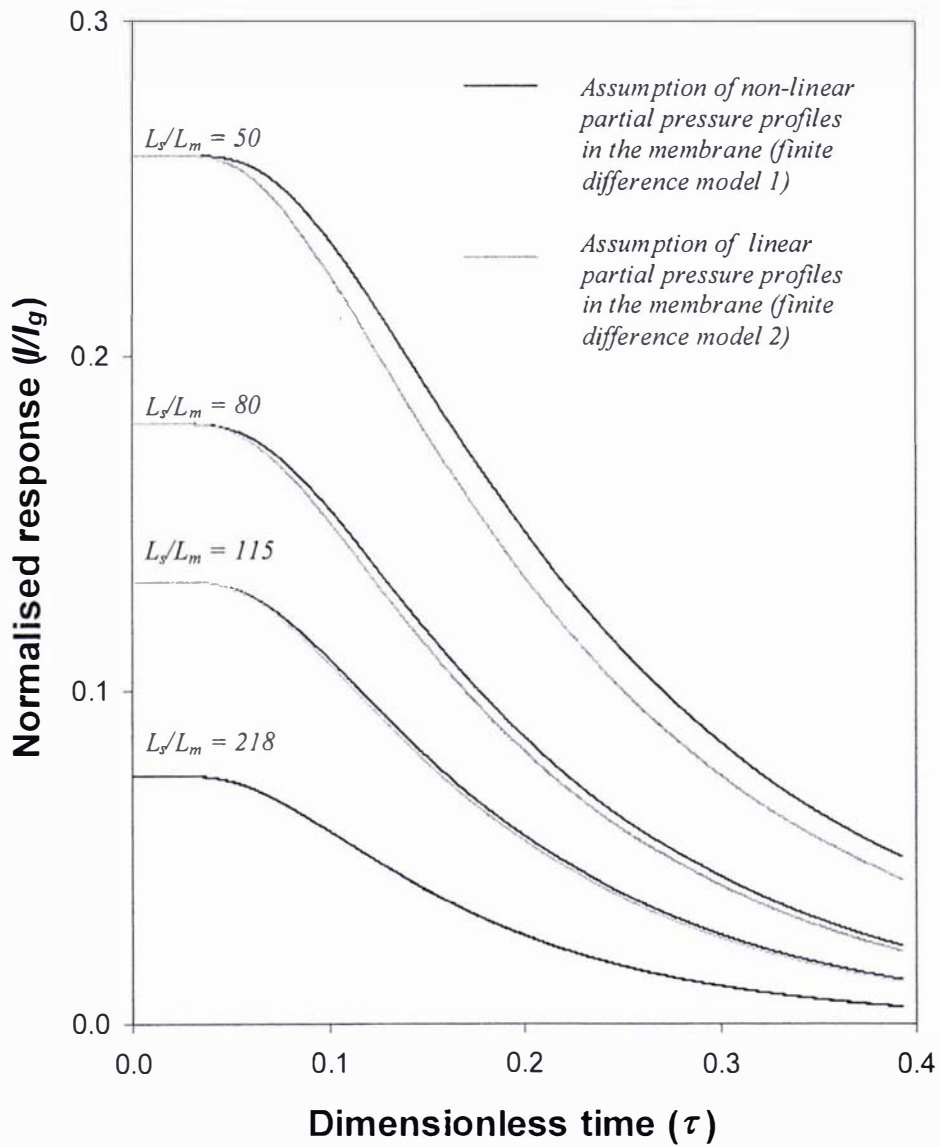
Figure 5.6   Simulated 'down-step' transients under the assumption of non-linear and linear membrane partial pressure profiles at various ratios of L_s/L_m.
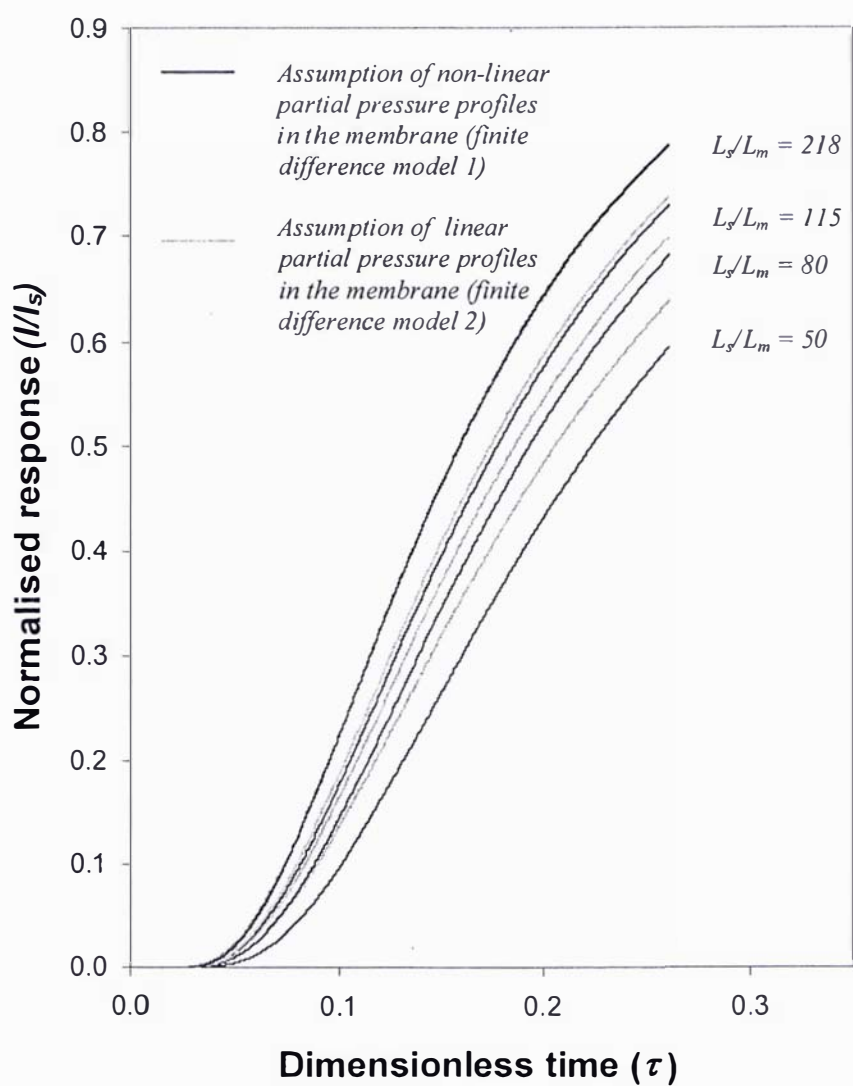
Figure 5.7   Simulated 'up-step' transients under the assumption of non-linear and linear membrane partial pressure profiles at various ratios of L_s/L_m.
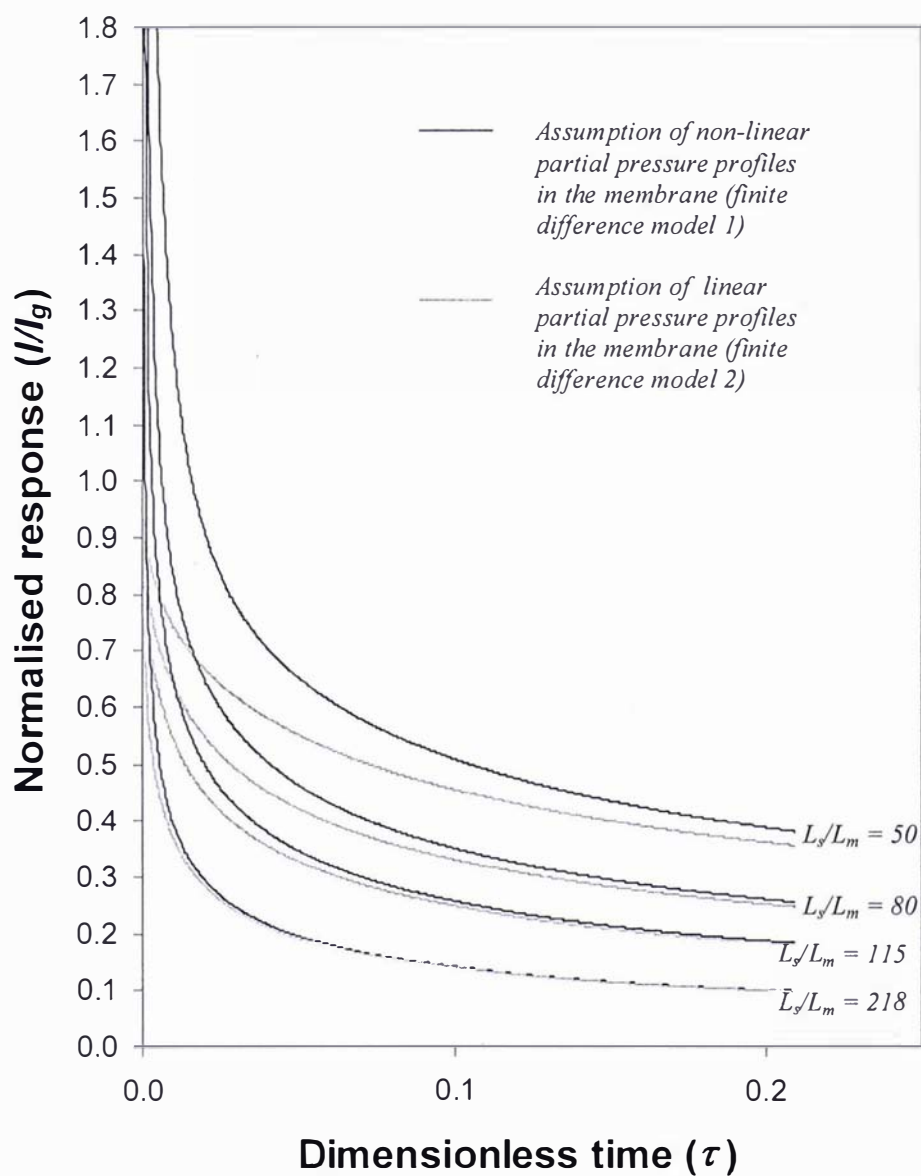
Figure 5.8   Simulated 'switch-on' transients under the assumption of non-linear and linear membrane partial pressure profiles at various ratios of L_s/L_m.
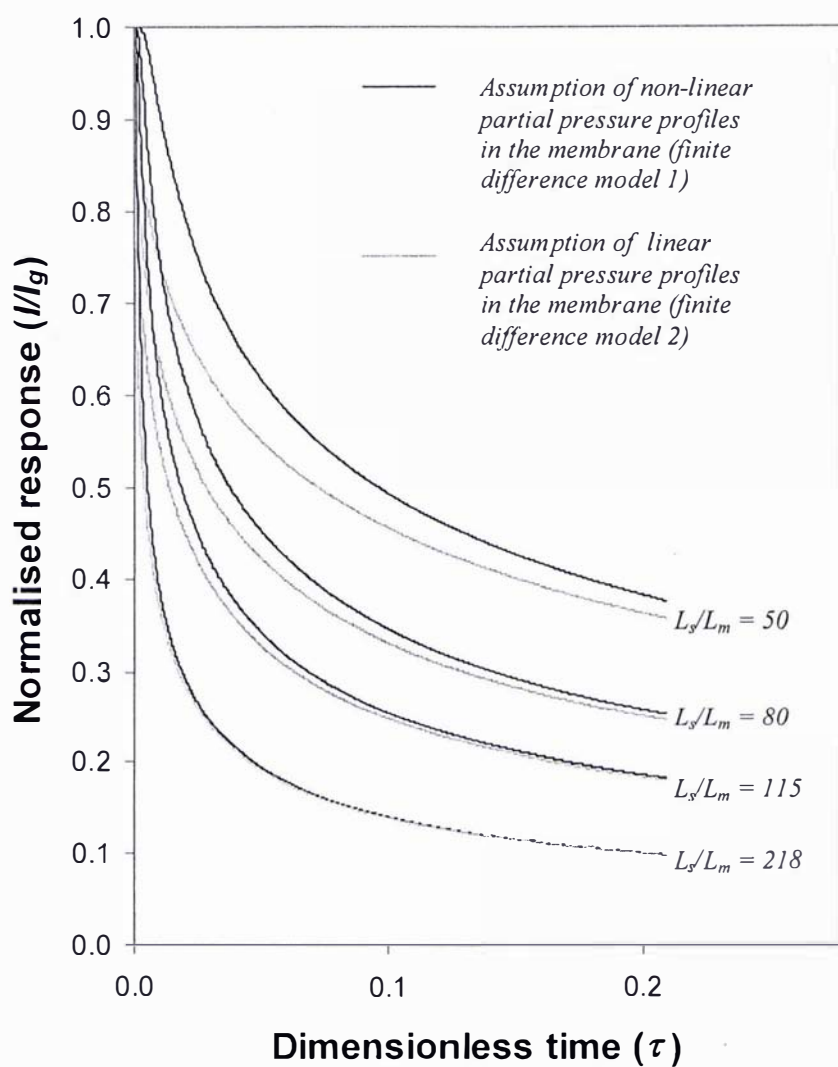
Figure 5.9   Simulated 'steady-state sample addition' transients under the assumption of non-linear and linear membrane partial pressure profiles at various ratios of L_s/L_m.

Note that in the bi-layer system the position in the system was denoted by x. In the single layer system the bottom boundary has moved from $x=0$ to $x=L_m$. To differentiate the two systems and to make the bottom boundary occur at zero position, positional variation in the single layer system is described by x', where $x'=x-L_m$. Hence the use of x' as opposed to x in equation 5.39 and the following two sections (5.5.1 and 5.5.2).

5.5.1 Down-step experiment analytical solution

For the 'down-step', the initial conditions are given by,

$$p_s = p_g \frac{\left(\dfrac{P_m}{L_m D_s S_s} x' + 1 \right)}{\left(\dfrac{P_m}{L_m D_s S_s} L_s + 1 \right)} \quad for \quad 0 \leq x' \geq L_s \quad t=0 \quad (5.40)$$

The boundary condition at the gas-liquid interface is given by,

$$p_s = 0 \quad x' = L_s, t > 0 \tag{5.41}$$

At the sample-membrane interface the boundary condition is given by,

$$\frac{\partial p_s}{\partial x'} = \frac{P_m}{L_m D_s S_s} p \quad x' = 0, t > 0$$

If the problem is made dimensionless such that x' is expressed as x'/L_s, and p_s as p_s/p_g, then the analytical solution for the normalised current transient as described by Ho *et al.* (1988) is given by,

$$\frac{I(t)}{I_g} = 2 \sum_{n=1}^{\infty} \frac{\beta_n^2 + Bi^2}{\beta_n^2 + Bi^2 + Bi} \frac{\sin \beta_n}{\beta_n} e^{-\beta_n^2 \tau} \tag{5.42}$$

208

where β_n's are the positive roots of the equation,

$$\beta \cot \beta + Bi = 0 \tag{5.43}$$

and,

$$Bi = \frac{I_g}{I_s} - 1 = \frac{P_m}{L_m} \frac{L_s}{D_s S_s} \text{ (dimensionless)} \tag{5.44}$$

Note that τ is dimensionless time as previously given in equation 5.38 ($\tau = D_s t / L_s^2$). It has been verified that this analytical solution gives the same solution as the numerical solution with adequate precision.

5.5.2 Sample steady-state addition experiment analytical solution

For the 'sample steady-state addition' method, the initial conditions are given by,

$$p_s = p_g \quad 0 \le x' \le L_s \qquad t=0 \tag{5.45}$$

The boundary condition at gas-sample interface is given by,

$$p_s = p_g \quad x' = L_s, t > 0 \tag{5.46}$$

The boundary condition at sample-membrane interface is given by,

$$\frac{\partial p_s}{\partial x'} = \frac{P_m}{L_m D_s S_s} p \quad x' = 0, t > 0 \tag{5.47}$$

Once again this problem is made dimensionless. The analytical solution to this problem has been described by Myers (1987) for heat transfer. By use of the heat and mass transfer analogy, the analytical solution for the normalised current transient is given by,

$$\frac{I(t)}{I_g} = 1 - \frac{Bi}{1+Bi} + 2Bi \sum_{n=1}^{\infty} \frac{(\sin \beta_n)^2}{\beta_n^2 + Bi(\sin \beta_n)^2} e^{-\beta_n^2 \tau} \qquad (5.48)$$

where β_n's are once again the positive roots of equation 5.43, and Bi is given by equation 5.44. It has been verified that this analytical solution gives the same solution as the numerical solution with adequate precision.

5.6 Data analysis

To use these analytical solutions to determine P_s, D_s and S_s the following procedure was employed. The steady-state current in the gas phase (p_g) was measured, giving I_g (see equation 5.3). Upon reaching steady-state with a sample solution layer in place at p_g, I_s was obtained (see equation 5.6).

This was done both for water (known properties) and an unknown sample solution. Equation 5.9 was then used to calculate the relative permeability (P_s/P_w) of the sample to water.

The transient currents are recorded as appropriate for the 'down-step' or 'steady-state sample addition' methods (see materials and methods section). $Bi=I/I_s-1$ can then be substituted into equation 5.42 or 5.48 as appropriate, and the diffusion coefficient varied until a fit is obtained. This can be done with the full data transient, a selected range of data, several data points, or a single data point. Doing this for both water and sample, the relative diffusivity of sample to water can be determined D_s/D_w. Because P_s/P_w is known (from the steady-state analysis), the relative solubility can also be determined S_s/S_w ($P=DS$). If the properties of oxygen in water are known, then those of the sample can be expressed in absolute terms if desired. This requires no explicit knowledge of the membrane properties.

The next section describes the results of the implementation of this procedure for both the 'down-step' and 'steady-state sample addition' methods, using a variety of standard solutions.

5.7 Validation of methodology against standard solutions

Figure 5.10 shows examples of data traces obtained for the 'sample steady-state addition' method. Trace (a) represents a smooth first order decay type pattern. This is the type of data trace that is expected based on the predictions of the discussed mathematical models. Trace (b) shows substantial deviation from the expected decay pattern. This could be due to inconsistent sample addition, and spreading over the membrane. Before the sample settles, mass transport may be convective, and only become diffusive at a later time when the sample stagnates. The same result could also be due to early temperature fluctuations and stabilisation, or displacement of the experimental device. All of these could potentially result in transitions between convective and diffusive mass transport.

Figure 5.11 shows example data traces for the 'down-step' experiment data collection. In this case curve (a) represents the expected transient, whilst curve (b) shows significant deviation in the form of a 'hump', evidenced by an increase in current after the step-change, before the expected decline is observed. The cause of this 'hump' is also likely to be due to mass transport being convective for a time. A likely cause is physical disturbance of the device as the gas partial pressure is step changed. Other possibilities include temperature differences between the gas before and after step-charge, or a difference in vapour pressure of these gases. A difference in vapour pressure could lead to surface evaporation or condensation, depending on the direction of the driving force. This could change the sample thickness, and also lead to temperature gradients which could, in turn, lead to convection. Convection could also result from surface disturbance of the sample by the gas flowing over it.

Precautions for avoiding all of these potential problems were described previously in this chapter. In practice, when transients were obtained that deviated from those expected for both 'sample steady-state addition' and 'down-step' data collection, these transients were discarded (it was verified that these transients produce inaccurate and highly variable results).
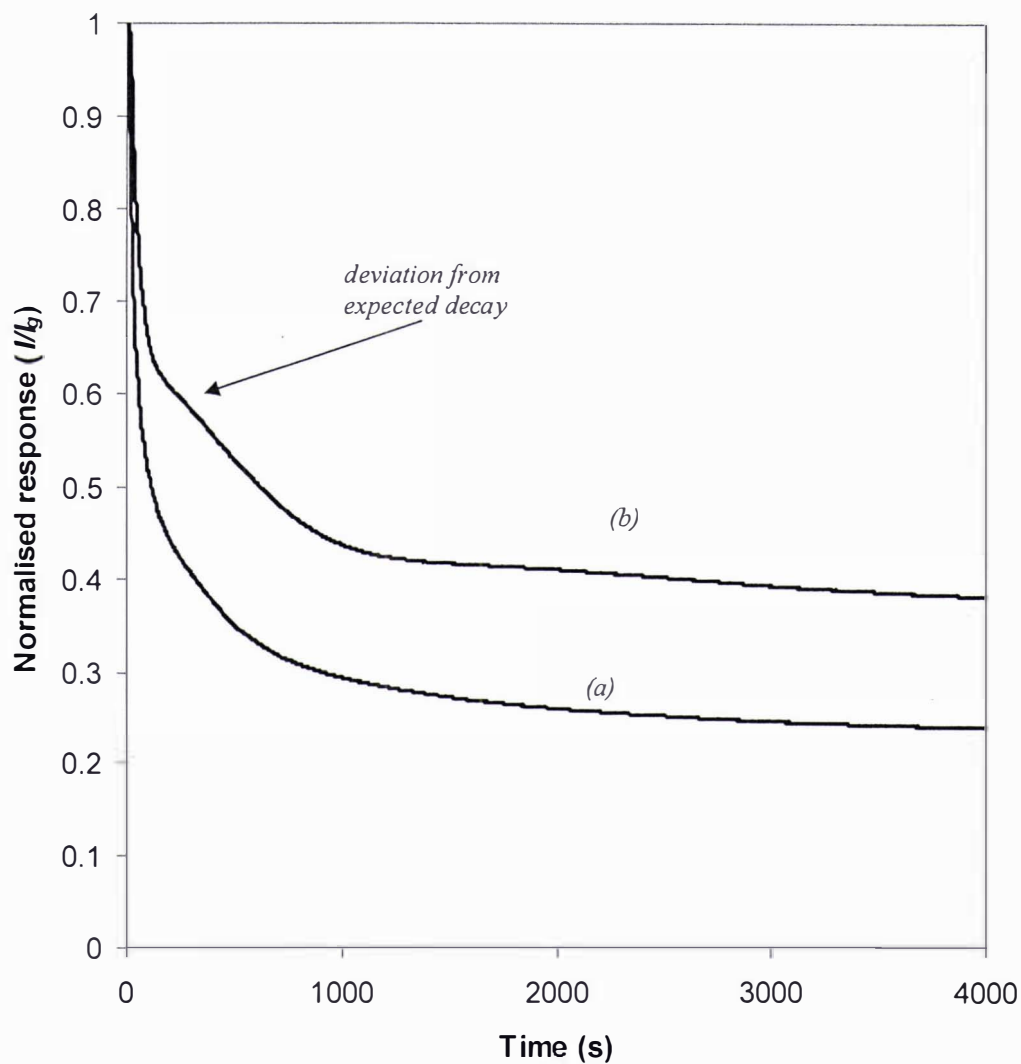
Figure 5.10   Experimental 'sample steady-state addition' traces showing (a) acceptable and (b) discarded experimental data.

The chart shows two curves (a) and (b) plotting Normalised response (I/I_g) on the y-axis (from 0.26 to 0.38) against Time (s) on the x-axis (from 0 to 700). An arrow labelled *deviation from expected decay* points to curve (b).
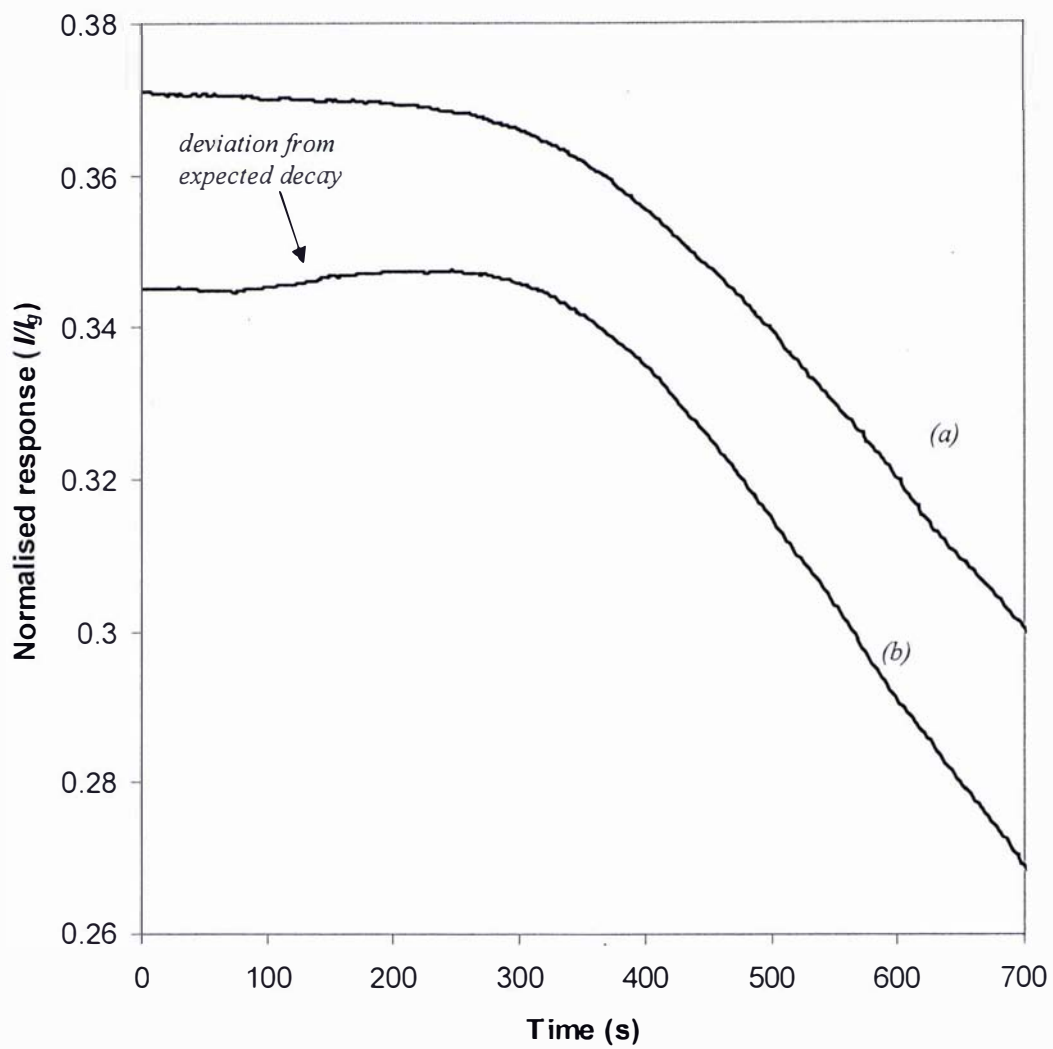
Figure 5.11   Experimental 'down-step' traces showing (a) acceptable and (b) discarded experimental data.
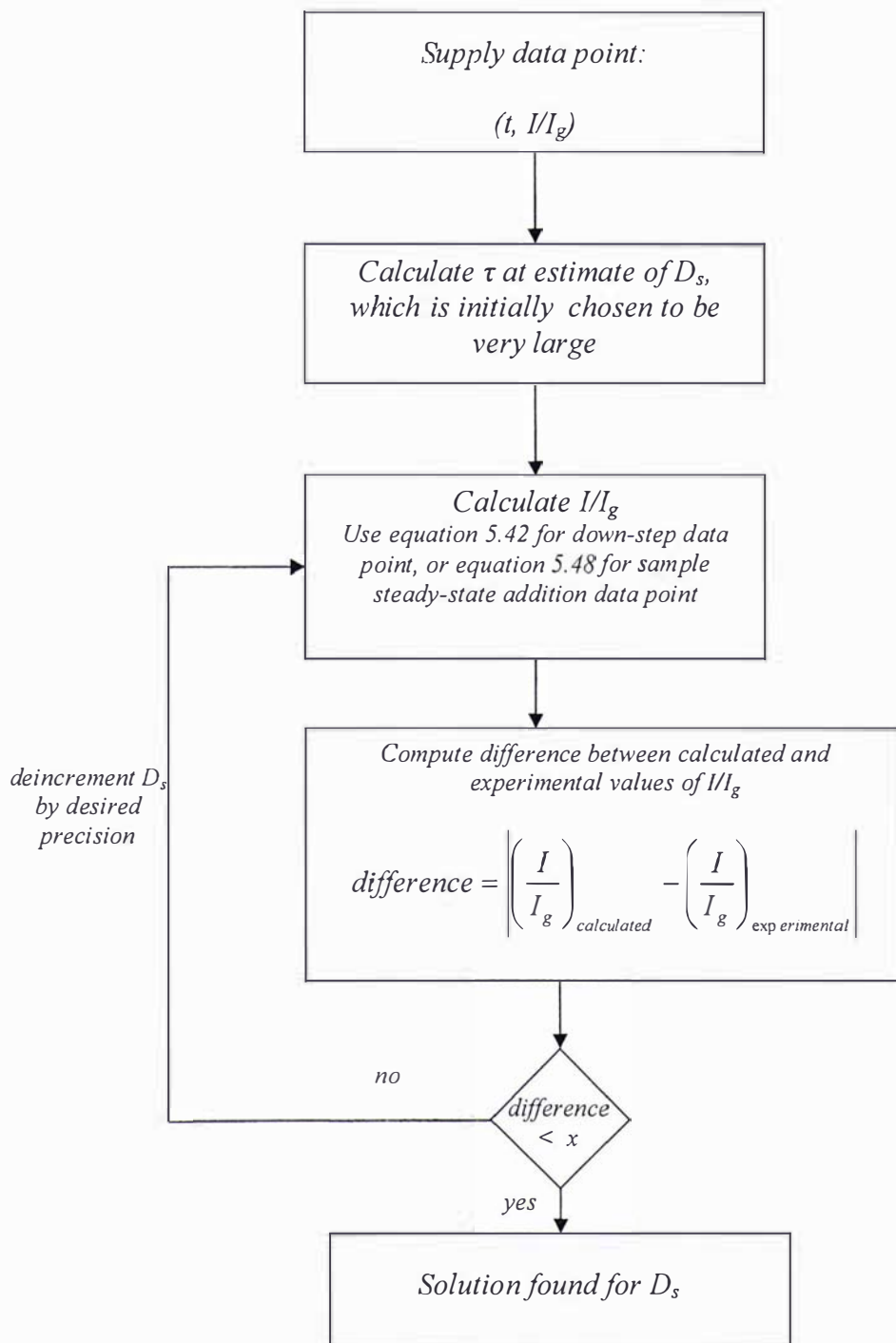
Figure 5.12   Algorithm for calculating diffusivity (ideally $x = 0$, however to save processing time x was chosen as 0.001. Precision used here was 0.01 x 10^{-9}).

Having obtained reliable transients, the diffusion coefficients were estimated at each data point according to the algorithm described in Figure 5.12. The question is which data provides the best estimates of D_s. Ideally, a plot of predicted D_s vs. t would be a straight line (horizontal), as the calculated value of D_s should be independent of the data point used to calculate it. However figures 5.6 to 5.9 show that it would not be appropriate to use all data when operating under the assumption of linear partial pressure profiles in the membrane. The use of data at early time values may result in large errors, as this assumption only becomes true at longer time values. Therefore, instead of D_s vs. t being the ideal straight line, it would be expected that early D_s estimates would be unstable, and tend toward a straight line as time increases.

Figures 5.13 and 5.14 show typical plots of D_s vs. t for sample steady-state addition and down-step experiments respectively, and suggest that this is indeed the case. In both cases, predicted D_s values are initially highly variable before declining to a stable value at larger time intervals. In similar work Ho *et al.* (1988) used a single data point to estimate D_s. This value was taken after a 3% decline in initial current was observed for the down-step. This work suggests that such an approach may not be appropriate if estimates of D_s are not yet stable. Another tempting approach to estimating D_s would be to use the value of D_s which obtains a best-fit between an observed current vs. time transient and a predicted one. This approach would be inappropriate due to the weight it would place on early data points for which the mathematical assumptions are known to be untrue. Therefore this work uses an estimate of D_s which is selected from the stable part of a D_s vs. t curve. A mean of 10 data points over the stable part of the curve was taken as the estimate of D_s. Although it is inappropriate to use data points from early time intervals, it should be noted that Figure 5.13 shows that the estimates of D_s for the 'sample steady-state addition' method do not stabilise until very long time values. At these longer time intervals steady-state is being approached (see Figure 5.8). Because the data is not changing much here, estimates of D_s should be viewed with caution. This does not apply to the down-step method where D_s estimates stabilise during the transient period of the current vs. time curve.

This process was carried out for both water and sample, and the relative permeability (P_s/P_w) calculated using equation 5.9 (assuming equal sample layer thickness). D_s and

D_w are calculated as described by Figure 5.12, and by selecting values from the appropriate part of the D vs. t curve. Thus the relative diffusivity could be calculated (D_s/D_w). Finally since $P = DS$, the relative solubility was calculated (S_s/S_w) as given by,

$$S_{rel} = \frac{P_{rel}}{D_{rel}} \qquad\qquad (5.49)$$

The results of the data analysis (i.e. determination of P_{rel}, D_{rel} and S_{rel}) are presented in Tables 5.3 and 5.4 for 'sample steady-state addition' and 'down-step' respectively, for a variety of sucrose and NaCl standards.

Included on Figures 5.13 and 5.14 is the typical value of the diffusion coefficient of oxygen in water. The proximity of the water value to the stable part of the curve indicates that the estimates provided by this method are of the order of magnitude expected for aqueous solutions. Although variability in the absolute predicted values of D was observed for both samples of the same concentration and water (particularly with the 'sample steady-state addition' method), this variability was reduced when diffusion coefficients were expressed relative to water.

The purpose of this work was to test the accuracy and precision of these methods in determining D_{rel} and S_{rel}, and, based on this, whether or not these methods were appropriate for the determination of these parameters in human follicular fluid.

The best approach to test how accurate these methods are comes from comparison with known values of solubility determined by titrative methods (MacArthur, 1916). At a glance, the mean relative solubilities for each standard compare reasonably well with known values from the literature for both 'steady-state sample addition' and 'down-step'. A more quantitative indication of accuracy can be obtained by assuming the S_{rel} values of MacArthur (1916) to be the 'gold standard' or true values. Taking the difference between these values and those experimentally determined generates a population of 32 differences. Assuming the differences are normally distributed,

216

whether or not these differences are significantly different from zero can be tested using a paired t-test. For the sample steady-state addition method this difference was not significantly different from zero ($p > 0.05$). For the down-step method this difference is marginal ($p < 0.01$).

This would suggest that both methods compare favourably with the data of MacArthur (1916), and that the sample steady-state addition method may be slightly more accurate. Having said that, it should be noted that the mean of the differences are comparable (0.020 for sample steady-state addition, 0.018 for down-step) and both are close to zero. The 'down-step' method produces relative solubility (S_{rel}) estimates with greater precision than the 'sample steady-state addition' method (SD of differences 0.033 and 0.063 respectively). For relative diffusivity (D_{rel}) estimates, the 'down-step' method produces more precise results for every standard solution. Given that it is desirable to detect variation in relative diffusivity of greater than 20% in follicular fluid, the 'down-step' method's maximum observed D_{rel} variability of SE = 2.2% suggests this method will be adequate for detecting large differences. The greater maximum D_{rel} variability of the sample steady-state addition method of SE = 4.7% would also be suitable to achieve this end. It appears that both methods would be suitable for determining large variability in follicular fluid D_{rel} and S_{rel}.

Further, the data in table 5.3 may somewhat overstate the case for the 'sample steady-state addition' method. It presents data only from suitable transients (see Figure 5.10). In practice this method required much higher rejection of unsuitable transients than the 'down-step' method. For this reason this method was discarded in favour of the 'down-step' method for the analysis of D_{rel} and S_{rel} in follicular fluid in the subsequent chapter. The 'sample steady-state addition' method could be improved by incorporating controlled and automated sample addition. Both methods would benefit from on-line sample layer thickness measurement. This would allow the detection of evaporation and condensation, and could also lead to improved results if the assumption of equal thickness between water and sample solutions is not ideal. Other improvements, such as optimisation of L_s/L_m to achieve faster response, may also be desirable. Such improvements combined with a compact, robust design could provide a device for convenient measurement of diffusivity and solubility.
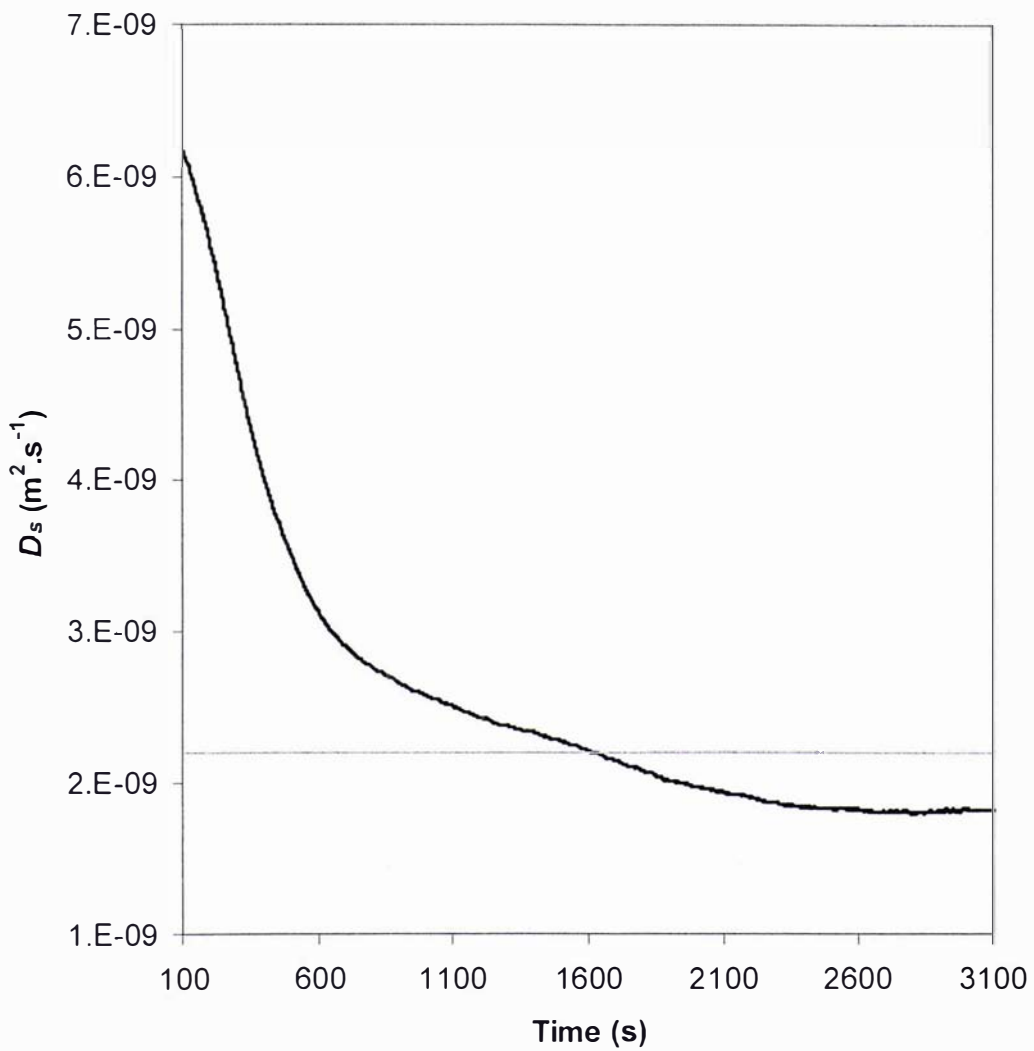
Figure 5.13   Change in predicted sample diffusion coefficient with time for 'steady-state sample addition'. Horizontal line indicates standard value for the oxygen diffusion coefficient in water at 25 °C (Lango *et al.,* 1996).
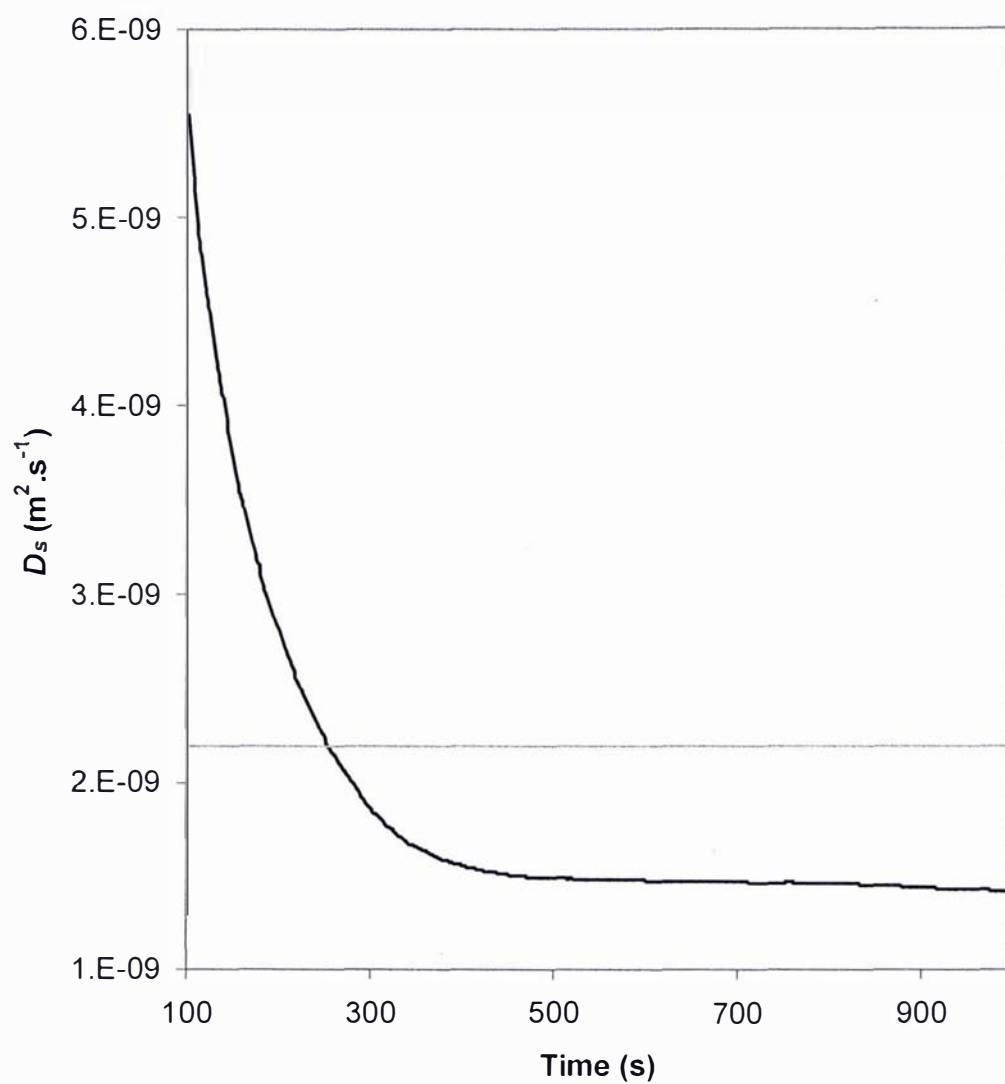
Figure 5.14   Change in predicted sample diffusion coefficient with time for 'down-step'. Horizontal line indicates standard value for the oxygen diffusion coefficient in water at 25 °C (Lango *et al.,* 1996).

	Relative P	Relative D	Relative S	Relative S (MacArthur, 1916)	Difference	Relative P (mean±SE)	Relative D (mean ±SE)	Relative S (mean ±SE)
1/8M Sucrose	0.858	0.924	0.929		-0.005			
	0.877	0.912	0.962	0.934	0.028	0.889±	0.915±	0.973±
	0.920	0.870	1.057		0.123	1.5	1.9	3.0
	0.899	0.954	0.942		0.008			
1/4M Sucrose	0.774	0.987	0.784		-0.050			
	0.790	0.958	0.825	0.834	-0.009	0.775±	0.908±	0.858±
	0.751	0.854	0.879		0.045	1.1	4.2	4.1
	0.786	0.832	0.945		0.111			
1/2M Sucrose	0.581	0.800	0.726		-0.034			
	0.621	0.889	0.699	0.760	-0.061	0.592±	0.826±	0.722±
	0.576	0.888	0.649		-0.111	1.7	4.7	4.8
	0.591	0.727	0.813		0.053			
1M Sucrose	0.345	0.606	0.569		0.015			
	0.322	0.666	0.483	0.554	-0.071	0.335±	0.606±	0.556±
	0.327	0.594	0.551		-0.003	1.9	3.7	5.1
	0.347	0.559	0.621		0.067			
1/4M NaCl	0.935	1.001	0.934		-0.021			
	0.901	0.987	0.913	0.955	-0.042	0.923±	0.964±	0.961±
	0.903	0.864	1.045		0.090	1.4	3.5	3.0
	0.954	1.003	0.951		-0.004			
1M NaCl	0.645	0.832	0.775		0.048			
	0.708	0.801	0.884	0.727	0.157	0.677±	0.816±	0.833±
	0.684	0.888	0.770		0.043	1.9	3.8	4.2
	0.670	0.741	0.904		0.177			
2M NaCl	0.443	0.790	0.561		0.033			
	0.447	0.852	0.525	0.528	-0.003	0.456±	0.854±	0.535±
	0.466	0.872	0.534		0.006	1.4	2.8	1.7
	0.468	0.901	0.519		-0.009			
3M NaCl	0.320	0.811	0.395		0.007			
	0.296	0.720	0.411	0.388	0.023	0.318±	0.797±	0.400±
	0.331	0.804	0.412		0.024	2.4	3.5	1.8
	0.326	0.853	0.382		-0.006			
				Mean	0.020			
				SD	0.063			
				n	32			

Table 5.3   Oxygen permeability, diffusivity, and solubility data for 'sample steady-state addition' method for various standard solutions (four replicates for each standard). Experimental values of relative solubility are compared to those of MacArthur 1916 by calculating the difference (experimental value minus MacArthur value).

	Relative P	Relative D	Relative S	Relative S (MacArthur, 1916)	Difference	Relative P (mean ±SE)	Relative D (mean ± SE)	Relative S (mean ± SE)
1/8M Sucrose	0.874	0.960	0.910		-0.024			
	0.901	0.980	0.919	0.934	-0.015	0.890± 0.7	0.959± 1.0	0.928± 1.2
	0.897	0.934	0.960		0.026			
	0.887	0.962	0.922		-0.012			
1/4M Sucrose	0.753	0.947	0.795		-0.039			
	0.794	0.908	0.874	0.834	0.040	0.775± 1.2	0.930± 1.3	0.833± 2.4
	0.765	0.954	0.802		-0.032			
	0.786	0.912	0.862		0.028			
1/2M Sucrose	0.579	0.730	0.793		0.033			
	0.600	0.809	0.742	0.760	-0.018	0.595± 1.4	0.776± 2.2	0.767± 1.9
	0.584	0.788	0.741		-0.019			
	0.615	0.777	0.792		0.032			
1M Sucrose	0.334	0.556	0.601		0.047			
	0.353	0.616	0.573	0.554	0.019	0.340± 2.3	0.584± 2.1	0.582± 2.0
	0.351	0.584	0.601		0.047			
	0.320	0.579	0.553		-0.001			
1/4M NaCl	0.911	0.931	0.979		0.024			
	0.962	0.977	0.985	0.955	0.030	0.929± 1.3	0.961± 1.2	0.966± 1.5
	0.934	0.954	0.979		0.024			
	0.908	0.983	0.924		-0.031			
1M NaCl	0.676	0.892	0.758		0.031			
	0.661	0.861	0.768	0.727	0.041	0.672± 1.6	0.858± 1.5	0.783± 2.5
	0.650	0.848	0.767		0.040			
	0.699	0.831	0.841		0.114			
2M NaCl	0.465	0.810	0.574		0.046			
	0.471	0.832	0.566	0.528	0.038	0.459± 1.2	0.841± 1.5	0.546± 2.5
	0.452	0.862	0.524		-0.004			
	0.448	0.861	0.520		-0.008			
3M NaCl	0.339	0.771	0.440		0.052			
	0.317	0.790	0.401	0.388	0.013	0.320± 2.5	0.772± 1.3	0.415± 3.3
	0.324	0.744	0.435		0.047			
	0.300	0.783	0.383		-0.005			
				Mean	0.018			
				SD	0.033			
				n	32			

Table 5.4   Oxygen permeability, diffusivity, and solubility data for the 'down-step' method for various standard solutions (four replicates for each standard). Experimental values of relative solubility are compared to those of MacArthur 1916 by calculating the difference (experimental value minus MacArthur value).

.

221

There may also be scope to investigate the incorporation of other boundary/initial conditions (e.g. 'Up-step') and investigation of whether this could further improve such a device.

5.8 Conclusions and recommendations

In this chapter a variety of methods were examined for determining the oxygen permeability, diffusivity and solubility of aqueous solutions. All methods involved coupling the steady-state and transient response of a Clark oxygen electrode whilst manipulating the boundary and initial conditions.

The 'steady-state sample addition' and 'down-step' methods were determined to be suitable for analysis of follicular fluid oxygen permeability, diffusivity and solubility. However, the 'down-step' method is more precise and experimentally reliable. Therefore only this method was used in the subsequent chapter to determine the variability of these parameters in follicular fluid.

The investigated methods could be improved through modification of diffusion cell design. Future work to investigate the incorporation of other boundary/initial conditions into the analysis is recommended, as this may further improve the accuracy and precision of measurements.

Chapter 6.   The physical and transport properties of human follicular fluid

The chemical composition of follicular fluid has been widely investigated. Physical and transport properties have received much less attention. The mathematical modelling work presented in this thesis suggests that these properties will play a role in the transport of substances through follicular fluid. In particular, variation in the permeability of oxygen through follicular fluid will impact on the amount of oxygen reaching the oocyte, and the rate at which this oxygen is transported. Furthermore, any great variation in the physical and transport properties of follicular fluid may make the comparison of dissolved oxygen in fluid from different follicles difficult.

The parameters investigated in this chapter are the density, osmolality, viscosity, oxygen permeability, oxygen diffusivity, and oxygen solubility of human follicular fluid. Values for these parameters are generally well documented in human plasma, where variability is minor (Trudnowski & Rico, 1974; Turitto & Slack 1998; Lowe & Barbenel 1988; Christoforides *et al.,* 1969; Lango *et al.,* 1996; Goldstick *et al.,* 1976). Follicular fluid is a derivative of plasma, and therefore these parameters might be expected to show small variability in follicular fluid also. If this is the case, the measurement of dissolved oxygen in follicular fluid will be simplified. On the other hand, if variability is large then it is possible that this variability may be related to the developmental capacity of the oocyte.

The aim of this chapter is to investigate how variable these physical and transport properties of follicular fluid are, and to compare them to those of human plasma. This information will be used to determine the impact this variability may have on the measurement of dissolved oxygen in follicular fluid.

6.1   Materials and methods

Follicular fluid samples were collected from patients undergoing IVF treatment at the ISIS clinic in Hamilton, New Zealand. Appropriate ethical approval and patient

consent were obtained prior to collecting samples. Samples were collected from 12 patients in standard IVF collection tubes (14 ml Falcon round bottom polystyrene tube, product no. 352057, Becton Dickinson Labware, NJ, USA). Due to the difficulty associated with consent and the extra burden of sample collection placed on the staff at the IVF clinic, sample sizes were constrained to a practical minimum.

Where possible, samples were collected from individual follicles, where this was not the case the number of follicles from which the total sample was composed was recorded. Samples which contained follicular flushing fluid were not considered. After retrieval, samples were transported on ice to the laboratory where all described analyses were performed as rapidly as possible.

Samples were qualitatively graded for blood contamination. Samples were given a score of 0 (no blood contamination), 1 (minimal blood contamination), 2 (moderate blood contamination), or 3 (heavy blood contamination), based on visual assessment of the sample.

Before analysis, all samples were centrifuged at 1500 g for 5 minutes according to the recommendations of Broviczeny *et al.,* (1984) for the measurement of plasma viscosity. This removes red blood cells and other cellular matter that may interfere with the analysis.

Density measurements were made using a high precision syringe (Bioanalytical Systems Inc., product no. MD-0100, Indiana, USA) fitted with a stainless steel guide. The syringe and steel guide were initially cleaned and dried before a tare weight was measured using a 4-place balance. The syringe and guide, as well as the follicular fluid sample of interest, were then placed in a water bath at 37 ± 0.5 °C and allowed at least 10 minutes to reach temperature. After this time a follicular fluid sample was drawn into the syringe and any air bubbles expelled. Excess fluid was then ejected by pushing the plunger against the steel guide. This ensured the same volume of fluid was sampled on each occasion. The resulting syringe, guide, and sample were then re-weighed. This process was repeated using a distilled water sample. After correction for tare weight, the relative density of the follicular fluid sample could be calculated

as the ratio of the follicular fluid sample weight to the water weight. Preliminary measurements conducted on water samples at 37 °C showed that the precision of this procedure was ± 2% (± CV, n=30).

Osmolality measurements were made using a vapour pressure osmometer (Wescor Inc., product no. M2448, Utah, USA). The device was calibrated according to the manufacturers instructions before each individual sample was analysed using calibration standards of 290 mOsmol.kg^{-1} and 1000 mOsmol.kg^{-1}. The manufacturer of this device reports its precision as approximately ± 2 mOsmol.kg^{-1}.

Viscosity measurements were made using a capillary viscometer (Cannon Instrument Co., product no. C403, Pennsylvania, USA) submerged in a water bath at 37 ± 0.5 °C. Before analysis, samples were submerged in the water bath and allowed at least 10 minutes to reach temperature. A 1 ml sample was then added to the viscometer and the time required for the sample to travel between the appropriate markings was recorded. After each sample was analysed the viscometer was rinsed several times with water, followed by several rinses with ethanol and acetone as required to clean the viscometer. The viscometer was then dried in an oven. Once dry, an equivalent water run was performed. Knowing the times for both follicular fluid (t_f) and water samples (t_w) to travel through the viscometer, the relative viscosity of the follicular fluid sample was calculated as,

$$\text{Relative Viscosity} = \frac{\rho_f t_f}{\rho_w t_w} \qquad (6.1)$$

where ρ_f / ρ_w is the relative density previously analysed for the same follicular fluid sample as described above. The precision of the viscometer used in this study was reported by the manufacturers as ± 0.16%.

The permeability, diffusivity, and solubility of follicular fluid samples was analysed according to the methodology described in Chapter 5. The key difference was that not enough follicular fluid was obtained to allow conditioning of the gas by passing it through a sub-sample of the fluid. Instead, gases were sparged through water. This

is seen to be a suitable measure since, given the low electrolyte content of follicular fluid, its vapour pressure is not likely to be significantly different from water to result in any evaporative or condensation problems. A sponge soaked with follicular fluid sample was placed over the top of the stainless steel cap of the diffusion cell.

6.2   Results and discussion

6.2.1 Density, osmolality, and viscosity

A total of 135 follicles were aspirated from 12 women. 88 fluid samples were collected in total, with 34 samples containing fluid from more than one follicle. Of the 88 fluid samples collected, 91% showed visual blood contamination. 54 fluid samples were aspirated as single follicles. Of these 54 samples, heavily blood contaminated samples were excluded from the analysis (score 3). The remaining 29 follicular fluid samples from single follicles were analysed for density, osmolality and viscosity.

Of the 29 samples tested only 6 were visually free of blood contamination (score 0), 10 had minimal blood contamination (score 1), and 12 had moderate blood contamination (score 2). For the parameters of density, osmolality, and viscosity the effect of blood contamination was investigated using a t-test for the difference between means. Testing the differences of the means of (0 score – 1 score), (0 score – 2 score), and (1 score – 2 score) revealed no significant differences for any of the parameters ($p > 0.05$ in all cases). This suggests that the minimal to moderate blood contamination of some samples has no detectable effect on the values of these parameters (density, osmolality, and viscosity). Hence, for each parameter the full sample size of 29 was included and taken to be representative of follicular fluid.

Table 6.1 presents a summary of the measurements of density, osmolality, and viscosity in human follicular fluid, including a comparison with human plasma. Figure 6.1 provides a visual comparison between human follicular fluid and human plasma for the same parameters.

	Follicular Fluid Mean ± SD (n=29)	Range	Human Plasma Range
Relative Density	1.022 ± 0.003	1.014 – 1.031	1.019 – 1.022 (Trudnowski & Rico, 1974)
Osmolality (mOsmol.kg^{-1})	281 ± 15	238 - 321	276 – 295 (Turitto & Slack 1998)
Relative Viscosity	1.707 ± 0.102	1.544 – 1.927	1.670 – 1.940 (Lowe & Barbenel 1988)

Table 6.1   Relative density, osmolality, and relative viscosity in human follicular fluid. Values for human plasma are included for comparison.

The relative density of human follicular fluid has not been reported before. Figure 6.1 suggests that the relative density of human follicular fluid is more variable than human plasma, though the human plasma range shows considerable overlap with the central part of the follicular fluid distribution. The two fluids appear to be very similar with respect to relative density.

This similarity is apparent for osmolality also, with the human plasma range once again showing overlap with the central part of the follicular fluid distribution. Again, follicular fluid appears to be more variable than plasma. This similarity suggests the lack of a concentration gradient between follicular fluid and plasma, although the plasma range is arguably slightly higher than the central follicular fluid distribution, which is possibly suggestive of a minor osmotic gradient. The lack of osmotic gradient between human follicular fluid and plasma has been noted before, and is suggested to be due to electrolyte contribution from granulosa cells, or an active mechanism of ion transport (Fisch *et al.* 1990). The mean osmolality reported here of 281 mOsmol.kg^{-1} is very similar to the value reported by Edwards (1974) of 280 mOsmol.kg^{-1} for human follicular fluid.

For relative viscosity, human follicular fluid and human plasma are also similar, with considerable overlap between the plasma range and the central part of the follicular fluid distribution. However, plasma shows wider variability relative to follicular fluid, compared to the measurements of density and osmolality. The alignment of the follicular fluid distribution suggests that follicular fluid may be generally slightly less viscous than human plasma. This may be due to its lower protein content (McNatty, 1978). The mean value of relative viscosity reported here of 1.707 is consistent with the value reported by Luck *et al.* (2000) of 1.830 for human follicular fluid.

The viscosity of a fluid can be used to predict the diffusivity of a solute through the fluid. A variety of empirical correlations have been derived to achieve this. The starting point for many of these correlations is the Stokes-Einstein equation (Akgerman & Gainer, 1972). Expressing this equation in units consistent with this work, the diffusion coefficient of oxygen through follicular fluid may be expressed as,

228
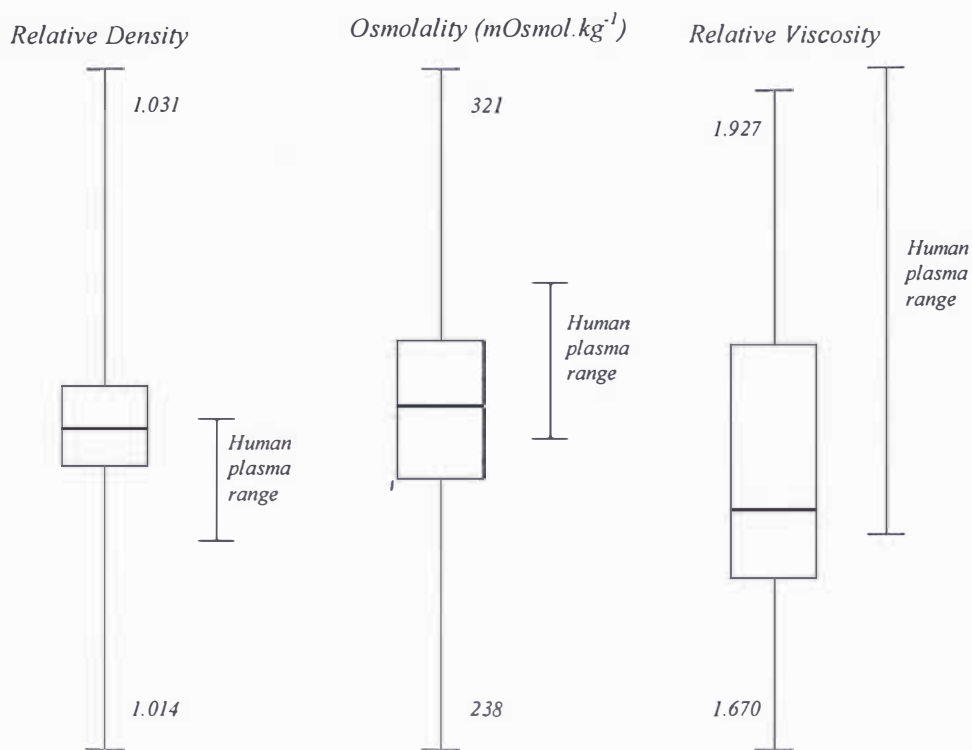
Figure 6.1   Boxplots of the density, osmolality, and viscosity of human follicular fluid samples. Whiskers represent the range (and define scale), while the box represents the upper quartile, median, and lower quartile. Ranges for human plasma obtained from the literature are included for comparison.

$$D_a = \frac{kT}{6\pi\mu_a r_{O_2}}$$
(6.2)

where k is the Boltzman constant, r_{O2} is the radius of an oxygen molecule and μ represents the kinematic viscosity. (D_a as defined in nomenclature). Note that the kinematic viscosity is given by viscosity multiplied by density.

The problem with the Stokes-Einstein equation is that it is not very accurate. Empirical variations of this equation have been developed to improve accuracy, including those of Wilke & Chang (1955), and Tyn & Calus (1975). These correlations introduce additional solvent and solute specific parameters to achieve improved accuracy as demonstrated through comparison with experimental values. However accuracy is typically limited to ±10 to 20%, and is often much worse. Unfortunately, other than viscosity, the specific solute parameters for follicular fluid or even human plasma are not available. However, the aqueous nature of these fluids dictates that these parameters can be assumed to be essentially the same as those of water. If this is the case, the relative diffusivity of oxygen in follicular fluid and plasma can then be calculated (relative to water). Because the viscosity of the solvent of interest appears in the denominator of Stokes-Einstein based correlations, the equation for relative diffusivity reduces to the same form for all these correlations (including the Stokes-Einstein equation itself), and is given by equation 6.3.

$$\frac{D_a}{D_w} = \frac{\mu_w}{\mu_a} \approx 1/(\text{Relative viscosity})$$
(6.3)

The right hand approximation can be made for dilute aqueous solutions whose density is essentially the same as that of water, as is the case for follicular fluid. In other words, equation 6.3 shows that the relative diffusivity of oxygen in follicular fluid and plasma can be approximated by the inverse of the relative viscosity. Using equation 6.3 and the relative viscosity range presented in table 6.1 gives a relative diffusivity range of 0.52 to 0.65. Although the absolute values of this range may be questionable due to the inaccuracy of the correlations, the width of the range may be a fair indication of the expected variability in the relative diffusivity of oxygen in

230

follicular fluid. The range spans 13% which suggests that diffusivity in human follicular fluid may not be highly variable. For human plasma the calculated range of relative diffusivity is 0.52 to 0.60. The reduced width of this range (8%) reflects the lower variability of human plasma viscosity compared with follicular fluid (which may be due to the much larger sample sizes upon which plasma estimates are based). Once again the absolute values may not be accurate, but a relative comparison suggests that oxygen diffusivity in plasma and follicular fluid should be similar, with diffusion through follicular fluid possibly slightly more rapid. The next section describes the actual experimental determination of relative diffusivity of oxygen in human follicular fluid, along with relative solubility and relative permeability.

6.2.2 Oxygen permeability, diffusivity, and solubility

The 29 single follicle samples included in the density, osmolality, and viscosity analysis were subjected to the diffusivity, solubility, and permeability analysis described in the previous chapter. Of these, 11 samples produced experimental data traces (plots of current vs. time) that were of an acceptable quality (see 5.7 for inclusion criteria).

Table 6.2 presents a summary of the measurements of diffusivity, solubility, and permeability in human follicular fluid, including a comparison with human plasma. Figure 6.2 provides a visual comparison between human follicular fluid and human plasma for the same parameters.

Values for the oxygen diffusivity, solubility, and permeability of human follicular fluid are reported for the first time here. Figure 6.2 shows that the ranges of diffusivity for human follicular fluid and human plasma show some overlap, although this overlap does not include the central part of the follicular fluid distribution. Although the oxygen diffusivity in both fluids is similar, this suggests that oxygen may diffuse more readily through human follicular fluid. This is consistent with the observations made via the prediction of relative diffusivity for follicular fluid and plasma in the previous section.

231

The magnitude of the experimental ranges of relative diffusivity are similar for follicular fluid and plasma, at 16%, and 15% respectively. These experimental ranges are larger than, but not dissimilar to, those predicted in the previous section of 13% and 8% for follicular fluid and plasma respectively. Also, as suggested, the absolute values of the predicted relative diffusivities and the experimental relative diffusivities are different, due most likely to the known inaccuracies of the predictive equations. For follicular fluid the experimental range is 0.78-0.94 compared with the predicted range of 0.52 to 0.65. For plasma the experimental range is 0.67-0.82 compared with the predicted range of 0.52 to 0.60. In both cases the predicted range is lower than the experimental range and shows no area of overlap.

For relative solubility, Figure 6.2 shows human follicular fluid to be similar to human plasma, with the ranges showing considerable overlap in the central region of the follicular fluid distribution. Oxygen solubility in human follicular fluid may be slightly more variable than that in plasma. Oxygen solubility in human follicular fluid may also be generally slightly higher than in plasma. This may once again be due to the lower protein content of follicular fluid. Protein displaces water which is the fraction of the fluid containing dissolved oxygen. Therefore, less protein will result in greater oxygen solubility. In any case, differences are very small.

The distribution of relative permeability does not provide much additional information as this parameter is simply the product of diffusivity and solubility ($P=DS$). Because the variability in relative diffusivity (SD = 5%) is greater than relative solubility (SD=2%), relative diffusivity has a greater impact on the distribution of relative permeability. This can be seen in Figure 6.2 with the box plots for diffusivity and permeability being very similar. As with diffusivity, there is common overlap between plasma and follicular fluid permeabilities, which does not include the central part of the follicular fluid distribution. Again this suggests that follicular fluid may be slightly more permeable to oxygen compared with plasma.

In any case, the absolute values of oxygen diffusivity, solubility, and permeability are not of key importance. What is important is how the variability of these parameters affects oxygen transport in the follicle, and the implications this variability has on the

232

measurement of dissolved oxygen in follicular fluid. Now that some quantitative information is available on the variability of these parameters, these issues are addressed in the following sections using the model developed in Chapter 4.

Although the variability is of primary importance to this work the accuracy of the values presented in this chapter should ideally be confirmed using a larger sample size and compared against human plasma values measured using the same methodology. Due to the added difficulty associated with obtaining human plasma and the fact that this work is interested mainly in the variability of these parameters, this was not considered any further here.

6.2.2.1 The effect of variability in follicular fluid oxygen diffusivity and solubility on the measurement of follicular fluid dissolved oxygen

It has been previously demonstrated in this work that the width of the 'zone of uncertainty' will be affected by the position of the oocyte or cumulus oocyte complex, C_{crit}, R_o, r_o, D_a, and S_a.

No specific data is available on the variability of C_{crit} and R_o, and as a result studies quantifying this are recommended. Variability in oocyte or cumulus-oocyte complex position has been simulated in this work through the antral, pre-ovulatory with no cumulus, and pre-ovulatory with cumulus models of oxygen transport in the follicle. Data on the variability of r_o is available and has been previously described. The variability in D_a, and S_a has been examined for the first time in this chapter. Combining this knowledge, Figure 6.3 represents the best estimate of the lower and upper limits of the zone of uncertainty. The lower limit has been calculated using an antral follicle with high antral fluid oxygen solubility. The upper limit was calculated using a pre-ovulatory follicle with cumulus, high oocyte diameter, low antral fluid oxygen diffusivity, and low antral oxygen solubility. The high oocyte diameter was described in Figure 4.18. Because of the small sample size, for the oxygen diffusivity and solubility measurements, the range of each parameter given in Table 6.2 is used as a conservative estimate of low and high values.

	Follicular Fluid Mean ± SD (n=11)	Range	Human Plasma Range
Relative Diffusivity	0.86 ± 0.05	0.78 – 0.94	0.67 – 0.82 (Lango *et al.*, 1996, Goldstick *et al.*, 1976)
Relative Solubility	0.91 ± 0.02	0.86 – 0.94	0.87 – 0.92 (Christoforides *et al.*, 1969)
Relative Permeability	0.79 ± 0.05	0.69 – 0.86	0.60 – 0.73 (Christoforides *et al.*, 1969, Lango *et al.*, 1996, Goldstick *et al.*, 1976)

Table 6.2   Relative diffusivity, relative solubility, and relative permeability of oxygen in human follicular fluid. Values for human plasma are included for comparison.
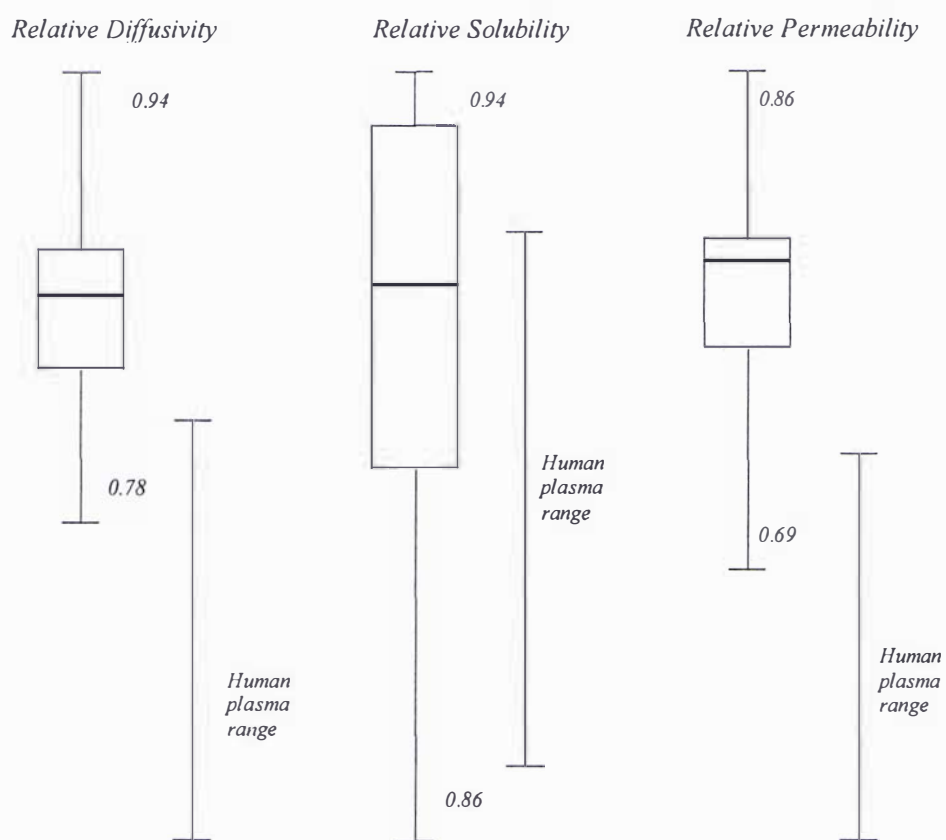
Figure 6.2   Box plots of the oxygen diffusivity, solubility, and permeability in human follicular fluid samples. Whiskers represent the range (and define scale), while the box represents the upper quartile, median, and lower quartile. Ranges for human plasma obtained from the literature are included for comparison.

Figure 6.3 shows the width of the zone of uncertainty to be from 5.6 to 7.3 vol%. This represents the best conservative estimate which takes into account variation in the cumulus-oocyte complex, oocyte size, follicular fluid diffusivity, and solubility. Any follicular fluid below 5.6 vol% oxygen will represent an oocyte not capable of maximum respiration. The oxygen status of the follicle will be uncertain between 5.6 and 7.3 vol%. Above 7.3 vol% the oocyte will be capable of maximal respiration.

If positional variation is removed by assuming that the oocyte is located eccentrically and essentially in the granulosa layer, the width of the zone of uncertainty reduces to 5.6 to 5.8 vol% (not shown on figure). Therefore, variability due to follicular fluid diffusivity and solubility is negligible. Different follicular fluid samples can be assumed to be the same in terms of these properties, and the measurement of concentration instead of partial pressure is not necessary.

Because knowledge of the location of the cumulus-oocyte complex may reduce the effect of positional variation, quantitative information on cumulus-oocyte position in human follicles would be helpful (as positional variation largely determines the width of the zone of uncertainty).

This work shows that the concept of measuring dissolved oxygen in follicular fluid as an indicator of oocyte potential is a valid one. The concept of a cut-off oxygen level and a zone of uncertainty has been demonstrated here through mathematical modelling. Perhaps the best way forward from here is to actually measure dissolved oxygen in follicular fluid and relate this to developmental competence. This may determine a value for any cut-off level, and the width of the zone of uncertainty, experimentally. A similar approach has already been used with success by Van Blerkom *et al.* (1997). The establishment of standard dissolved oxygen ranges for use by IVF clinics would be ideal. To achieve this will first require reliable and convenient means to analyse follicular fluid dissolved oxygen. Therefore, issues concerning the actual measurement of dissolved oxygen are the subject of Chapters 7 and 8.
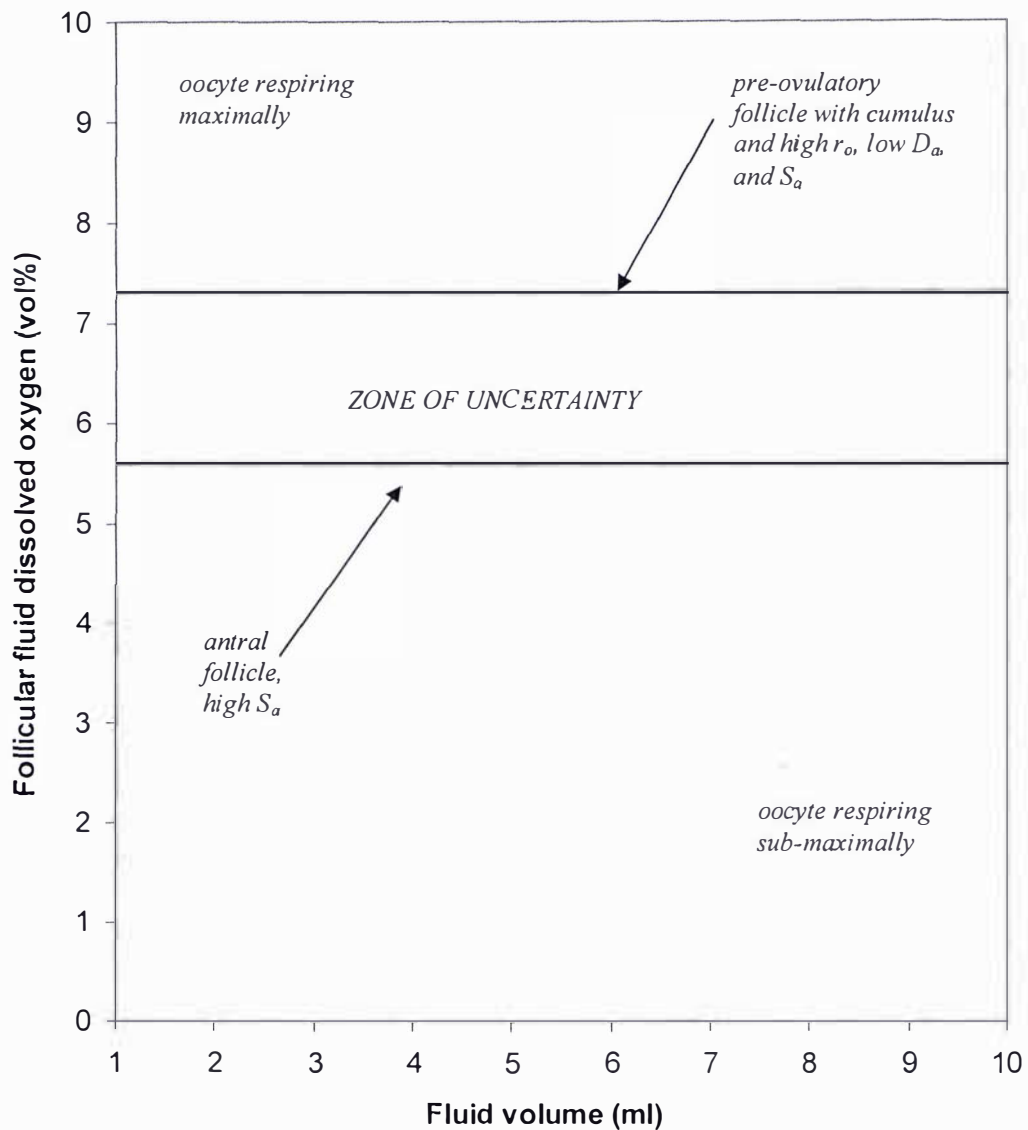
Figure 6.3   Minimum follicular fluid dissolved oxygen required to sustain the oocyte at 99% maximal respiration (IVF sized follicle range). The antral and pre-ovulatory with cumulus models can be used to set the lower and upper bounds of the zone of uncertainty respectively, and reflect the positional uncertainty of the cumulus-oocyte complex. The parameters of oocyte size, follicular fluid diffusivity, and solubility are used in combination to obtain the maximal width of the zone of uncertainty based on knowledge of variability in these parameters (including the measurements of D_a and S_a reported here).

6.3 Conclusions and recommendations

The physical and transport properties of follicular fluid are not highly variable. These parameters are very similar to their values in plasma, of which follicular fluid is a derivative. Of these parameters, follicular fluid density, oxygen permeability, diffusivity, and solubility were reported for the first time.

The lack of variability in the oxygen diffusivity and solubility of follicular fluid means that these parameters have very little impact on the analysis of follicular fluid dissolved oxygen. The effect of positional variation of the cumulus-oocyte complex seems to be more important. Therefore it is recommended that this be quantified, along with the variability in the oxygen consumption kinetics of human oocytes.

The work presented to this point appears to justify the pursuit of the measurement of follicular fluid dissolved oxygen as an indicator of oocyte potential. It is suggested that a cut-off level and associated zone of uncertainty exist which can be used to classify the oxygen status of the follicle/oocyte. Further measurement may confirm the existence of these concepts and allow them to quantified in some form as standardised guidelines. Before this can be achieved a reliable and convenient method for the analysis of follicular fluid dissolved oxygen levels needs to be established. Variability in reported follicular fluid dissolved oxygen suggests that this has not yet been achieved, and is therefore the subject of the following two chapters.

Chapter 7.   Follicular fluid changes during IVF aspiration

The work of the previous chapters has shown that the measurement of dissolved oxygen levels in follicular fluid can, in theory, provide an indicator of the respiratory status of the oocyte. As a result, the focus of this work now shifts toward practical issues associated with the measurement of dissolved oxygen in human follicular fluid.

It might be thought that the analysis of dissolved oxygen in follicular fluid could most simply be achieved by collecting the fluid after IVF aspiration and subjecting it to a standard method of oxygen analysis (e.g. using a Clark electrode). However, such an approach assumes that the gaseous composition of the fluid is unchanged by the aspiration process. To this end changes in pH are also of interest, as these will be related to the carbonate/bicarbonate equilibrium and may result from changes in the dissolved carbon dioxide content of follicular fluid.

Dissolved oxygen analysis may be further complicated by the presence of blood in follicular fluid. Due to its haemoglobin content, blood can act as a massive oxygen source and sink. As blood contamination is common in IVF aspiration it is important to understand the implications of this on the analysis of dissolved oxygen in follicular fluid.

IVF aspiration may also affect the temperature of follicular fluid. Temperature will affect the solubility of oxygen in the fluid and also the response of oxygen sensing devices such as the Clark electrode. Therefore, any temperature changes caused by aspiration need to be understood so that measurement and data analysis can be performed reliably.

Finally, any device that is ultimately incorporated into the IVF aspiration kit for the purposes of fluid sampling and/or analysis must not represent any increased risk of shear damage to the oocyte. Exactly what represents an increased risk is not clear. Therefore a baseline needs to be established by determining what effect current IVF

aspiration has on the oocyte.

This chapter investigated changes in follicular fluid during IVF aspiration; specifically changes in dissolved oxygen levels, pH, blood contamination, and temperature. The physical effects of aspiration on the cumulus-oocyte complex were also investigated. The results are discussed in relation to their practical implications on the analysis of dissolved oxygen in follicular fluid in the IVF clinic.

7.1 Materials and methods

7.1.1 Aspiration system

The aspiration set-up and measurement sites are shown in Figure 7.1. The aspiration kits used were Follicle Aspiration Sets (Swedmed Lab International AB, Billdal, Sweden, article no. A-161025s-1). These aspiration sets have a needle length of 30 cm (OD 1.6 mm, ID 1.1 mm), and a functional tubing length of 58.5 cm from needle to collection vial. Samples were collected in Sealable Sampling Tubes (Swedmed Lab International AB, article no. D-7030). Aspiration was performed using a vacuum pump operated at flow rates between 8 and 22 ml/min.

7.1.2 Follicular fluid

Follicular fluid was collected from the ovaries of cows killed at a local abattoir, and served as a model system. Ovaries were collected after slaughter and placed in warm saline. Upon collection ovaries were transported to the laboratory as rapidly as possible and fluid was extracted (typically within an hour of collection) . Fluid was either used immediately or stored on ice for use the following day, after which it was discarded.
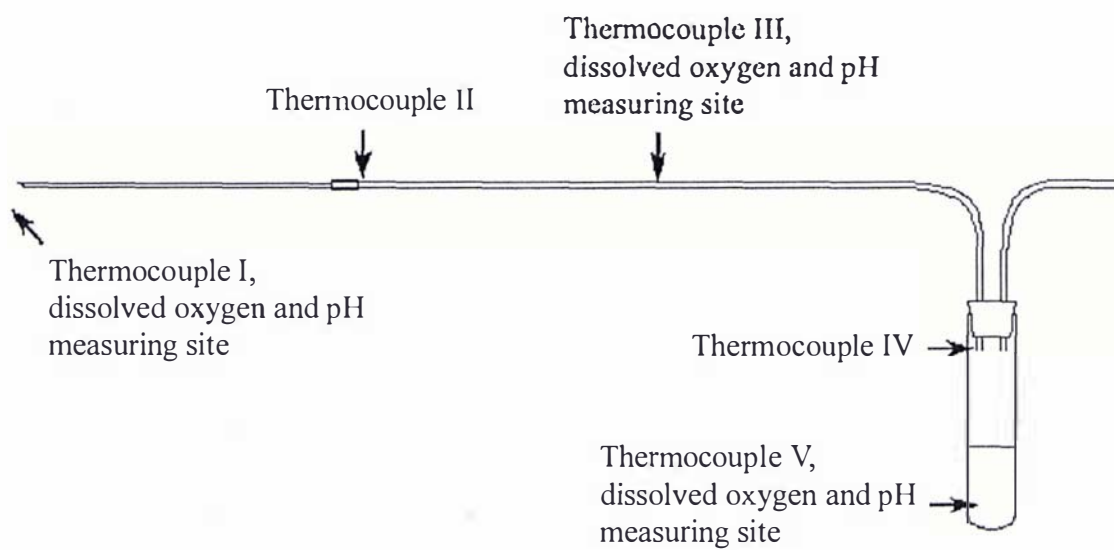
Figure 7.1   Aspiration set-up and measurement sites.

7.1.3 Oxygen measurements

Dissolved oxygen was analysed using a Clark-style oxygen electrode (Diamond General Corp., Ann Arbor, USA, product no. 733). The probe was calibrated by equilibrating bovine follicular fluid with instrument grade standard gas mixtures containing 0, 5, and 21 vol% oxygen. Samples of 2.5 ml of follicular fluid were prepared by sparging with both nitrogen and 21 vol% oxygen so that a spectrum of dissolved oxygen levels in the fluid was created. The response of the probe in the fluid was recorded before aspiration, and immediately after, by placing the probe in the bulk collection vial. Fluid flow rate was controlled between 18 - 20 ml/min. Measurements were made at 25 ± 0.5 °C as the probe precision was greater at this temperature than at 37 °C. Note that oxygen measurements and the pH and temperature measurements detailed in the following sections were measured independently of one another during separate sets of aspirations under the conditions described in this and the following sections for that particular measurement.

Additional runs were carried out where a 1ml fluid sample was withdrawn from the midpoint of the tubing line using a gas tight syringe. The dissolved oxygen of the sample was then immediately measured. This was done so that the cause of any changes in dissolved oxygen could be identified. The standard aspiration kit was modified to include a 3 cm length of silicon tubing at the midpoint of the tubing line. This allowed the tubing line to be punctured with a needle, and a sample withdrawn as aspiration proceeded.

7.1.4 pH measurements

The pH was measured using a standard pH electrode which was calibrated according to the manufacturer's instructions (Metrohm Ltd., Herisau Switzerland, product no. 6.0234.100). The procedure was identical to that employed for dissolved oxygen analysis, except that samples were equilibrated with 5 vol% carbon dioxide before aspiration. Follicular fluid was also equilibrated with 3 vol% carbon dioxide so that a standard curve for pH change as a function of dissolved carbon dioxide could be generated. All measurements were made at 37 ± 0.5 °C.

7.1.5 Temperature measurements

27-gauge thermocouples of type T and K were placed at various positions in the aspiration device (Figure 7.1). They were connected to a TC-08, 8 Channel Thermocouple Data Logger (Pico Technology Ltd., Cambridgeshire, United Kingdom), and a laptop computer equipped with the software PicoLog for Windows (Pico Technology Ltd.). Thermocouples were calibrated by testing in a ice/water slurry, and boiling water. Offsets among thermocouples were also determined at 37 °C, by placing thermocouples in a common fluid at this temperature.

The follicular fluid to be aspirated was placed in a water bath (Contherm Scientific Company, Lower Hutt, New Zealand, product no. 370) and controlled at 37 ± 0.5 °C. The tip of the needle was placed in the fluid, with the remaining functional length immersed in the water bath and insulated with polystyrene to prevent heat losses. This was done so that the clinical situation (in which the functional length of the needle is inside the body) could be simulated. The remainder of the collection device was at ambient conditions of 21 ± 0.5 °C. Fluid flow rate was altered between 8 and 22 ml/min so that its effect on heat losses could be determined. Fluid was aspirated until steady state temperatures were observed.

Additional aspirations were carried out with the collection vial insulated so that the magnitude of convective heat losses to the ambient environment could be determined. Aspirations were also carried out after the collection tube had first been heated to 37 °C and insulated, so that the amount of heat lost to heating the collection tube material could be determined through comparison with previous trials.

7.1.6 Cell shear measurements

In this work changes in the morphological appearance of the cumulus-oocyte complex were used as a measure of the shear which it was exposed to during aspiration.

The IVF aspiration kits used were the same as those described above except that one of three sampling devices was placed in the middle of the tubing line. The development of these devices and their effects on the cumulus-oocyte complex and dissolved oxygen levels in follicular fluid are described in the next chapter. The data, reported in this chapter, on cell shear was collected with device A in place (see Figure 8.2). The cell shear data reported here refers to those complexes passing through the aspiration kit without being trapped/sampled by device A. Such complexes are assumed to have undergone normal IVF aspiration. Any complexes passing into device A (sampled) are reported on in the next chapter.

Ovaries were collected in the same way described in section 7.1.2. Individual follicles were then aspirated using a needle, test tube, and vacuum pump. The mixture of follicular fluid, oocytes, and other cellular material resulting from aspiration of the ovaries was placed in a water bath at 39 °C where the cellular matter was allowed to settle to the bottom of the tube. The cellular sediment was then removed and placed in a Petri dish on a heated stage at 39 °C. Oocytes were then located using low power light microscopy, and removed using a Pasteur pipette.

Upon removal oocytes were matured according to the guidelines developed by the Reproductive Technology group, AgResearch Ltd., New Zealand (see appendix A for detailed guidelines). Maturation was performed to allow the appearance of the oocyte and surrounding cumulus cell mass to more closely resemble human cumulus-oocyte complexes which are generally already mature when aspirated.

After maturation, a single cumulus-oocyte complex was placed in a Petri dish together with a 5 ml sample of follicular fluid. The cumulus oocyte complex was then digitally photographed under low power light microscopy. On the heated stage the cumulus-oocyte complex was then aspirated along with the follicular fluid. Aspiration of the cumulus-oocyte complex was viewed under light microscopy to ensure that it had entered the aspiration kit. The bulk of the fluid was allowed to travel through to the main collection tube, with a 1 ml sample being extracted from the middle of the tubing line using one of three sampling devices (effects of sampling on the cumulus-oocyte complex reported in the following chapter).
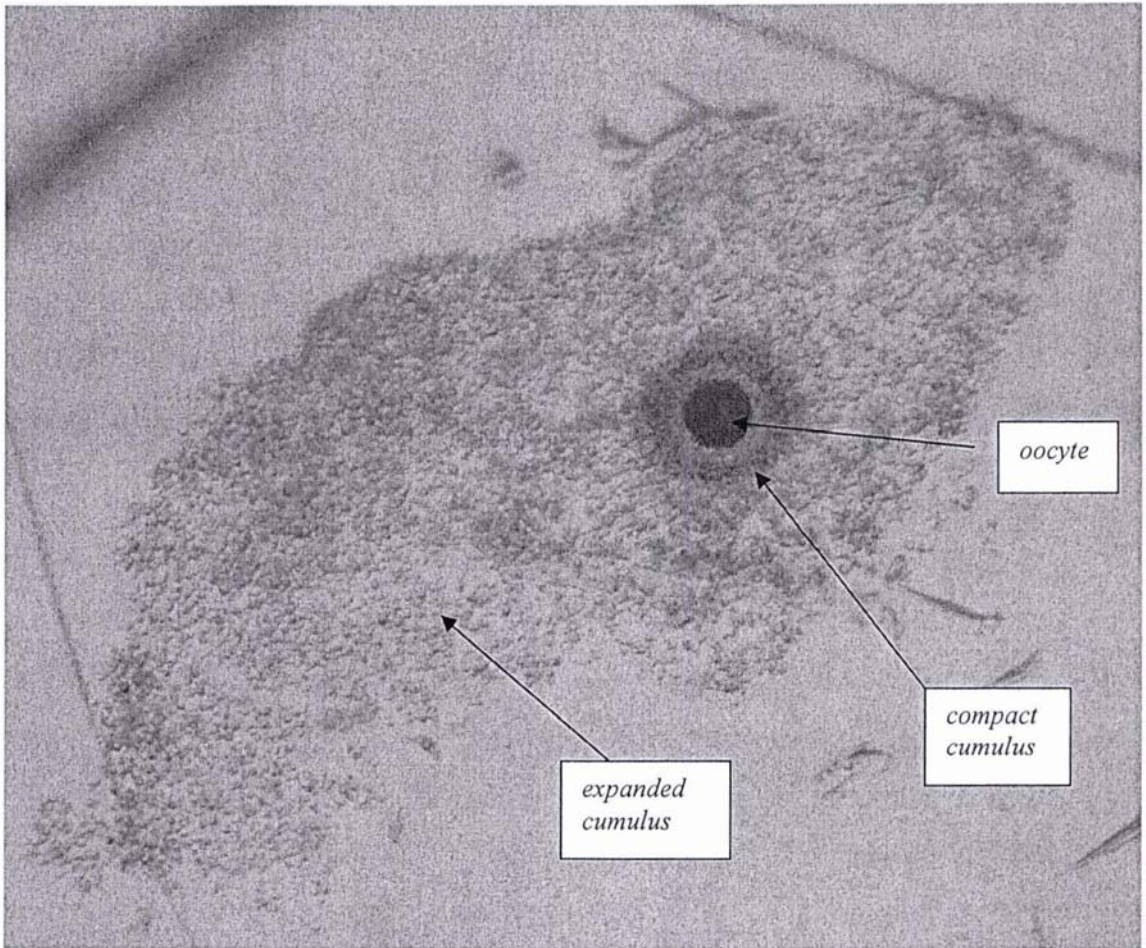
Figure 7.2   A typical bovine cumulus-oocyte complex after maturation in synthetic media.

After aspiration, the cumulus-oocyte complex was searched for in both the 1 ml sample, and the bulk collection vial. Whether or not the cumulus-oocyte complex was found was recorded. The oocyte was visually examined for any signs of a damaged *zona pellucida* (membrane enclosing oocyte) with the result being recorded. The cumulus-oocyte complex was then once again photographed under light microscopy. A typical image of a cumulus-complex is shown in Figure 7.2.

The before and after aspiration digital images of the cumulus-oocyte complexes were subsequently subjected to a semi-quantitative analysis to determine the effects of aspiration and sampling on the cumulus-oocyte complex. The measured parameters included Total cumulus area, Compact cumulus area, Expanded cumulus area, Compact cumulus coverage, Expanded cumulus coverage, Voidage, Compact cumulus sphericity, and Expanded cumulus sphericity. Each of these parameters is detailed below.

Figure 7.3 provides a visual description of some of the parameters discussed below. The area of the oocyte was calculated first. Using Adobe Photoshop 7.0 (Adobe Systems Inc., California, USA) the area of the oocyte can be selected using the lasso tool. Using the histogram function, the number of pixels occupied by the oocyte was calculated (P_1). In the same way the total number of pixels occupied by the oocyte and the compact cumulus (P_2) cells was calculated (note that the compact cumulus is most likely representative of the *corona radiata*, and the expanded cumulus of the *cumulus oophorus*. However, because these cells are grouped here according to a qualitative visual assessment of the cells and not a detailed assessment of the nature of the cells, these terms have been avoided). Thus, the Compact cumulus area expressed as a ratio relative to the oocyte area was calculated as,

$$\text{Compact cumulus} = \frac{P_2 - P_1}{P_1} \tag{7.1}$$

In the same way the total pixels occupied by the entire cumulus-oocyte complex (P_3) can be used to calculate the area occupied by the expanded cumulus, expressed relative to the oocyte's area. Unlike the compact cumulus area, the expanded cumulus

246

area consists of large fluid voids as well as cellular matter, and is given by,

$$\text{Expanded cumulus (cells and fluid)} = \frac{P_3 - P_2}{P_1} \tag{7.2}$$

Adobe Photoshop's threshold tool can also be used to select just the pixels occupied by the darker cellular matter of the expanded cumulus cell region (P_4). The fluid voidage of the expanded cumulus cells is then given by,

$$\text{Voidage} = \frac{P_3 - P_2 - P_4}{P_3 - P_2} \tag{7.3}$$

Compact cumulus coverage was manually assessed using a protractor to estimate the amount of the oocyte circumference which is surrounded by compact cumulus cells (0 to 360°), with the result expressed as a fraction of 360°. Expanded cumulus coverage was expressed in the same way and represents the proportion of the oocyte that is surrounded by the expanded cumulus mass. Most often this proportion was simply one. For example the cumulus-oocyte complex of Figure 7.3 would have both compact and expanded cumulus coverage proportions equal to one.

The compact cumulus sphericity was estimated to provide some indication as to how close the compact cumulus mass is to being circular in shape. The minimum distance (d_{min}) from the centre of the oocyte to the outer edge of the compact cumulus mass was manually measured using a ruler to the nearest mm of a printed image. In the same way the maximum distance (d_{max}) was measured. If the radius of the oocyte was also measured (r_o), the compact cumulus sphericity expressed as a ratio between 0 and 1 (one being circular) is defined as,

$$\text{Compact cumulus sphericity} = \frac{1 + d_{min}/r_o}{1 + d_{max}/r_o} \tag{7.4}$$
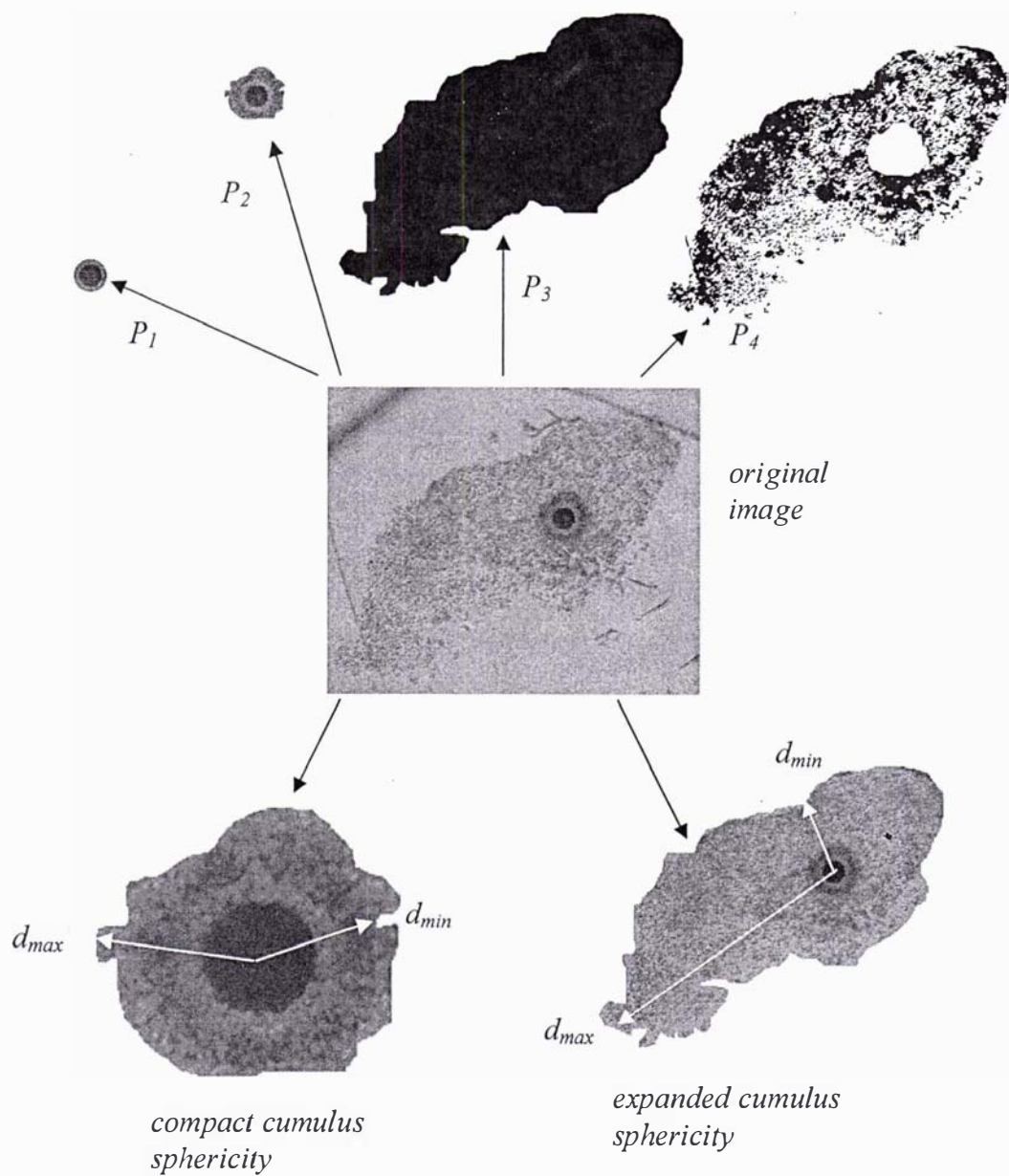
Figure 7.3   Visual description of various measured parameters used to provide a
semi-quantitative description of the cumulus-oocyte complex. Refer to text or
nomenclature section for description of symbols.

248

The Expanded cumulus sphericity was calculated in the same way except that d_{min} is now the minimum distance from the oocyte centre to the outer edge of the expanded cumulus mass and d_{max} is the maximum distance.

The parameters described above were measured before and after aspiration with the results being used to determine the impact of aspiration on the cumulus-oocyte complex. The procedure described is semi-quantitative, as it requires some judgement on the part of the investigator. However it represents a significant improvement over purely qualitative assessments.

7.2   Results and discussion

7.2.1 Dissolved oxygen changes during aspiration

The effect of IVF aspiration on dissolved oxygen levels in follicular fluid is presented in Figure 7.4. The solid line shown in Figure 7.4 is the $y=x$ line which represents where data would fall if no changes in dissolved oxygen levels were observed. All reported dissolved gas levels have been corrected for water vapour pressure.

The deviation of data from the $y=x$ line indicates that aspiration causes significant rises in the dissolved oxygen content of follicular fluid particularly at lower initial levels ($p<0.01$). The mean increase in dissolved oxygen in follicular fluid throughout the range is 5 ± 2 vol% ($\pm$SD, n=15). Also included in Figure 7.4 is data showing the effect of sampling fluid from the middle of the tubing line using a syringe.

When fluid is sampled from the tubing line there is no significant change in fluid dissolved oxygen levels ($p=0.307$). This indicates that the cause of change in dissolved oxygen levels is due to mixing with air in the collection tube.

Aspiration of follicular fluid raises the dissolved oxygen levels of the fluid. This is caused by air/fluid contact in the collection tube, and as a result the dissolved oxygen levels of the fluid tend towards 21 vol% (the concentration in ambient air). Such a rise

in dissolved oxygen is unlikely to have a negative affect on oocyte viability, particularly if the follicle was in a hypoxic state prior to aspiration. However, it is possible that elevated oxygen levels may negatively affect the oocyte by causing an elevation in the level of reactive oxygen species (ROS).

This result highlights the need for sampling precautions when analyzing oxygen levels in follicular fluid. The magnitude of the changes in dissolved oxygen will vary from system to system, but will be present if aspiration includes significant gas-liquid contact. Fluid cannot simply be aspirated into the bulk collection tube and analyzed for oxygen. To avoid changes in dissolved oxygen, fluid sampling and/or measurement needs to take place before the collection vial is reached (alternatively the aspiration kit could be redesigned to eliminate gas/liquid contact). This may be one of the reasons for the large variation in reported literature values of dissolved oxygen in follicular fluid (Table 7.1).

The variability observed in Table 7.1 may suggest that the analytical measures used to prevent changes in follicular fluid oxygen levels are also highly variable. Most of the reported mean values of dissolved oxygen are statistically significantly different from one another. The large variation (7 to 17 vol%) in reported values of dissolved oxygen in follicular fluid suggests that either the populations are different, or that analytical errors are present. Inadequate attention to avoidance of oxygen level changes during fluid sampling may explain the variation observed in these reports.
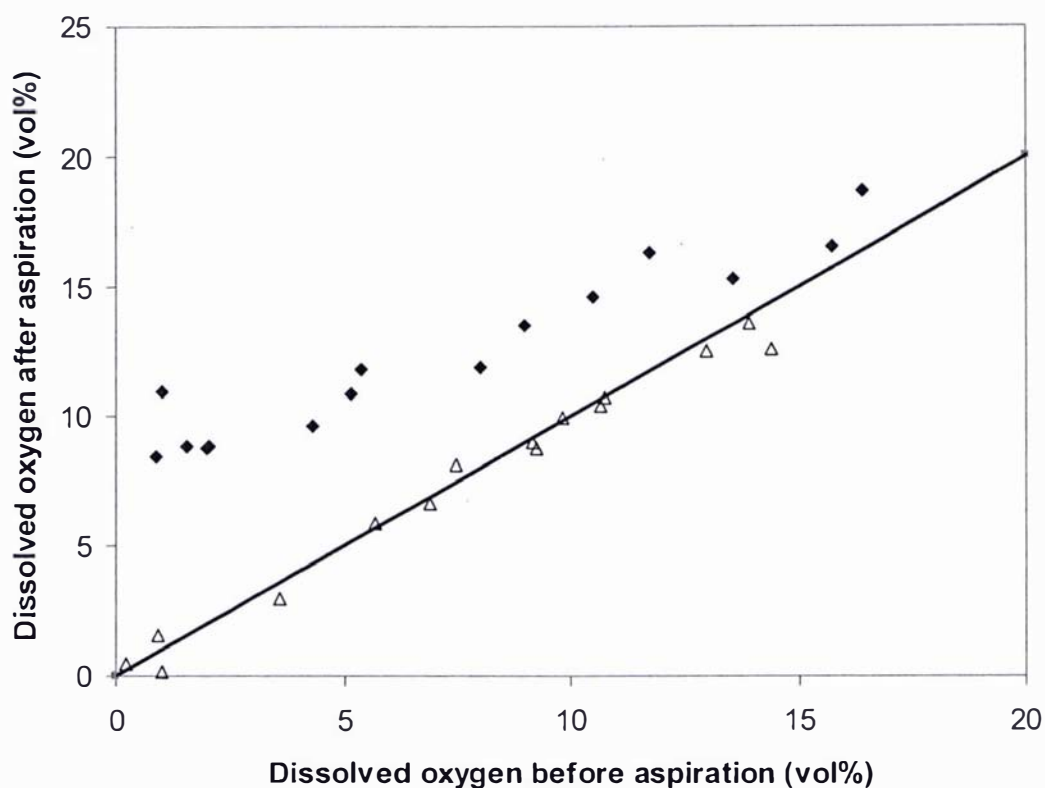
Figure 7.4. Comparison of the dissolved oxygen in follicular fluid before aspiration with that in the collection vial, or when sampled from tubing line before the collection vial (see position III, Figure 7.1). Symbols: ♦ - fluid in collection tube; Δ - fluid from position III. Straight line is $y=x$.

Reference	Mean reported follicular fluid dissolved oxygen (vol%±SD)	Follicular fluid source	Air contamination control	Blood contamination control
Shalgi et al., 1972	7.1 ± 2.8 (n=36)	Hysterectomy	Yes (capillary sample)	Yes
Fraser et al., 1973	9.9 ± 3.6 (n=12)	Hysterectomy	Yes (samples with air bubbles rejected)	Yes
Fischer et al., 1992	7.9 ± 1.3 (n=20)	IVF	Yes (capillary sample)	Not stated
Imoedemhe et al., 1993	16.6±2.6 (n=107)	IVF	Yes (paraffin oil)	Not stated
Van Blerkom et al., 1997	Not Stated (n=1079)	IVF	Not stated	Slightly amber accepted
Huey et al., 1999	13.2±3.2 (n=80)	IVF	Not stated	Slightly amber accepted

Table 7.1   Variation in reported values of follicular fluid oxygen levels.

7.2.2 pH changes during aspiration

The results of the investigation of the effects of IVF aspiration on the pH of follicular fluid are presented in Figure 7.5.

Aspiration results in a statistically significant change in fluid pH ($p<0.01$). The pH rises an average of 0.04 ± 0.01 pH units ($\pm SD$, n=15). When fluid is sampled directly from the tubing line no significant change in fluid pH is observed ($p=0.15$), with a mean change of 0.00 ± 0.01 pH units ($\pm SD$, n=15).

The change in pH is most likely caused by a reduction in the CO_2 levels in the fluid. The pH of follicular fluid is a function of CO_2 levels in the fluid. This relationship was observed with the fluid used in this study by equilibrating it with gas containing varying levels of CO_2. When follicular fluid is contacted with air in the collection tube (which has low CO_2 levels) the CO_2 levels in the fluid decrease. Based on this relationship, the pH rise observed in this study is likely to be caused by a drop in CO_2 of approximately 0.5 vol%. This small rise in pH and drop in dissolved CO_2 is unlikely to have major physiological significance. However, it does further demonstrate that gas compositional changes occur during IVF aspiration. Once again, this can be avoided if fluid sampling and/or measurement occurs before the collection vial.

7.2.3 IVF aspiration and blood contamination

Previous data gathered as part of this work showed that 91% of follicular fluid samples are visibly contaminated with blood (see section 6.2.1). It is therefore very important to understand how this blood contamination affects any potential follicular fluid analysis, both in terms of its dissolved oxygen levels but also with respect to other potential analytes.
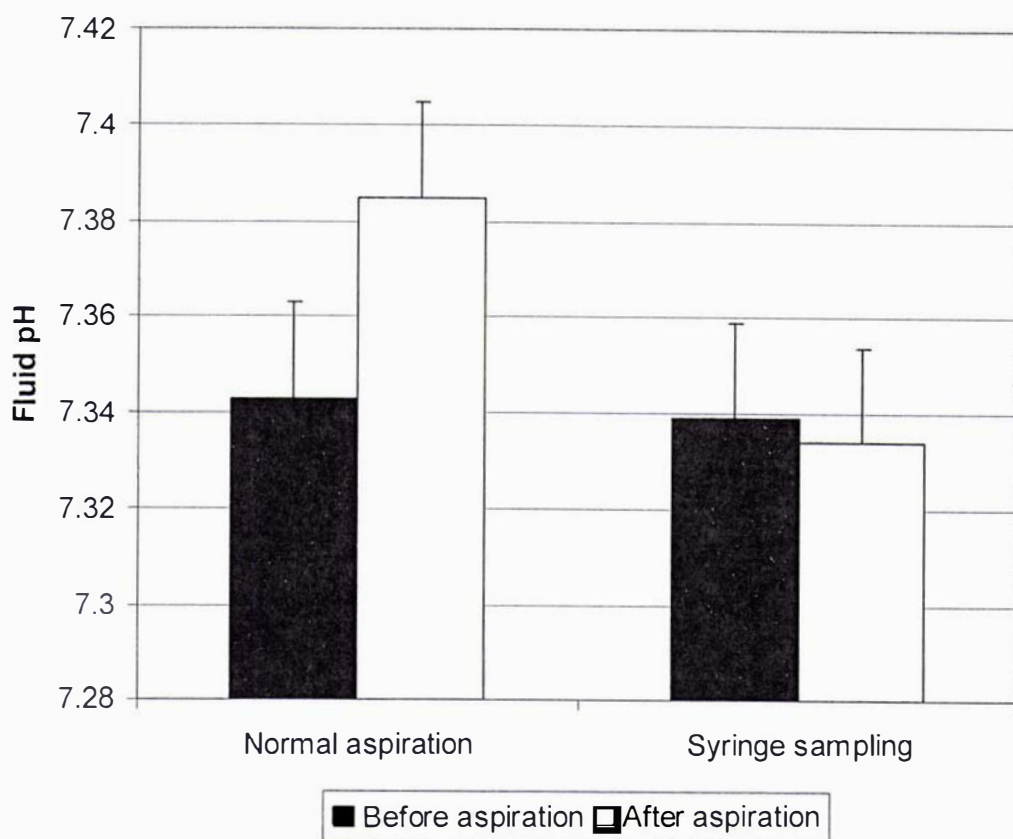
Figure 7.5   Mean change in pH of follicular fluid before and after aspiration, for both normal aspiration and when fluid is sampled from the tubing line. Error bars show standard deviation.

7.2.3.1 Blood contamination and follicular fluid dissolved oxygen

Blood, by virtue of its haemoglobin content, is a massive oxygen sink. Blood contains two forms of oxygen, that which is bound to haemoglobin, and dissolved oxygen which can be considered as freely dissolved in the plasma portion of blood.

An instant before mixing of blood with follicular fluid, oxygen will exist as oxygen bound to haemoglobin in blood, oxygen dissolved in the plasma portion of the blood, and oxygen dissolved in follicular fluid. After contamination by mixing, oxygen will exist as oxygen bound to haemoglobin in the mixture, and free dissolved oxygen in the mixture,

$$
\begin{array}{c}
\text{Oxygen} \\
\text{bound} \quad \text{to} \\
\text{haemoglobin} \\
\text{in blood}
\end{array}
+
\begin{array}{c}
\text{Oxygen} \\
\text{dissolved} \\
\text{in plasma}
\end{array}
+
\begin{array}{c}
\text{Oxygen} \\
\text{dissolved} \quad \text{in} \\
\text{follicular} \\
\text{fluid}
\end{array}
=
\begin{array}{c}
\text{Oxygen} \\
\text{bound} \quad \text{to} \\
\text{haemoglobin} \\
\text{in mixture}
\end{array}
+
\begin{array}{c}
\text{Oxygen} \\
\text{dissolved} \quad \text{in} \\
\text{mixture}
\end{array}
\quad (7.5)
$$

The fraction of haemoglobin that is saturated by oxygen (Y_H) is described by the Hill equation and is a function of the partial pressure of dissolved oxygen (pO_2)(Fournier, 1998).

$$
Y_H = \frac{pO_2{}^n}{P_{50}^n + pO_2{}^n} \qquad (7.6)
$$

Where n represents the degree of cooperative binding between oxygen and haemoglobin, and P_{50} represents the partial pressure of the oxygen at which 50% of the binding sights are full (constant for a given system/animal). Now, incorporating the Hill equation (equation 7.6) and equation 7.5, and assuming the solubility of oxygen in follicular fluid and plasma are equal (justified by the work of Chapter 6), and that each haemoglobin molecule is capable of binding 4 oxygen molecules, the following oxygen balance can be written.

$$4C_H V_b \frac{pO_{2b}^n}{P_{50}^n + pO_{2b}^b} + pO_{2b} S_p V_b \varepsilon + pO_{2f} S_p V_{ff} = 4C_H V_b \frac{pO_{2m}^n}{p_{50}^n + pO_{2m}^n} + pO_{2m} (V_{ff} + V_b \varepsilon) S_p$$

(7.7)

Table 7.2 provides estimates and descriptions for the various parameters of equation 7.7. It should be noted that equation 7.7 assumes that both the degree of cooperative binding of oxygen to haemoglobin (n), and the P_{50} remain the same before and after mixing. In practice it is well understood that these parameters are effected by temperature (Reeves, 1980), pH (Samaja et al., 1981), CO_2 levels (Kwant et al., 1988) and 2,3-diphosophoglycerate (DPG) concentration (Samaja et al., 1981). However, both follicular fluid and blood can be assumed to be at or close to body temperature at the point of mixing, and the pH and CO_2 levels of blood and follicular fluid have been shown to be similar (Fischer et al., 1992; Fisch et al., 1990; Shalgi et al., 1972). DPG is a molecule found within the red blood cells which reduces the oxygen binding capacity of haemoglobin. Provided red blood cells are not significantly ruptured, this relationship can be assumed to be unaffected.

Of the parameters listed in Table 7.2, void fraction (ε) and the haemoglobin concentration of blood (C_H) have been calculated through information from a variety of sources. Fournier (1998b) gives the number of red blood cells per ml of whole blood as 4.8×10^9 for females, and the mean volume of red blood cells as 95 μm^3.cell^{-1}. From this the volume fraction of blood occupied by cells can be calculated for females as,

$$Cell\ fraction = 1 - \varepsilon = 4.8 \times 10^4\ \frac{cells}{ml}\ x\ 95 \frac{\mu m^3}{cell}\ x\ \frac{1}{10^{18}}\frac{m^3}{\mu m^3}\ x\ 10^6\ \frac{ml}{m^3} = 0.456 \quad (7.8)$$

and hence the void fraction (ε) is 1-(1- ε), or 54.4%.

Truskey et al. (2004) gives the molecular mass of haemoglobin as 64,500 g/mol and Fournier (1998b) gives the concentration of haemoglobin as 0.335 g/mol of red blood cells. Hence the concentration of haemoglobin in blood, C_H, can be calculated as follows,

$$C_H = 0.335 \frac{g}{ml\,RBC's} \times 0.456 \frac{ml\,RBC's}{ml\,blood} \times \frac{1}{64,000} \frac{mol}{g} \times 10^6 \frac{ml}{m^3} = 2.37 \frac{mol}{m^3 blood}$$

(7.9)

Having estimated all the required parameters, equation 7.7 can be solved for the partial pressure of the blood/follicular fluid mix after contamination (pO_{2m}). It cannot be solved explicitly and hence an iterative solution was employed.

Figure 7.6 shows the solution of equation 7.7 as the degree of blood contamination is varied for a 5ml follicular fluid sample at a variety of initial dissolved oxygen levels in the follicular fluid (0, 3, 5, 7 vol %). The figure shows that the level of dissolved oxygen in the contaminated follicular fluid increases as the level of blood contamination increases. The blood itself is initially at approximately 12.5 vol% (95 mmHg) and if extended, each of the curves in Figure 7.6 tends to this value. The closer the initial follicular fluid dissolved oxygen is to the level of dissolved oxygen in blood, the slower the rate of increase with increasing blood contamination level. However, even at a starting level of 7 vol% the increase in dissolved oxygen level is greater than 1 vol% with a small 2% blood contamination.

At 5 vol%, which is a fair estimate for a typical value of follicular fluid dissolved oxygen, the increase is obviously even greater. Such increases are certainly great enough to cause significant error in the measurement of dissolved oxygen in contaminated samples. Given that 91% of follicular fluid samples present with blood contamination that is visible and likely at a level of at least 2%, this means that meaningful dissolved oxygen data can only be gathered from a very small number of follicles. As the aim of dissolved oxygen measurement is to make comparisons among follicles then this would give rise to a very limited data set.

Symbol	Value	Units	Description	Reference
C_H	2.37	mol.m^{-3}	Haemoglobin concentration of blood	Multiple, see discussion below
V_b	n/a	m^3	Volume of blood (varied parameter)	n/a
pO_{2b}	95	mmHg	Partial pressure of oxygen in blood (assumed arterial)	(Fournier, 1998)
S_p	0.00123	mol.m^{-3}.mmHg^{-1}	Solubility of oxygen in plasma, and follicular fluid	Chapter 4
ε	0.544	Dimensionless	Void fraction of blood	See discussion
pO_{2f}	n/a	mmHg	Partial pressure of oxygen in follicular fluid (varied parameter)	n/a
V_{ff}	5x10^{-6}	m^3	Volume of follicular fluid	Chapter 4
P_{50}	26	mmHg	Partial pressure at which ½ the haemoglobin sites are occupied with oxygen	(Fournier,1998, Clerbaux *et al.*, 1993)
n	2.34	Dimensionless	Degree of cooperative binding of oxygen and haemoglobin	(Fournier,1998, Clerbaux *et al.*, 1993)
pO_{2m}	n/a	mmHg	Calculated parameter	n/a

Table 7.2   Parameter estimates for blood contamination calculations.
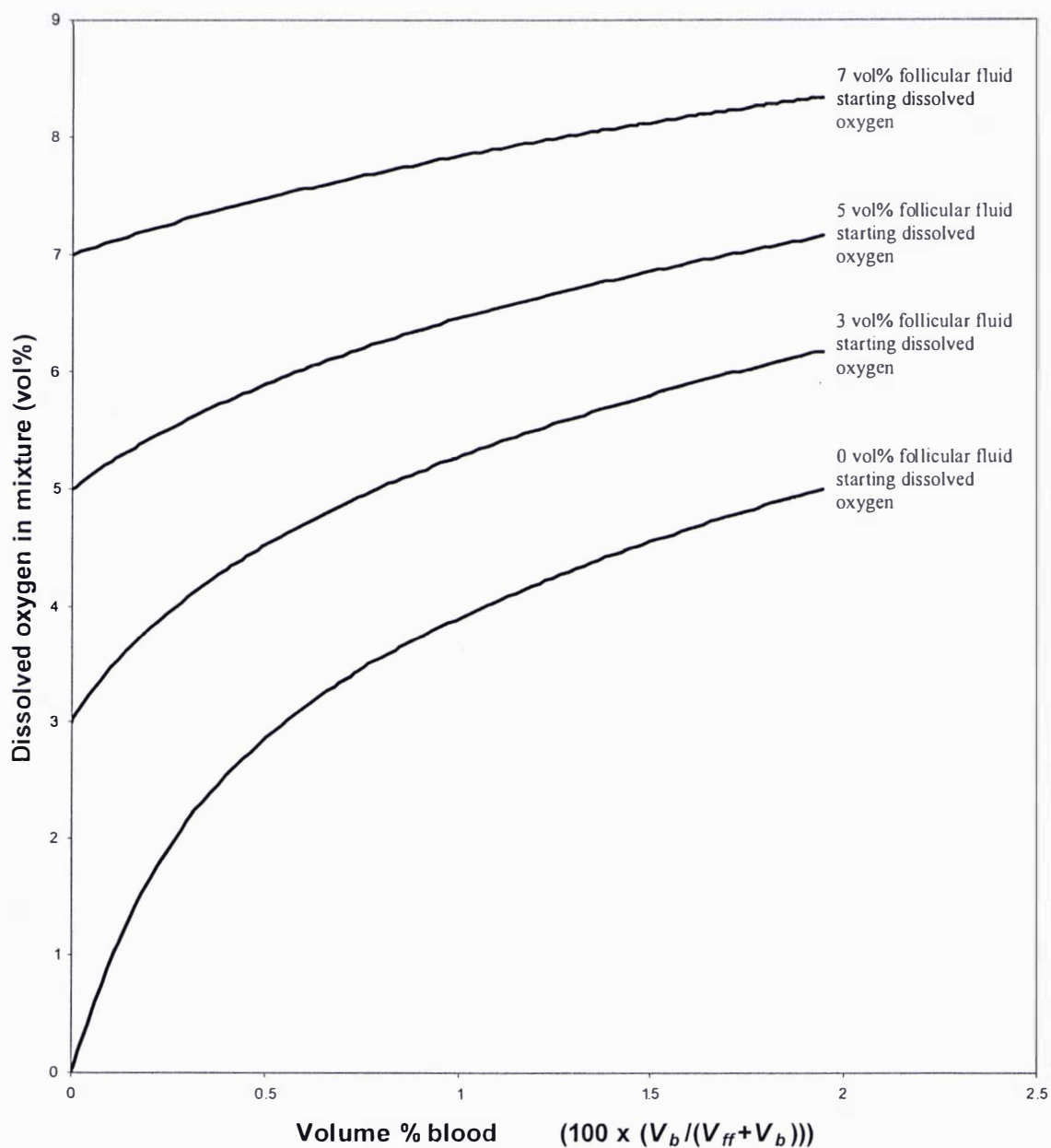
Figure 7.6   Changes in dissolved oxygen of a 5 ml follicular fluid sample with various initial dissolved oxygen levels upon contamination with blood.

One potential way around this problem would be to measure the pO_2 of the mixture and attempt to back calculate the dissolved oxygen level of the original uncontaminated sample. This would require knowledge of all the parameters of equation 7.7 (excluding pO_{2f} which we want to calculate). Practically, this would require measurement of additional parameters including P_{50} and n, as these are known to vary significantly within individuals of the same species (Clerbaux *et al.*, 1993). When this requirement is combined with the need for centrifugation of the sample to measure the amount of red blood cells, such an exercise quickly becomes impractical.

Given the great effect of blood contamination on the apparent measured level of dissolved oxygen in follicular fluid, it is interesting to look at how literature studies which attempted to analyse oxygen levels in follicular fluid coped with this problem. Two earlier studies which obtained follicular fluid samples during hysterectomy operations (Shalgi *et al.*, 1972, Fraser *et al.*, 1973) rejected blood contaminated samples. It is likely that the increased access to the ovaries afforded by the hysterectomy operation allowed these studies to keep blood contamination at a negligible value. Of the IVF studies where blood contamination is of greater frequency, two studies gave no indication of any control over blood contamination (Fischer *et al.*, 1992, Imoedemhe *et al.*, 1993), while the other two accepted slightly amber specimens (Van Blerkom *et al.*, 1997, Huey *et al.*, 1999). It is not possible to be categorical without further knowledge of the procedures employed in these studies, but it is likely that all four IVF studies suffered from oxygen analysis errors due to blood contamination. The implication is that the values of dissolved oxygen in follicular fluid may have been over reported to varying but unknown degrees.

Van Blerkom *et al.* (1997) stated that highly blood contaminated samples could be centrifuged, the red blood cells removed, and subsequently analysed for dissolved oxygen with no effect on the dissolved oxygen levels. Although no supporting evidence was provided, this is worthy of further investigation as it may represent a valuable tool for avoiding the problems of blood contamination in follicular fluid oxygen analysis. Apart from this proposed centrifugation method, the only other likely alternative to obtaining reliable follicular fluid dissolved oxygen measurements is to obtain a sample free of blood.

7.2.3.2   Blood contamination and other analytes

Although the effects of blood contamination on oxygen levels seems to have been given some consideration, the effect of blood contamination on other analytes in follicular fluid appears to have been overlooked. This is in spite of the very large number of studies which have analysed non-oxygen components in follicular fluid, both in humans and animals. Most commonly, samples are centrifuged with the red blood cells being removed before analysis of the parameter of interest. This approach fails to acknowledge that blood is a mixture of red blood cells and plasma. After centrifugation the remaining fluid will be a mixture of follicular fluid and plasma, and the measured concentration of analyte (C_a) will be given by,

$$C_a = \frac{C_p V_p + C_f V_{ff}}{V_p + V_{ff}} \tag{7.10}$$

What the investigator actually wants to measure is the concentration of the analyte in follicular fluid (C_{ff}), and by following the above procedure is actually measuring the concentration of the analyte in the mixture (C_a). Whether knowingly or not, the assumption has been made that the concentration of the analyte in plasma and follicular fluid are approximately equal ($C_p \approx C_{ff}$), and/or the volume of plasma is negligible ($V_p \approx 0$), as this is the only way that $C_{ff} \approx C_a$.

The assumption that $V_p \approx 0$ is unlikely to be justified, at least a good deal of the time. In the clinical work carried out in this thesis, follicular fluid samples with red blood cell sediments occupying 1/3 to greater than 1/2 of the sample volume were frequently observed. Because blood is composed of approximately a 50:50 mixture by volume of plasma and red blood cells, then the fluid phase of a sample containing 1/3 total volume of RBC's will in fact be a 50:50 mix of plasma and follicular fluid. In this case the only thing that can save the analysis is if the concentration of the analyte in follicular fluid and plasma are the same or very similar. Regardless, it is certainly not good experimental practice. Once again the analysis could be saved by rearranging equation 7.10 for C_f and back calculating its value. To do this, the volume of

261

plasma could be calculated from the volume of RBC's (V_{RBC}) that were obtained from centrifugation.

$$V_p = \frac{V_{RBC}\varepsilon}{1-\varepsilon} \qquad (7.11)$$

This, of course, makes the assumption that a general value of ε can be used, otherwise this value would have to be measured. Also, a sample of plasma would need to be analysed for C_p. V_f could also be inferred from the total less V_p. Although this entire procedure is possible it is certainly not very practical. The best alternative is to obtain a sample free of blood contamination. This does not help the many investigations which have already published data for various follicular fluid species. It is therefore possible that some published data may have been affected by one of three problems.

1. Over reporting of levels of the analyte in follicular fluid due to the concentration of the analyte being higher in blood than in follicular fluid.

2. Under reporting of the levels of an analyte in follicular fluid due to the concentration of that analyte being lower in blood than in follicular fluid.

3. Failure to detect small but significant variability in follicular fluid samples, due to the analyte concentrations being sufficiently similar in the follicular fluid and blood.

7.2.4 Temperature changes during aspiration

The steady state temperatures at each thermocouple position (refer to Figure 7.1 for thermocouple positions) are shown in Table 7.3, and graphically in Figure 7.7. From follicle to collection tube, fluid temperature drops by an average of 7.7°C (T I to T V). 83% of this temperature drop occurs after the fluid falls from the tubing exit to the bottom of the collection tube (T IV to T V). The rate of heat loss Φ_L (W) across any part of the system will be related to the temperature drop across that part of the system ($\Delta\theta$) according to equation 7.12.

Flow rate (ml/min)	Ambient	I	II	III	IV	V
8	21.4	37.5	36.6	36.1	35.6	27.8
9	21.2	36.6	35.8	35.3	34.9	27.9
9	21.4	37.3	36.4	35.9	35.4	28.0
10	21.4	36.4	35.5	35.2	34.7	28.0
13	21.2	36.9	36.1	35.8	35.5	29.2
14	21.1	36.8	36.0	35.8	35.6	29.2
15	21.3	37.2	36.5	36.3	36.1	30.0
15	21.3	37.1	36.3	36.1	35.9	29.3
16	21.3	37.3	36.5	36.4	36.1	30.2
20	21.3	36.7	36.0	36.0	35.9	29.3
21	21.3	36.8	36.2	36.3	36.3	30.4
22	21.0	36.9	36.5	36.5	36.4	32.1
n	12	12	12	12	12	12
Mean	14.3	21.3	37.0	36.2	36.0	35.7	29.3
Std. Dev.	4.8	0.1	0.3	0.3	0.4	0.5	1.3

Table 7.3   Temperature of follicular fluid (°C) at positions indicated in Figure 7.1, for a standard aspiration kit.
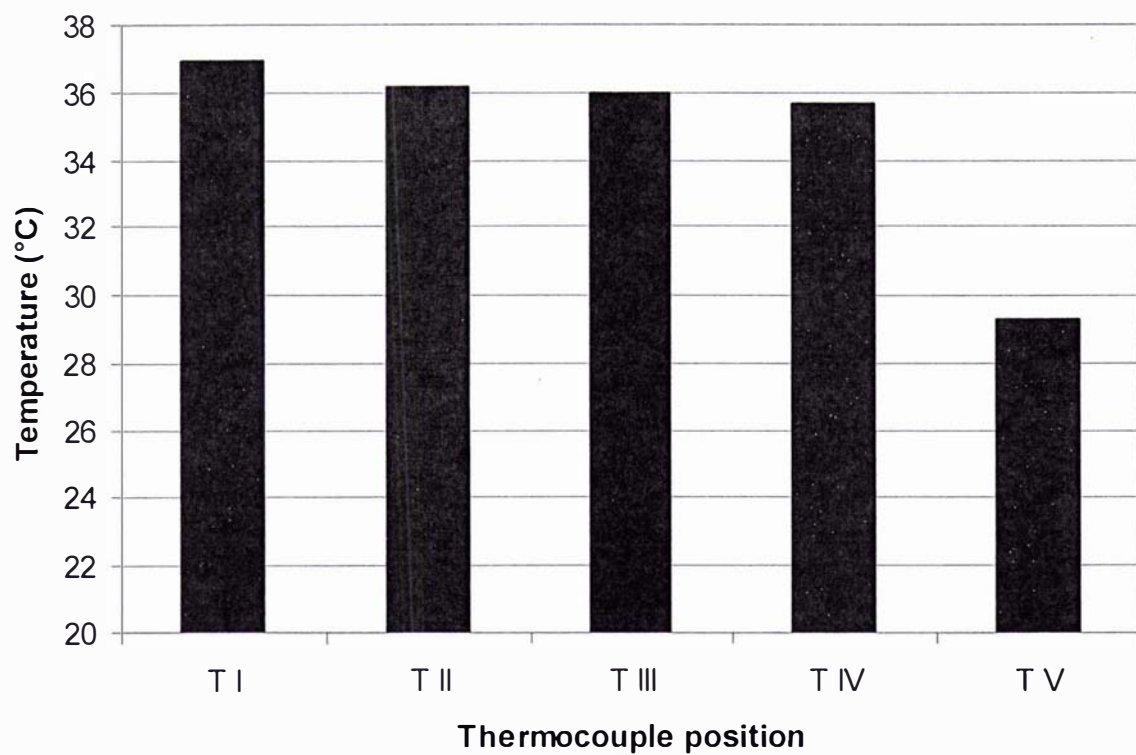
Figure 7.7   Mean temperature of follicular fluid during aspiration at positions indicated in Figure 7.1.

$$\phi_L = mc_{pff}\Delta\theta \qquad\qquad (7.12)$$

where m is the fluid flow rate (kg.s^{-1}), and c_{pff} is the heat capacity of follicular fluid.

Therefore the proportion of the total heat loss over any part of the system will simply be the ratio of the temperature drop over that part of the system ($\Delta\theta$) to the total temperature drop over the entire system ($\Delta\theta_{tot}$). This relationship is described by equation 7.13.

$$Proportion\ of\ total\ heat\ lost = \frac{mC_{pff}\Delta\theta}{mC_{pff}\Delta\theta_{tot}} = \frac{\Delta\theta}{\Delta\theta_{tot}} \qquad\qquad (7.13)$$

According to equation 7.13 the 83% temperature drop observed as the fluid falls from the tubing exit to the bottom of the collection tube (T IV to T V), translates to 83% of the total system heat losses. Therefore the mean percentage contributions to heat loss in the system are 10% from follicle to needle, 7% from needle to collection tube entry, and 83% within the collection tube itself.

Equation 7.12 can be used to calculate the absolute rate of heat losses over each part of the system, and the results used to examine any relationship between heat loss and flow rate. Calculation of the heat loss contribution of each part of the system requires an estimate of the heat capacity of follicular fluid (c_{pff}). This can be achieved through the use of equation 7.14 (Choi & Okos, 1986).

$$c_{pff} = X_1 c_{p1} + X_2 c_{p2} + ...X_n c_{pn} \qquad\qquad (7.14)$$

where for the 1st to nth components of follicular fluid, X is the weight fraction and c_p is the heat capacity of that particular component.

The general composition of follicular fluid has been previously determined (McNatty, 1978), and can be approximated as a mixture of 93 wt% water, 6 wt% protein, with the remaining 1 wt% being made up by other compounds such as electrolytes. At

37 °C the specific heat capacity of water is 4300 J.kg^{-1}.K^{-1} (Liley *et al.,* 1997), and that of protein 2050 J.kg^{-1}.K^{-1} (Choi & Okos, 1986). Therefore, using equation 7.3 the heat capacity of follicular fluid is estimated as 4200 J.kg^{-1}.K^{-1}. Calculation of heat losses also requires the conversion of flow rate in ml.min^{-1} to kg.s^{-1}, which can be achieved if the density of follicular fluid is known. At 37 °C the density of water is 993.3 kg.m^{-3} (Liley *et al.,* 1997), and the mean relative density of follicular fluid from Chapter 6 is 1.022. Therefore the density of follicular fluid is 993.3 x 1.022 = 1015.2 kg.m^{-3}. Assuming the values of follicular fluid heat capacity and density to be constant throughout the temperature range observed in this study, equation 7.12 can be used to relate the rate of heat loss through the system to the flow rate. Performing these calculations reveals that down the needle and tubing lines, rate of heat loss is relatively constant and independent of flow rate throughout the tested range. However, from the tubing exit to the bottom of the collection vial (T IV to T V), the rate of heat loss appears to be related to the flow rate. This relationship is shown in Figure 7.8.

Figure 7.8 shows a trend for a greater rate of heat loss as flow rate increases through the aspiration kit. To understand this relationship, and the sources of heat loss within the system, further heat transfer theory can be applied. There are three possible sources of heat loss in the collection vial. Heat may be lost as a result of the fluid heating the collection vial. Once the tube has been heated, further losses may occur through the walls of the vial to the environment. Finally, heat may be lost due to water evaporation from the follicular fluid or as convective heat loss to the air in the collection vial (lost down the vacuum line), and these final sources are referred to here as internal system heat loss.

The large fluid temperature drop in the collection vial was further investigated to determine the cause of this heat loss. Table 7.4 shows the temperature drops observed from thermocouple IV to V when various combinations of collection vial heating and insulation are employed at a flow rate of 14 ml/min. $\Delta\theta_1$ is the temperature drop when aspiration is performed normally. $\Delta\theta_2$ is the temperature drop when the collection vial is heated and then insulated prior to aspiration. $\Delta\theta_3$ is the temperature drop when the collection vial is insulated only prior to aspiration.
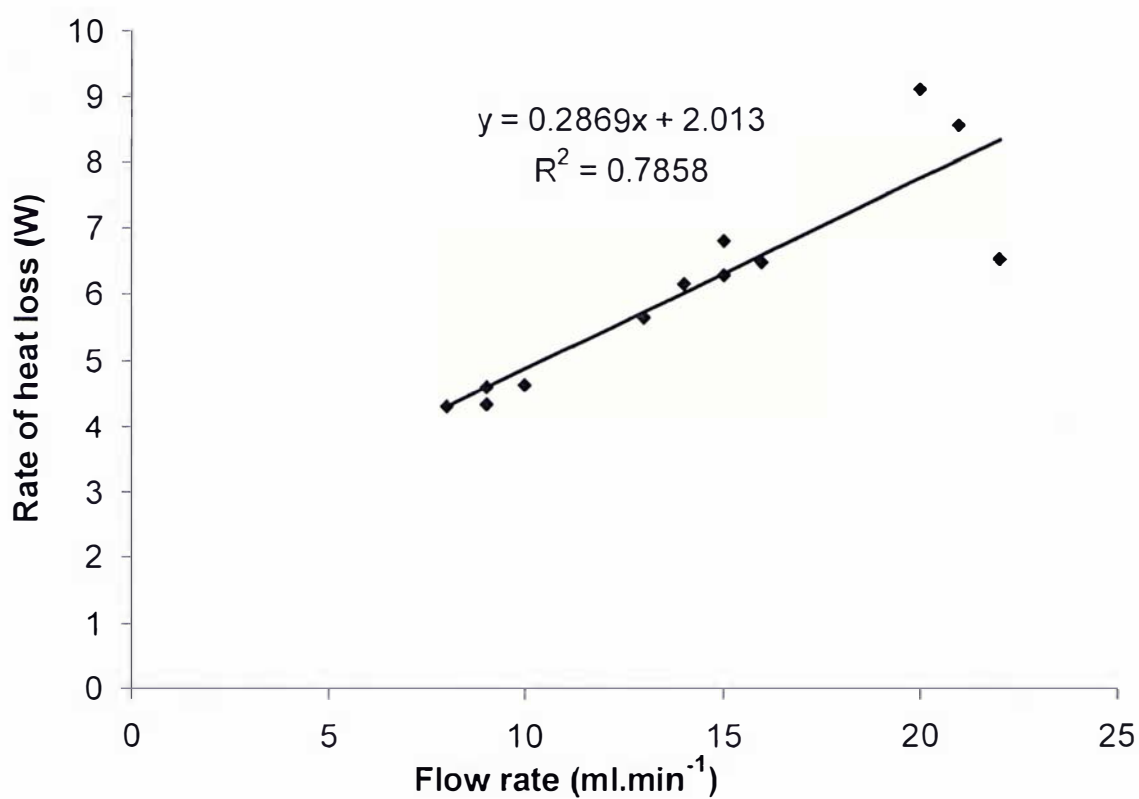
Figure 7.8   Rate of heat loss from the tubing exit to the bottom of the collection vial (T IV to T V) as a function of flow rate.

Flow rate (ml/min)	$\Delta\theta_1$	$\Delta\theta_2$	$\Delta\theta_3$
14	6.0	5.2	6.1
14	6.1	5.1	5.8
14	6.9	5.5	6.4
14	6.9	5.5	6.8
14	6.1	4.9	5.8
14	6.0	5.0	5.9
14	6.6	5.6	6.4
14	6.9	5.4	6.4
14	5.9	4.8	6.2
14	6.5	5.4	6.4
n	10	10	10
Mean	6.4	5.3	6.2
Std. Dev.	0.4	0.3	0.3

Table 7.4   Temperature drop from thermocouple IV to V under different heating conditions (°C). $\Delta\theta_1$ is the temperature drop when aspiration is performed normally. $\Delta\theta_2$ is the temperature drop when the collection vial is heated and then insulated prior to aspiration. $\Delta\theta_3$ is the temperature drop when the collection vial is insulated only prior to aspiration.

Therefore, $\Delta\theta_1$ can be considered the mean temperature drop due to internal system heat losses (most likely due to evaporation), collection vial heating, and convective heat losses to the environment. $\Delta\theta_2$ is the mean temperature drop due only to internal system heat losses. $\Delta\theta_3$ is the mean temperature drop due to internal system heat losses and collection vial heating.

From these values the mean relative contributions of heat losses over the collection vial can be calculated. These are the internal system heat losses, collection vial heating, and convective losses to the environment.

$$\% \text{ Internal system heat losses} = \frac{100}{1} \times \frac{\Delta\theta_2}{\Delta\theta_1} = 82\% \pm 2\% \text{ (mean} \pm 95\% \text{ CI)}$$

$$(7.15)$$

$$\% \text{ Heat loss due to collection vial heating} = \frac{100}{1} \times \frac{(\Delta\theta_1 - \Delta\theta_2) - (\Delta\theta_1 - \Delta\theta_3)}{\Delta\theta_1} = 15\%$$

$\pm 2\%$ $\hspace{6cm}$ (7.16)

$$\% \text{ Heat loss due to convective heat loss} = \frac{100}{1} \times \frac{(\Delta\theta_1 - \Delta\theta_3)}{\Delta\theta_1} = 2\% \pm 2\%$$

$$(7.17)$$

The major source of heat loss comes from internal system heat losses. The suggested mechanism for this internal system loss is discussed below.

The results presented here show that IVF aspiration induces a temperature drop in follicular fluid. This temperature drop has a total mean steady-state value of 7.7°C at an average flow rate of 14.3 ml/min. Only 1.3 °C of this temperature drop is the result of the fluid flowing from the follicle to the point where it enters the collection vial (TI to TIV). Because these results are for steady state, the initial temperature drop will be slightly greater as the tubing line is being heated. This effect will be largest for the first aspiration of an IVF procedure. This loss could be prevented by heating and insulating the tubing line, thus preventing any losses due to heating the line and

269

convective losses to the atmosphere. The remaining 6.4 °C temperature drop occurs after the follicular fluid has entered the collection vial (TIV to TV). Heat losses due to warming the collection vial, and convective losses to the environment, account for only 17% of the temperature drop.

The remainder of the heat loss is due to internal system heat losses. This heat loss could be caused by convective losses to the air in the collection vial and/or evaporation of water in the collection tube. In the vacuum environment of the collection tube the thermal mass of air will be very small, and hence convective heat losses via mixing with air in the collection tube are likely to be negligible. Thus the dominant contributor to internal system heat losses is likely to be evaporation. The low pressure environment of the collection vial lowers the vapour pressure of water, and creates improved conditions for evaporation. If the dominant source of heat loss from thermocouple IV to V is assumed to be due to evaporation of water from the collection vial, the mass of fluid lost in this manner can be approximated.

The enthalpy of vaporisation of water (ΔH_{vap}) is approximately 43000 J.mol^{-1} (Liley *et al.*, 1997) at 36 °C (the approximate tube exit temperature). The temperature drop in the total fluid mass of Y (kg) due to evaporation will be related to the heat lost via the evaporation of y (kg) of fluid according to equation 7.18.

$$Yc_{pff}\Delta\theta_2 = y\frac{1000\Delta H_{vap}}{M_{H_2O}} \tag{7.18}$$

where M_{H2O} is the molecular mass of water (g.mol^{-1}).

Therefore the weight percentage of the total fluid lost to evaporation will be given by,

$$\text{Wt\% of fluid lost to evaporation} = \frac{y}{Y}x\frac{100}{1} = \frac{C_{pff}\Delta\theta_2 M_{H_2O}}{10\Delta H_{vap}} = 0.9\% \tag{7.19}$$

The temperature drop observed requires that less than 1% of the mass of follicular fluid be evaporated. This water vapour would likely be lost down the vacuum line,

270

and such a small quantity would not be readily detected. At low flow rates the temperature drop from the tubing exit to the collection vial is greater than at high flow rates. This is due to the increased residence time of fluid in the collection tube. The actual rate of heat loss is higher at high flow rates than at low ones from the tubing exit to the collection vial. This is likely due to the increased applied vacuum at higher flow rates. The larger vacuum lowers the vapour pressure of water and enhances evaporative heat losses.

It is important to note that the experimental set-up used is intended as a characteristic representation of the IVF process. Observed temperature drops will likely vary from clinic to clinic based on the particular aspiration kit used, the magnitude of the applied vacuum, degree of collection vial heating, and thermal mass of the collection vial. If the collection vial were to be heated and had high thermal mass then the observed temperature drop in the fluid would be buffered by the heat from the vial walls. This effect was not observed in this work as the polystyrene collection vials used have very low thermal mass.

However, though the magnitude may vary, evaporation and an associated temperature drop will occur regardless of the particular system, provided aspiration occurs in a vacuum environment. This will occur as the droplets fall through the vacuum to the bottom of the collection vial where the fluid may be reheated.

The observed temperature drops will result in an increase in the oxygen solubility of follicular fluid. The enhanced ability of the fluid to store oxygen will have an impact on the magnitude of the observed changes in dissolved oxygen levels. If the sample can be obtained without oxygen contamination then the change in solubility does not represent a problem. Furthermore, if fluids are sampled and removed for analysis they will need to be returned to a common temperature before measurement takes place. This may not be such an issue if measurement can be performed in-line where changes in temperature have been shown to be minimal. Therefore, the idea of sampling and/or measurement of the dissolved oxygen in follicular fluid, before the collection vial is reached, is also supported by the implications of the temperature drops observed here.

Although not the primary objective of this work, it is important to consider that the temperature drops for standard IVF aspiration reported here may also have implications with regard to oocyte integrity.

Such a large and rapid temperature drop is unlike any the oocyte will have experienced in its previous history. Most IVF clinics place the collected fluid on a heated block after aspiration, if there is to be a delay before the embryologist searches the fluid for the oocyte(s). Oocyte searching usually takes place on a heated stage. As a result, the retrieval process takes the environment of the oocyte from around 37°C pre aspiration to approximately 29°C immediately post aspiration, before returning to around 37°C.

Research suggests that human oocytes exposed to room temperature can have disrupted spindles and chromosomal dispersal (Almeida & Bolton 1995). These effects can be reversed if oocytes are returned to 37°C within 2 min, but not after 10 min. Similar research indicated that human oocyte spindles become completely dis-assembled after exposure to room temperature for 5 min (Wang *et al.*, 2001). These spindles recovered after 20 min of re-warming. Oocytes exposed to 28°C and 25°C for 10 min and then re-warmed were found to have limited recovery. Wang *et al.* (2001) concluded that maintenance of temperature at 37°C during in-vitro oocyte manipulation is likely to be important to normal fertilization and subsequent embryo development. Research conducted on pig oocytes after 44 hours of maturation showed similar spindle dis-assembly after cooling to 24°C, with limited spindle recovery regardless of the cooling time (Liu *et al.*, 2003). Reduced pregnancy rates were found. This may suggest that in the human work, although the spindle was observed to return to normal, the oocyte may in fact have reduced developmental capacity in the form of lower pregnancy rates. Obviously to continue with transfer in the above human studies would not be ethical, and hence pregnancy rates were not measured. Rigorous temperature control during intracytoplasmic sperm injection (ICSI) has also been shown to improve pregnancy rates (Wang *et al.*, 2002).

These results suggest that the IVF aspiration temperature drop measured in this work may compromise the developmental capacity of some oocytes, particularly if re-

warming does not take place quickly. IVF clinics need to take particular care in ensuring temperature control of follicular fluid if there are to be delays before oocyte searching. The disparity between pregnancy rates between various fertilization centres is well documented (Munne *et al.,* 1997). Differences in clinical operating practices with regard to fluid temperature control may be another factor contributing to such variance.

7.2.5   Effects of IVF aspiration on the Cumulus-oocyte complex

149 bovine cumulus-oocyte complexes were aspirated without the oocyte being sampled by device A, and hence are considered to have undergone standard IVF aspiration. Of these 149 oocytes, none were lost, although some took considerable time to find. All 149 were examined by light microscopy. None showed any evidence of damage to the zona-pellucida or oocyte.

The controlled setup of this study differs from the *in-vivo* situation. Here each oocyte was viewed as it entered the aspiration system, thus ensuring that it had indeed been aspirated. After this point, the only way an oocyte could be lost would be if it were completely destroyed or became caught up in the internal structure of the system. The latter case would be expected to present as an aspiration in which an additional oocyte appeared. So, setting aside human error in searching and finding oocytes, the only way in which an oocyte could be permanently lost in this system is via destruction.

When oocytes are aspirated from actual ovaries without any prior knowledge of the position of the oocyte, and visual identification prior to aspiration is impossible, recovery rates would be expected to be much lower. This is the case in bovine studies which have reported recovery rates ranging from approximately 25-85% (Fry *et al.,* 1993; Smith *et al.,* 1994; Bols *et al.,* 1996; Bols *et al.,* 1997). Further, these studies have demonstrated that recovery rate depends on vacuum pressure (Fry *et al.,* 1993; Smith *et al.,* 1994; Bols *et al.,* 1996), needle gauge (Fry *et al.,* 1993; Smith *et al.,* 1994; Bols *et al.,* 1996), needle bevel (Fry *et al.,* 1993; Smith *et al.,* 1994; Bols *et al.,* 1997), operator (Smith *et al.,* 1994) and day of aspiration (Smith *et al.,* 1994). It is

most likely that the interaction of these parameters with the internal follicle contributes to the large variability in recovery rates. This work further suggests that the fact that the oocyte cannot be visualised also plays a major role in its non-recovery.

Bols *et al.* (1997) and Horne *et al.* (1996) also reported an artificial setup where oocytes were collected and identified prior to aspiration. Bols *et al.* (1997) aspirated 50 cumulus-oocyte complexes at a time, from a Petri dish. At flow rates comparable with this work, Bols *et al.* (1997) reported a recovery rate ranging from 72 to 84% over a variety of needle types. In an artificial system, such low recovery rates are surprising. Assuming human counting error to be negligible, this implies that 16 to 28% of oocytes were either destroyed by aspiration or lost, never to be recovered. It should be noted that the system of aspiration used by Bols *et al.* (1997) was designed for use in cattle and differs from the human system used here, by virtue of its short needle. In any case, an aspiration system which apparently destroys or permanently loses such a high proportion of oocytes is quite alarming. The loss rate reported by Bols *et al.* (1997) (16 to 28%) is clearly in stark contrast to that reported here (0%) and may be a result of differences in human and bovine aspiration systems. It is important to note that higher recovery rates are expected in artificial systems such as that used by Bols *et al.* (1997), Horne *et al.* (1996) and in this work. This is likely because in such artificial systems that cumulus-oocyte complex is first recovered and then used for experiment. In real IVF both in animals and humans the initial recovery will likely be compromised as some cumulus-oocyte complexes remain tethered to the follicle wall or may be lost between aspirations as the needle is moved from follicle to follicle.

In the artificial system setup by Horne *et al.* (1996), three oocytes were aspirated at a time from a test tube using a setup which, like that reported here, is designed to mimic the human IVF aspiration system. Horne *et al.* (1996) reported that at flow rates comparable with this investigation no oocytes were destroyed, with all of them being recovered. This is consistent with the observations reported here. This further highlights the differences between bovine and human systems. Such a difference may, in fact, be desirable. The bovine system is most likely concerned with presenting the

maximum number of oocytes. Although this would also seem to be a sensible goal for human systems, ethical considerations dictate that human IVF aspiration is more concerned with aspirating undamaged oocytes.

As already stated, of the 149 oocytes aspirated in this study, none were found to have cracked or damaged zona pellucidae. Similarly, Cohen *et al.* (1986) found that, of 165 oocytes recovered using a vacuum pump aspiration system in a real human IVF clinic, only one had a cracked zona pellucidae. Using a test statistic designed to test the equality of two proportions (Sokal & Rohlf, 1969), it was found that the proportion of the cracked zona pellucidae reported here cannot be considered different from that reported in the human IVF clinic by Cohen *et al.* (1986) (p=0.168). This lends support to the experimental setup used here being a fair replication of standard IVF aspiration.

Of the 149 cumulus-oocytes that underwent standard IVF aspiration, 123 were subjected to the digital image analysis previously described. Images were recorded both before and after aspiration. This work allowed the impact of aspiration on the cumulus-oocyte complex to be determined.

The results of this investigation are displayed in Figures 7.9 and 7.10 in terms of the parameters previously described for cumulus-oocyte complex analysis. Included in the figures are the test statistics relevant to the particular parameter. A summary of the analysis is provided in Table 7.5. All of the measured parameters are paired observations and therefore require the use of test statistics for paired observations if the maximum is to be learned from the data. Rather than testing for a significant difference between the means of the before and after populations, whether or not the mean difference of the paired observations is significantly different from zero has been tested (a paired comparison). To use the standard t-test statistic requires that the paired observations be normally distributed. For each measured parameter, the assumption of normality was examined by inspecting histograms and normal-quantile plots of each data set of differences. For the parameters of voidage, and expanded cumulus sphericity the distributions were sufficiently normal. The remaining distributions showed deviation from normality. In some cases this presented in the form of a number of outliers, skewing the distribution. Upon examination, no reason

could be established for the rejection of such outliers, and hence, for all remaining distributions, the assumption of normality was rejected. In these cases, data transformation was attempted by various means and found to be unsatisfactory.

Consequently, a non-parametric test statistic was used, namely Wilcoxons signed ranked test for paired observations (Sokal & Rohlf, 1969b). The exceptions to this were the measures of compact cumulus coverage and the expanded cumulus coverage. In the cases of both compact and expanded cumulus coverage the great majority of measurements showed complete coverage both before and after aspiration. Further, when a change in coverage was observed it was most often only partial. As a result the mean value of the parameters, is skewed greatly toward one (Figure 7.10(b)) and cannot be considered a fair indication of the underlying phenomena. This is not the case for the other parameters whose means are not affected greatly by the outliers, as these were infrequent observations in a large sample. As a result of this, the test statistic deemed most appropriate for use with the compact and expanded cumulus coverage data is one based on the difference between two proportions (Sokal & Rohlf, 1969). To use this statistic, observations were expressed as the proportion of the population before or after aspiration that had less than complete coverage. The statistic tests whether or not these proportions are significantly different before and after aspiration. In table 7.5 the values reported for compact and expanded cumulus coverage represent the increase in the proportion of the population that shows less than complete coverage.

Table 7.5 shows that differences were significant at the 5% level for all parameters other than compact cumulus coverage and voidage. Although aspiration is resulting in statistically significant changes in the majority of measured parameters, this information, coupled with the visual descriptions of Figures 7.9 and 7.10, gives insight into the practical and biological significance of the changes.

(a)

(b)
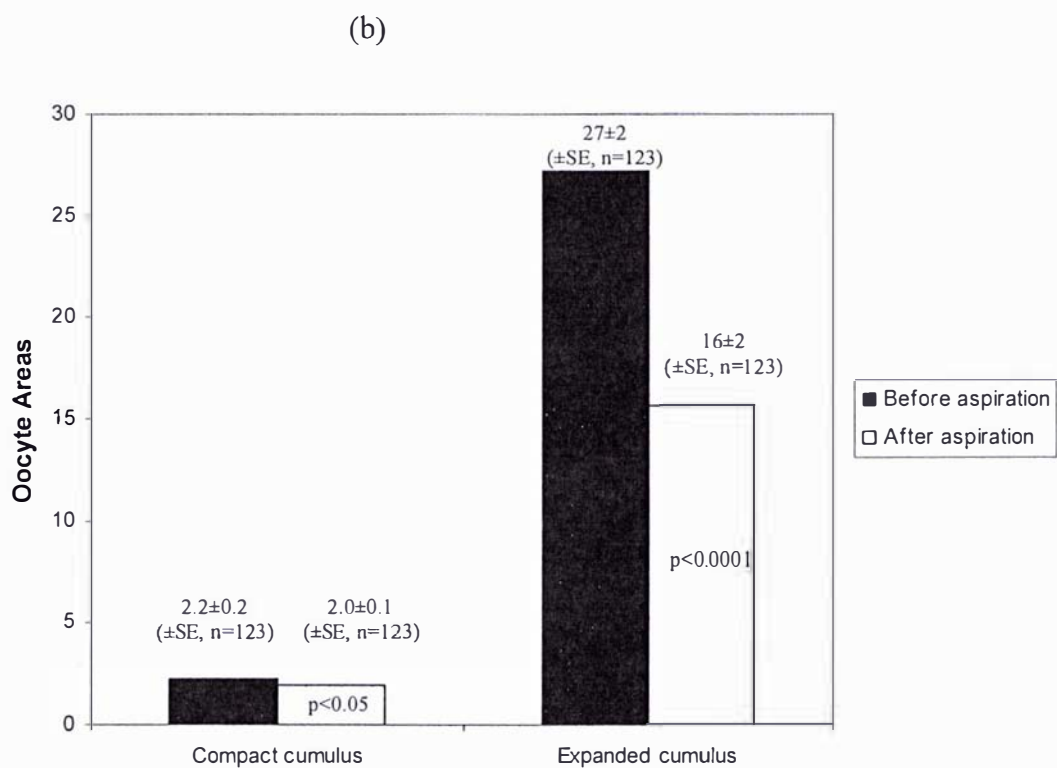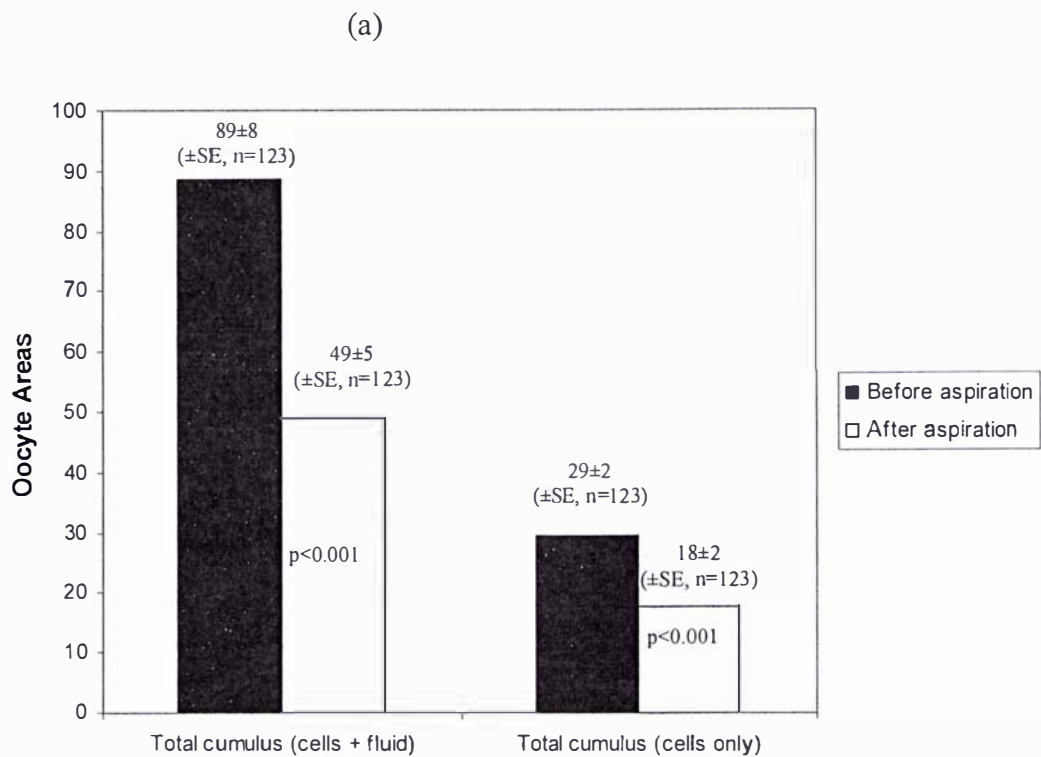
Figure 7.9   Effect of IVF aspiration on the area of cumulus cells surrounding the oocyte.

(a)

(b)
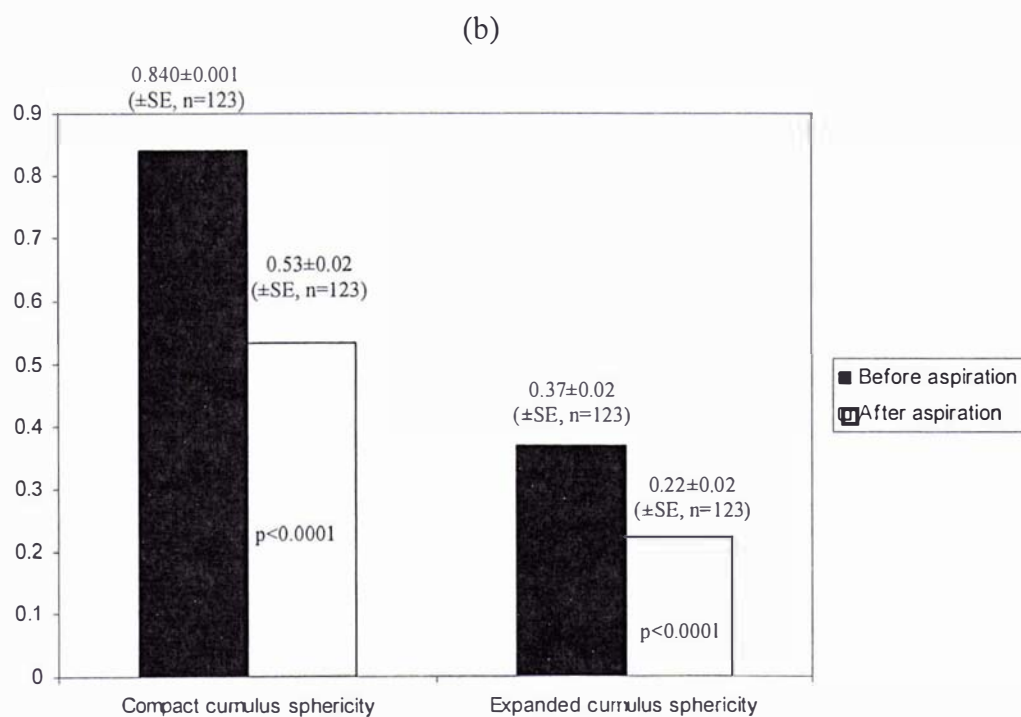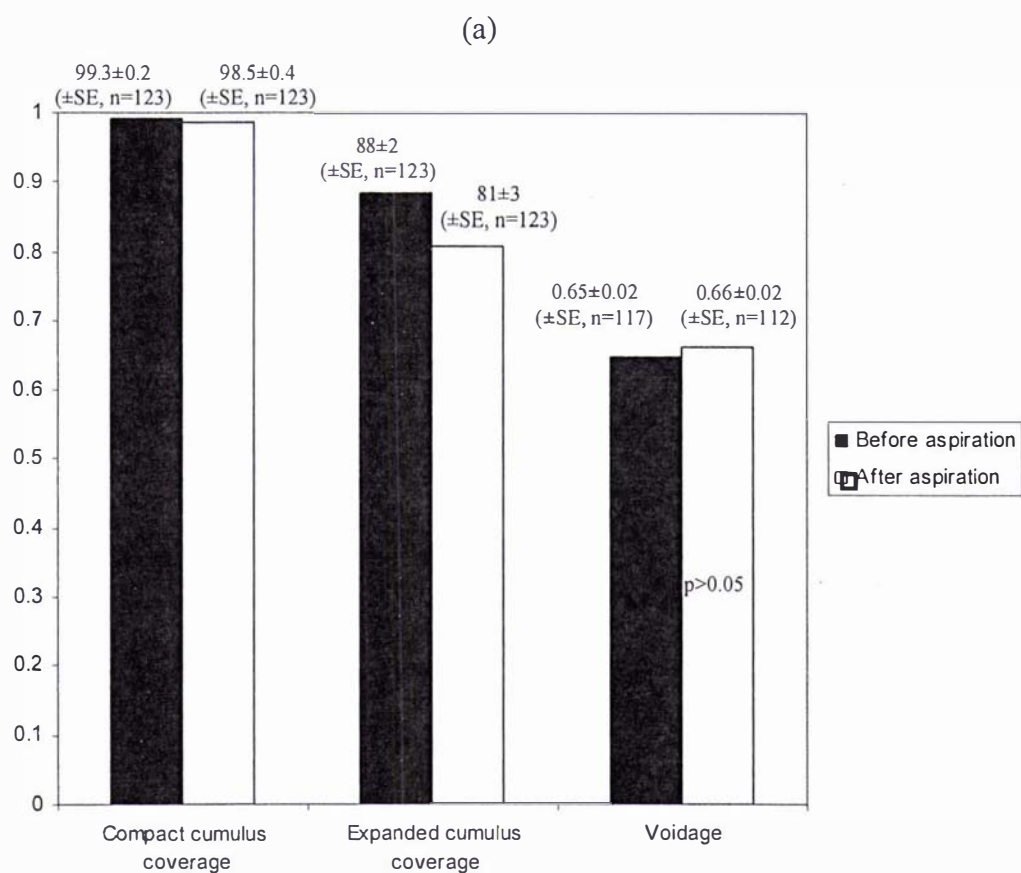
Figure 7.10   Effect of IVF aspiration on the coverage, voidage, and sphericity of cumulus cells.

	Difference (after-before)	SE	Test statistic	Reference	p
Total cumulus (cells and fluid) (oocyte areas)	-39	7	Wilcoxons signed raked test for paired observations	(Sokal & Rohlf, 1969b)	p<0.001 *
Total cumulus (cells only) (oocyte areas)	-12	2	Wilcoxons	(Sokal & Rohlf, 1969b)	p<0.001 *
Compact cumulus (oocyte areas)	-0.3	0.1	Wilcoxons	(Sokal & Rohlf, 1969b)	p<0.05 *
Expanded cumulus (oocyte areas)	-11	2	Wilcoxons	(Sokal & Rohlf, 1969)	p<0.001 *
Compact cumulus coverage	0.07	n/a	Test statistic for difference between proportions	(Sokal & Rohlf, 1969)	p>0.05
Expanded cumulus coverage	0.18	n/a	Test statistic for difference between proportions	(Sokal & Rohlf, 1969b)	p<0.01 *
Voidage	0.03	0.01	t-test for paired comparisons	(Sokal & Rohlf, 1969c)	p>0.05
Compact cumulus sphericity	-0.3	0.02	Wilcoxons	(Sokal & Rohlf, 1969b)	p<0.001 *
Expanded cumulus sphericity	-0.15	0.02	t-test for paired comparisons	(Sokal & Rohlf, 1969c)	p<0.001 *

Table 7.5   Summary of paired observations analysis of the effects of IVF aspiration on the cumulus-oocyte complex. All differences are mean values, apart from compact and expanded cumulus coverage, the values for which represent the increase in the proportion of not fully covered observations. * indicates a significant difference at a minimum of the 5% level.

The total cumulus mass decreased by a mean value of 39 oocyte areas, due to aspiration. This is both a large and statistically significant change. This change included both cellular and fluid areas. Of this reduction, 12 oocyte areas are the result of a loss of cumulus cell mass, which is also statistically significant. Of this 12 oocyte areas, only 0.3 is due to a statistically significant loss of compact cumulus cells, with remainder due to expanded cumulus. Because the change in voidage is not statistically significant, the loss in total cumulus cells of 39 oocyte areas can simply be considered a loss in cumulus cells with an accompanying loss of the fluid associated with it, without any expansion or contraction of the cellular material relative to the fluid. The loss of 0.3 oocyte areas of compact cumulus cells amounts to approximately a 14% reduction in this cell mass. Although these cells are in the closest proximity to the oocyte, such a small loss is not likely to be of great concern, although it does indicate that the shear forces imposed by aspiration do reach the vicinity of the oocyte, even if their impact is not great.

The reduction of 11 oocyte areas of expanded cumulus cells translates to a 41% reduction in this cellular mass. This indicates that these cells are greatly affected by the forces of aspiration. Because of the peripheral location of these cells relative to the oocyte they can be considered to play a somewhat sacrificial role, protecting the oocyte. In spite of the large loss in expanded cumulus mass, the fact that the voidage does not change suggests that the magnitude of shear strain relative to the strength of the cumulus-oocyte complex is not large. If they were severe, large dispersion in the cellular mass might be expected.

90% of oocytes were surrounded completely by compact cumulus cells with no significant difference observable after aspiration. This indicates that although a small amount of compact cumulus cells are stripped off by aspiration, this process does not lead to a loss of the cells immediately adjacent to the oocyte surface. Hence the oocyte is not exposed, or at least not any more so than it was before aspiration. In contrast only 72% of oocytes are completely surrounded by expanded cumulus with this reducing to a statistically significant 54% after aspiration. Once again the cells appear to play a protective role.

The compact cumulus mass can be considered more spherical than the expanded cumulus mass, with both undergoing a statistically significant reduction in sphericity of 0.3 and 0.15 respectively upon aspiration. This shows that both compact and expanded cumulus masses are deformed by aspiration. The impact of such deformation on the oocyte is not known, although the forces required to deform cumulus cells would certainly be far smaller than those required to deform the oocyte.

In summary, this semi-qualitative analysis has shown that IVF aspiration imposes sufficient force on the cumulus-oocyte complex to strip away a large proportion of expanded cumulus cells. However this phenomenon is reduced in the vicinity of the oocyte and suggests that the expanded cumulus cells play a protective role. After aspiration, the oocyte is, generally, still well surrounded by cumulus cells which undergo moderate distortion, but this is not particularly severe as evidenced by the lack of damage to the oocyte itself. This contrasts with similar work done using a bovine IVF aspiration kit (Bols *et al.,* 1997). At comparable flow rates using a variety of different needle types, this work found that between 16 and 28% of aspirated cumulus-oocyte complexes had all their expanded cumulus stripped away. As with oocyte recovery rate, this once again highlights the apparent comparative severity of the bovine system. The most comparable work to this investigation was carried out using a human IVF aspiration kit (Horne *et al.,* 1996). The results were only qualitative, but the conclusions reached by the authors were similar to those described here, i.e. the morphological appearance of the cumulus-oocyte complexes is generally unaltered by standard IVF aspiration under commonly encountered conditions, particularly if the cumulus was regular, compact and refractile. Further, the authors suggested that intact cumulus may offer protection during oocyte collection, a suggestion supported by the more quantitative analysis reported here.

Therefore a baseline which describes the effects of IVF aspiration on the cumulus-oocyte complex has been established. This can be used as a standard with which to compare sampling and/or measurement devices to ensure they do not represent any increased risk of shear damage to the oocyte. Although this methodology can be used to compare such devices it should not necessarily be considered a good indication of the true magnitude of shear damage caused by IVF aspiration itself. This is because

the cumulus-oocyte complexes used were matured in-vitro and come from bovine follicles. Furthermore these cumulus-oocyte complexes underwent multiple aspirations (initial recovery followed by experimental aspiration).

7.3   Conclusions and recommendations

It has been demonstrated in this chapter that IVF aspiration causes significant changes in the gaseous composition of follicular fluid. Aspiration results in an increase in the dissolved oxygen levels of follicular fluid, and a decrease in carbon dioxide levels. These changes are due to gas liquid contact in the collection vial. These changes dictate that the reliable sampling and/or measurement of follicular fluid gas composition (in particular dissolved oxygen) must take place before the collection vial is reached.

Mathematical modelling of blood contaminated follicular fluid has also demonstrated that small amounts of blood contamination give rise to large changes in the dissolved oxygen levels in follicular fluid. Therefore, if follicular fluid dissolved oxygen levels are to be measured, samples must be free of blood contamination.

IVF aspiration also causes significant drops in the temperature of follicular fluid. The majority of this drop occurs in the collection vial and is due to evaporation of water from the follicular fluid in the vacuum environment of the collection vial. The solubility of oxygen in follicular fluid is affected by temperature, as are the responses of many oxygen sensing devices. Therefore, understanding these temperature changes is important to the reliable measurement of dissolved oxygen in follicular fluid. Once again, these results suggest that oxygen analysis may be more appropriate before the collection vial is reached, where changes in temperature are minimal.

IVF aspiration causes minimal changes to the cumulus-oocyte complex. Aspiration results in the stripping of small amounts of expanded cumulus from the cumulus-oocyte complex, as well as small deformation in the shape of the cumulus-oocyte complex. Aspiration does not appear to damage the oocyte itself. These effects of IVF aspiration on the cumulus-oocyte complex can serve as a basis of comparison for determining the effects of any modifications to the IVF aspiration system.

This chapter has shown that IVF aspiration causes significant changes in follicular fluid. The following chapter investigates how these changes can be overcome so that the dissolved oxygen levels in follicular fluid can be measured reliably. The issue of overcoming blood contamination is discussed further, and fluid sampling devices are compared to standard IVF aspiration with respect to cell shear.

Chapter 8. Practical aspects of the sampling and analysis of dissolved oxygen in follicular fluid

The work of previous chapters has facilitated an understanding of how reliable dissolved oxygen measurements could be made. Most notably, samples or measurements must be performed before the collection vial is reached, and must be free of blood contamination.

This chapter details the design of a device for the collection of samples for the analysis of oxygen in follicular fluid. The performance of the device is tested with respect to obtaining a follicular fluid sample with unchanged oxygen levels, and it is compared to standard IVF aspiration in terms of cumulus-oocyte complex damage. Consideration is given to the practical aspects of making dissolved oxygen measurements in follicular fluid, and to the integration of such techniques into clinical practice. The focus of future investigations are suggested.

8.1 Materials and methods

The effects of three sampling devices on the cumulus-oocyte complex, and the dissolved oxygen levels in follicular fluid were experimentally investigated. The IVF aspiration kit used in this work was the same as that described in Chapter 7, except that one of three sampling devices was placed in the middle of the tubing line. Figure 8.2 depicts each of these sampling devices. The sampling devices are designed to withdraw a 1 ml follicular fluid from the tubing line.

The effect of each sampling device on the dissolved oxygen levels of follicular fluid was investigated in the same manner as described in Chapter 7. Dissolved oxygen levels were measured before aspiration. Follicular fluid samples were then aspirated as described in Chapter 7 at 14 ml/min. A 1 ml sample was drawn from the middle of the tubing line. The dissolved oxygen levels in the sample were then measured. All

dissolved oxygen measurements were performed in the same manner as described in Chapter 7 at 25°C.

8.2 Follicular fluid sampling alternatives

Dissolved oxygen measurements in follicular fluid remain unchanged before the collection vial of a IVF aspiration kit. Based on this, three alternative approaches to the sampling and/or measurement of dissolved oxygen are suggested and pictured in Figure 8.1.

In-line sampling refers to the process where a volume of fluid is sampled from the main tubing line, while the remainder of the fluid is allowed to flow as normal through to the collection vial. The fluid sample can then be used for the analysis of dissolved oxygen in follicular fluid.

In-line measurement refers to the situation where an oxygen measurement device is placed inside the tubing line and continuously monitors the oxygen levels in the fluid as it flows past.

In-follicle measurement refers to the case where the oxygen sensing device is located in the needle. The sensor could either respond to the oxygen levels in the fluid as the needle punctures the follicle or alternatively, independently puncture the follicle, make a measurement and retract prior to needle puncture. Each of these alternatives has their own advantages and disadvantages, and these can be most objectively viewed in relation to the system constraints.

(a) In-line sampling

sample here

collection vial

(b) In-line measurement

measure here
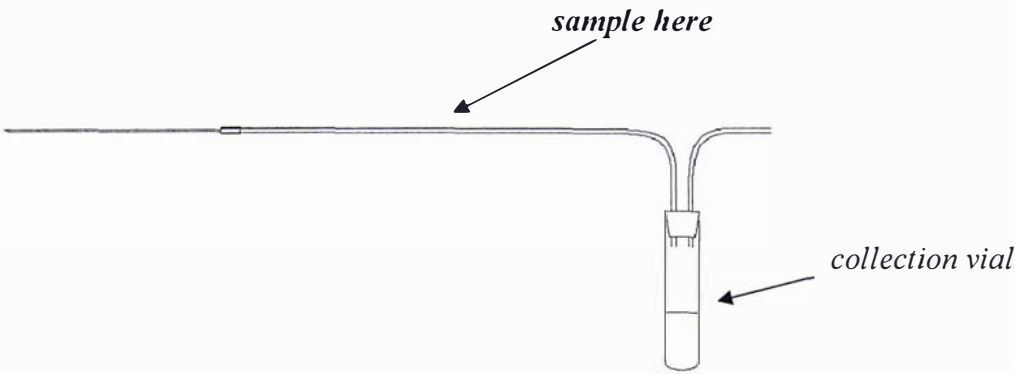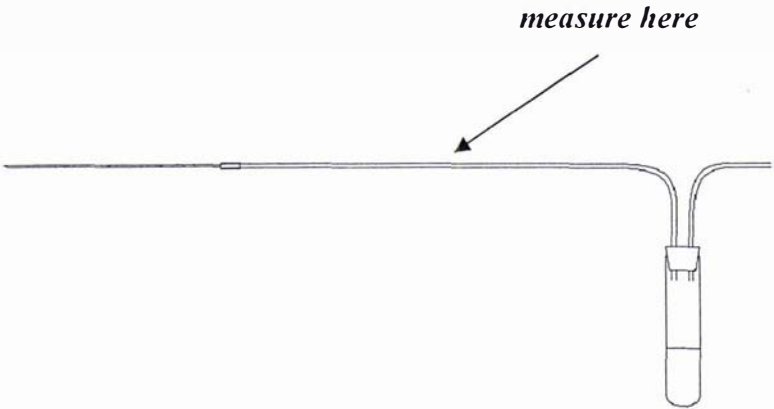
(c) In-follicle measurement

measure here
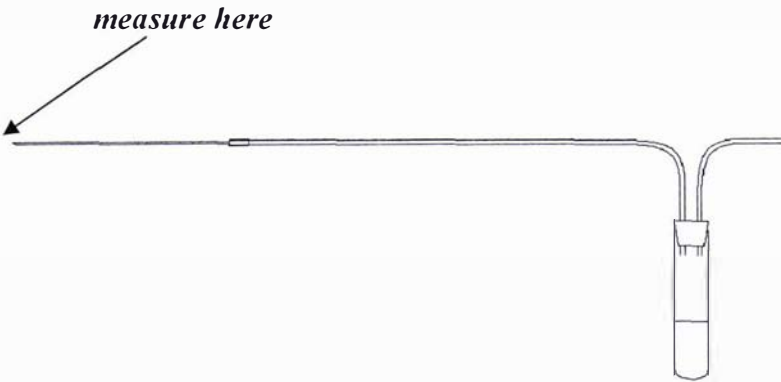
Figure 8.1   Suggested alternative approaches to the sampling and/or measurement of dissolved oxygen in follicular fluid.

8.2.1 System constraints

For any device to be appropriate for use in the IVF clinic, it must conform to a number of constraints. The constraints must consider technical, practical and safety issues. After considerable discussion with representatives from Fertility Associates Ltd., including doctors, nurses and administrators, the following constraints were arrived at. The system must,

- Present the sample to the measurement device with unchanged oxygen levels that are representative of those of the follicle of origin.
- Cause no increased risk of shear damage to the oocyte, compared to current IVF aspiration.
- Cause no increased toxicity risk to the oocyte, compared to current IVF aspiration.
- Meet clinical requirements for sterility.
- Be practical for clinical use.
- Be achievable within the limitations of available time and resources.

The requirement to deliver the sample to the measurement device with unchanged oxygen levels implies that the measurement device is capable of analysing the oxygen levels in the sample with appropriate accuracy and precision, and this will be assumed to be the case here. Previous work (see section 7.2.2) demonstrated that oxygen levels in follicular fluid are sufficiently unchanged before the bulk collection vial. However, blood contamination must also be eliminated if sample oxygen levels are to be unchanged. For in-line sampling, this could be achieved if flow down the tubing line is plug flow. If this is the case, fluid would be expected to present as slugs of clean follicular fluid and blood, becoming mixed, only once the collection vial is reached. Clean samples could then be obtained manually by sampling, only when fluid is visibly free of blood. This process could potentially be automated by using a sensor to detect blood contamination.

For in-line measurement, this problem could be simplified, as it is likely that slugs of follicular fluid and blood would give vastly different oxygen signals, making

287

differentiation between blood and follicular fluid possible using the same sensor that is analysing the oxygen levels. This requires that the response time of the sensor is sufficiently rapid. The sensor would need to rapidly produce a steady-state response to a follicular fluid slug before encountering a blood sample.

Such response times would likely need to be < 1s, which is difficult to achieve with a typical Clark-style oxygen electrode. More recently, fluorescence techniques have become commercially available that may be capable of rapid response times in this range. The requirement for rapid response becomes even more important if significant oxygen gradients exist within the follicular fluid. This would mean that the response times would need to be close to instantaneous, if the oxygen gradient profile in the fluid is to be reliably reproduced by the trace of the measurement device. Significant oxygen gradients in the follicular fluid may provide even more of a problem for the in-line sampling method. Here only a small portion of the fluid is drawn off for analysis, and if this fluid sample is not representative of the oxygen levels in the fluid the validity of the entire analysis must be questioned. However, the modelling work of Chapter 4 demonstrated that large oxygen gradients are unlikely to exist, and hence measurement or sampling in this way is justified. Ideally, the lack of oxygen gradients across the follicular fluid should be verified experimentally. Obtaining bulk values of follicular oxygen for comparison with other follicles greatly simplifies any attempts to measure follicular oxygen

In-follicle measurement could provide a way to completely overcome blood contamination, by measuring directly in the essentially undisturbed follicle. Such a device could then either make a point measurement of oxygen in the follicle or even map oxygen levels across the fluid space if desired.

For in-line sampling, the requirement of delivering an unchanged sample to the measurement device includes ensuring the oxygen levels in the sample remain stable, if there is to be a time delay before analysis.

The requirement to avoid additional shear damage to the oocyte during any modified IVF aspiration is obviously a very important one. If the oocyte is damaged then any

attempts to determine its quality through oxygen analysis are somewhat in vain. Of the three alternatives, in-line sampling provides the most potential for oocyte shear damage. This is because the oocyte could be potentially included in the sample, after which it would have to be expelled, thus exposing it to additional shear forces. Therefore the design of any sampling device should include ways to eliminate the possibility of the oocyte being sampled, or at the very least minimize the frequency of this occurrence. If it is possible that the oocyte will be sampled, then any sampling device should incorporate an opening wide enough to ensure the oocyte can travel freely through it. Failure to do so could result in the oocyte being punctured or compressed.

In-line sampling, in-line measurement and in-follicle measurement all have the ability to damage the oocyte by virtue of the fact they provide additional surfaces to which the oocyte is exposed and can therefore be punctured or entangled on. Entanglement may be a particular problem when the disperse nature of a cumulus-oocyte complex is considered. Therefore, any sharp protruding surfaces may be problematic. Any sampling system that includes valves may be particularly dangerous, as this could provide a site where the oocyte could become trapped or destroyed. Any unnecessary dead space should be avoided for the same reasons. Ultimately, whether a device provides any increased risk of shear damage to the oocyte needs to be tested thoroughly by experiment.

The requirement of no increased toxicity risk to the oocyte is also very important. However, standard tests are in place which determine whether a material is suitable for medical use, and, in particular, suitable for use in the proximity of oocytes/embryos. Ideally this issue can be avoided completely by constructing any device from materials which have already passed toxicity tests. Where this is not possible, the material(s) in question will require testing and modification if they do not meet requirements. In the case of in-line sampling, meeting such requirements should be readily achievable. The medical community takes blood samples from patients on a routine basis. If the sampling of follicular fluid is considered analogous to this, then meeting requirements through the use of the same or similar materials should be possible.

For in-line measurements and in-follicle measurements this matter is perhaps not quite as simple. Any measurement device is likely to be constructed of unique materials that will require testing. Having said that, Clark-style oxygen sensors are used within catheters for online blood gas measurement, as are fluorescence based probes. For in-follicle measurements toxicity must be considered, not only in relation to the oocyte, but also in relation to the patient, as the measurement device now resides *in-vivo*, and this may further complicate the implementation of this technology.

The sterility constraint requires that any sampling and/or measurement device needs to be capable of meeting the current requirements of sterile operation of IVF clinics. For an in-line sampling device, utilisation of pre-packaged sterile components such as syringes and catheters, or comparable re-usable sterilisable components, mean that this should be easily achieved. Collection of fluid samples from individual follicles may also mean that sampling devices need to be detached and re-attached throughout the duration of the pick-up. This will require that any sampling port is capable of sealing when this is taking place, so as to maintain the integrity of the sterile IVF kit by protecting it from atmospheric exposure.

In-line measurement and in-follicle measurement will likely see the measurement device in place for the duration of the procedure, and therefore these components will only need to be sterile at the outset. Measurement devices could, in theory, be disposable, and therefore only require sterile manufacture. However, in practice the relative expense of such components is likely to require them to be re-used from patient to patient. This means that any measurement device must be capable of withstanding cleaning and sterilisation. Auto-clave sterilisation is preferable, as this is a readily available facility to most IVF clinics. Traditional Clark-style electrodes are not auto-clavable and would therefore require sterilisation via less convenient methods, such as treatment with ethylene oxide or radiation methods. At least some oxygen measuring fluorescence probes are capable of being autoclaved, and may therefore be more desirable in this respect.

The constraint of practical clinical use requires that any device be capable of fitting

into the IVF clinic with minimal disruption or modification to current operating practices. In-line measurement and in-follicle measurement both have the potential to cause the least disruption to current clinical practice. These devices would presumably be in place before the procedure starts. During the procedure, data could be automatically logged for later analysis. Perhaps the biggest challenge would be the logistical exercise of keeping track of which data is relevant to which oocyte. Such logistics would also be required for in-line sampling, with the additional burden of taking a sample. This will be particularly cumbersome if manual sampling is to be employed. This would likely require the dedicated use of an extra pair of hands. Given that the IVF procedure usually involves a doctor at the needle end and a nurse at the collection vial end, there is very limited space for an additional operator to be involved in sample collection. It is of great importance that any sampling and/or measurement does not add significantly to the length of the time required for what is generally an unpleasant procedure for the patient. Any device must also be robust, such that failure is a virtual impossibility. Any leakage or other serious flaws could result in oocyte loss and/or compromise the continuation of the procedure. Discussions with Fertility Associates staff highlighted the desire to maintain current staffing requirements. Whilst any additional staffing requirements should be kept to a minimum, additional staffing requirements will be likely, whether through additional preparation and data analysis time or through the manual collection of samples. Practical clinical use is, however, of utmost importance. Any device that is to be cumbersome will simply not be used by clinic staff.

The constraint of achievability refers to the technological challenge of each of the proposed alternatives in relation to the available time and resources, as well as the short and long term goals of the program. The relative technological challenge presented by each alternative is clear cut. In-line sampling is the least challenging, followed by in-line measurement, with in-follicle measurement being the most technologically challenging alternative. Given that it has yet to be established that measuring follicular oxygen on a routine basis is worthwhile or desirable for IVF clinics, and that IVF clinics need to be convinced that measuring oxygen will provide them with some real advantage (such as an increase in the number of live births), the majority of the remainder of this chapter focuses on the design and testing of an in-

line sampling device intended for use in clinical trials (i.e. it may be foolhardy to devote substantial resource to developing challenging technology if a genuine need for this technology is yet to be established). If the results of clinical trials using such a device were to provide evidence that may convince IVF clinics that measuring oxygen is worthwhile, then further development of the in-line and in-follicle measurement alternatives would be appropriate.

8.2.2 In-line sampling device design and testing

In view of the constraints previously discussed, three alternative in-line sampling devices were proposed as depicted in Figure 8.2.

Each device was constructed to be capable of being placed in the IVF tubing line. It was intended that the follicular fluid flows through the device on its way to the bulk collection vial, during which time a sample of the desired volume is drawn off (the maximum sample volume is 1 ml in each case). The devices are placed in the tubing line, as it has previously been shown that follicular fluid oxygen levels are unchanged at this location.

Device A consists of a Perspex block inside which a length of silicon tubing is placed. The Perspex block also contains a slot and needle guide which was designed in this case to support a 1 ml Hamilton glass syringe (product no. 1001, Hamilton Company, Reno, NV, USA). The syringe is fitted with a 21 gauge needle having an internal diameter of 495 μm. The mean diameter of a human oocyte is 116 μm (Tsuji *et al.*, 1985), meaning that the syringe is easily large enough to accommodate the oocyte if it is mistakenly sampled. This is important, as a needle which is too narrow may result in oocyte deformation or fracture. The work done here also shows that the mean diameter of a bovine cumulus-oocyte complex is 4.5 oocyte diameters. Assuming the bovine system to be an appropriate model of the human system, and that the oocyte diameter is 116 μm, this equates to 520 μm. The maximum observed diameter of an oocyte-cumulus complex was 1100 μm. Because both of these values are greater than the internal diameter of the needle (495 μm) this suggests that syringe sampling will result in some deformation of the cumulus-oocyte complex. The internal diameter

of the needle of the standard IVF kit used in this investigation was 1100 μm^3. Whether by chance or design this suggests that even the largest cumulus-oocyte complexes will be able to travel down the IVF needle with a much smaller chance of deformation than the sampling device designed here. The small needle of device A may also result in the oocyte-cumulus complex becoming entangled on it, which could lead to oocyte loss. Some degree of cumulus deformation or loss is unlikely to be problematic, where as oocyte damage or loss is unacceptable. Therefore, whether or not any device presents a risk to the oocyte, needs to be established before any clinical work can proceed.

The internal diameter of the needle could be made larger to accommodate large cumulus-oocyte complexes. However, doing this comes at the cost of potential analytical errors due to the greater amount of air in the dead-space of the needle. Air in the dead-space of the syringes results in air bubbles in the sample. It is well established that such bubbles result in significant error in the analysis of oxygen in blood (Mueller *et al.,* 1976; Biswas *et al.,* 1982; Ishikawa *et al.,* 1974). Similar results have been observed in plasma (Mahoney *et al.,* 1991) and water (Scott *et al.,* 1971) suggesting that this will also be a problem in follicular fluid. Therefore, regardless of the fluid, it is prudent to strictly avoid such bubbles for reliable results. If bubbles are present they must be expelled immediately. To avoid bubbles the dead-space of the syringe can be flushed with a sterile fluid before sample. Ideally this fluid should be oxygen free. This will also result in a small error, however this will be much smaller than if the dead space contained gas. This is due to the fact that nitrogen and oxygen are both sparingly soluble in aqueous solutions, and therefore the liquid flushed deadspace will contain negligible amounts of gas which will have little effect on the gas composition of the bulk sample.

Device A was designed so that the needle punctures the silicon tubing, a sample is drawn, and the syringe subsequently removed. Upon syringe removal the silicon tubing reseals. This is extremely important as it protects the sterile integrity of the IVF kit between samples. It also ensures that when a sampling syringe is not in place and a vacuum is applied, no fluid is lost due to leakage. Again this is very important as fluid loss could potentially lead to oocyte loss.

Device A
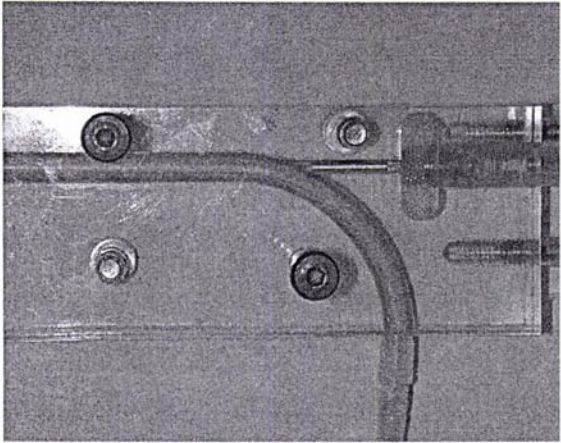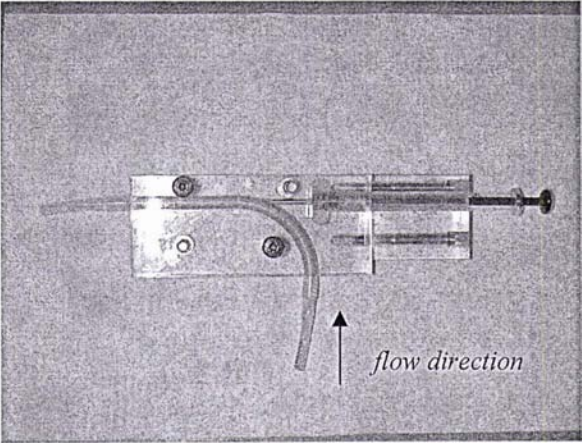
Device B
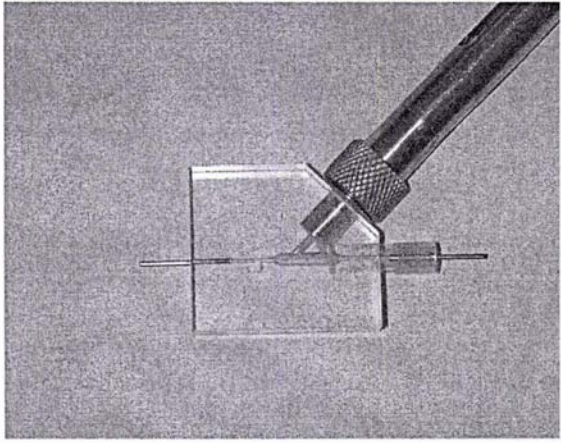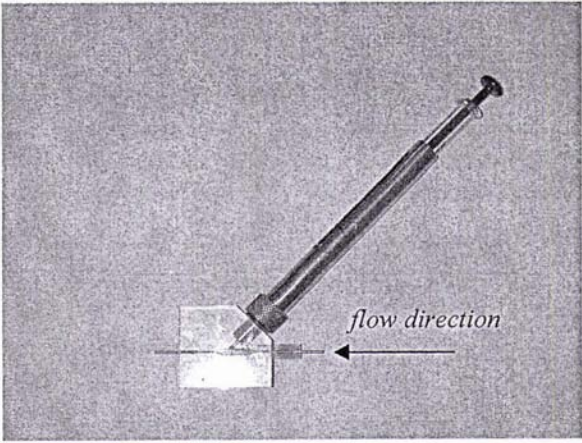
Device C

Figure 8.2   In-line sampling devices.

Device A also has a U bend in the silicon tubing line with the needle opening being aligned with the direction of flow. Both of these measures are intended to reduce the chance that the oocyte is sampled. Centrifugal force around the bend should guide the oocyte to the outer edge of the tubing away from the needle tip. The alignment of the needle opening with the direction of the flow makes it more difficult for the oocyte to be sampled by ensuring it is not propelled directly into this opening.
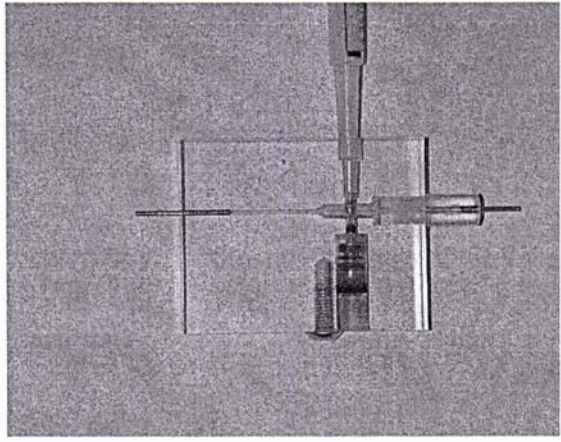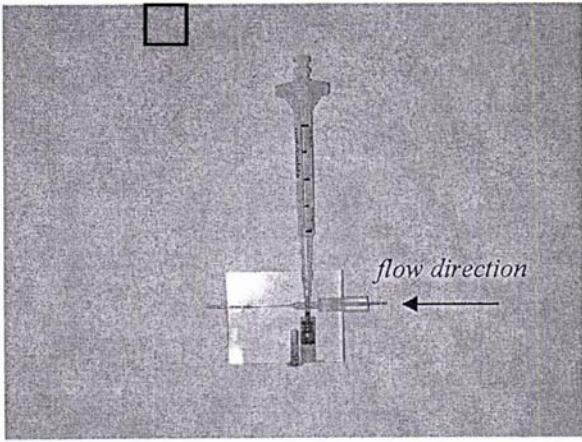
After sampling the fluid should be analysed as rapidly as possible, as permeation of oxygen from the atmosphere through the walls of the syringe and into the fluid could result in pre-analytical errors. The selection of a glass syringe helps to prevent this. The oxygen levels of water (Scott *et al.,* 1971) and blood (Mahoney *et al.,* 1991, Wu *et al.,* 1997) have been shown to be stable for longer periods when samples are drawn into glass as opposed to plastic syringes. To further reduce the changes in oxygen due to delays, samples can also be stored on ice. This has been shown to significantly stabilise the oxygen levels of blood (Biswas *et al.,* 1982; Beaulieu *et al.,* 1999). The metabolic oxygen consumption of white blood cells stored on ice is negligible (Eldridge & Fretwell, 1965; Fletcher & Barber, 1966), and this is likely to contribute to this stabilisation. Furthermore, the reduced permeability of materials to oxygen at lower temperatures is also likely to slow any significant changes in oxygen levels of samples stored on ice. If any cumulus or granulosa cells are present in a follicular fluid sample, storage on ice will likely slow the metabolism of these cells also, and hence stabilise the oxygen levels. It is, of course, absolutely essential that if the oocyte has been accidentally sampled, it is identified and removed before ice storage of the sample.

Both devices B and C have been designed with the same intention as device A, which is to obtain a follicular fluid sample with unchanged oxygen levels. These devices differ largely in the way they attempt to cope with the resealing of the sample port between samples. Device B is based on the concept of a catheter. It features a Perspex block through which the fluid flows. At an angle to the main line is a sample line which extends up to a needle guide. The needle guide can be readily detached, a rubber septum is placed at the base, and the needle guide refitted. This allows a Hamilton syringe to slide down the needle guide, at which point its needle punctures

the septum and the needle resides in the sample line. The rubber septum once again allows the resealing of the device in between samples. The angling of the sample port with the direction of bulk flow is once again intended to reduce the likelihood of oocyte sampling.

Device C is more mechanically complex. It features a flow-through Perspex block as per device B. The sample port is perpendicular to the direction of bulk flow and accommodates a 1.25 ml Eppendorf syringe (1.25 ml Combitips Eppendorf GmbH, Hamburg, Germany). The syringe is locked in place by pushing it against a stainless steel tube attached to a spring. Doing this introduces a hole in the stainless steel tubing into the main tubing line, allowing a sample to be drawn into the syringe. Upon syringe removal the spring is released, the stainless steel tube is moved up and the hole in it is no longer in the main tubing line, and hence the system reseals. Device C has the advantage of having no needle for the cumulus-oocyte complex to become entangled on. It has the disadvantages of not including any precautions to prevent oocyte sampling, the possibility of the oocyte being squashed by the spring mechanism, and incorporates a plastic syringe rather than a glass one. These issues could be resolved if this device was found to be worth pursuing.

To this point each device is largely concerned with obtaining a sample with unchanged oxygen levels, not causing any shear damage to the oocyte and maintaining the sterile integrity of the IVF kit through the ability to reseal between samples. It is advisable to test the performance of the devices in relation to these parameters. Once a device can satisfactorily meet these requirements it would then be considered appropriate to progress to addressing the other constraints which deal with material toxicity, the ability to be sterilised, and the practicality of clinical use and integration.

8.2.2.1 Sampling with unchanged oxygen levels

The ability of each device (A, B and C) to obtain a sample of follicular fluid with unchanged oxygen levels was investigated (see section 8.1 for methods).

Figure 8.3 shows the before and after sampling oxygen measurements in follicular fluid plotted against each other for all three devices. In each plot the solid straight line is $y=x$, upon which data would be expected to fall if no changes in oxygen levels were observed after sampling. For each device the data fell close to the $y=x$ line, which at first glance suggests that no major changes in dissolved oxygen have been caused by sampling. The exception to this is the marked outlier of Device B. When this measurement was made, significant bubbling in Device B was observed, presumably due to leakage in the rubber septum.

The distributions of the differences were inspected using normal quantile plots and histograms. For all three devices the distribution of the differences were normal, and hence a paired t-test could be used to examine whether or not the mean of the differences is significantly different from zero. For devices A, B (excluding bubbling run) and C it was found that there is no statistically significant difference between the before and after measurements ($p = 0.34$, $p = 0.25$ and $p = 0.20$ for devices A, B and C respectively).

Figure 8.4 shows a Bland-Altman plot for each of the three devices. Here the difference between the paired before and after measurements vs. their mean is plotted, a useful tool for assessing the agreement between two measurement methods (Bland & Altman, 1986). It is also useful for detecting any proportional bias between before and after measurements (Shaw *et al.,* 2001). A lack of bias is indicated by data scattered randomly about the mean line with the majority of data falling within the limits of $\pm 2SD$. The outlier of device B was excluded from Figure 8.4, from which it can be seen that no proportional bias seems to be apparent for any of the devices A, B and C.

This analysis suggests that all three devices are suitable for obtaining samples of follicular fluid unchanged, particularly if the explained outlier of device B is removed. Upon further investigation it was found that bubbling was a consistent problem with device B which became apparent after the rubber septum had been punctured multiple times. Such bubbling could potentially lead to leakage, and for this reason device B was discarded from any future analysis and deemed to be unsuitable for use in an IVF

clinic in its current state.

8.4.2.2 Sampling without shear damage to the oocyte

For the remaining devices, A and C, the effect of these devices on oocyte loss, and the shear forces placed on the cumulus-oocyte complex was investigated using the methods previously described in section 7.1.6.

Oocytes aspirated through device C were not always located immediately, and were recorded as lost. Subsequent runs would then often produce multiple oocytes. This indicated that the oocytes were being held up within the device. After a number of aspirations, visible build up of cellular material, presumably cumulus cells was observed on the internal surfaces of the sampling device. Device C was therefore deemed to be unsuitable for use in the IVF clinic and further investigation on this device ceased.

Of 170 aspirations through device A, 149 resulted in the oocyte proceeding directly through to the bulk collection tube as per normal IVF. The remaining 21 oocytes were located in the sample syringe. No oocytes were lost and no oocyte damage was observed. Thus there is no evidence that the oocyte is damaged more by sampling via device A than by normal IVF. This conclusion may be in part due to the small sample size (n=21) of sampled oocytes. Ideally a larger sample size would be required to determine the difference between damage caused by normal IVF aspiration and syringe sampling. However because oocyte sampling is essentially an event with a low probability (21/170 = 0.12), obtaining a sample size of 100 sampled oocytes would require an estimated 100/0.12 = 833 total aspirations. As this is only a prototype device, an investigation of that magnitude would be a waste of time and resources. For now it is sufficient to show that device A in its basic form is worthy of further development. Once a final device is arrived at, more stringent testing involving a larger sample size would be warranted, as it needs to be demonstrated beyond doubt that any device will not damage the oocyte before it is used in the IVF clinic.
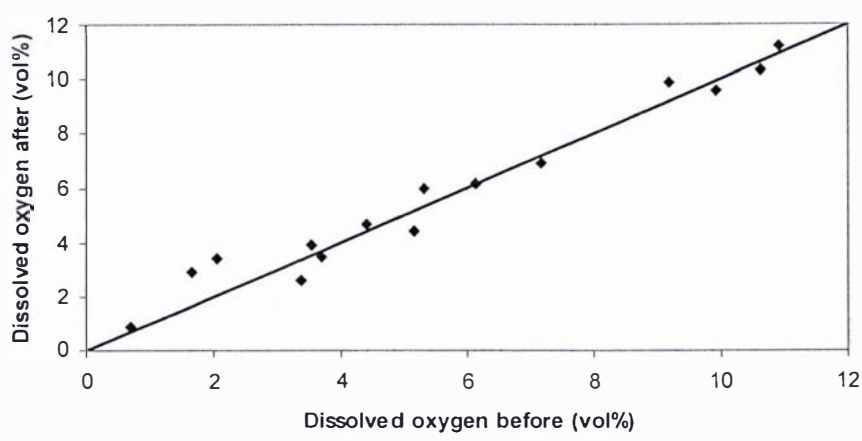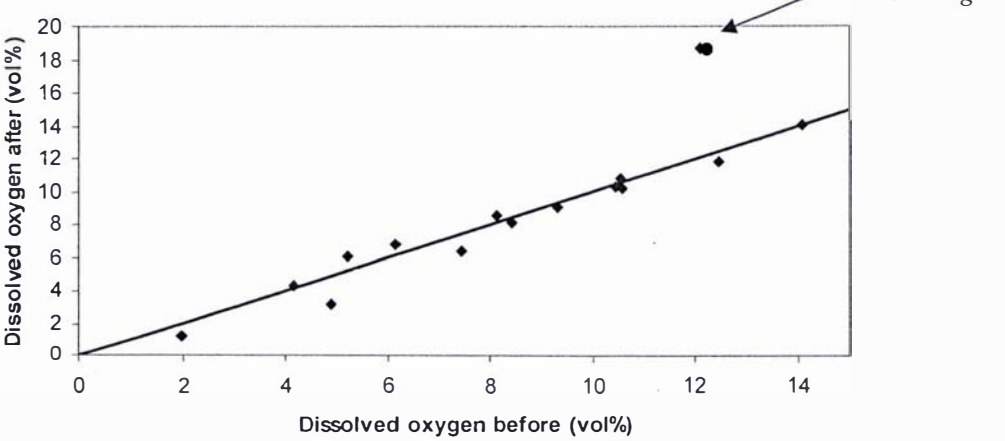
Figure 8.3   Dissolved oxygen levels before and after sampling using devices A, B, and C. In each case the solid line is that of $y=x$.

Device A
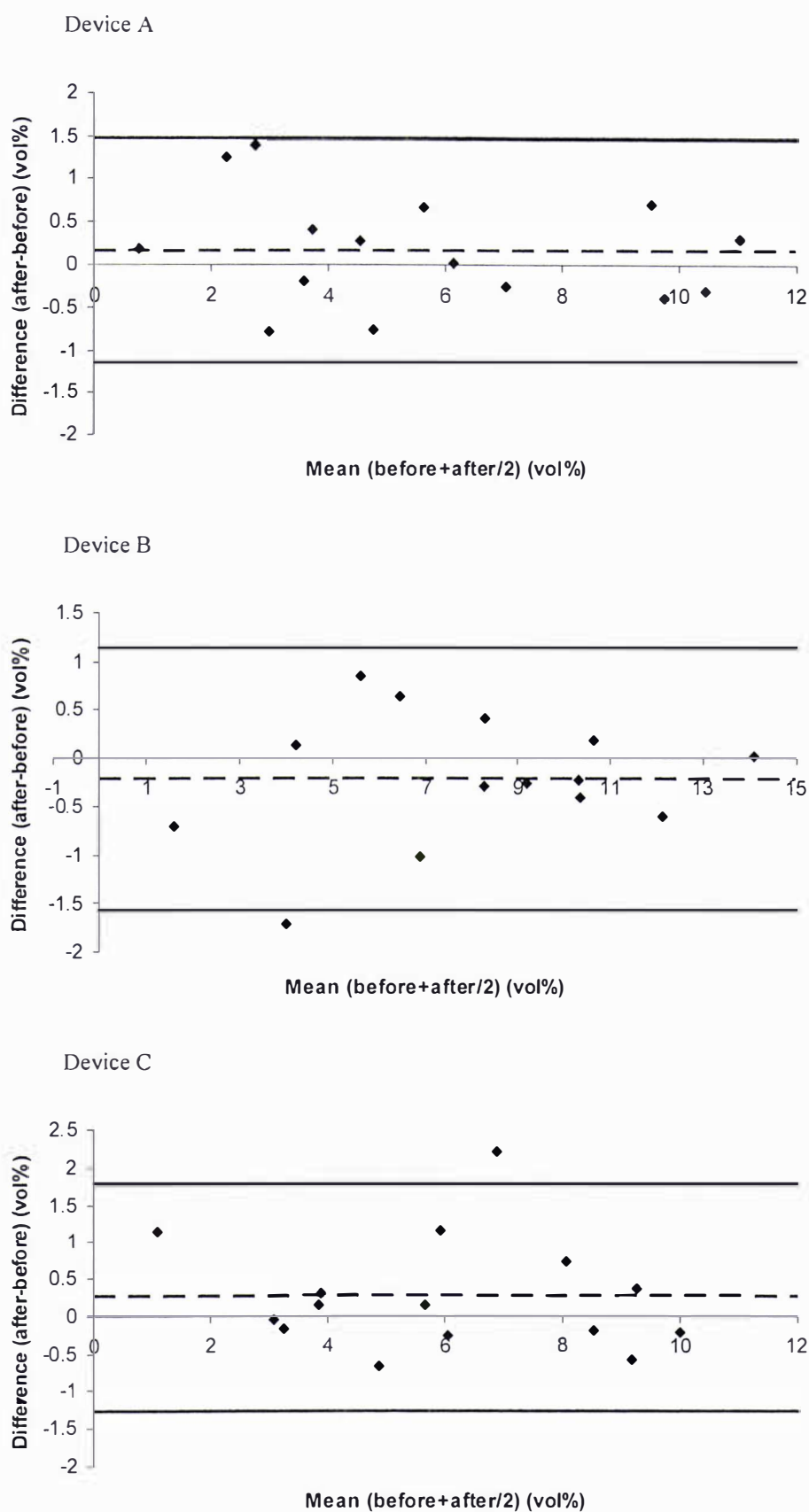
Device B

Device C

Figure 8.4   Bland-Altman Plots for devices A, B and C.

This investigation involved aspirating 5ml of follicular fluid from which a sample of 1ml was drawn, with the remaining 4ml being allowed to flow through to the bulk collection tube. If oocyte sampling was considered a random event, one would expect the probability of the oocyte appearing in any given sample to be $1/5 = 0.2$. In fact, as al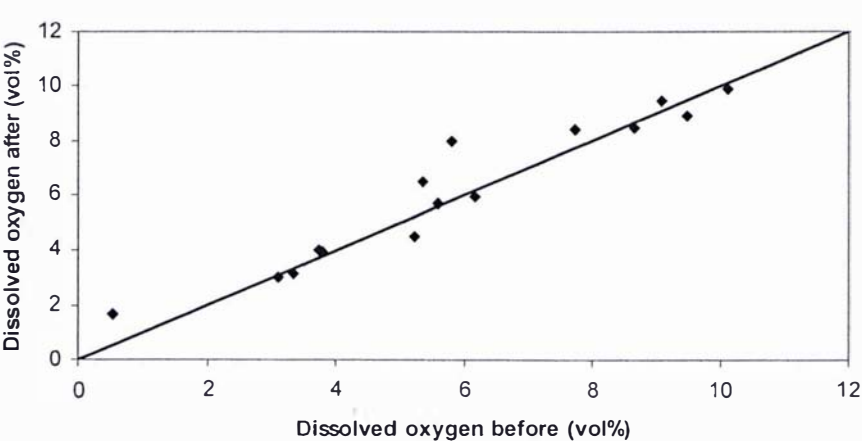ready stated, the experimentally determined probability was only 0.12. Testing whether or not 0.12 is significantly different from the theoretical value of 0.2 (Sokal & Rohlf, 1969) gives $p < 0.001$, indicating that the values are different. This suggests that the described design features of device A which were intended to reduce the likelihood of the oocyte being sampled have been effective in doing so.

Of the 21 cumulus-oocyte complexes that were located in the sample syringe, 14 were subjected to image analysis, and the parameters previously described were calculated. The important question to be answered here was whether or not there was a difference, in terms of the measured parameters, between normal aspiration and syringe sampling. For the large standard IVF sample the parameters total cumulus (cells + fluid), total cumulus (cells only), compact cumulus and expanded cumulus sphericity were determined to have non-normal distributions (Chapter 7). As a result Wilcoxons non-parametric paired t-test was used to investigate the difference between the paired data in Chapter 7. Because these parameters showed non-normal distributions for the standard IVF sample, a non-parametric test was also used to test whether or not the two data sets of standard IVF and syringe sampling were different. In this case the Mann-Whitney non-parametric test was appropriate (Sokal & Rohlf, 1969b).

The difference between the compact cumulus coverage and expanded cumulus coverage was previously tested using a test statistic for the difference between two proportions. This test is particularly inappropriate when one sample is small (Sokal & Rohlf, 1969), and hence the difference between these parameters for normal IVF (n=123) and syringe sampling (n=14) was not tested. For the remaining two parameters of voidage and compact cumulus sphericity which showed normal distributions, a two sample t-test comparing the difference between two means (Moore & McCabe, 1993) was used to investigate the difference between normal IVF

and syringe sampling. For the parameters total cumulus (cells + fluid), total cumulus (cells only), compact cumulus, and expanded cumulus, no evidence was found to reject the null hypothesis that normal IVF and syringe sampling are equal (p>0.05 in all cases). Hence for these parameters it can be stated that there is no evidence that syringe sampling causes any greater reduction in cumulus mass compared to normal IVF. The lack of difference may, in part, be due to the small sample size, but it would appear at this early prototype stage that a device based on the principles of device A is worthwhile pursuing.

A t-test for the difference between means for fluid voidage also revealed no significant difference between normal IVF and syringe sampling (p>0.05).

For the two remaining parameters, expanded and compact cumulus sphericity, significant differences were detected. Using the Mann-Whitney test it was found that there is evidence that the changes in expanded cumulus sphericity caused by normal IVF aspiration are not the same as those caused by syringe sampling (p<0.001). Similarly, using a t-test for the difference between means, it was found that the mean change in compact cumulus sphericity caused by normal aspiration was significantly different from that caused by syringe sampling (p<0.001).

Figure 8.5 shows the box plots for the distributions of the changes for normal IVF aspiration compared to syringe sampling, for compact cumulus sphericity (a) and expanded cumulus sphericity (b). These plots reveal that, for both compact and expanded cumulus, the distributions of differences in sphericity are closer to zero and generally less negative for syringe sampling, particularly for expanded cumulus. Although the syringe sampling distributions are skewed, it indicates that much of the data is positive. For normal IVF aspiration the distribution of differences for expanded cumulus is almost exclusively negative. Coupled with the knowledge that these differences are statistically significant, this suggests that syringe sampling can not only result in a smaller reduction in cumulus sphericity but can also act to increase it.

As previously discussed, the needle of the sampling syringe is smaller than the typical cumulus-oocyte complex. It is theorised here that when cumulus masses are drawn

down the sample needle, they are being deformed to the shape of the cylindrical needle. This is ultimately detected in the data as a more spherical appearance. In summary, apart from an increase in the sphericity of the cumulus cells, device A appears not to have a major impact on the cumulus-oocyte complex.

More samples are desirable to verify this difference, but such work should be left until a final design has been arrived at. Device A is also capable of sampling follicular fluid with unchanged oxygen levels. For these reasons it is recommended that a device based on the principles of device A be further developed through to the stage where it can be used in the IVF clinic.

8.2.3 From prototype to clinic

Taking a promising device from the prototype stage through to the stage of real life clinical use requires consideration of the remaining system constraints. Namely, the device needs to be constructed from non-toxic materials, to be sterilisable, and practical for clinic use. Furthermore, any device which meets these requirements will need to be re-tested to ensure that it does not change oxygen levels, damage the cumulus-oocyte complex, and is capable of maintaining a seal between the ambient environment and the sterile environment of the IVF kit.

Achieving all of this is no small task, and as a result it has been the subject of a Master's degree in bioprocess engineering (Harding, 2005). The work of this Master's thesis had two objectives. Firstly to take a follicular fluid sampling device from the prototype stage through to a state where it is suitable for use in IVF clinical trials. And secondly to use this device to measure oxygen levels in the follicular fluid of women.

(a) Compact Cumulus Sphericity
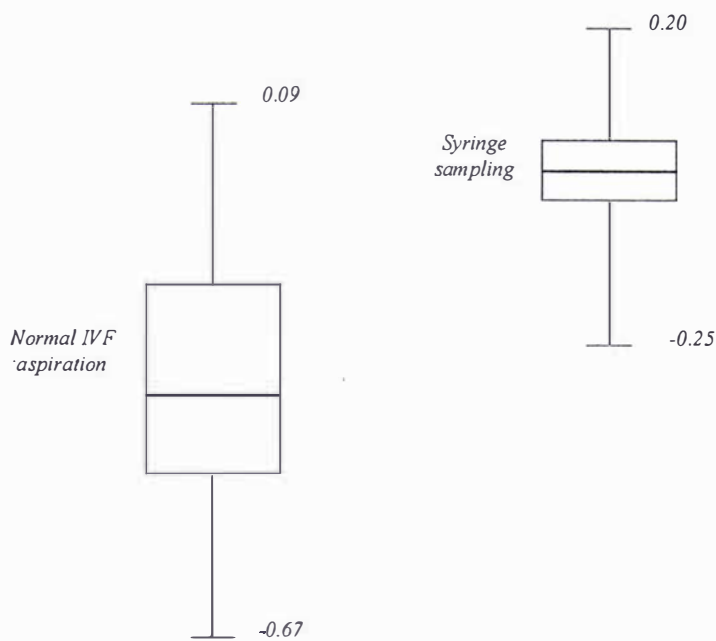
(b) Expanded Cumulus Sphericity
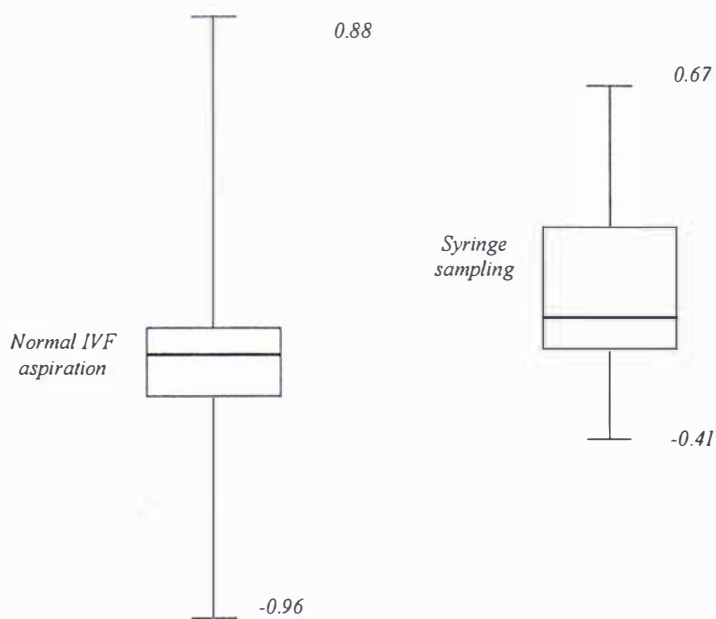
Figure 8.5   Box plots of differences (after aspiration-before) for cumulus sphericity, for normal IVF and syringe sampling. Adjacent box plots are on common scale which is defined by the whiskers. Whiskers represent range, with the box showing upper and lower quartiles, as well as the median.

Figure 8.6 depicts the device designed for clinic use. The device consists of a small stainless steel guide surrounding a short length of silicon tubing. The device is designed to take an 18 gauge needle through the needle guide. The needle punctures the tubing and is fitted with a glass luer-tip 1ml tuberculin syringe (Popper & Sons Inc, New York, USA) through which a sample is drawn. The basic principle of the device is therefore similar to device A. This device is much more easily assembled than device A due to the removal of the Perspex block. It is also readily sterilisable, and has been constructed from materials which passed embryo toxicity tests. The device is also considerably lighter, and less bulky, therefore allowing it to be more easily incorporated into the IVF procedure for which space is at a premium.

Aside from these improvements there are several key differences between this device and device A. Firstly the bend in the tubing has been removed. It is possible that this may undesirably increase the frequency with which the oocyte is sampled. Secondly, the 21 gauge needle has been replaced with an 18 gauge needle. This will mean that a greater portion of cumulus-oocyte complexes will easily fit down the needle which could result in reduced shear stress. However, the increased dead volume of this needle may make it more difficult to obtain a sample with unchanged oxygen levels. Finally, the device has been designed so that the needle remains in place between samples with the syringe barrel being swapped over. This means that there will be periods of time between samples where the IVF kit will be open to the unsterile atmosphere. Furthermore, if a syringe barrel is not in place (for example if sampling has ceased but further follicles are to be aspirated) and aspiration continues fluid may flow out the unsealed sample port, which could result in oocyte loss. The reason the device was designed in this way was to avoid multiple punctures of the silicon tubing, in the fear that this may lead to leakage. If this was deemed to be the best approach to sampling, the whole device could be designed as a single solid structure incorporating a needle guide and flow through cell, with the silicon tubing discarded. Such a device could be completely constructed from stainless steel, glass or some suitable material.

As already stated, having modified the device, the next step would be to perform rigorous re-testing to ensure the device did not change oxygen levels and did not cause any shear damage to the oocyte over and above normal aspiration.
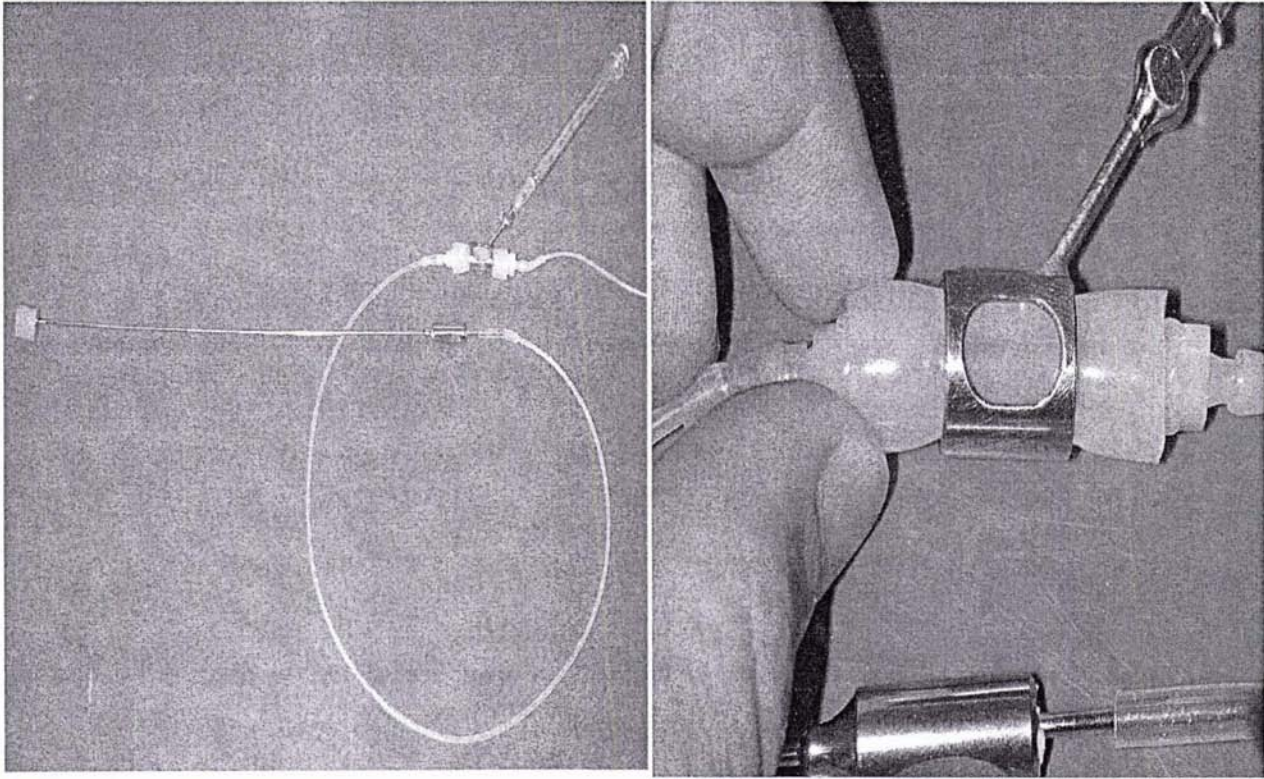
305

Figure 8.6   The improved sampling device (taken from Harding, 2005).

Unfortunately, the ability of the improved device to sample follicular fluid oxygen unchanged was not tested. The impact of the device on the shear forces placed on the oocyte was indirectly examined. Rather than using real cumulus-oocyte complexes and the semi-quantitative analysis described in this work, a simplified qualitative procedure was employed. Nineteen fibrinogen clots were cut into 3mm lengths, aspirated and sampled using the improved device. A qualitative visual assessment was then made as to whether the clot had been damaged by comparing before and after photographs. Typical before and after images are shown in Figure 8.7.

The author concluded that the clots were not damaged by taking into account their size. It appears from Figure 8.7 that the clot seems to have undergone significant deformation. The idea behind this work was that the fibrinogen clots were larger and more brittle than cumulus-oocyte complexes, and therefore if they were not damaged it would be unlikely that the cumulus-oocyte complex would be. This logic is sound, but the deformation observed in figure 8.7 suggests that these clots are not particularly brittle. It is recommended here that this device be more rigorously tested for cumulus-oocyte damage, using a better model system (for example, real cumulus-oocyte complexes), before this device is used substantially in the clinic. Doing so will reduce the need to speculate and infer from one system to another, and allow the clearer identification of any risks before clinical use.

The 18-gauge needle used to aspirate the fibrinogen clots pictured in Figure 8.12 has an internal diameter of 0.838 mm. Before aspiration the clot was jagged and would not fit between the rungs of the mm scale shown. After aspiration it was uniform and of similar thickness to the mm scale, and indeed the 0.838 mm internal diameter of the needle through which it was drawn. It is suggested here that the clot may have been compressed uniformly by the needle it was drawn down. This is a phenomenon similar to the suggested reason for the increase in sphericity of the cumulus masses aspirated in this work. Although speculative, these two independent results lend support to the idea of the needle deforming objects which are drawn through it. It also suggests that the fibrinogen clots may be more deformable than brittle.
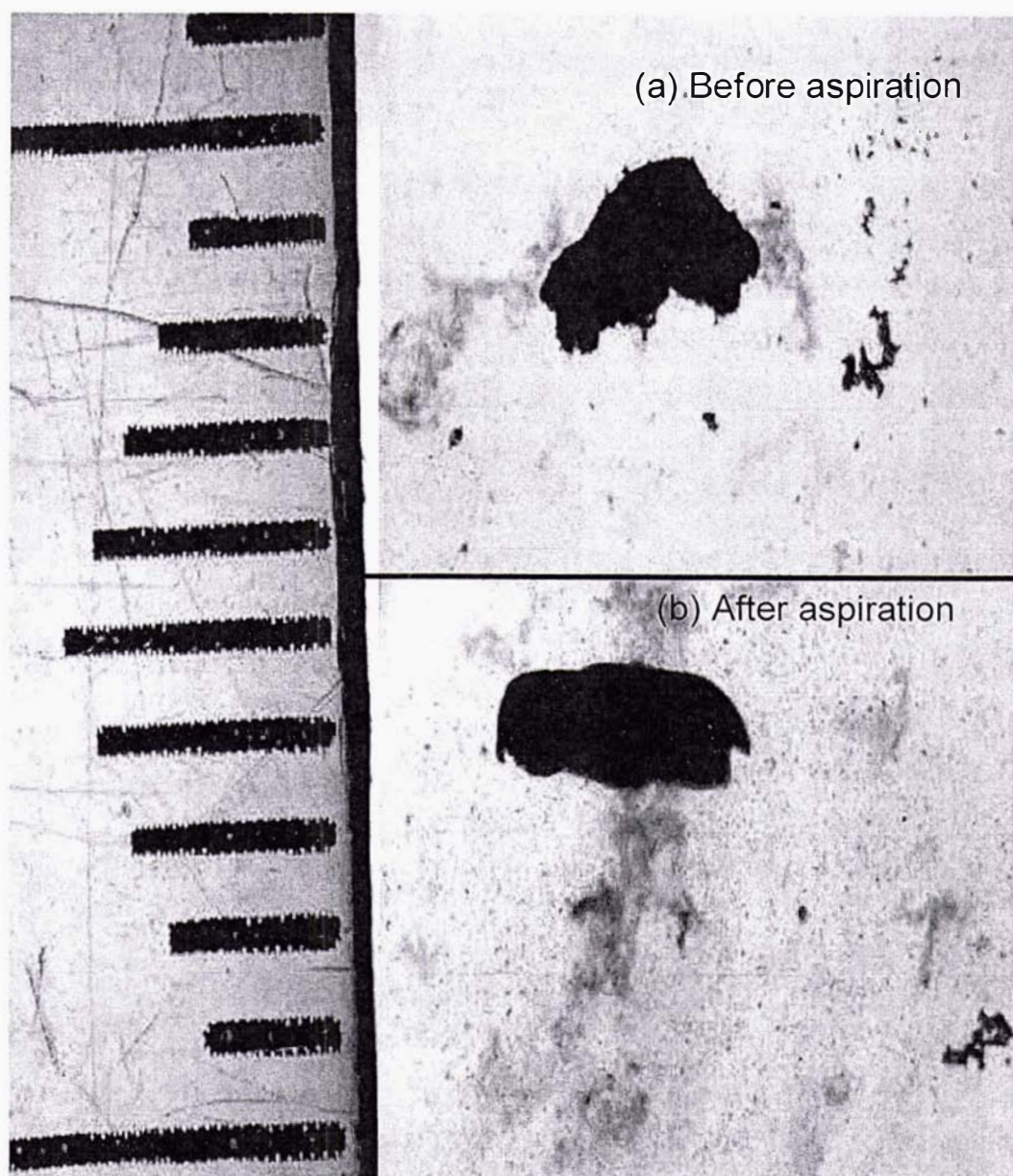
Figure 8.7   Typical fibrinogen clots before and after aspiration (taken from Harding 2005). Divisions on scale = 1 mm.

The improved sampling device was tested in the clinic. It did not perform adequately with leakage and bubbling being observed. The reason the device failed seems to be due to failure to appropriately test the system in the laboratory. The failure of the device greatly eroded the confidence of the clinicians involved in the concept of sampling follicular fluid for subsequent analysis, and no oxygen measurements have been made to date.

8.2.4 In-line measurement

As in-line sampling seems unlikely to get off the ground, the wider program of which this thesis is a part has shifted focus to in-line measurement. As well as the advantages already discussed which in-line measurement offers, it seems to also be met with more favour by clinicians.

Although clinical use is likely some time away, preliminary results (Figure 8.8) show some promise. Figure 8.8 shows the results of oxygen measurement before and after aspiration, using a fluorescence probe (Collier, Personal Communication, 2006). The data seems to be quite linear but are uniformly off-set from the $y=x$ line. This is believed to be due to the oxygen in the tubing line, which is more readily detected by the more precise fluorescence probe. This issue can likely be resolved by the use of tubing with reduced oxygen permeability. The concept of in-line measurement has been made possible by the recent commercial availability of suitable oxygen fluorescence probes. These probes appear to be more reproducible than traditional Clark-style electrodes and have reduced response times. All the constraints will once again have to be resolved, but this seems to be at least the short term future of oxygen measurement in follicular fluid.
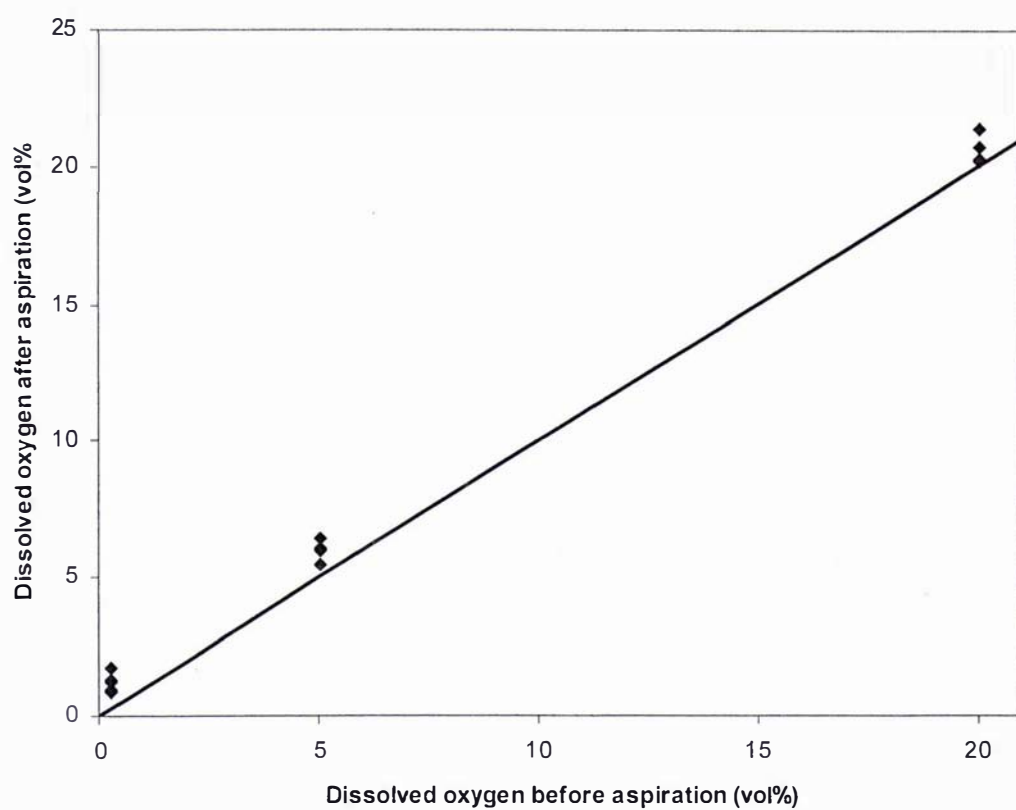
Figure 8.8   Oxygen before and after aspiration as measured by an in-line fluorescence probe (Collier, personal communication).

8.3   Conclusions and recommendations

A prototype in-line follicular fluid sampling device (Device A) did not appear to result in any major increase in cumulus cell stripping when compared with normal IVF aspiration. The sampling device did however deform the cumulus-oocyte to a more spherical shape. This was likely due to the diameter of the needle sampling port being smaller than some cumulus-oocyte complexes. At this prototype stage it appears that an in-line sampling device could be used in an IVF clinic without resulting in any increased risk to the oocyte, and hence the patients chance of a successful outcome.

The same sampling device could also be used to sample follicular fluid with unchanged oxygen levels, provided the sample is free of blood contamination. Blood contamination can potentially be avoided during in-line sampling if flow down the tubing line is plug flow. Blood contamination is an issue that needs to be dealt with if analysis of follicular fluid dissolved oxygen levels are to be incorporated into the IVF clinic.

Trials of in-line sampling devices in the IVF clinic proved to be unsuccessful due to failure to appropriately simulate the IVF aspiration process in the laboratory. As a result, clinicians' confidence in an in-line sampling device appears to have been eroded to the point that it is unlikely such a device will be used in the IVF clinic.

The immediate future of dissolved oxygen analysis may involve in-line measurement using a fluorescence oxygen probe. Early work with such a device is promising from an analytical viewpoint, and the concept of in-line measurement seems to be favoured by clinicians.

Chapter 9.   Conclusions and recommendations

In contrast to the previous work of Gosden & Byatt-Smith (1986), this work has shown that it is likely that oxygen can reach the oocyte in the pre-antral follicle. This is largely due to improved estimates of oxygen diffusivity through the granulosa cell layer, and the inclusion of fluid voidage.

Whether or not oxygen actually reaches the oocyte in the pre-antral follicle will depend on the follicle size, voidage, and degree of vascularisation. The distribution of vascularisation also plays a role, with symmetrically distributed vascularisation resulting in a more even oxygenation of the follicle, as well as more total oxygen in the follicle.

Regardless of follicle size, voidage, and vascularisation, the follicle will eventually reach a size beyond which it cannot grow without becoming at least partially anoxic. This work has demonstrated that antrum formation represents a way in which the follicle can continue to grow, and yet avoid the formation of anoxic regions. Comparison of predictions to published data has shown that the growing human antral and pre-ovulatory follicles increase their size in such a way that is consistent with overcoming the formation of anoxic regions.

Specific model predictions are that oocyte respiration will become sub maximal at follicular fluid volumes below approximately 4ml, vascularisation levels below 38%, or fluid dissolved oxygen levels below 5.1 vol%. These values are consistent with observations in the literature.

Mathematical modelling also indicated that oxygen gradients across the fluid antrum are negligible except in the vicinity of the oocyte or cumulus-oocyte complex. The oxygen concentration in the follicular fluid can be assumed to be at one representative bulk concentration. This assumption simplifies the practical analysis of dissolved oxygen in follicular fluid.

This work has also shown that the dissolved oxygen levels in the follicular fluid can provide a simple measure of the respiratory status of the oocyte. The measurement of follicle vascularisation can also be used to achieve this but requires knowledge of additional parameters, and is therefore considered inferior to the measurement of dissolved oxygen levels in follicular fluid.

The predictions of the mathematical modelling described in this thesis are limited by the accuracy and precision of the parameter values used. In an effort to improve the predictions of the model, measurements of follicular fluid oxygen diffusivity and solubility were carried out. These had not been previously measured, and the quantification of these parameters allowed the uncertainty of the predictions to be reduced.

Having established the potential value of the measurement of dissolved oxygen levels in follicular fluid, this work then focused on the practical aspects of measuring oxygen in fluid collected from IVF patients. It was demonstrated that IVF aspiration causes significant changes in the dissolved oxygen levels of follicular fluid. As a result, follicular fluid sampling and/or measurement must be carried out before the collection vial is reached, if changes in oxygen levels are to be avoided.

It was also demonstrated that IVF aspiration causes changes in the pH and temperature of follicular fluid, as well as morphological changes in the cumulus-oocyte complex.

The design of a device which is capable of sampling follicular fluid with unchanged oxygen levels was detailed. This device performed poorly when an attempt was made to use it in a clinic, and it is unlikely to be used on a regular basis in IVF clinics.*

Preliminary investigation into in-line measurement of follicular fluid dissolved oxygen levels was promising, and this may be at least the short term future for analysis of dissolved oxygen in follicular fluid. Ultimately, any device which intends to find its way into common clinical use will need to overcome many constraints. The most important of these is being robust and practical enough to fit in with daily

313

clinical practice.

Future experimental work aimed at gaining improved parameter estimates is recommended. This will improve the quality of information obtained from the models. In particular, studies into the oxygen consumption kinetics of the oocyte would be beneficial. Knowledge of how the oxygen consumption of the oocyte changes with time, and how various oxygen levels impact on the oocyte, will allow the model to be used to investigate the implications on follicle development.

The pursuit of dissolved oxygen measurement in follicular fluid appears to be worthwhile. Therefore, it is recommended that progress toward its measurement continues, at least for use in clinical trials. There is no substitute for real world data.

Ultimately the relationship between follicular fluid oxygen levels and oocyte health needs to be conclusively established. If it is established that it would be beneficial to measure follicular fluid dissolved oxygen routinely, then its analysis needs to reach the point where it can be seamlessly integrated into clinical routine. This will likely be a challenging exercise. If appropriate, standard oxygen ranges which relate to oocyte viability should be produced and used in the clinic.

Dissolved oxygen measurement in clinical practice must meet a number of constraints. Arguably, in-line measurement and in –follicle measurement are the best methods to achieve this. However, an in-line sampling device was developed because it is the least challenging technically. Three designs were initially tested of which device A proved the best in laboratory tests. Attempts by another investigator in a separate Master's project to use a similar device in an IVF clinic failed. The result was an undermining of clinician confidence in in-line sampling. Subsequently, it is unlikely to be pursued further.

Chapter 10.   References

Agarwal A, Gupta S, Sharma RK. Role of oxidative stress in female reproduction. Reproductive Biology and Endocrinology, 3, 28-49, 2005.

Akgerman A, Gainer JL. Predicting gas-liquid diffusivities. Journal of Chemical and Engineering Data, 17, 372-377, 1972.

Akita K. Diffusivities of gases in Aqueous Electrolyte Solutions. Industrial and Engineering Chemistry Fundamentals, 20, 89-94, 1981.

Almeida PA, Bolton VN. The effect of temperature fluctuations on cytoskeletal organisation and chromosomal constitution of the human oocyte. Zygote, 3, 357-365, 1995.

Arain S, Weiss S, Heinzle E, John GT, Krause C, Klimant I. Gas sensing in microplates with optodes: Influence of oxygen exchange between sample, air, and plate material. Biotechnology and Bioengineering, 90, 271-280, 2005.

Attaran M, Pasqualotto E, Falcone T, Goldberg JM, Miller KF, Agarwal A, Sharma RK. The effect of follicular fluid reactive oxygen species on the outcome of in vitro fertilization. International Journal of Fertility and Womens Medicine, 45, 314-320, 2000.

Barroso G, Barrionuevo M, Rao P, Graham L, Danforth D, Huey S, Abuhamad A, Oehninher, S. Vascular endothelial growth factor, nitric oxide, leptin follicular fluid levels correlate negatively with embryo quality in IVF patients. Fertility and Sterility, 72, 1024-1026, 1999.

Battino R, Rettich TR, Tominaga T. The solubility of oxygen and ozone in liquids. Journal of Physical Chemical Reference Data, 12, 163-178, 1983.

Beaulieu M, Lapointe Y, Vinet B. Stability of pO_2, pCO_2, and ph in fresh blood samples stored in a plastic syringe with low heparin in relation to various blood-gas and hematological parameters. Clinical Biochemistry, 32, 101-107, 1999.

Bhal P, Pugh N, Chui D, Gregory L, Walker S, Shaw R. The use of transvaginal power doppler ultrasonography to evaluate the relationship between perifollicular vascularity and outcome in in-vitro fertilization treatment cycles. Human Reproduction, 14, 939-945, 1999.

Biswas CK, Ramos JM, Agroyannis B, Kerr DNS. Blood gas analysis: effect of air bubbles in syringe and delay in estimation. British Medical Journal, 284, 923-927,1982.

Bland JM, Altman DG. Statistical methods for assessing agreement between two methods of clinical measurement. Lancet, 8476, 307-310, 1986.

Bols PEJ, Van Soom A, Ysebaert MT, Vandenheede JMM, de Kruif A. Effects of aspiration vacuum and needle diameter on cumulus oocyte complex morphology and developmental capacity of bovine oocytes. Theriogenology, 45, 1001-1014, 1996.

Bols PEJ, Ysebaert MT, Van Soom A, de Kruif A. Effects of needle tip bevel and aspiration procedure on the morphology and developmental capacity of bovine compact cumulus oocyte complexes. Theriogenology, 47, 1221-1236, 1997.

Brinsden PR. (Ed) A Textbook of In Vitro Fertilization and Assisted Reproduction (3rd Ed.), Taylor & Francis, Oxford, 2005.

Broviczeny KG, Dintenfass L, Fukada E, Harkness J, Lewis SM, Phillips MJ, Rewald E, Ruhenstroth-Bauer G, Shukla JB, Verwilghen RL, Seaman GVF, Schmid-Schonbein H, De Clark F. Recommendation for a selected method for the measurement of plasma viscosity. Journal of Clinical Pathology, 37, 1147-1152, 1984.

Chiang SH, Toor, HL. Interfacial resistance in the absorption of oxygen by water. AIChE Journal, 5, 165-168, 1959.

Choi Y, Okos MR. Effects of Temperature and composition on the thermal properties of foods. In, Food Engineering and Process Applications (Vol. 1), Jelen P (Ed.), Elsevier Applied Science, London, 1986.

Christoforides C, Laasberg LH, Hedley-White J. Effect of temperature on solubility of O_2 in human plasma. Journal of Applied Physiology, 26, 56-60, 1969.

Chui D, Pugh N, Walker S, Shaw R. Follicular vascularity - the predictive value of transvaginal Doppler ultrasonography in an in-vitro fertilization programme: a preliminary study. Human Reproduction, 12, 191-196, 1997.

Clark AR, Stokes YM, Lane M, Thompson JG. Mathematical modelling of oxygen concentration in bovine and murine cumulus-oocyte complexes. Reproduction, 131, 999-1006, 2006.

Clerbaux TH, Gustin P, Detry B, Cao ML, Frans A. Comparative study of the oxyhaemoglobin dissociation curve of four mammals: man, dog, horse and cattle. Biochemistry and Physiology A-Physiology. 106A, 687-694, 1993.

Cohen J, Avery S, Campbell S, Mason BA, Riddle A, Sharma V. Follicular aspiration using a syringe suction system may damage the zona pellucida. Journal of in Vitro Fertilization and Embryo Transfer. 3, 224-226, 1986.

Cohen J. Organs of Reproduction. In, Reproduction, Butterworths, London, 1977.

Collier W. Personal communication. Food and Health, AgResearch Grasslands, Private Bag 11008, Palmerston North, New Zealand.

Daniel SA, Armstrong DT, Gore-Langton RE. Growth and development of rat oocytes in vitro. Gamete Research, 24, 109-121, 1989.

Cussler EL. Measurement of Ternary diffusion. In, Multicomponent Diffusion, Churchill SW (Ed.), Elsevier Scientific Publishing Company, Amsterdam, 1976.

Delforge JP, Thomas K, Roux F, De Siqueira JC, Ferin J. Time relationships between granulosa cells growth and luteinization, and plasma luteinizing hormone discharge in human.1. A morphometric analysis. Fertility and Sterility, 23, 1-11, 1972.

Dhar A, Dockery P, Turner K, Lenton EA, Cooke ID. The human ovarian granulosa cell: a stereological approach. Journal of Anatomy, 188, 671-676, 1996.

Dionne KE, Colton CK, Yarmush ML. A microperifusion system with environmental control for studying insulin secretion by pancreatic tissue. Biotechnology Progress, 7, 359-368, 1991.

Dittmer DS, Grebe RM (Eds.). Handbook of Respiration, pg. 7, Saunders, Philadelphia, 1958.

Duda JL, Vrentas JS. Laminar liquid jet diffusion studies. AIChE Journal, 14, 286-294, 1968.

Duncan WW, Glew MJ, Wang XJ, Flaherty SP, Matthews CD. Prediction of in-vitro fertilization rates from semen variables. Fertility and Sterility, 59, 1233-1238, 1993.

Dutta A, Popel AS. A theoretical analysis of intracellular oxygen diffusion. Journal of Theoretical Biology, 176, 433-445, 1995.

Edwards RG. Follicular Fluid. Journal of Reproduction and Fertility, 37, 189-219, 1974.

Eldridge F and Fretwell LK. Change in oxygen tension of shed blood at various temperatures. Journal of Applied Physiology, 21, 790-792, 1965.

Ferrell RT, Himmeblau DM. Diffusion coefficients of nitrogen and oxygen in water. Journal of chemical and engineering data, 12, 111-115, 1967.

Findlay ALR. The development of reproductive function.. In, reproduction and the Fetus, Edward Arnold (Publishers) Ltd., 1984.

Fisch B, Goldberg I, Ovadia J, Tadir Y. Physiochemical properties of follicular fluid and their relation to in vitro fertilization (IVF) outcome. Journal of in Vitro Fertilization and Embryo Transfer, 7, 67-73, 1990.

Fischer B, Kunzel W, Kleinstein J, Gips H. Oxygen tension in follicular fluid falls with follicle maturation. European Journal of Obstetrics Gynaecology and Reproductive Biology, 43, 39-43, 1992.

Fletcher G, Barber JL. Effect of sampling technique on the determination of paO_2 during oxygen breathing. Journal of applied physiology, 21, 463-468, 1966.

Fournier RL. Oxygen Transport in Biological Systems. In, Basic Transport Phenomena in Biomedical Engineering, Taylor and Francis, Philadelphia, 1998.

Fournier RL. The physical and flow properties of blood. In, Basic Transport Phenomena in Biomedical Engineering, Taylor and Francis, Philadelphia, 1998b.

Fraser I., Baird D, Cockburn F. Ovarian venous blood pO_2, pCO_2, and pH in Women. Journal of Reproduction Fertility, 33, 11-17, 1973.

Friedman CI, Seifer DB, Kennard EA, Arbogast L, Alak B, Danforth DR,. Elevated level of follicular fluid vascular endothelial growth factor is a marker of diminished pregnancy potential. Fertility and Sterility, 70, 839-839, 1998.

Fry RC, Simpson TL, Squires TJ, Miles MA, Niall E. Oocyte recovery is influenced by needle type and aspiration pressure. Presented at the Australian Society for Reproductive Biology 25th annual conference, 1993.

Goldstick TK, Ciuryla VT, Zukerman L. Diffusion of oxygen and blood. Advanced Experimental Medical Biology, 75, 183-190, 1976.

Gosden RG, Byatt-Smith JG. Oxygen concentration gradient across the ovarian follicular epithelium: model, predictions and implications. Human Reproduction, 1, 65-68, 1986.

Gosden RG, Hunter RHF, Telfer E, Torrance C, Brown N. Physiological factors underlying the formation of ovarian follicular fluid. Journal of Reproduction and Fertility, 82, 813-825, 1988.

Gregory L, Leese HJ. Determinants of oocyte and preimplantation embryo quality: metabolic requirements and the potential role of cumulus cells. JBFS 1(2), Hum. Reprod.11 Natl. Suppl., 96-102, 1996.

Gull I, Geva E, Lerner-Geva L, Lessing JB, Wolman I, Amit A. Anaerobic glycolysis - the metabolism of the preovulatory human oocyte. European Journal of Obstetrics Gynaecology and Reproductive Biology, 85(2), 225-228, 1999.

Gwatkin RBL, Haidri AA. Oxygen requirements for maturation of hamster oocytes. Journal of Reproduction Fertility, 37, 127-129, 1973.

Hahn CEW. Electrochemical analysis of clinical blood-gas, gases and vapours. The Analyst, 123, 57R-86R, 1998.

Harding HA. Product development specifications for a follicular sampling device for use in a human in-vitro fertilisation clinic. Thesis for the degree of Masters of Engineering, Massey University, Palmerston North, 2005.

Hashimoto S, Minami N, Takakura R, Yamada M, Imai H, Kashima, N. Low oxygen tension during in vitro maturation is beneficial for supporting the subsequent development of bovine cumulus-oocyte complexes. Molecular Reproduction and Development, 57, 353-360, 2000.

Hills BA. Respiration of tissue as a medium of heterogeneous permeability. Bulletin of Mathematical Biophysics, 32, 219-235, 1970.

Ho CS, Ju L, Baddour RF, Wang DIC. Simultaneous measurements of oxygen diffusion coefficients and solubilities in electrolyte solutions with a polarographic oxygen electrode. Chemical Engineering Science, 43, 3093-3107, 1988.

Horne R, Bishop CJ, Reeves G, Wood C, Kovacs GT. Aspiration of oocytes for in-vitro fertilization. Human Reproduction Update, 2, 77-85, 1996.

Houghton FD, Thompson JG, Kennedy CJ, Leese HJ. Oxygen consumption and energy metabolism of the early mouse embryo. Molecular Reproduction and Development, 44, 476-485, 1996.

Huey S, Abuhamad A, Barroso G, Hsu M-I, Kolm P, Mayer J, Oehninger S. Perifollicular blood flow Doppler indices, but not pO_2, pCO_2, or pH, predict oocyte developmental competence in in vitro fertilization. Fertility Sterility, 72, 707-712, 1999.

Hunter RHF, Einer-Jenson N Greve T. Presence and significance of temperature gradients among different ovarian tissues. Microscopy Research and Technique, 69, 501-507, 2006.

Huyser C, Fourie FLR, Wolmarans L. Spectrophotometric absorbance of follicular fluid: A selection criterion. Clinical Assisted Reproduction, 9, 539-544, 1992.

Imoedemhe DAG, Chan RCW, Ramadan IAG, Sigue AB. Changes in follicular fluid gas and pH during carbon dioxide pneumoperitoneum for laparoscopic aspiration and their effect on human oocyte fertilizability. Fertility Sterility, 59, 177-182, 1993.

Ishikawa S, Fornier A, Borst C, Segal MS. The effects of air bubbles and time delay on blood gas analysis. Annals of Allergy, 33, 72-77, 1974.

Jansen R, DeCherney A. Overcoming Infertility: A Compassionate Resource for Getting Pregnant, W H Freeman & Co, 1998.

Jones DP, Kennedy FG. Intracellular Oxygen supply during hypoxia. American Journal of Physiology, 243, C247-C253, 1982.

Jones DP, Kennedy FG. Analysis of intracellular oxygenation of isolated adult cardiac myocytes. American Journal of Physiology, 250, C384-C390, 1986.

Jones DP. Effect of mitochondrial clustering on O_2 supply in hepatocytes. American Journal of Physiology. 247, C83-C89, 1984.

Jones RE. The Female Reproductive System. In, Human Reproductive Biology (2nd Ed.), Academic Press, San Diego, 1997.

Ju L, Ho CS, Babbour RF. Simultaneous measurements of oxygen diffusion coefficients and solubilities in fermentation media with polarographic oxygen electrodes. Biotechnology and Bioengineering, 31, 995-1005, 1988.

Kiekhofer W, Holmen GJ, Peckman B. Some chemical characteristics of ovarian and parovarian cystic fluids. Obstetrics Gynaecology, 20, 471-483, 1962.

Kim KH, Oh DS, Jeong JH, Shin BS, Joo BS, Lee KS. Follicular blood flow is a better predictor of the outcome of in vitro fertilization-embryo transfer than follicular fluid vascular endothelial growth factor and nitric oxide concentrations. Fertility and Sterility, 82, 586-592, 2004.

Knight DC, Tyler JP, Driscoll GL. (2001). Follicular flushing at oocyte retrieval: a reappraisal. Australian and New Zealand Journal of Obstetrics and Gynaecology, 41, 210-213, 2001.

Krieger IM, Mulholland GW, Dickey CS. Diffusion coefficients for gases in liquids from the rates of solution of small gas bubbles. The Journal of Physical Chemistry, 71, 1123-1129, 1967.

Kwant G, Oeseburg B, Zwart A, Zijlstra WG. Human whole-blood O_2 affinity: effect of CO_2. Journal of Applied Physiology, 64, 2400-2409, 1988.

Lango T, Morland T, Brubakk AO. Diffusion coefficients and solubility coefficients for gases in biological fluids and tissues: a review. Undersea & Hyperbaric Medicine, 23, 247-272, 1996.

Lee M, Ben-Rafael Z, Meloni F, Mastroianni L, Flickinger G. Relationship of human oocyte maturity, fertilization, and cleavage to follicular fluid prolactin and steroids. Journal of In Vitro Fertilization and Embryo Transfer, 4, 168-172, 1987.

Leese HJ, Lenton EA. Glucose and lactate in human follicular fluid: concentrations and interrelationships. Human Reproduction 5: 915-919, 1990.

Lequarre AS, Vigneron C, Ribaucour F, Holm P, Donnay I, Dalbies-Tran R, Callesen H, Mermillod P. Influence of antral follicle size on oocyte characteristics and embryo development in the bovine. Theriogenology, 63, 841-859, 2001.

Liley PE, Thomson GH, Friend DG, Daubert TE, Buck E. Physical and Chemical Data. In, Perry's Chemical Engineers' Handbook (7th Ed.), Perry RH, Green DW (Eds.), McGraw-Hill, New York, 1997.

Liu RH, Sun QY, Li YH, Jiao LH, Wang WH. Effects of cooling on meiotic spindle structure and chromosome alignment within in vitro matured porcine oocytes. Molecular Reproductive Development, 65, 212-218, 2003.

Lowe GDO, Barbenel, JC. Plasma and Blood Viscosity. In, Clinical Blood Rheology – Volume I, Lowe GDO (Ed), CRC Press, Florida, 1988.

Luck MR, Ye J, Almislimani H, Hibberd S. Follicular fluid rheology and the duration of the ovulatory process. Journal of Reproduction and Fertility, 120, 411-421, 2000.

MacArthur CG. Solubility of oxygen in salt solutions and the hydrates of these salts. The Journal of Physical Chemistry, 495-502, 1916.

Magnusson C, Hillensjo T, Tsafriri A, Hultborn R, Ahren K. Oxygen consumption of maturing rat oocytes. Biology of Reproduction, 17, 9-15, 1977.

Magnusson C, Hillensjo T, Hamberger L, Nilsson L. Oxygen consumption by human oocytes and blastocysts grown in vitro. Human Reproduction, 1, 183-184, 1986.

Mahoney JJ, Harvey JA, Wong RJ, Van Kessel AL. Changes in oxygen measurements when whole blood is stored in iced plastic glass syringes. Clinical Chemistry, 37, 1244-1248, 1991.

Malamitsi-Puchner A, Sarandakou, A, Baka SG, Tziotis J, Rizos D, Hassiakos, D, Creatsas, G. Concentrations of angiogenic factors in follicular fluid and oocyte-cumulus complex culture medium from women undergoing in vitro fertilization: association with oocyte maturity and fertilization. Fertility and Sterility. 76, 98-101, 2001.

Manarang-Pangan S, Menge AC. Immunologic studies on human follicular fluid. Fertility and Sterility, 22, 367-372, 1971.

Maxwell JC. A treatise on electricity and magnetism. Clarendon Press, Oxford, 1873.

McNatty KP. Follicular Fluid. In, The Vertebrate Ovary – comparative biology and evolution, Jones RE (Ed.), Plenum Press, New York, 1978.

McNatty KP. Hormonal correlates of follicular development in the human ovary. Australian Journal of Biological Science, 34, 249-268, 1981.

McShane PM. Infertility. John Wiley and Sons, New York, 1997.

Meyerhoff ME. In vivo blood-gas and electrolyte sensors: progress and challenges. Trends in Analytical Chemistry, 12, 257-266, 1993.

Moore DS, McCabe GP. Inference for Distributions. In, Introduction to the practice of statistics (2nd Ed.), W.H Freeman and Company, New York, 1993.

Mossman HW, Duke KL. General microscopic structure of the mammalian ovary. In, Comparative morphology of the mammalian ovary, The University of Wisconsin Press, Wisconsin, 1973.

Mueller RG, Lang GE, Beam JM. Bubbles in samples for blood gas determinations-potential source of error. American Journal of Clinical Pathology, 65, 242-249,1976.

Muller WA. Developmental Biology, Spinger-Verlag, New York, 1996.

Munne S, Magli C, Adler A, Wright, G, deBoer K, Mortimer D, Tucker M, Cohen J, Gianaroli L. Treatment-related chromosome abnormalities in human embryos. Human Reproduction, 12, 780-784, 1997.

Murdin AD, Kirkby NF, Wilson R, Spier RE. Immobilized hybridomas: oxygen diffusion. In, Animal Cell Biotechnology (Vol. 3), Academic Press, 1988.

Myers GE. Separation of Variables. In, Analytical methods in conduction heat transfer, Genium Publishing Corporation, New York, 1987.

Nagy Z, Liu J, Cecile J, Silber S, Devroey P, Vansteirteghem A. Using ejaculated, fresh, and frozen-thawed epididymal and testicular spermatozoa gives rise to comparable results after intracytoplasmic sperm injection. Fertility and Sterility, 63, 808-815, 1995.

Nargund G, Bourne T, Doyle P. Association between ultrasound indices of follicular blood flow, oocyte recovery, and preimplantation embryo quality. Human Reproduction, 11, 109-113, 1996.

Neeman m, Abramovitch R, Schiffenbaur YS, Tempel C. Regulation of angiogenesis by hypoxic stress: from solid tumours to the ovarian follicle. International Journal of Experimental Pathology, 78, 57-70, 1997.

Ng ST, Chang T, Jackson Wu TC. Prediction of the rates of fertilization, cleavage, and pregnancy success by cumulus-coronal morphology in an in vitro fertilization program. Fertility and Sterility, 72, 412-417, 1999.

Nicholson C. Diffusion and related transport mechanisms in brain tissue. Reports on Progress in Physics, 64, 815-884, 2001.

Oyawoye O, Gadir AA, Garner A, Constantinovici N, Perrett C, Hardiman P. Antioxidants and reactive oxygen species in follicular fluid of women undergoing IVF: relationship to outcome. Human Reproduction, 18, 2270-2274, 2003.

Pasqualotto EB, Agarwal A, Sharma RK, Izzo VM, Pinotti JA, Joshi NJ, Rose BI. Effect of oxidative stress in follicular fluid on the outcome of assisted reproductive procedures. Fertility and Sterility, 81, 973-976, 2004.

Pauly S. Permeability and Diffusion Data. In, Polymer Handbook (4th ed.), Abe A, Bloch DR (Eds.), John Wiley and Sons, New York, 1999.

Perloff WH, Schultz J, Farris EJ, Balin H. Some aspects of the chemical nature of human ovarian follicular fluid. Fertility and Sterility, 6, 11-17, 1955.

Peters H, McNatty, KP. Morphology of the Ovary. In, The ovary – a correlation of structure and function in mammals, Granada Publishing, London, 1980.

Quigley MM, Wolf DP, Maklad NF, Dandekar PV, Sokoloski JE. Follicular size and number in human in vitro fertilization. Fertility and Sterility, 38, 678-681, 1982.

Reeves RB. The effect of temperature on the oxygen equilibrium curve of human blood. Respiration Physiology, 42, 317-328, 1980.

Richmond KN, Shonat RD, Lynch RM, Johnson PC. Critical pO_2 of skeletal muscle in vivo. American Journal of Physiology, 277, H1831-H1840, 1999.

Riley MR, Muzzio FJ, Buettner HM, Reyes SC. Monte carlo calculation of effective diffusivities in two- and three- dimensional heterogeneous materials of variable structure. American Journal of Physiology, 49, 3500-3503, 1994.

Riley MR, Muzzio FJ, Buettner HM, Reyes SC. Diffusion in heterogeneous media: application to immobilized cell systems. AIChE Journal, 41, 691-700, 1995.

Riley MR, Muzzio FJ, Buettner HM, Reyes SC. A simple correlation for predicting effective diffusivities in immobilized cell systems. Biotechnology and Bioengineering, 49, 223-227, 1996.

Rumsey WL, Schlosser C, Nuutinen EM, Robiolio M, Wilson DF. Cellular energetics and the oxygen dependence of respiration in cardiac myocytes isolated from adult rat. The journal of Biological Chemistry, 265, 15392-15399, 1990.

Samaja M, Mosca A, Luzzana M, Rossi-Berardi L, Winslow RM. Equations and nomogram for the relationship of human blood P_{50} to 2,3-diphosphoglycerate, CO_2 and H^+. Clinical Chemistry, 27, 1856-1861,1981.

Schoolcraft WB, Schlenker T, Gee M, Jones GS, Jones HW. Assisted hatching in the treatment of poor-prognosis in-vitro fertilization candidates. Fertility and Sterility, 62, 551-554, 1994.

Scott PV, Horton JN, Mapleson WW. Leakage of oxygen from blood and water samples stored in plastic and glass syringes. British Medical Journal, 3, 512-516, 1971.

Scott RT, Hofmann GE, Muasher SJ, Acosta AA, Kreiner DK, Rosenwaks Z. Correlation of follicular diameter with oocyte recovery and maturity at the time of transvaginal follicular aspiration. Journal of in Vitro Fertilization and Embryo Transfer, 6, 73-75, 1989.

Shalgi R, Kraicer PF, Soferman N, Rimon A, Pinto M. Proteins of human follicular fluid: The blood follicle barrier. Fertility Sterility, 24, 429-434, 1973.

Shalgi R, Kraicer PF, Soferman N. Gases and electrolytes of human follicular fluid. Journal of Reproduction Fertility, 28, 335-340, 1972.

Shalgi R, Kraicer PF, Soferman N. Human Follicular Fluid. Journal of Reproduction and Fertility, 31, 515-516, 1972b.

Shaw AD, Li Z, Thomas Z, Stevens CW. Assessment of tissue oxygen tension: comparison of dynamic fluorescence quenching and polarographic electrode technique. Critical Care, 6, 76-80, 2001.

Shostak S. (1991). Embryology: an introduction to developmental biology, HarperCollins, New York, 1991.

Simonetti S, Veeck LL, Jones HW. Correlation of follicular fluid volume with oocyte morphology from follicles stimulated by human menopausal gonadotropin. Fertility and Sterility, 44, 177-180, 1985.

Sloane E. Reproductive Anatomy. In, Biology of Women (2nd Ed.), John Wiley and Sons, New York, 1985.

Smith JF, Tervit HR, McGowan LT, Pugh PA. Effect of aspiration system on the recovery and development of sheep follicular oocytes. AgResearch internal document, Hamilton, New Zealand, 1994.

Sokal RR, Rohlf FJ. Analysis of Frequencies. In, Biometry, Emerson R, Kennedy D, Park RB, Beadle GW, Whitaker DM (Eds.), W.H Freeman and Company, 1969.

Sokal RR, Rohlf FJ. Assumptions of Analysis of Variance. In, Biometry, Emerson R, Kennedy D, Park RB, Beadle GW, Whitaker DM (Eds.), W.H Freeman and Company, 1969b.

Sokal RR, Rohlf FJ. Two-Way Analysis of Variance. In, Biometry, Emerson R, Kennedy D, Park RB, Beadle GW, Whitaker DM (Eds.), W.H Freeman and Company, 1969c.

Stangel JJ. Fertility and Conception: an essential guide for childless couples, 30-42, Paddington Press, 1979.

Sugiura K, Pendola FL, Eppig JJ. Oocyte control of metabolic cooperativity between oocytes and companion granulosa cells: energy metabolism. Developmental Biology 279, 20-30, 2005.

Tai RC, Chang H. Oxygen transport in heterogeneous tissue. Journal of Theoretical Biology, 43, 265-276, 1974.

Tan SL, Bennett S, Parsons J. Surgical techniques of oocyte collection and embryo transfer. British Medical Bulletin, 46, 628-642, 1990.

Tan SL, Royston P, Campbell S, Jacobs HS, Betts J, Mason B, Edwards RG. Cumulative conception and livebirth rates after in-vitro fertilization. Lancet, 339, 1390-1394, 1992.

Tham MK, Walker RD, Gubbins KE. Diffusion of oxygen and hydrogen in aqueous potassium hydrogen solutions. Journal of Physical Chemistry, 74, 1747-1751, 1970.

Thompson JG, Partridge RJ, Houghton FD, Cox CI, Leese HJ. Oxygen uptake and carbohydrate metabolism by in vitro derived bovine embryos. Journal of Reproduction and Fertility, 106, 299-306, 1996.

Trudnowski RJ, Rico RC. Specific gravity of blood and plasma at 4 and 37 °C. Clinical Chemistry, 20, 615-616, 1974.

Truskey GA, Yuan F, Katz DF. Transport of Gases Between Blood and Tissues. In, Transport Phenomena in Biological Systems, Pearson Prentice Hall, New Jersey, 2004.

Truskey GA, Yuan F, Katz DF. Transport in Porous Media. In, Transport Phenomena in Biological Systems, Pearson Prentice Hall, New Jersey, 2004b.

Tsuji K, Sowa M, Nakano R. Relationship between human oocyte maturation and different follicular sizes. Biology of Reproduction., 32, 413-417, 1985.

Turitto V, Slack SM. Blood and related fluids. In, Handbook of Biomaterial Properties, Black J, Hastings G (Eds.), Chapman and Hall, London, 1998.

Tyn MT, Calus WF. Temperature and concentration dependence of mutual diffusion-coefficients of some binary-liquid systems. Journal of Chemical and Engineering Data, 20, 310-316, 1975.

Van Blerkom J, Henry G. Oocyte dysmorphism and aneuploidy in meiotically mature human oocytes after ovarian stimulation. Human Reproduction, 12, 1610-1614, 1992.

Van Blerkom J. Intrinsic factors affecting the outcome of laboratory assisted conception in the human. In, The Biological Basis of Early Reproductive Failure in the Human: Applications to Medically-Assisted Conception, Van Blerkom J (Ed.), Oxford University Press, Oxford, 1994.

Van Blerkom J, Davis P, Lee J. ATP content of human oocytes and developmental potential and outcome after in-vitro fertilization. Human Reproduction, 10, 415-454, 1995.

Van Blerkom J. The influence of intrinsic and extrinsic factors on the developmental potential and chromosomal normality of the human oocyte. Journal of the Society for Gynaecologic Investigation, 3, 3-11, 1996.

Van Blerkom J. Can the developmental competence of early human embryos be predicted effectively in the clinical IVF laboratory? Human Reproduction, 12, 1610-1614, 1997.

Van Blerkom J, Antczak M, Schrader R. The development potential of the human oocyte is related to the dissolved oxygen content of follicular fluid: association with vascular endothelial growth factor levels and perifollicular blood flow characteristics. Human Reproduction, 12, 1047-1055, 1997.

Van Blerkom J. Epigenetic influences on oocyte developmental competence: perifollicular vascularity and intrafollicular oxygen. Journal of Assisted Reproduction and Genetics, 15, 226-234, 1998.

Van Blerkom J. Intrafollicular influences on human oocyte developmental competence: perifollicular vascularity, oocyte metabolism and mitochondrial function. Human Reproduction, 15, 173-188, 2000.

Veeck LL, Edward Wortham JW, Witmyer J, Acosta AA, Garcia JE, Jones GS, Jones HW. Maturation and fertilization of morphologically immature human oocytes in a program of in vitro fertilization. Fertility and Sterility, 39, 594-602, 1983.

Vivian JE, King CJ. Diffusivities of slightly soluble gases in water. AIChE Journal, 10, 220-221, 1964.

Wagner MG, St. Clair, PA. Are In vitro fertilization and embryo transfer of benefit to all? Lancet, 2, 1027-1030, 1989.

Wang WH, Meng L, Hacket RJ, Odenbourg R, Keefe DL. Limited recovery of meiotic spindles in living human oocytes after cooling-rewarming observed using polarized light microscopy. Human Reproduction, 2374-2378, 2001.

Wang WH, Meng L, Hackett RJ, Oldenbourg R, Keefe DL. Rigorous thermal control during intracytoplasmic sperm injection stabilizes the meiotic spindle and improves fertilization and pregnancy rates. Fertility and Sterility, 77, 1274-1277, 2002.

Waterstone JJ, Parsons JH. A prospective study to investigate the value of flushing follicles during transvaginal ultrasound-directed follicle aspiration. Fertility and Sterility, 57, 221-223, 1992.

Weiner-Megnazi Z, Vardi L, Lissak A, Shnizer S, Reznick AZ, Ishai D, Lahav-Baratz S, Shiloh H, Koifman M, Dirnfeld M. Oxidative stress indices in follicular fluid as measured by the thermochemiluminescence assay correlate with outcome parameters in in vitro fertilization. Fertility and Sterility, 82, 1171-1176, 2004.

Wikland M, Lennart E, Hamberger. Transvesical and transvaginal approaches for the aspiration of follicles by the use of ultrasound. Annals of the New York Academy of Science, 442, 184-192, 1985.

Wilke CR, Chang P. Correlation of diffusion coefficients in dilute solutions. AICHE Journal, 1, 264-270, 1955.

Wu, EY, Barazanji, KW, and Johnson RL. Sources of error in A-aDo2 calculated from blood stored in plastic syringes. Journal of Applied Physiology 82,196-202, 1997.

Zeitz J, McNamee P, Toner JP. Assisted reproductive technology in the United States: 1998 results generated from the American Society for Reproductive Medicine/Society for assisted reproductive technology registry. Fertility and Sterility, 77, 18-31, 2002.

Appendix A. Procedure for the maturation of bovine cumulus-oocyte complexes

This document describes the procedure for maturation of oocytes collected from bovine ovaries obtained from the local abattoir and the subsequent examination of the effect of aspiration using a standard Swedmed FTD kit, and a set of modified apparatus (most probably a modified plastic syringe).

Equipment required:

Microscope with heated stage

Waterbath

Incubator with atmosphere of 5% CO_2 in air

Standard and modified FTD kit

Consumables required:

Maturation media

- Aspiration media
- H199 + 10% FCS
- B100 + 10% FCS
- IVM hormones
- Bovine ovaries

Maturation procedure

The maturation media (supplied by Ruakura) should be prepared ahead of time if possible. A Petri dish (or as many as will be required) containing IVM hormones and the containers of H199 + 10% FCS (cap tightened) and B199 + 10% FCS (cap loose) should be placed in the incubator with an atmosphere of 5% CO_2 in air to equilibrate for at least 2 hours.

All work with the oocytes should be carried out on a warm microscope stage (39°C)

and in the incubator at 39°C.

Bovine ovaries collected from the abattoir are stored in warm saline and should be transferred to the lab as soon as possible. Aspirate the oocytes and follicular fluid from the follicles into warmed tubes by suction using a vacuum pump. When each aspiration tube is sufficiently full, place it in the waterbath at 39°C while aspirating the remaining oocytes.

Prepare the Petri dishes while leaving the tubes to sit for a few minutes so that the contents can settle.

Place 4 (+) Petri dishes on a warm box. To the first add a few mls of aspiration medium. If there are a lot of oocytes to be matured, more than one Petri dish of aspiration medium may be required. To the second and third add a few mls of H199 + 10% FCS, and to the fourth add a few mls of B199 + 10% FCS. (The final Petri dish containing the IVM hormones should already be prepared and calibrated with CO_2 at 39°C.)

Using a Pasteur pipette attached to a syringe with a piece of silicone tubing, aspirate the oocytes from the follicular fluid (sediment in the bottom of the aspiration tube), place them in a Petri dish containing aspiration medium and allow to settle. The remaining follicular fluid should be stored in the fridge for later use in testing the aspiration kits.

On the warm microscope stage, search the Petri dish for oocytes. Pick up the oocytes using a Pasteur pipette / syringe and transfer to the first Petri dish containing H199 + 10% FCS. In order not to miss any oocytes, it may be easier to grid the Petri dish with a scalpel before starting and search the grid one square at a time until the entire dish has been searched.

Transfer the oocytes to the second Petri dish containing H199 + 10% FCS.

Transfer the oocytes to the Petri dish containing B199 + 10% FCS. Immediately start

transferring the oocytes to the dish containing IVM hormones. (The time left in the B199 + 10% FCS medium should be minimised to avoid pH changes.)

Continue until all oocytes are in the IVM medium and then incubate at 39°C in an atmosphere of 5% CO_2 in air for 22-24 hours (or until ready to use them).